



Dipl.-Ing. Mike Alexander Lagler, BSc.

# **Influence of Optimising Prosumers on Rural Distribution Networks**

## **DOCTORAL THESIS**

to achieve the university degree of  
Doktor der technischen Wissenschaften

submitted to

**Graz University of Technology**

### **Supervisor**

Univ.-Prof. DDipl.-Ing. Dr.techn. Robert Schürhuber  
Institute of Electrical Power Systems  
Graz University of Technology

Prof. Dr.-Ing. Christian Becker  
Institute of Electrical Power and Energy Technology  
Hamburg University of Technology

Graz, June 2021

– *meiner Familie* –

# Acknowledgements

Nach fünf Jahren als Universitätsassistent am Institut für Elektrische Anlagen und Netze an der TU Graz, darf ich auf eine höchst interessante und lehrreiche Zeit zurückblicken, in der es mir nicht nur gelungen ist, meine fachliche Expertise im Bereich der Elektrotechnik zu erweitern, sondern auch wertvolle zwischenmenschliche Kontakte zu knüpfen. Es ist mir daher ein ausgesprochen großes Anliegen, jenen Personen gegenüber meinen Dank und meine Wertschätzung zum Ausdruck zu bringen, die mich auf meinem Weg zur Promotion stets hilfreich begleitet haben.

So danke ich an dieser Stelle insbesondere Univ.-Prof. DDipl.-Ing. Dr.techn. Robert Schürhuber, der nicht nur als hervorragender Betreuer meines Dissertationsvorhabens fungierte, sondern auch als Vorgesetzter ein Höchstmaß an fachlicher und sozialer Kompetenz unter Beweis stellte und Prof. Dr.-Ing. Christian Becker, Leiter des Instituts für Elektrische Energietechnik der Technischen Universität Hamburg, der sich mit großem Interesse bereit erklärt hat, neben Prof. Schürhuber die wissenschaftliche Begutachtung der vorliegenden Arbeit zu übernehmen.

Ein großer Dank gilt auch Dipl.-Ing. Dr.techn. Ernst Schmautzer, der es mir im Rahmen zahlreicher gemeinsamer Projekte ermöglichte, in meiner Persönlichkeit als Teamplayer zu wachsen sowie dem Institut für Wärmetechnik an der TU Graz insbesondere Dr. Richard Heimrath, DI Werner Lerch und Dr. Daniel Brandl für die gelungene Projektzusammenarbeit und die Unterstützung bei diversen Anliegen im Bereich der Wärmetechnik.

Meinen Arbeitskollegen danke ich für die gemeinsame produktive und nicht zuletzt auch lustige Zeit, die wir mit einander zugebracht haben. Es bedarf einer besonderen Würdigung, wenn sich ein kollegiales Arbeitsverhältnis zu einem freundschaftlichen Miteinander entwickelt.

Als Zeichen meiner Wertschätzung sei in dieser Danksagung auch mein ehemaliger Vorgesetzter Em.Univ.-Prof. Dipl.-Ing. Dr.techn. Lothar Fickert erwähnt, welcher mir selbst in seinem wohlverdienten Ruhestand noch als mentaler Coach beim Erreichen meiner beruflichen Ziele zur Seite steht.

Der wohl größte Dank richtet sich jedoch an meine Familie. Liebe Mama, lieber Papa, liebe Oma, lieber Christian ihr habt mir nicht nur mein Studium ermöglicht, sondern wart auch zeit meines Lebens die beste Unterstützung, die ich mir nur hätte wünschen können. Meine Dissertation als Höhepunkt meiner wissenschaftlichen Tätigkeit sei daher euch gewidmet.

*Mike Alexander Lagler*

## **AFFIDAVIT**

I declare that I have authored this thesis independently, that I have not used other than the declared sources/resources, and that I have explicitly indicated all material which has been quoted either literally or by content from the sources used. The text document uploaded to TUGRAZonline is identical to the present doctoral thesis.

---

Date, Signature

## Abstract

A plethora of factors are currently leading to significant changes in both the planning and operation of distribution networks and systems such as single-family houses, commercial and industrial buildings. These factors include the increasing share of decentralised energy generation and storage systems in distribution networks, the integration of electric vehicles, the coupling of electrical and thermal systems, as well as the increased and easy use of Information and Communication Technologies (ICT). The primary actors in this situation, formerly known as consumers of energy and power, have now become so-called prosumers (producers and consumers) who feed energy back into the network at specific times.

Hybrid energy systems combine cross-sectoral energy sources and supply systems as well as energy distribution and storage all into one compact system. The aim thereby is to substitute fossil energy sources with primarily renewably generated electricity or other renewable energy sources and sustainable forms of energy use.

The use of new meter functions and services (smart metering) enables market-dependent dynamic or special consumer/prosumer tariffs while taking the availability of electrical energy in the network into account. In the simplest case, the consumer can be motivated by the visualisation of tariffs, consumption and costs to increase their energy efficiency. By optimising the use of distributed generation systems, e.g., photovoltaic or solar thermal systems, energy storages and demand-side management, the prosumer can respond to dynamic tariffs and obtain e.g., an economically optimal advantage. Accordingly, this optimisation by the prosumers influences the load flow conditions in low- and medium-voltage networks.

Therefore, a powerful simulation model has been developed to model, simulate and analyse the behaviour and steady-state energy flows of such hybrid energy systems such as optimising prosumers. Using linear optimisation algorithms, the optimal use of decentralised energy generation and storage systems in the example of a single-family house is determined. The simulation model considering different optimisation objectives, desired energy services (heating, cooling, electrical energy services), external boundary conditions, e.g., building structure and weather, individual technical components, as well as selected energy tariffs. Furthermore, the developed simulation model is used to analyse how the high penetration of optimising prosumers influences rural distribution networks.

Keywords: Hybrid energy system, photovoltaic, storage, sector coupling, prosumer, single-family house, linear optimisation, MILP, low voltage distribution network, load-flow calculation, energy tariffs

## Kurzfassung

Der steigende Anteil dezentraler Energieerzeugungs- sowie Speicheranlagen in den Verteilnetzen, die Integration von Elektrofahrzeugen, die Kopplung von elektrischen und thermischen Systemen sowie die steigende und einfache Nutzung von Informationstechnologien (IKT) führen zu starken Veränderungen in den Verteilnetzen und in Anlagen wie Einfamilienhäuser, Gewerbe und der Industrie. Vormalig reine Energie- und Leistungskonsumenten werden nun zu sogenannten Prosumern (Producer und Consumer), welche zu bestimmten Zeiten z.B. elektrische Energie in das Netz rückspeisen.

Ein hybrides Energiesystem – z.B. in einem Einfamilienhaus – weist eine intelligente Kopplung der Energieerzeugungs- und Speicheranlagen des Strom-, Wärme- und Kältesektors auf. Durch diese sektorenübergreifende Kopplung kann der elektrische sowie thermische Energiebedarf ökonomisch und/oder ökologisch effizient gedeckt werden. Hybride Energiesysteme haben zum Ziel, fossile Energieträger durch überwiegend regenerativ erzeugten Strom, andere erneuerbare Energiequellen sowie durch nachhaltige Formen der Energienutzung zu substituieren.

Die Verwendung neuer Zählerfunktionen und -dienste (Smart Metering) ermöglicht marktabhängige dynamische oder spezielle verbraucher- und prosumerorientierte Tarife. Im einfachsten Fall kann der Verbraucher dazu motiviert werden, seine Effizienz zu steigern oder sein Verbraucherverhalten durch den erhöhten Informationsgewinn zu ändern, z.B. durch Berücksichtigung der aktuellen Tarifsituation, des Eigenverbrauchs oder der damit verbundenen Kosten. Durch die optimierte Nutzung der dezentralen Erzeugungsanlagen (z.B. Photovoltaik und Solarthermie) sowie der Energiespeicher kann der Verbraucher oder Prosumer gegebenenfalls auf dynamische Tarife reagieren und z.B. seinen wirtschaftlich oder ökologisch optimalen Vorteil erzielen.

Es wurde ein umfangreiches Simulationsprogramm entwickelt, mit welchem das Verhalten sowie die stationären Energieflüsse solcher hybrider Energiesysteme, wie optimierende Prosumer, modelliert, simuliert und analysiert werden können. Mit linearen Optimierungsalgorithmen wird der optimale Einsatz von dezentralen Energieerzeugungs- und Speichersystemen am Beispiel eines Einfamilienhauses ermittelt. Das entwickelte Simulationsprogramm berücksichtigt unterschiedliche Optimierungsziele, gewünschte Energiedienstleistungen (Heizung, Kühlung, elektrische Energiedienstleistungen), äußere Randbedingungen (z.B. Gebäudestandard, Wetter), die eingesetzten technischen Anlagen sowie ausgewählte Energietarife. Darüber hinaus wird mit Hilfe des entwickelten Simulationsprogramms der Einfluss von optimierenden Prosumern auf ländliche Verteilnetze untersucht.

Schlüsselwörter: Hybride Energiesysteme, Photovoltaik, Speicher, Sektorkopplung, Prosumer, Einfamilienhaus, lineare Optimierung, MILP, Niederspannungsnetz, Lastflussrechnung, Energietarife

# Contents

<b>List of Symbols and Abbreviations</b>	<b>x</b>
<b>1 Introduction</b>	<b>1</b>
1.1 Scope of Research . . . . .	2
1.2 Research Methods . . . . .	2
1.3 Research Questions . . . . .	3
1.4 Scientific Contribution and Publications of the Author . . . . .	4
<b>2 Methodology, Modelling and Calculations</b>	<b>7</b>
2.1 Hybrid Energy Systems . . . . .	7
2.1.1 Prosumer – Overview . . . . .	8
2.2 Simulation Model – ProsOpt . . . . .	10
2.2.1 Optimisation of Hybrid Energy Systems . . . . .	12
2.3 Weather . . . . .	24
2.4 Energy Demand . . . . .	28
2.4.1 Electrical Energy Demand – Domestic Appliances and Lighting	30
2.4.2 Heating and Cooling Demand . . . . .	31
2.4.3 Domestic Hot Water . . . . .	36
2.4.4 Home Presence of Electric Vehicle . . . . .	38
2.5 Economic and Ecologic Assumptions . . . . .	39
2.6 Distributed Energy Generation and Storage Systems . . . . .	42
2.6.1 Photovoltaic System . . . . .	42
2.6.2 Electrical Energy Storage System . . . . .	48
2.6.3 Electric Vehicles . . . . .	54
2.6.4 Solar Thermal System . . . . .	58
2.6.5 Heat Pumps and Air Conditioners . . . . .	62
2.6.6 Domestic Gas Boiler . . . . .	64
2.6.7 District Heating . . . . .	65
2.6.8 Thermal Energy Storage . . . . .	66
2.7 Load Flow Calculations . . . . .	68
<b>3 Optimisation of Hybrid Energy Systems</b>	<b>70</b>
3.1 Degree of Autonomy and Self-Consumption of a Prosumer . . . . .	74
3.2 Economic Optimum of a Prosumer . . . . .	79
3.3 Impact of Energy Tariffs on Prosumer Behaviour . . . . .	84
3.4 Storage Strategies: Forecast versus Self-Consumption . . . . .	87
3.5 Economical and Ecological Optimisation of a Prosumer . . . . .	89

---

<b>4</b>	<b>Influence of Prosumers on Distribution Networks</b>	<b>95</b>
4.1	Increasing Hybridisation Levels of Households . . . . .	99
4.2	Dynamic Energy Tariffs and Peak-Shaving . . . . .	105
4.3	Impact of Voltage and Reactive Power Control on the Distribution Network . . . . .	110
<b>5</b>	<b>Summary and Outlook</b>	<b>120</b>
	<b>References</b>	<b>131</b>
	<b>Appendices</b>	<b>139</b>
<b>A</b>	<b>Methodology, Modelling, Calculations</b>	<b>139</b>
<b>B</b>	<b>Solar Irradiance</b>	<b>141</b>
<b>C</b>	<b>Influence on Distribution Networks</b>	<b>148</b>

# List of Figures

1.1	Overview of sectors . . . . .	1
2.1	Comparison between the generation of a PV system and electrical demand of a single-family house . . . . .	7
2.2	Schematic illustration of the modelled hybrid energy system – Prosumer	9
2.3	Overview of the simulation model ProOpt . . . . .	10
2.4	Overview hybrid energy system - optimisation . . . . .	14
2.5	Measured ambient temperature and solar irradiance – Graz Austria .	24
2.6	Illustration of the composition of solar irradiance . . . . .	25
2.7	Comparison of solar irradiance at various alignments of surfaces . . .	27
2.8	Energy demand of the residential sector in Austria, 2017/18 . . . . .	28
2.9	LoadProfileGenerator (LPG) - activity selection by a person . . . . .	29
2.10	Electrical demand of a chosen household . . . . .	30
2.11	Overview of the internal and external factors influencing the thermal behaviour of a building. . . . .	31
2.12	Heating and cooling power of the house with an annual heating demand of $75 \frac{\text{kWh}}{\text{m}^2}$ and annual cooling demand of $6 \frac{\text{kWh}}{\text{m}^2}$ . . . . .	35
2.13	Comparison of the calculated heating and cooling demand with the results of the simulation software IDA ICE from EQUA Simulation AB	36
2.14	Domestic hot water demand of a chosen household . . . . .	37
2.15	EV home presence of a chosen household . . . . .	38
2.16	Static, HT/NT and dynamic tariff models . . . . .	39
2.17	Methodical representation of the calculation process of the PV system	42
2.18	Efficiency of a PV module as a function of the ambient temperature $\vartheta_a$ and the solar irradiance $G$ . . . . .	43
2.19	Efficiency of the inverter $\eta_{AC}$ as a function of the active power output of the PV modules . . . . .	44
2.20	Reactive power capability for inverter-based generators . . . . .	45
2.21	Voltage-reactive power mode for inverter-based generators . . . . .	46
2.22	Active power-power factor mode for inverter-based generators . . . .	47
2.23	Voltage-active power mode for inverter-based generators . . . . .	47
2.24	Schematical representation of a PV-Storage system and exemplary a comparison of the PV generation, the household’s electrical demand, and the charging and discharging of an EES at limited charging/discharging power . . . . .	51
2.25	Operation strategy – self-consumption . . . . .	53
2.26	Operation strategy – peak-shaving . . . . .	53
2.27	Operation strategy – forecast . . . . .	54
2.28	Electric Vehicle - V2G model . . . . .	57

2.29	Collector efficiency for different temperature differences . . . . .	59
2.30	Schematic representation of a solar thermal system . . . . .	61
2.31	Thermal power output - performance data of a representative air source heat pump . . . . .	62
2.32	Soil temperature $\vartheta_{\text{soil}}$ as an annual curve and at various depths . . . .	63
2.33	Implemented heat supply by district heating . . . . .	65
2.34	Schematic illustration of the used TES model . . . . .	67
2.35	Methodology - load flow calculations . . . . .	69
3.1	Correlation between demand and the generation of the PV system . .	72
3.2	Degree of autonomy and self-consumption of prosumers – Scenarios S1 to S4 . . . . .	76
3.3	Economic optimum of a prosumer . . . . .	82
3.4	Impact of energy tariffs on optimising prosumer storage charging behaviour . . . . .	85
3.5	Forecast-based versus traditional storage strategy - difference in degree of autonomy and degree of self-consumption . . . . .	88
3.6	Sensitivity analyses of annual energy costs - heat pump as the primary heating system . . . . .	92
3.7	Sensitivity analyses of annual CO <sub>2</sub> emissions - heat pump as the primary heating system . . . . .	93
4.1	Low-voltage network, consisting of four feeders and the considered thirteen prosumers . . . . .	96
4.2	Active power flow $p_T$ across the transformer, transformer loading $i_T$ and LV-network losses $s_{\text{loss}}$ – Scenario N1-N4: <u>N1</u> : District heating, w/o photovoltaic's and electrical energy storages <u>N2</u> : Heat pumps, thermal energy storages with heating cartridges, home charging of the electric vehicles, w/o photovoltaic's and electrical energy storages <u>N3</u> : N2 with photovoltaic's added <u>N4</u> : N2 with photovoltaic's and electrical energy storages added . . . . .	100
4.3	Line loading - scenarios N1 to N4 <u>N1</u> : District heating, w/o pho- tovoltaic's and electrical energy storages <u>N2</u> : Heat pumps, thermal energy storages with heating cartridges, home charging of the electric vehicles, w/o photovoltaic's and electrical energy storages <u>N3</u> : N2 with photovoltaic's added <u>N4</u> : N2 with photovoltaic's and electrical energy storages added . . . . .	102
4.4	Node voltages – scenario N1 to N4, <u>N1</u> : District heating, w/o pho- tovoltaic's and electrical energy storages <u>N2</u> : Heat pumps, thermal energy storages with heating cartridges, home charging of the electric vehicles, w/o photovoltaic's and electrical energy storages <u>N3</u> : N2 with photovoltaic's added <u>N4</u> : N2 with photovoltaic's and electrical energy storages added . . . . .	103

4.5	Active power flow $p_T$ across the transformer, transformer loading $i_T$ and LV-network losses $s_{\text{loss}}$ – Scenario N4-N7 <u>N4</u> : Heat pumps, thermal energy storages with heating cartridges, home charging of the electric vehicles, photovoltaic's, electrical energy storages, static energy tariffs and PCC limits set to 17.3 kVA <u>N5</u> : N4 with dynamic energy tariffs <u>N6</u> : N4 performing peak-shaving with PCC limits set to 8 kVA <u>N7</u> : N4 with dynamic energy tariffs and performing peak-shaving with PCC limits set to 8 kVA . . . . .	106
4.6	Line loading – scenarios N4 to N7 <u>N4</u> : Heat pumps, thermal energy storages with heating cartridges, home charging of the electric vehicles, photovoltaic's, electrical energy storages, static energy tariffs and PCC limits set to 17.3 kVA <u>N5</u> : N4 with dynamic energy tariffs <u>N6</u> : N4 performing peak-shaving with PCC limits set to 8 kVA <u>N7</u> : N4 with dynamic energy tariffs and performing peak-shaving with PCC limits set to 8 kVA . . . . .	107
4.7	Node voltages – scenarios N4 to N7 <u>N4</u> : Heat pumps, thermal energy storages with heating cartridges, home charging of the electric vehicles, photovoltaic's, electrical energy storages, static energy tariffs and PCC limits set to 17.3 kVA <u>N5</u> : N4 with dynamic energy tariffs <u>N6</u> : N4 performing peak-shaving with PCC limits set to 8 kVA <u>N7</u> : N4 with dynamic energy tariffs and performing peak-shaving with PCC limits set to 8 kVA . . . . .	108
4.8	Active power flow $p_T$ across the transformer, transformer loading $i_T$ and LV-network losses – Scenarios N4 and N8 to N10 <u>N4</u> : Heat pumps, thermal energy storages with heating cartridges, home charging of the electric vehicles, photovoltaic's, electrical energy storages, static energy tariffs, PCC limits set to 17.3 kVA and the inverters are operating in a constant power factor mode $\cos(\varphi) = 1$ <u>N8</u> : N4 and the inverters are operating in a constant power factor mode $\cos(\varphi) = 0.95$ (under-excited) <u>N9</u> : N4 and the inverters are operating in volt-var mode <u>N10</u> : N4 and the inverters are operating in watt-cos $\varphi$ mode . . . . .	111
4.9	Line loading – scenario N4 and N8 to N10 <u>N4</u> : Heat pumps, thermal energy storages with heating cartridges, home charging of the electric vehicles, photovoltaic's, electrical energy storages, static energy tariffs, PCC limits set to 17.3 kVA and the inverters are operating in a constant power factor mode $\cos(\varphi) = 1$ <u>N8</u> : N4, inverters are operating with a constant power factor of 0.95 (under-excited) <u>N9</u> : N4 and the inverters are operating in volt-var mode <u>N10</u> : N4 and the inverters are operating in watt-cos $\varphi$ mode . . . . .	113

4.10	Node voltages - scenarios N4,N8 - N10 <u>N4</u> : Heat pumps, thermal energy storages with heating cartridges, home charging of the electric vehicles, photovoltaic's, electrical energy storages, static energy tariffs, PCC limits set to 17.3 kVA and the inverters are operating in a constant power factor mode $\cos(\varphi) = 1$ <u>N8</u> : N4, inverters are operating with a constant power factor of 0.95 (under-excited) <u>N9</u> : N4 and the inverters are operating in volt-var mode <u>N10</u> : N4 and the inverters are operating in watt-cos $\varphi$ mode . . . . .	115
4.11	Characteristic curves of the volt-var mode and the watt-cos $\varphi$ mode for feeder II . . . . .	116
B.1	Illustration of Sun's declination $\delta$ . . . . .	141
B.2	Yearly sum of solar irradiation incident on optimally-inclined south-orientated photovoltaic modules – Europe . . . . .	142
B.3	Monthly and yearly solar irradiation of three different cities . . . . .	143
B.4	Position of the sun in the sky . . . . .	144
B.5	Solar path . . . . .	145
B.6	Overview of the different angles . . . . .	146

# List of Tables

2.1	Domestic warm water quantities and temperatures per use and different apartment sizes . . . . .	36
2.2	Levelised Costs of Energy (LCE) for the used technologies and energy tariffs, typical prices in Austria, 2018 . . . . .	40
2.3	CO <sub>2</sub> equivalents or global warming potential (GWP) of the technologies used . . . . .	41
2.4	Characteristics of Li-ion batteries . . . . .	48
2.5	Characteristics of Pb-A batteries . . . . .	49
2.6	Efficiencies of gas boiler . . . . .	65
2.7	Overview of the different node types - load flow calculation . . . . .	68
3.1	Initial parameter settings - Prosumer (Scenario S1) . . . . .	73
3.2	Scenarios – Annual energy demand according to the individual main scenarios . . . . .	75
3.3	Considered CAPEX and energy tariffs . . . . .	80
3.4	Parameter settings - economical and ecological optimisation of a prosumer . . . . .	90
3.5	Assumed initial values of levelised costs of energy (LCE) and CO <sub>2</sub> equivalents . . . . .	91
4.1	Electrical parameters of the network components . . . . .	96
4.2	Defined scenarios - network analysis . . . . .	98
A.1	Comparison of typical overall heat transfer coefficients $U$ for different building types . . . . .	139
A.2	Typical values for the total energy transmittance $g$ of transparent components . . . . .	139
A.3	Thermal conductivity $k_{\text{soil}}$ , volumetric heat capacity $C_{\text{soil}}$ for different kinds of soil . . . . .	140
B.1	Albedo values $\alpha$ for different surfaces . . . . .	147
C.1	Energy demand of households connected to B1 to B13 . . . . .	148

# Abbreviations

AC	Air conditioning system
CAPEX	Capital expenditure
CD	Cooling demand
CHP	Combined heat and power
COP	Coefficient of performance
CT	Cold temperature
DH	District heating
DHW	Domestic hot water
DWH	Domestic water heating
EER	Energy efficiency ratio
EES	Electrical energy storage
EV	Electric vehicle
EVCS	Electric vehicle charging station
G2V	Grid to vehicle
HC	Heating cartridge
HD	Heating demand
HP	Heat pump
HT	High temperature
HVAC	Heating, ventilation and air conditioning
HX	Heat exchanger
ICT	Information and communication technologies
IEAN	Institute of Electrical Power Systems
LCE	Levelised cost of energy
LCOE	Levelised cost of electricity
LT	Low temperature
LV	Low voltage
MILP	Mixed integer linear programming
MV	Medium voltage
OPEX	Operating expenditure
PCC	Point of common coupling
Prosumer	Producer + consumer
PV	Photovoltaic
ST	Solar thermal
TES	Thermal energy storage
V2G	Vehicle to grid

# 1 Introduction

A plethora of factors are currently leading to significant changes in both the planning and operation of distribution networks and systems such as single-family houses, commercial and industrial buildings. These factors include the increasing share of decentralised energy generation and storage systems in distribution networks, the integration of electric vehicles, the coupling of electrical and thermal systems, as well as the increased and easy use of Information and Communication Technologies (ICT). The primary actors in this situation, formerly known as consumers of energy and power, have now become so-called prosumers (producers and consumers) who feed energy back into the network at specific times.

Hybrid energy systems combine cross-sectoral energy sources and supply systems as well as energy distribution and storage all into one compact system. The aim thereby is to substitute fossil energy sources with primarily renewably generated electricity or other renewable energy sources and sustainable forms of energy use. The basis of optimal and energy-efficient system design and operation is the knowledge of the interaction of the system components and their interdependencies.

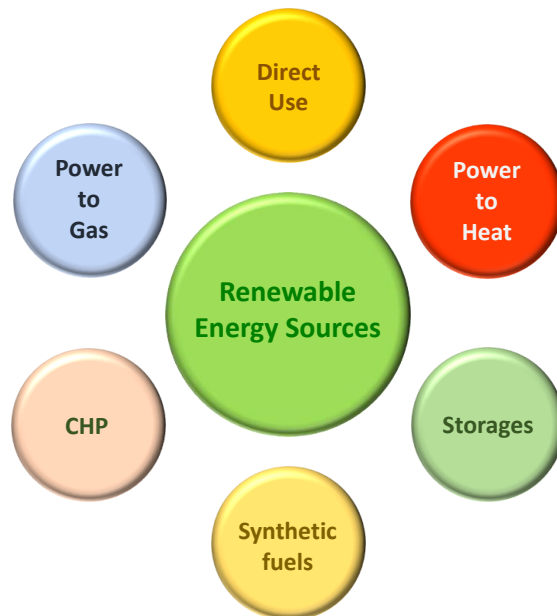


Figure 1.1: Overview of sectors

The use of new meter functions and services (smart metering) enables market-dependent dynamic or special consumer/prosumer tariffs while taking the availability of electrical energy in the network into account. In the simplest case, the consumer

can be motivated by the visualisation of tariffs, consumption and costs to increase their energy efficiency. Using weather and demand forecast methods combined with optimisation algorithms, a prosumer can respond to dynamic tariffs and optimally operate the distributed generation systems, e.g., photovoltaic or solar thermal systems, energy storages, and demand control. Accordingly, prosumers' forecast-based operation influences the load flow conditions in low- and medium-voltage networks.

## 1.1 Scope of Research

In the context of this thesis, a simulation model has been developed which can model, simulate and analyse hybrid energy systems. This simulation model is used to determine the optimal use of decentralised energy generation and storage systems, taking into account the coupling of thermal and electrical systems. Using optimisation algorithms, the economic or ecological objectives of the prosumers are analysed, considering different desired energy services (heating, cooling, electrical energy services), external boundary conditions (e.g., building structure, weather) as well as selected energy- and power-based tariffs. The developed simulation model is additionally used to determine the influence of multiple independently optimised prosumers on a typical rural low voltage distribution network.

### Non-Goals:

The following objectives are not the aim of this thesis and the developed simulation model:

- Development of simulated technologies, e.g., heat pump, photovoltaic system
- Dynamic calculations of thermal and electrical systems
- Steady state and transient stability analysis
- Frequency stability in future networks
- Short circuit calculations
- Influence of energy communities on distribution networks

## 1.2 Research Methods

In this thesis, a simulation model developed using the software MATLAB is used to analyse the behaviour and steady-state energy flows of hybrid energy systems such as single-family households (prosumers) in distribution networks. Based on the simulation model, the optimal use of the distributed energy generation and storage systems is determined using linear optimisation (MILP – Mixed Integer Linear Programming) taking into account the desired energy services, external boundary conditions (e.g., weather) and cost functions of the individual components. The objectives of optimisation can be technical – optimal use of generated energy for electricity, heating and cooling –, economical as well as ecological.

The influence of optimised prosumers on the distribution network is determined by coupling the simulation model of a prosumer with a time series-based load flow

calculation of a typical distribution network. Furthermore, this thesis shows how far the network operator can control the load flow by introducing selected dynamic tariffs. Different methods of dynamic tariffs, as well as different optimisation objectives of the consumers/prosumers, are compared and presented in this thesis.

### 1.3 Research Questions

Research Question	Section
Which combinations of different technologies result in an economic, ecological or technical optimum?	3.5
How sensitive is the overall hybrid energy system to variations in system components, e.g., photovoltaic- or electrical energy storage capacity?	3.1, 3.5
Which degree of autonomy or self-consumption of a hybrid energy system can be achieved under realistic environmental conditions?	3.1
How scalable or transferable is the developed simulation model to other hybrid energy systems, such as industry?	2.2
What influence have optimised prosumers on the load flow conditions, e.g., loading and voltage levels in rural distribution networks?	4
How can electrical energy storage systems optimally used or dimensioned in hybrid energy systems?	3.4
How is the operation of hybrid energy systems of optimising prosumers influenced by fluctuating electricity and heat production, and variable tariffs?	3.3, 4.2

## 1.4 Scientific Contribution and Publications of the Author

As a university assistant at the Institute of Electrical Power Systems (IEAN) of the Graz University of Technology, research in the fields of smart grids, network planning, hybrid energy systems, optimisation of energy systems, distributed power generation and storage systems were performed. The research results have been published as scientific contributions and publications in national and international conferences as well as in research reports. Below, the author's contributions and publications are listed.

### Journals

T. Wieland, M. Reiter, E. Schmautzer, L. Fickert, M. A. Lagler, S. Eberhart: „Gleichzeitigkeitsfaktoren in der elektrischen Energieversorgung – Konventioneller & probabilistischer Ansatz“, e&i Elektrotechnik und Informationstechnik, Springer-Verlag, Wien, Austria, 2014

### Conferences

M. A. Lagler, R. Schürhuber, R. Heimrath, T. Mach, M. J. Müller: „Interaction of hybrid energy systems with the power network on the example of an industrial company“, CIRED Workshop, Berlin, Germany, 2020

M. A. Lagler, R. Schürhuber, E. Schmautzer, R. Heimrath, T. Mach, M. J. Müller: „Effizienzsteigerung in komplexen hybriden Energiesystemen am Beispiel eines Industriebetriebes“, 16. Symposium Energieinnovation, Graz, Austria, 2020

D. Herbst, M. A. Lagler, R. Schürhuber, E. Schmautzer, L. Fickert, A. Einfalt, H. Brunner, D.-L. Schultis, T. Frühwirth, W. Prügler: „Zukünftige Anforderungen an NS-Netze und deren Lösungsansätze am Beispiel POSYCO“, 16. Symposium Energieinnovation, Graz, Austria, 2020

M. A. Lagler, R. Schürhuber, E. Schmautzer: „Influence of Optimizing Prosumers on Urban Distribution Networks“, ETG-Kongress 2019, Esslingen am Neckar, Germany, 2019

M. A. Lagler, E. Schmautzer, R. Schürhuber: „Ökonomische und ökologische Optimierung eines hybriden Energiesystems am Beispiel eines Einfamilienhauses“, 11. Internationale Energiewirtschaftstagung, Vienna, Austria, 2019

M. A. Lagler, E. Schmautzer, R. Schürhuber: „Sensitivities in Hybrid Energy Systems“, 8<sup>th</sup> Solar Integration Workshop, Stockholm, Sweden, 2018

M. A. Lagler, E. Schmautzer, R. Schürhuber, W. Lerch, R. Heimrath, T. Mach: „Creation of a Hybrid Simulation Model“, International Sustainable Energy Conference - ISEC 2018, Graz, Austria, 2018

M. A. Lagler, E. Schmautzer, R. Schürhuber: „Sensitivitäten in Hybriden Energiesystemen“, 15. Symposium Energieinnovation, Graz, Austria, 2018

M. Fürnschuß, M. A. Lagler, E. Schmautzer: „Bedarfsorientierte Konzeptionierung von Photovoltaikanlagen“, 15. Symposium Energieinnovation, Graz, Austria, 2018

M. A. Lagler, E. Schmautzer, M. Grobbauer, J. Gratzner, G. M. Michtner: „Modellierung eines industriellen hybriden Energiesystems unter Einbeziehung dezentraler Energieerzeugung und -speicherung“, 10. Internationale Energiewirtschaftstagung, Vienna, Austria, 2017

M. A. Lagler, E. Schmautzer, S. Forsthofer: „Modellierung eines hybriden Energiesystems unter Berücksichtigung dezentraler Energieerzeugung und -speicherung am Beispiel eines Einfamilienhauses mit Anbindung an das öffentliche Elektrizitätsnetz“, Forum Econogy 2016, Linz, Austria, 2016

M. A. Lagler, T. Wieland, E. Schmautzer: „Computer-Based Analysis of an Urban 20 kV Medium-Voltage Network“, Universities Power Engineering Conference, Coimbra, Portugal, 2016

## Poster

M. A. Lagler, E. Schmautzer, R. Schürhuber: „Ökonomische und ökologische Optimierung eines hybriden Energiesystems am Beispiel eines Einfamilienhauses“, 11. Internationale Energiewirtschaftstagung, Vienna, Austria, 2019<sup>1</sup>

## Presentations

E. Schmautzer, M. A. Lagler: „Neue Anforderungen an die Mittel- und Niederspannungs-Stromversorgung im städtischen und ländlichen Raum“, 55. Fachtagung der Österreichischen Gesellschaft für Energietechnik im OVE, Salzburg, Austria, 2017

## Relevant Research Reports

M. A. Lagler, E. Schmautzer, R. Heimrath, et al.: „REsys - Regelungsstrategien zur Effizienzsteigerung komplexer hybrider Energiesysteme“, Klima- und Energiefonds, Energieforschungsprogramm - 1. Ausschreibung, Austria, 2019

E. Schmautzer, M. A. Lagler, T. Wieland: „Smart City Project Graz - Anhang 2: Scientific Monitoring – Grätzel-Demo“, Smart Energy Demo – FIT for SET 2. Ausschreibung, Austria, 2017

---

<sup>1</sup> Winner of Best Poster Award (Plurality voting)

L. Fickert, E. Schmutzner, T. Wieland, M. Lagler, T.Höhn, M. Grobbauer, J. Reckenzaun: „Smart City Project Graz - Arbeitspaket 3, Task 2, Niederspannungs-Gleichspannungsnetz“, Smart Energy Demo – FIT for SET 2. Ausschreibung, Austria, 2017

L. Fickert, E. Schmutzner, T. Wieland, M. Lagler, T.Höhn, M. Grobbauer, J. Reckenzaun: „Smart City Project Graz - Subtask 6.4 Monitoringkonzept“, Smart Energy Demo – FIT for SET 2. Ausschreibung, Austria, 2017

W. Lerch, R. Heimrath, T. Mach, T. Wieland, M. Reiter, M. A. Lagler, E. Schmutzner und M. Gratzl-Michlmair: „Rahmenplan Energie Energy City Graz-Reinighaus - Annexbericht 5: Modellierung des Bedarfs an und der Versorgung mit Wärme und elektrischem Strom“, Bundesministerium für Verkehr, Innovation und Technologie, Österreich, 2015

# 2 Methodology, Modelling and Calculations

## 2.1 Hybrid Energy Systems

Since consumption and generation of energy do not coincide in every time step, it is necessary to purchase or sell energy at suboptimal tariffs, or to adapt the load profile, e.g., consumer behaviour, accordingly. A further possibility to cover the demand is to use energy storages or demand-side management. The following Figure 2.1 compares a typical generation profile of a photovoltaic system with the electrical demand of a single-family house for two exemplarily chosen working days in summer.

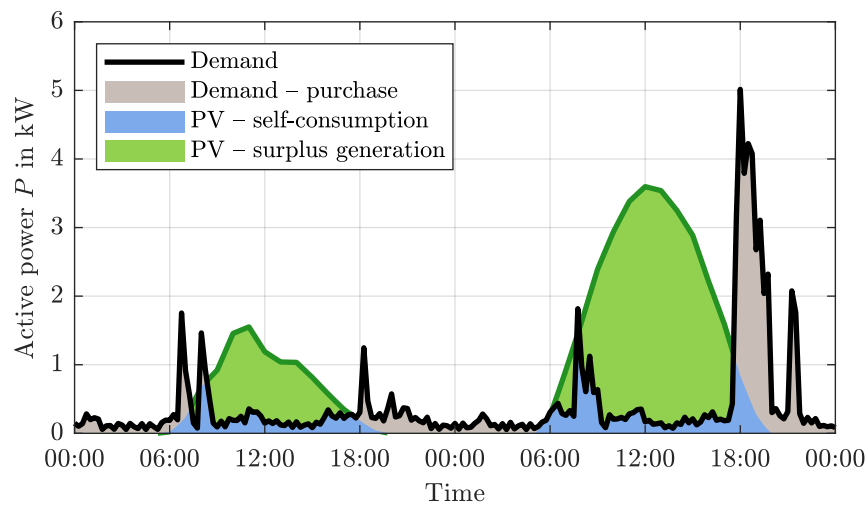


Figure 2.1: Comparison between the generation of a PV system and electrical demand of a single-family house

The generation of the photovoltaic system and the demand of a single-family house do not coincide in every time step. Therefore, a photovoltaic system can be mounted demand-oriented to utilise generation optimally, e.g., to a western orientation for higher generation in the afternoon. Furthermore, a coupling of the electrical and thermal systems to a so-called hybrid energy system increases the overall system's optimal utilisation.

A hybrid energy system intelligently combines energy generation and distribution systems as well as energy storage systems for electricity, heating and cooling. An

intelligent coupling of thermal and electrical systems, can spare resources, saves energy costs, as well as increases the perceived comfort.

However, this coupling requires optimal cooperation of the electrical and thermal system components, which are sensitive to internal and external influences (e.g., usage, geographic and topological situation), technical design (e.g. old, refurbished, new), economic constraints and ecological priorities (e.g. local or global aspects).

In this thesis, the sensitivities of various parameters on a hybrid energy system are investigated, such as:

- **Environmental impacts**, e.g., geographical location, fluctuations of the weather
- **Grid-side impacts**, e.g., existing energy supply concept, flexible purchase and selling prices for thermal and electrical energy, and electrical power
- **Economic influences**, e.g., local and global influences on electricity, gas and oil prices as well as their availability
- **Consumer behaviour**, e.g., desired energy services, load profile, power and energy management possibilities
- **Funding**, e.g., influence and decision criteria for future investments, optimal investment time
- **Efficiency of system components**, e.g., LV and MV network connection, photovoltaic system (PV), electricity, heat and cold systems, control systems, control/regulation and optimisation

### 2.1.1 Prosumer – Overview

Traditionally, single-family houses were consumers with a predictable load profile, periodically repeated over days and weeks. These loads' behaviour has been changing in recent years due to the fall in price and development of renewable generation and storage systems, the more accessible use of Information and Communication Technologies (ICT), the changing environmental awareness of people, and the push for more autonomy. The

- increasing share of decentralised energy generation and storage systems,
- the integration of electric vehicles,
- and the coupling of electrical and thermal systems

leads to significant changes in the planning and operation of distribution networks and systems such as single-family houses, businesses, and industry. Previously pure consumers are now turning into producers and are changing into so-called prosumers (*producers + consumers*). With the help of ICT methods and optimisation algorithms, prosumers can react to market-dependent dynamic or consumer and prosumer-oriented tariffs in order to achieve a previously defined optimum.

The following Figure 2.2 gives an overview of a prosumer by the example of a single-family house and shows commonly used technologies for energy supply and storage. Figure 2.2 shows the technologies considered in the developed simulation model (see

Section 2.2) and represent not a recommendation for simultaneous implementation of all these technologies in a single-family house.

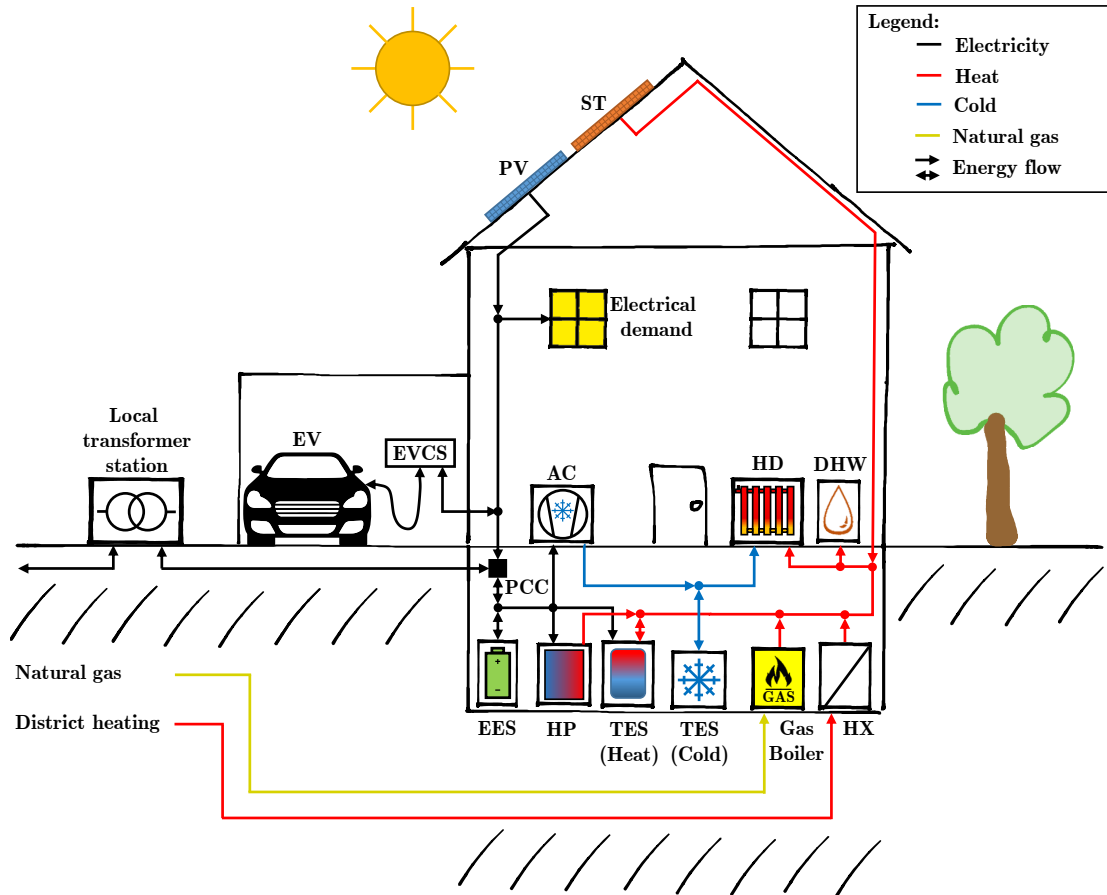


Figure 2.2: Schematic illustration of the modelled hybrid energy system – Prosumer

Based on the developed simulation model, the optimal use of decentralised energy generation and storage systems for prosumers is determined. Several decentralised energy generation and storage systems, as shown in Figure 2.2, cover the energy demand of the hybrid energy system. The key components for coupling the thermal and electrical energy systems to a hybrid energy system are

- the heat pump (HP),
- the air conditioning system (AC)
- and the heating cartridges of the thermal energy storage.

Furthermore, the thermal energy demand of the hybrid energy system depends mainly on the environmental conditions (weather), as well as on the construction of the building.

## 2.2 Simulation Model – ProsOpt

The simulation model ProsOpt, developed with the software MATLAB, analyses the behaviour of optimising prosumers. In ProsOpt the thermal and electrical systems of the prosumer are intelligently coupled to a hybrid energy system. The simulation model performs steady-state energy flow calculations. An energy management model determines the optimal use of the distributed energy generation and storage systems. A linear optimisation algorithm (MILP – Mixed Integer Linear Programming) takes the desired energy services, external boundary conditions (e.g., weather) and cost functions of the individual components into account to find an optimal solution.

ProsOpt is structured into four interdependent main parts – Inputs, Settings, Calculations and Optimisation –, which get executed in this order. The following Figure 2.3 gives an overview of the simulation model ProsOpt.

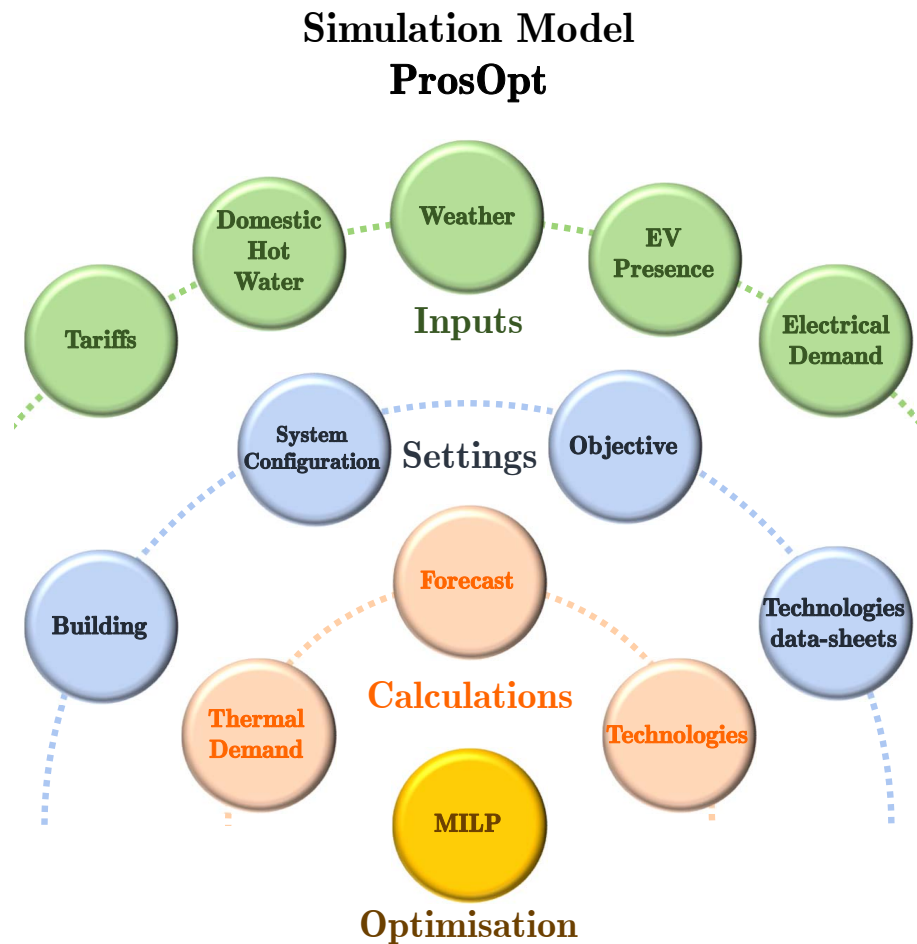


Figure 2.3: Overview of the simulation model ProsOpt

ProsOpt, designed as a Matlab function, aims to simulate the steady-state energy flow of optimising prosumer in single-family houses. As a Matlab function, the simulation model provides a standalone application for a detailed analysis of prosumers and can operate as a subroutine in load flow calculations.

The input data must contain a time and data vector, where the time vector must coincide for all input data. To ensure a uniform time resolution of the input data, the input data's smallest time resolution, e.g., hourly, is used. Data with a higher time resolution is adapted accordingly. Since long-term forecasts of weather and demand have a high degree of uncertainty, the optimisation algorithm should take a short forecast time of, e.g. the upcoming three days (72 hours) into account.

By optimising the use of distributed generation systems and energy storages, the prosumer can respond to dynamic tariffs, if defined as the optimisation objective, to obtain an economically optimal advantage. A sufficiently large number of optimising consumers and prosumers have an impact on the load flow conditions in low and medium voltage networks. In addition to economic objectives, further optimisation objectives can be considered, for example:

**Technical objectives:**

- Increase of the degree of autonomy / degree of self-consumption of the prosumer

**Ecological objectives:**

- CO<sub>2</sub>-equivalents of system components and of the overall system

The application of ProsOpt for optimising hybrid energy systems of prosumers is explained in more detail in Section 3 for selected scenarios.

## Applications

The following list outlines possible applications for the developed simulation model ProsOpt according to the energy-based analysis of prosumers.

- Optimisation of the prosumers operation considering various objectives, such as increasing the degree of self-consumption or achieving an economically or ecologically optimal advantage.
- Dimensioning and optimal operation of generation and storage systems.
- Coupling a prosumer's thermal and electrical energy system.
- Analysis of various energy tariffs' influence on the operation of prosumers.
- Integration of electric vehicles including Vehicle2Grid / Grid2Vehicle.
- Determination of the behaviour of optimising prosumers in low-voltage distribution networks taking into account voltage and reactive power control.
- Investigation of specific building construction designs on the energy demand.

## Transferability

The design of the methodology of the developed simulation model is transferable to other hybrid energy systems, e.g., industrial companies. The methodology of ProsOpt was also implemented in the project "REsys - Regelungsstrategien zur Effizienzsteigerung komplexer hybrider Energiesysteme" funded by the Austrian "Klima- und Energiefonds" as a part of the "Energieforschungsprogramm 2015". In

this project, models, simulations and analyses of an industrial company were built on measured and statistical data. By the use of ICT-methods and expert's knowledge, smart control strategies are developed and subsequently tested in simulations and on a real industrial hybrid energy system.

However, detailed analyses of the hybrid energy system to be modelled are necessary. At least the following data and documents must be available:

- System layouts such as circuit diagrams, e.g., system manuals of the PV system
- Hydraulic system layouts
- Data-sheets of the main system components, e.g., PV, transformers
- Control settings of the system and relevant operational data
- Weather data
- Building structure and system diagram

## 2.2.1 Optimisation of Hybrid Energy Systems

The simulation model ProsOpt is used to couple the thermal and electrical subsystems of a prosumer, shown in Figure 2.2, together to a hybrid energy system. With ProsOpt, the optimal use of the decentralised energy generation and storage systems can be determined based on scenarios using mixed-integer linear programming (MILP), depending on various objective functions. By optimising the use of distributed generation systems (e.g., photovoltaics, solar thermal energy) and energy storages the consumer or prosumer can respond to dynamic tariffs and obtain, e.g. an economically optimal advantage.

The method of linear programming represent procedures for the mathematical solution of a specific class of linear extreme value problems with constraints. In the mathematical context, an optimisation determines the maximum or the minimum of a function  $F(\mathbf{x})$ . This function  $F(\mathbf{x})$  is defined here on a (restricted) state space. The decisions to be made by the optimisation algorithm, e.g., choosing the shortest possible way, are represented by variables  $\mathbf{x}$  (degrees of freedom). To determine an optimal solution of the optimisation problem, exact methods such as decision tree (Branch&Bound and Branch&Cut algorithms) and cutting-plane methods can be applied [1]. Mixed-integer problems can be described in the form<sup>1</sup>

$$\min_{\mathbf{x}} \mathbf{c}^T \cdot \mathbf{x} \text{ subject to } \begin{cases} \mathbf{x} \\ \mathbf{A}_{\text{neq}} \cdot \mathbf{x} \leq \mathbf{b}_{\text{neq}} \\ \mathbf{A}_{\text{eq}} \cdot \mathbf{x} = \mathbf{b}_{\text{eq}} \\ \mathbf{l}_b \leq \mathbf{x} \leq \mathbf{u}_b \end{cases} \quad (2.1)$$

$\mathbf{x}$	Variables (unknowns)
$\mathbf{A}_{\text{neq}}, \mathbf{A}_{\text{eq}}$	In- and equality system matrix
$\mathbf{b}_{\text{neq}}, \mathbf{b}_{\text{eq}}$	In- and equality constants (knowns)
$\mathbf{l}_b, \mathbf{u}_b$	Lower and upper boundary of unknown variables
$\mathbf{c}^T$	Objective function

<sup>1</sup> Definition: Bold lowercase correspond to a column vector; bold uppercase correspond to a matrix

with the variables  $\mathbf{x} = [\mathbf{x}_r, \mathbf{x}_h]^\top \in \mathbb{R}^{r+h}$  as integers  $\mathbf{x}_r = [x_1, x_2 \dots x_r]^\top \in \mathbb{Z}^r$  and as real numbers  $\mathbf{x}_h = [x_1, x_2 \dots x_h]^\top \in \mathbb{R}^h$ . Binary variables are integers that can take only the values 0 and 1. The system of linear equations consists of  $m$  equations and  $n = r + h$  unknowns, with which the equality system matrix  $\mathbf{A}_{\text{eq}}$  can be defined with  $\mathbf{A}_{\text{eq}} \in \mathbb{R}^{m \times n}$ . The same applies to the system of linear inequations. The linear system of inequations can be specified with  $\mathbf{A}_{\text{neq}} \in \mathbb{R}^{k \times n}$  for  $k$  inequalities and  $n$  unknowns [2].

The mathematical optimisation supports the solving of practical problems, e.g., in the fields of logistics, transport, finance, communication and design. In the following, MILP is used to solve specific problems of hybrid energy systems, such as storage management or the most efficient use of the available systems. A advantage of MILP is that variables could also be integers or binary, e.g., on-off decisions of systems. In MILP, mathematical modelling and profound knowledge of the entire system in order to properly set up the variables and the mathematical formulation of their relationship to each other is of crucial relevance [1].

The following five essential parts mathematically describe the entire hybrid energy system:

- system configuration
- objective function
- weather and demand as a function of time
- modelling of system components
- optimisation algorithm

The linear equality constraints ( $\mathbf{A}_{\text{eq}} \cdot \mathbf{x} = \mathbf{b}_{\text{eq}}$ ) form a system of linear equations described by the equality system matrix  $\mathbf{A}_{\text{eq}}$ , several unknowns  $\mathbf{x}$  (energy flow) and known coefficients  $\mathbf{b}_{\text{eq}}$  (demand, ...). In special cases, like the thermal energy storage, modelled with two different temperature zones, see Section 2.6.8, linear inequality constraints ( $\mathbf{A}_{\text{neq}} \cdot \mathbf{x} \leq \mathbf{b}_{\text{neq}}$ ) must be used.

The optimisation algorithm, under the specification of an objective function  $\mathbf{c}^\top \cdot \mathbf{x}$  (e.g., minimising cost or increase the degree of autonomy), solves the optimisation problem. The system matrix  $\mathbf{A}_{\text{eq}}$ , together with defined boundaries ( $\mathbf{l}_b, \mathbf{u}_b$ ), represents the physical connections of all technical systems as well as the possible directions of the energy flow. The simulation model uses the energy flows – integral of power at a fixed time resolution – instead of power flows, since the states of charge of the storages require the physical quantity “energy” and choosing a uniform quantity for all variables avoids possible mix-ups.

To account long-term effects, the optimisation is performed in a temporal time resolution of 15 minutes over the time span of one year. Since long-term forecasts of weather and demand, especially the electricity demand, have a high degree of uncertainty, the optimisation algorithm always takes into account the upcoming three days (72 hours) in advance.

Figure 2.4 gives an overview of the hybrid energy system based on the prosumer shown in Figure 2.2, with links to the detailed description of the relevant system component in this thesis. The hybrid energy system is characterised by the energy

flows, represented by arrows, the system components, and the energy sources and sinks.

## System Overview - Optimisation

<b>Legend:</b>	PCC ... Point of Common Coupling	TES ... Thermal Energy Storage
	V2G/G2V ... Vehicle to Grid / Grid to Vehicle	$x$ ... Energy in kWh
	EES ... Electrical Energy Storage	HT/LT/CT ... High, low and cold temperature

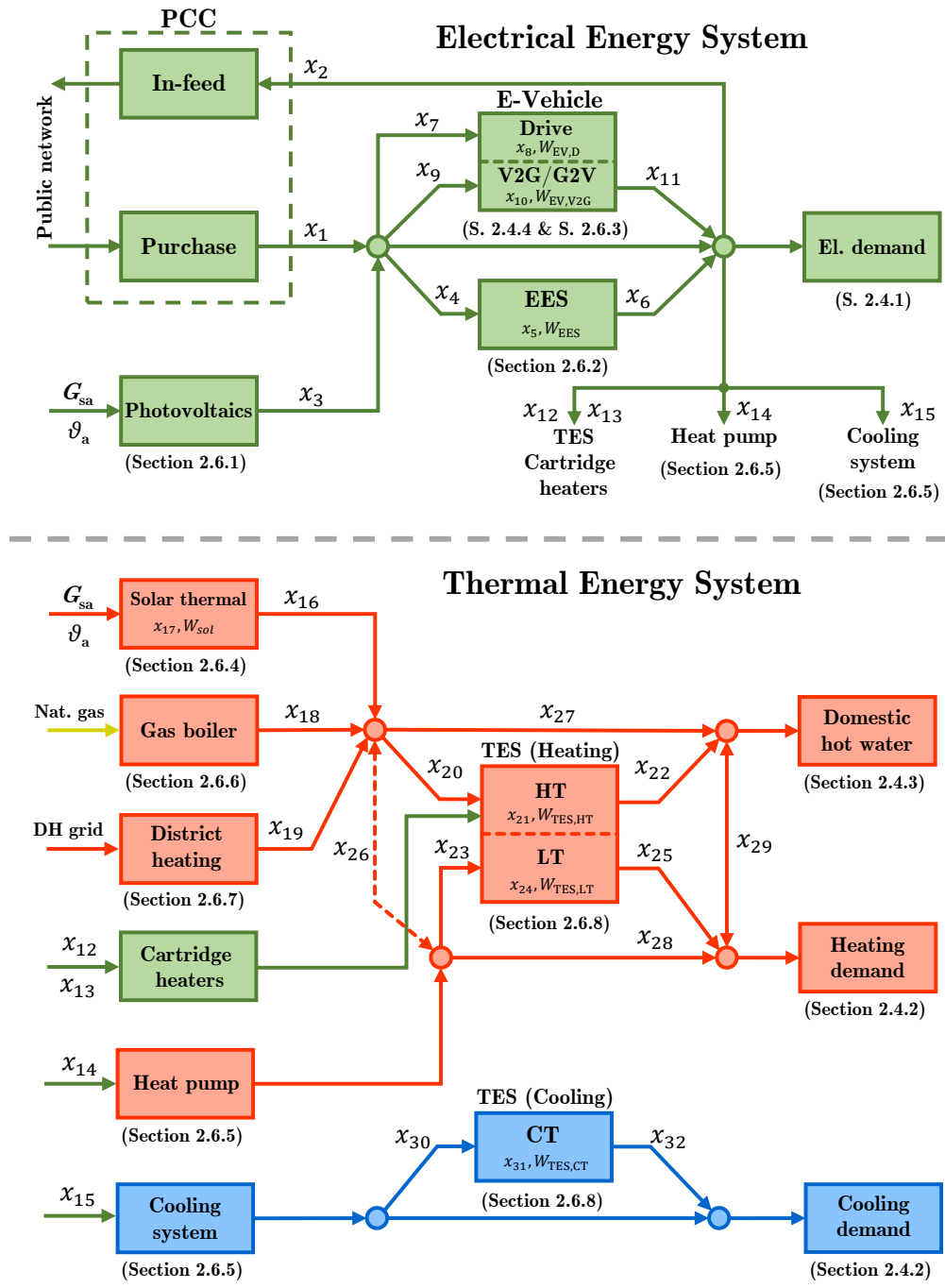


Figure 2.4: Overview hybrid energy system - optimisation

## Objectives

The objective function can be based on economic (most economical use of system components), technical (optimal use of decentralised energy sources, optimal autonomy), given scenarios (e.g., gas heating disabled), and ecological criteria (CO<sub>2</sub> equivalence).

## Constraints and Boundaries

The system shown in Figure 2.4 is mathematically described as follows. The elements of the system matrix  $\mathbf{A}_{\text{eq}}$  contain the efficiencies, conversion factors and losses for each technology and system component. The known variables  $\mathbf{b}_{\text{eq}}$  consider the demand, as well as initially the state of charge of the storage systems. In the following, the linear equality ( $\mathbf{A}_{\text{eq}} \cdot \mathbf{x} = \mathbf{b}_{\text{eq}}$ ) and inequality ( $\mathbf{A}_{\text{neq}} \cdot \mathbf{x} \leq \mathbf{b}_{\text{neq}}$ ) constraints are described in their general form.

$$\underbrace{\begin{pmatrix} a_{\text{eq},11} & a_{\text{eq},12} & \cdots & a_{\text{eq},1n} \\ a_{\text{eq},21} & a_{\text{eq},22} & \cdots & a_{\text{eq},2n} \\ \vdots & \vdots & & \vdots \\ a_{\text{eq},m1} & a_{\text{eq},m2} & \cdots & a_{\text{eq},mn} \end{pmatrix}}_{\mathbf{A}_{\text{eq}}} \cdot \underbrace{\begin{pmatrix} x_1 \\ x_2 \\ \vdots \\ x_n \end{pmatrix}}_{\mathbf{x}} = \underbrace{\begin{pmatrix} b_{\text{eq},1} \\ b_{\text{eq},2} \\ \vdots \\ b_{\text{eq},m} \end{pmatrix}}_{\mathbf{b}_{\text{eq}}} \quad (2.2)$$

$$\underbrace{\begin{pmatrix} a_{\text{neq},11} & a_{\text{neq},12} & \cdots & a_{\text{neq},1n} \\ a_{\text{neq},21} & a_{\text{neq},22} & \cdots & a_{\text{neq},2n} \\ \vdots & \vdots & & \vdots \\ a_{\text{neq},k1} & a_{\text{neq},k2} & \cdots & a_{\text{neq},kn} \end{pmatrix}}_{\mathbf{A}_{\text{neq}}} \cdot \underbrace{\begin{pmatrix} x_1 \\ x_2 \\ \vdots \\ x_n \end{pmatrix}}_{\mathbf{x}} \leq \underbrace{\begin{pmatrix} b_{\text{neq},1} \\ b_{\text{neq},2} \\ \vdots \\ b_{\text{neq},k} \end{pmatrix}}_{\mathbf{b}_{\text{neq}}} \quad (2.3)$$

The variables  $\mathbf{x}$  are limited by boundaries ( $\mathbf{l}_b \leq \mathbf{x} \leq \mathbf{u}_b$ ), resulting in the maximum transferred power or the maximum capacity of the respective storages.

The system, shown in Figure 2.4, consists of  $n = 32$  variables,  $m = 13$  equations and  $k = 2$  inequalities. The equations and inequalities of (2.2) and (2.3) are only valid for a single point in time. In order to achieve optimal storage management, it is essential to consider the next hours using a forecast of the demand and the weather. Based on (2.2) and (2.3) the size of the vectors and matrices of the constraints changes according to the considered next hours of the forecast with the total number of time steps  $T$ , e.g., a forecast of 72 hours with a temporal time resolution of 15 minutes corresponds to a total number of time steps  $T = 288$ . Thus the constraints increase to  $\mathbf{A}_{\text{eq}}^{(m \times n) \cdot T} \cdot \mathbf{x}^{n \cdot T} = \mathbf{b}_{\text{eq}}^{m \cdot T}$  and  $\mathbf{A}_{\text{neq}}^{(k \times n) \cdot T} \cdot \mathbf{x}^{n \cdot T} = \mathbf{b}_{\text{neq}}^{k \cdot T}$ .

In the beginning of the optimisation at the time index  $i = 1$ , with  $i \in \{1, 2, \dots, T\}$ , the storage levels must be initialised. The resulting storage level from step  $i$  corresponds to the initial storage level of the next step ( $i + 1$ ). Using the example of the electrical energy storage (EES), the following relationship is obtained, whereby the specific

matrix elements such as charging and discharging efficiencies are neglected for easier understanding.

$$\begin{aligned}
 i = 1 : & \quad -x_4 + x_5 + x_6 = W_{\text{EES}} \\
 i = 2 : & \quad -x_5^{(1)} - x_4^{(2)} + x_5^{(2)} + x_6^{(2)} = 0 \\
 & \quad \quad \quad \vdots \\
 i = T : & \quad -x_5^{(T-1)} - x_4^{(T)} + x_5^{(T)} + x_6^{(T)} = 0
 \end{aligned} \tag{2.4}$$

As shown in Figure 2.4, the variables  $\mathbf{x}$  correspond to the hybrid energy system's energy flow. Taking the electrical energy storage system (EES) as an example, the variables  $x_4^{(i)}$  represent the charging energy,  $x_5^{(i)}$  the state of charge and  $x_6^{(i)}$  the storage's discharge energy. In the first time step ( $i = 1$ ), the state of charge of the storage  $W_{\text{EES}}$  is initialised. The EES system's operation results in a new state of charge  $x_5^{(1)}$ , which is used as an initial value for the next time step ( $i = 2$ ). In this way, the EES systems state of charge is transferred to the next time step until the last time step  $T$  is reached. Due to this forwarding of the respective state of charge of the storage system  $x_5^{(i-1)}$ , the optimisation algorithm MILP makes an optimal operation of the EES possible.

The elements of the system matrices and the boundaries of the variables are explained in more detail below. A detailed description of the technologies and demand can be found in the respective sections 2.4 and 2.6.

### Photovoltaic System (Section 2.6.1)

The model to calculate a photovoltaic system (PV) uses weather data (solar irradiance, ambient temperature), technical characteristics of the PV modules and inverters (data sheets), azimuthal orientations and inclinations of the PV modules to determine the expected energy output of the PV system. Exact knowledge of the weather data is assumed - in practice: forecast data would be taken. The electrical energy generation is considered in the optimisation algorithm as follows.

$$\begin{aligned}
 \dots + x_3^{(i)} + \dots &= 0 \quad i \in \{1, 2, \dots, T\} \\
 l_{b,3}^{(i)} &\leq x_3^{(i)} \leq u_{b,3}^{(i)}
 \end{aligned}$$

with (2.5)

$$\begin{aligned}
 l_{b,3}^{(i)} &= 0 \\
 u_{b,3}^{(i)} &= P_{\text{PV,AC}}(G_{\text{sa}}(t), \vartheta_a(t)) \cdot \Delta t
 \end{aligned}$$

$\Delta t$	Time resolution in h
$\vartheta_a$	Ambient air temperature in °C
$G_{\text{sa}}$	Solar irradiance in W/m <sup>2</sup>
$i$	Time index
$l_b, u_b$	Lower and upper boundary of variable $x$ in kWh
$P_{\text{PV,AC}}$	AC power output of the PV system in kW according to Equation (2.26)
$t$	Time
$x_3$	Output Energy of the PV system for the time span $\Delta t$ in kWh

### Electrical Energy Storage (Section 2.6.2)

The purpose of an electrical energy storage (EES) system is to store energy in order to provide a demand-oriented supply [3]. In ProsOpt, the electrical energy storage considers the capacity, the maximum charging and discharging power as well as the losses resulting from the operation of the storage via the round-trip efficiency and the self-discharge rate.

$$\begin{aligned}
 i = 1 : & -x_4 \frac{\eta_{\text{EES,ch}}}{(1 - \eta_{\text{EES,self}})} + x_5 \frac{1}{(1 - \eta_{\text{EES,self}})} + x_6 \frac{1}{\eta_{\text{EES,disch}}(1 - \eta_{\text{EES,self}})} = W_{\text{EES}} \\
 & \vdots \\
 i \geq 2 : & -x_5^{(i-1)} - x_4^{(i)} \frac{\eta_{\text{EES,ch}}}{(1 - \eta_{\text{EES,self}})} \dots \\
 & + x_5^{(i)} \frac{1}{(1 - \eta_{\text{EES,self}})} + x_6^{(i)} \frac{1}{\eta_{\text{EES,disch}}(1 - \eta_{\text{EES,self}})} = 0 \\
 & l_{b,j}^{(i)} \leq x_j^{(i)} \leq u_{b,j}^{(i)}
 \end{aligned} \tag{2.6}$$

with

$$\begin{aligned}
 j & \in \{4, \dots, 6\} \\
 i & \in \{1, 2, \dots, T\} \\
 l_{b,4}^{(i)} & = 0 \quad u_{b,4+(i-n)} = P_{\text{EES,ch}} \cdot \Delta t \\
 l_{b,5}^{(i)} & = 0 \quad u_{b,5+(i-n)} = W_{\text{EES,cap}} \cdot \text{DoD} \\
 l_{b,6}^{(i)} & = 0 \quad u_{b,6+(i-n)} = P_{\text{EES,disch}} \cdot \Delta t
 \end{aligned}$$

$\Delta t$	Time resolution in h
$\eta_{\text{EES,ch}}, \eta_{\text{EES,disch}}$	Charging/discharging efficiency in pu
$\eta_{\text{EES,self}}$	Self-discharge rate in pu
DoD	Depth of Discharge in pu
$i$	Time index
$l_b, u_b$	Lower and upper boundary of variables $x$ in kWh
$P_{\text{EES,ch}}, P_{\text{EES,disch}}$	Maximum charging/discharging power in kW
$W_{\text{EES,cap}}$	Maximum capacity of EES in kWh
$x_4$	Charging energy of the EES in kWh
$x_5$	State of charge of the EES in kWh
$x_6$	Discharging energy of the EES in kWh

### Electric Vehicle (Section 2.6.3)

The integration of electric vehicles (EVs) increases the electricity demand of households. ProsOpt implements the EV in two different ways. On the one hand, as an electrical load and on the other hand as an electrical energy storage with time-related home presence and absence. As shown in the Figure 2.28, the capacity of the EV can be split. One part (drive) is used to use the car in an ordinary way. Which means, the vehicle is optimally charged during its home presence. On arrival, based on an average mileage of the vehicle, the remaining capacity is determined by a stochastic number. The reserved Vehicle2Grid/Grid2Vehicle (V2G/G2V) part is used as an electrical energy storage for optimised operation of the hybrid energy system.

Storage capacity of the EV for driving (D):

$$\begin{aligned}
 i = 1 : & -x_7 \frac{\eta_{EV,ch}}{(1 - \eta_{EV,self})} + x_8 \frac{1}{(1 - \eta_{EV,self})} = W_{D,init} \\
 & \vdots \\
 i \geq 2 : & -x_8^{(i)} - x_7^{(i)} \frac{\eta_{EV,ch}}{(1 - \eta_{EV,self})} + x_8^{(i)} \frac{1}{(1 - \eta_{EV,self})} = 0 \\
 & l_{b,j}^{(i)} \leq x_j^{(i)} \leq u_{b,j}^{(i)}
 \end{aligned} \tag{2.7}$$

with

$$\begin{aligned}
 j & \in \{7, 8\} \\
 i & \in \{1, 2, \dots, T\} \\
 l_{b,7}^{(i)} & = 0 \quad u_{b,7}^{(i)} = P_{EV,ch} \cdot \Delta t \\
 l_{b,8}^{(i)} & = 0 \quad u_{b,8}^{(i)} = W_{EV} \cdot DoD \cdot (1 - k)
 \end{aligned}$$

$\Delta t$	Time resolution in h
$\eta_{EV,ch}$	Charging efficiency in pu
$\eta_{EV,self}$	Self-discharge rate in pu
DoD	Depth of Discharge in pu
$i$	Time index
$k$	Percentage share of the storage capacity $W_{EV}$ for V2G/G2V
$l_b, u_b$	Lower and upper boundary of variables $x$ in kWh
$P_{EV,ch}$	Maximum charging power in kW
$W_{D,init}$	Storage Capacity (Drive) in kWh (Initialisation)
$W_{EV}$	Overall storage capacity of the vehicle in kWh
$x_7$	Charging energy of the EV reserved for driving in kWh
$x_8$	State of charge of the EV reserved for driving in kWh

Storage capacity of the EV for providing V2G/G2V:

$$\begin{aligned}
 i = 1 : & -x_9 \frac{\eta_{EV,ch}}{(1 - \eta_{EV,self})} + x_{10} \frac{1}{(1 - \eta_{EV,self})} + x_{11} \frac{1}{\eta_{EV,disch}(1 - \eta_{EV,self})} = W_{V2G,init} \\
 & \vdots \\
 i \geq 2 : & -x_{10}^{(i-1)} - x_9^{(i)} \frac{\eta_{EV,ch}}{(1 - \eta_{EV,self})} \dots \\
 & + x_{10}^{(i)} \frac{1}{(1 - \eta_{EV,self})} + x_{11}^{(i)} \frac{1}{\eta_{EES,disch}(1 - \eta_{EES,self})} = 0 \\
 & l_{b,j}^{(i)} \leq x_j^{(i)} \leq u_{b,j}^{(i)}
 \end{aligned} \tag{2.8}$$

with

$$\begin{aligned}
 j & \in \{9, 10, 11\} \\
 i & \in \{1, 2, \dots, T\} \\
 l_{b,9}^{(i)} & = 0 \quad u_{b,9}^{(i)} = P_{EV,ch} \cdot \Delta t \\
 l_{b,10}^{(i)} & = 0 \quad u_{b,10}^{(i)} = W_{EV} \cdot DoD \cdot k \\
 l_{b,11}^{(i)} & = 0 \quad u_{b,11}^{(i)} = P_{EV,disch} \cdot \Delta t
 \end{aligned}$$

$\Delta t$	Time resolution in h
$\eta_{EV,ch}, \eta_{EV,disch}$	Charging/discharging efficiency in pu
$\eta_{EV,self}$	Self-discharge rate in pu
DoD	Depth of Discharge in pu
$i$	Time index
$k$	Percentage share of the storage capacity for V2G/G2V
$l_b, u_b$	Lower and upper boundary of variables $x$ in kWh
$P_{EV,ch}, P_{EV,disch}$	Maximum charging/discharging power in kW
$W_{EV}$	Overall storage capacity of the Vehicle in kWh
$W_{V2G,init}$	Storage Capacity for V2G/G2V in kWh (initialisation)
$x_9$	Charging energy for the storage capacity of the EV (V2G/G2V) in kWh
$x_{10}$	State of charge of the EV (V2G/G2V) in kWh
$x_{11}$	Discharging energy of the EV (V2G/G2V) in kWh

The variables  $x_7^{(i)}$  and  $x_9^{(i)}$  in sum cannot exceed the charging power (inequality).

$$x_7^{(i)} + x_9^{(i)} \leq P_{EV,ch} \cdot \Delta t \text{ with } i \in \{1, 2, \dots, T\} \quad (2.9)$$

$\Delta t$	Time resolution in h
$i$	Time index
$P_{EV,ch}$	Maximum charging/discharging power in kW
$x_7$	Charging energy of the EV reserved for driving in kWh
$x_9$	Charging energy of the EV reserved for V2G/G2V in kWh

### Solar Thermal System (Section 2.6.4)

In solar thermal systems, solar thermal collectors convert the solar irradiance into heat. The efficiency of a solar collector results from the absorbed solar irradiance reduced by thermal losses. For a detailed mathematical description of the solar thermal system see Section 2.6.4.

$$\begin{aligned}
 i = 1 : x_{16} \cdot (1 - l_{\text{pipe}}) + x_{17} &= W_{\text{sol,init}} \cdot (1 - l_{\text{sol}}) + \eta_0(\theta(t)) \cdot \frac{G_c(t) \cdot A_{\text{sol}}}{1000} \cdot \Delta t + \\
 &\frac{a_{\text{sol}} \cdot A_{\text{sol}}}{1000} \cdot (\vartheta_a(t) - \vartheta_{\text{ref}}) \cdot \Delta t \\
 &\vdots \\
 i \geq 2 : -x_{17}^{(i-1)} \cdot (1 - l_{\text{sol}}) + x_{16}^{(i)} \cdot (1 - l_{\text{pipe}}) + x_{17}^{(i)} &= \\
 &\frac{G_c(t) \cdot A_{\text{sol}}}{1000} \cdot \Delta t + \frac{a_{\text{sol}} \cdot A_{\text{sol}}}{1000} \cdot (\vartheta_a(t) - \vartheta_{\text{ref}}) \cdot \Delta t
 \end{aligned} \quad (2.10)$$

$$l_{b,j}^{(i)} \leq x_j^{(i)} \leq u_{b,j}^{(i)}$$

with

$$j \in \{16, 17\}$$

$$i \in \{1, 2, \dots, T\}$$

$$l_{\text{pipe}} = \frac{k_p \cdot L_p}{W_{p,\text{max}}} \cdot (\vartheta_{\text{out}}(t) - \vartheta_{\text{in}}(t)) \cdot \Delta t \quad l_{\text{sol}} = \frac{a_{\text{sol}} \cdot A_{\text{sol}}}{V_{\text{sol}} \cdot \rho_w \cdot c_w \cdot \frac{1}{3600 \frac{\text{s}}{\text{h}}}} \cdot \Delta t$$

$$l_{b,16}^{(i)} = 0$$

$$u_{b,16}^{(i)} = W_{p,\text{max}}$$

$$l_{b,17}^{(i)} = W_{\text{sol}}(\vartheta_a(t))$$

$$u_{b,17}^{(i)} = W_{\text{sol}}(\vartheta_{\text{sol,max}})$$

$\Delta t$	Time resolution in h
$\eta_0$	Theoretical collector efficiency in pu
$\theta$	Incidence angle to the collector surface in $^\circ$
$\vartheta_a$	Ambient temperature in $^\circ\text{C}$
$\vartheta_{in}$	Indoor room temperature of the building $^\circ\text{C}$
$\vartheta_{out}$	Outlet temperature of the water from the solar thermal system in $^\circ\text{C}$
$\vartheta_{ref}$	Reference temperature for energy calculation in $^\circ\text{C}$
$\vartheta_{sol,max}$	Maximum allowed temperature of the solar thermal system in $^\circ\text{C}$
$\rho_w$	Density of water in $\text{kg}/\text{m}^3$ ( $\rho_w = 1000 \text{ kg}/\text{m}^3$ )
$A_{sol}$	Surface area of solar thermal collectors in $\text{m}^2$
$a_{sol}$	Loss coefficient in $\frac{\text{W}}{\text{m}^2\text{K}}$
$c_w$	Specific heat capacity of water in $\text{J}/(\text{kg} \cdot \text{K})$ ( $c_w = 4.1813 \text{ J}/(\text{kg} \cdot \text{K})$ )
$G_c$	Irradiance on solar collector in $\frac{\text{W}}{\text{m}^2}$
$i$	Time index
$k_p$	Thermal conductivity of the pipes in $\text{W}/(\text{m} \cdot \text{K})$
$l_b, u_b$	Lower and upper boundary of variables $x$ in kWh
$L_p$	Length of the pipe system of the house in m
$l_{pipe}$	Loss coefficient for transferring energy via the pipe system of the house in pu
$l_{sol}$	Overall loss coefficient of solar thermal system in pu
$t$	Time
$V_{sol}$	Volume of solar thermal system in $\text{m}^3$
$W_{p,max}$	Maximum transferable energy over the pipe system in kWh
$W_{sol,init}$	Stored energy in solar thermal system in kWh (Initialisation)
$x_{16}$	Output Energy of the solar thermal system for the time span $\Delta t$ in kWh
$x_{17}$	Stored Energy of the solar thermal system for the time span $\Delta t$ in kWh

## Heat Pumps and Air Conditioners (Section 2.6.5)

To simulate compression heat pumps and air conditioners, a catalogue data lookup approach is used. This approach is well suited to simulate heat pumps and air conditioners using the manufacturer's specifications in combination with mathematical fit functions. The mathematical fit functions determined for the electric power consumption  $P$  and the thermal power output  $\dot{Q}$  can be used to calculate the COP (Coefficient of Performance) or, in the case of air conditioners, the EER (Energy Efficiency Ratio). In the case of heat pumps, air-source heat pumps – ambient air temperature  $\vartheta_a$  source – and ground-source heat pumps – soil temperature  $\vartheta_{soil}$  source – can be simulated. The air conditioning system uses the indoor temperature of the conditioned building areas as a source for calculating the performance ratio  $EER$ .

$$\begin{aligned} \dots + x_{14}^{(i)} \cdot \text{COP}(\vartheta_{flow}, \vartheta_{source}(t)) \cdot (1 - l_{pipe}) + \dots &= 0 & i \in \{1, 2, \dots, T\} \\ \dots + x_{15}^{(i)} \cdot \text{EER}(\vartheta_{flow}, \vartheta_{source}(t)) \cdot (1 - l_{pipe}) + \dots &= W_c \end{aligned}$$

$$l_{b,j}^{(i)} \leq x_j^{(i)} \leq u_{b,j}^{(i)}$$

with

$$j \in \{14, 15\}$$

$$l_{pipe} = \frac{k_p \cdot L_p}{W_{p,max}} \cdot (\vartheta_{flow}(t) - \vartheta_{in}(t)) \cdot \Delta t$$

$$l_{b,14}^{(i)} = 0 \quad u_{b,14}^{(i)} = P_{HP,max} \cdot \Delta t$$

$$l_{b,15}^{(i)} = 0 \quad u_{b,15}^{(i)} = P_{AC,max} \cdot \Delta t$$

(2.11)

$\Delta t$	Time resolution in h
$\vartheta_{\text{flow}}$	Flow temperature of the heating system in °C
$\vartheta_{\text{in}}$	Indoor room temperature of the building °C
$\vartheta_{\text{source}}$	Source temperature for HP or AC in °C
$i$	Time index
$k_{\text{p}}$	Thermal conductivity of the pipes in W/mK
$l_{\text{b}}, u_{\text{b}}$	Lower and upper boundary of variables $x$ in kWh
$L_{\text{p}}$	Length of the pipe system of the house in m
$l_{\text{pipe}}$	Loss coefficient for transferring energy via the pipe system of the house in pu
$P_{\text{HP,max}}, P_{\text{AC,max}}$	Maximum power of the heat pump or the air conditioning system in kW
$t$	Time
$W_{\text{c}}$	Cooling demand in kWh
$W_{\text{p,max}}$	Maximum transferable energy over the pipe system in kWh
$x_{14}$	Thermal output energy of heat pump in kWh
$x_{15}$	Thermal output energy of air conditioner in kWh

### Domestic Gas Boiler (Section 2.6.6)

Conventional heating systems like domestic gas boiler are heating systems that use the chemically bound energy in fossil fuels to heat water. In a gas boiler, natural gas is burned in a combustion chamber, and water is heated by means of the released heat energy via a heat exchanger to cover the heat demand of a household. The domestic gas boiler is taken into account by its efficiency and the maximum heating power. In ProsOpt, the efficiency must be related to the GHV (gross heating value) to calculate condensing gas boiler.

$$\dots + x_{18}^{(i)} \cdot \eta_{\text{gas}} \cdot (1 - l_{\text{pipe}}) + \dots = 0 \quad i \in \{1, 2, \dots, T\}$$

$$l_{\text{b},18}^{(i)} \leq x_{18}^{(i)} \leq u_{\text{b},18}^{(i)}$$

with

(2.12)

$$l_{\text{pipe}} = \frac{k_{\text{p}} \cdot L_{\text{p}}}{W_{\text{p,max}}} \cdot (\vartheta_{\text{flow}}(t) - \vartheta_{\text{in}}(t)) \cdot \Delta t$$

$$l_{\text{b},18}^{(i)} = 0 \quad u_{\text{b},18}^{(i)} = P_{\text{gas,max}} \cdot \Delta t$$

$\Delta t$	Time resolution in h
$\eta_{\text{gas}}$	Efficiency of the domestic gas boiler in pu
$\vartheta_{\text{flow}}$	Flow temperature of the heating system in °C
$\vartheta_{\text{in}}$	Indoor room temperature of the building °C
$i$	Time index
$k_{\text{p}}$	Thermal conductivity of the pipes in W/mK
$l_{\text{b}}, u_{\text{b}}$	Lower and upper boundary of variables $x$ in kWh
$L_{\text{p}}$	Length of the pipe system of the house in m
$l_{\text{pipe}}$	Loss coefficient for transferring energy via the pipe system of the house in pu
$P_{\text{gas,max}}$	Maximum thermal power output of the domestic gas boiler in kW
$t$	Time
$W_{\text{p,max}}$	Maximum transferable energy over the pipe system in kWh
$x_{18}$	Thermal output energy of the gas boiler in kWh

## District Heating (Section 2.6.7)

District heating (DH) is a type of heating system from which customers can obtain thermal energy via a heat distribution network. As a system boundary, the energy transfer station is used as an interface (heat exchanger) between the DH distribution system and the building heating system. ProsOpt takes the heat exchanger into account through its efficiency and the maximum heat output.

$$\dots + x_{19}^{(i)} \cdot \eta_{\text{DH}} \cdot (1 - l_{\text{pipe}}) + \dots = 0 \quad i \in \{1, 2, \dots, T\}$$

$$l_{\text{b},19}^{(i)} \leq x_{19}^{(i)} \leq u_{\text{b},18}^{(i)}$$

with

$$l_{\text{pipe}} = \frac{k_{\text{p}} \cdot L_{\text{p}}}{W_{\text{p},\text{max}}} \cdot (\vartheta_{\text{flow}}(t) - \vartheta_{\text{in}}(t)) \cdot \Delta t$$

$$l_{\text{b},19}^{(i)} = 0 \quad u_{\text{b},19}^{(i)} = P_{\text{gas},\text{max}} \cdot \Delta t$$

$\Delta t$	Time resolution in h
$\eta_{\text{gas}}$	Efficiency of the heat exchanger
$\vartheta_{\text{flow}}$	Flow temperature of the heating system in °C
$\vartheta_{\text{in}}$	Indoor room temperature of the building °C
$i$	Time index
$k_{\text{p}}$	Thermal conductivity of the pipes in W/mK
$l_{\text{b}}, u_{\text{b}}$	Lower and upper boundary of variable $x$ in kWh
$L_{\text{p}}$	Length of the pipe system of the house in m
$l_{\text{pipe}}$	Loss coefficient for transferring energy via the pipe system of the house in pu
$P_{\text{DH},\text{max}}$	Maximum thermal power output of the heat exchanger in kW
$t$	Time
$W_{\text{p},\text{max}}$	Maximum transferable energy over the pipe system in kWh
$x_{19}$	Thermal output energy of the energy transfer station in kWh

## Thermal Energy Storages (Section 2.6.8)

In this thesis, sensible thermal energy storage devices are considered for the short-term balance, for a timespan of hours, between generation and demand for heating and cooling. According to Steen et al. [4] a thermal storage with three mixed zones – high (HT), low (LT) zones and the cold fresh water (CW) zones – is modelled as shown in Figure 2.34. For the cold storage only two zones – cold (CT) and cold fresh water (CW) zones – are necessary. The stored energy in the TES and the losses are calculated according to equations (2.42) and (2.43). The following equations (2.14) show the mathematical integration of a TES in the optimisation algorithm MILP on the example of the high-temperature zone of a TES (Heating). The same concept is also used for the low-temperature zone TES and the cold storage. A detailed description of the modelling of TES and the respective temperature zones are explained in Section 2.6.8.

$$\begin{aligned} i = 1 : & -x_{12} \cdot \eta_{\text{HC1}} - x_{13} \cdot P_{\text{HC2}} \cdot \Delta t \cdot \eta_{\text{HC2}} - \\ & x_{20} + x_{21} \cdot (1 + k_{\text{TES}}) + x_{22} \cdot (1 - l_{\text{pipe}}) = W_{\text{TES,HT,init}} \\ & \vdots \end{aligned} \quad (2.14)$$

$$\begin{aligned}
 i \geq 2 : & -x_{21}^{(i-1)} - x_{12}^{(i)} \cdot \eta_{\text{HC1}} - x_{13}^{(i)} \cdot W_{\text{HC2}} \cdot \eta_{\text{HC2}} - \\
 & x_{20}^{(i)} + x_{21}^{(i)} \cdot (1 + k_{\text{TES,HT}}) + x_{22}^{(i)} \cdot (1 - l_{\text{pipe}}) = 0 \\
 & l_{\text{b},j}^{(i)} \leq x_j^{(i)} \leq u_{\text{b},j}^{(i)}
 \end{aligned}$$

with

$$j \in \{12, 13, \dots, 21\}; i \in \{1, 2, \dots, T\}$$

$$l_{\text{pipe}} = \frac{k_{\text{p}} \cdot L_{\text{p}}}{W_{\text{p,max}}} \cdot (\vartheta_{\text{flow}}(t) - \vartheta_{\text{in}}(t)) \cdot \Delta t$$

$$k_{\text{TES}} = U_{\text{TES}} \cdot A_{\text{TES}} \cdot \frac{1}{W_{\text{TES,HT,max}}} \cdot (\vartheta_{\text{TES,HT}}(t) - \vartheta_{\text{in}}(t))$$

$$l_{\text{b},12}^{(i)} = 0 \quad u_{\text{b},12}^{(i)} = P_{\text{HC1}} \cdot \Delta t$$

$$l_{\text{b},13}^{(i)} = 0 \quad u_{\text{b},13}^{(i)} = 1 \quad \text{with } x_{13}^{(i)} \in \mathbb{N}$$

$$l_{\text{b},20}^{(i)} = 0 \quad u_{\text{b},12}^{(i)} = W_{\text{TES,ch}} \cdot \Delta t$$

$$l_{\text{b},21}^{(i)} = 0 \quad u_{\text{b},12}^{(i)} = W_{\text{TES,max}}$$

$$l_{\text{b},22}^{(i)} = 0 \quad u_{\text{b},12}^{(i)} = W_{\text{TES,disch}} \cdot \Delta t$$

$\Delta t$	Time resolution in h
$\eta_{\text{HC1}}, \eta_{\text{HC2}}$	Efficiency of heating cartridges in pu
$\vartheta_{\text{flow}}$	Flow temperature of the heating system in °C
$\vartheta_{\text{in}}$	Indoor room temperature of the building °C
$\vartheta_{\text{TES,HT}}$	Temperature of HT zone in °C
$A_{\text{TES}}$	Surface of the TES to the surrounding in m <sup>2</sup>
$i$	Time index
$k_{\text{p}}$	Thermal conductivity of the pipes in W/mK
$k_{\text{TES,HT}}$	Loss coefficient of TES to the surroundings in pu
$l_{\text{b}}, u_{\text{b}}$	Lower and upper boundary of variables $x$ in kWh
$L_{\text{p}}$	Length of the pipe system of the house in m
$l_{\text{pipe}}$	Loss coefficient for transferring energy via the pipe system of the house in pu
$P_{\text{HC1}}, P_{\text{HC2}}$	Maximum power of heating cartridges in kW
$t$	Time
$U_{\text{TES}}$	Overall heat transfer coefficient of the TES in W/m <sup>2</sup> K
$W_{\text{p,max}}$	Maximum transferable energy over the pipe system in kWh
$W_{\text{TES,HT,init}}$	Initialised storage level in kWh
$W_{\text{TES,HT,max}}$	Maximum storable energy in HT zone of TES (heating) in kWh
$x_{12}$	Charging energy of heating cartridge 1 (variable power) in kWh
$x_{13}$	Charging energy of heating cartridge 2 (constant power) in kWh
$x_{20}$	Charging energy of the TES (HT zone) in kWh
$x_{21}$	State of charge of the TES (HT zone) in kWh
$x_{22}$	Discharging energy of the TES (HT zone) in kWh

The variables  $x_{21}^{(i)}$  and  $x_{24}^{(i)}$  in sum cannot exceed the maximum storage level of the TES (inequality).

$$x_{21}^{(i)} \cdot \frac{1}{W_{\text{TES,HT,max}}} + x_{24}^{(i)} \frac{1}{W_{\text{TES,LT,max}}} \leq 1 \quad \text{with } i \in \{1, 2, \dots, T\} \quad (2.15)$$

$W_{\text{TES,LT,max}}$	Maximum storage level of LT zone of the TES (heating) in kWh
$W_{\text{TES,HT,max}}$	Maximum storage level of HT zone of the TES (heating) in kWh
$x_{21}$	State of charge of the TES (HT zone) in kWh
$x_{24}$	State of charge of the TES (LT zone) in kWh

## 2.3 Weather

The influence of the weather in the form of, e.g., ambient temperature, solar irradiance, clouds and wind has a significant influence on the energy production and efficiency of distributed generation systems and consumer behaviour such as heating, cooling, lighting.

In addition to gravitation (tides) and geothermal energy, the Sun is Earth's largest regenerative energy source, with an annual amount of energy of  $3.9 \cdot 10^{24} \text{ J} = 1.08 \cdot 10^{18} \text{ kWh}$  emitted on the surface of the Earth. On Earth, this energy source reflects in solar irradiance, ambient temperature, wind and precipitation. This energy source can be used through technical transformation by, e.g., photovoltaic systems and heat pumps, to cover a part of the global energy demand of electricity, heat and cold [5]. Appendix B contains further basic information on solar irradiance.

The ambient temperature  $\vartheta_a$  and the solar irradiance  $G$  are characterized by a strongly fluctuating behaviour. The following Figure 2.5 shows the measured values of ambient temperature  $\vartheta_a$  (left) and solar irradiance  $G$  (right) of an exemplary year in Graz, Austria.

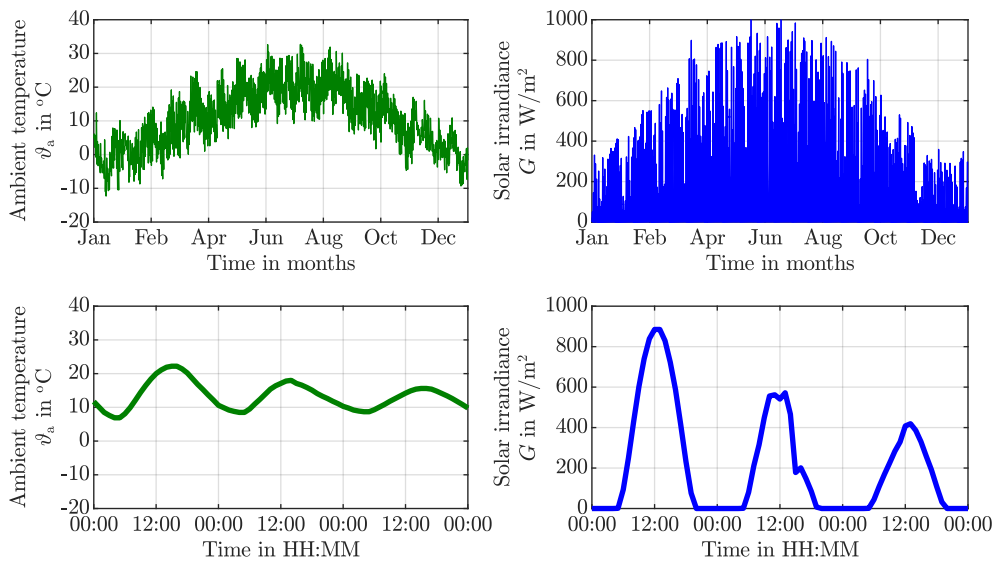


Figure 2.5: Measured ambient temperature (left) and solar irradiance (right) – Graz Austria

The Figure 2.5 shows the daily – three exemplary chosen days – and seasonal fluctuations of ambient temperature  $\vartheta_a$  and solar irradiance  $G$  of real measured data in the year 2016. These fluctuations lead to a strongly fluctuating generation of electricity and heat of generation systems such as photovoltaic and solar thermal systems.

The data of the ambient temperature  $\vartheta_a$  and solar irradiance  $G$  is essential for the modelling of decentralised renewable generation systems and the calculation of the heating and cooling demand of buildings.

The extraterrestrial irradiance  $G_a$  ( $[G_a] = \text{W}/\text{m}^2$ ) is reduced on its way through the atmosphere. There are different physical effects like reflection and absorption of the Earth's atmosphere, Rayleigh and Mie scattering (elastic scattering of electromagnetic waves on spherical objects), see Figure 2.6. The solar irradiance  $G$  is separated into the following parts:

- **Direct beam irradiance  $G_{\text{dir}}$ :**  
Extraterrestrial irradiance ( $G_a$ ) minus atmospheric losses
- **Diffuse irradiance  $G_{\text{diff}}$ :**  
Irradiance caused by atmospheric reflection and Rayleigh and Mie scattering
- **Reflected irradiance  $G_{\text{refl}}$ :**  
Solar irradiance reflected on the environment (depending on the terrestrial Albedo  $\alpha$  – see Appendix B)

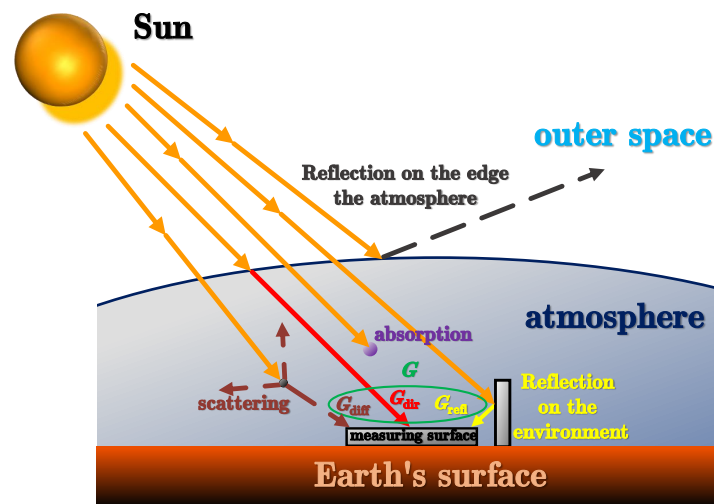


Figure 2.6: Illustration of the composition of solar irradiance (adapted, [6])

The solar irradiance  $G$ , composed of direct  $G_{\text{dir}}$ , the diffuse irradiance  $G_{\text{diff}}$  and the reflected irradiance  $G_{\text{refl}}$ , is measured on a horizontal surface with a pyranometer, see Figure 2.6.

$$G = G_{\text{dir}} + G_{\text{diff}} + G_{\text{refl}} \quad (2.16)$$

On clear days the direct irradiance  $G_{\text{dir}}$  dominates. If there are clouds present, the solar irradiance is scattered by the water molecules in the troposphere. This scattering increases the diffuse irradiance  $G_{\text{diff}}$  and reduces the direct irradiance  $G_{\text{dir}}$  compared to a sunny day.

The solar irradiance  $G$  gets reflected by the environment, e.g., buildings or trees. The degree of diffuse reflection of surfaces is indicated by the Albedo  $\alpha$ . The Table B.1 in the Appendix B lists Albedo values  $\alpha$  for different types of surfaces. The reflected irradiance  $G_{\text{refl}}$  is calculated with the measured solar irradiance using an anisotropic approach [6].

In order to determine the output of renewable generation systems such as photovoltaic systems (Section 2.6.1) and solar thermal systems (Section 2.6.4), as well as

the heating and cooling demand (Section 2.4.2), the horizontally measured global irradiance  $G$  needs to be calculated for differently oriented and inclined surfaces, as described subsequently.

### Conversion of Horizontally Measured Solar Irradiance on Arbitrarily Oriented and Inclined Surfaces

The direct part of the horizontal solar irradiance  $G_{\text{dir}}$  can be converted to an arbitrarily oriented and inclined surface, see Figure B.6. The solar irradiance directly incident on an arbitrarily aligned surface  $G_{\text{sa,dir}}$  can be calculated at any time with the Equation (2.17) from the horizontal direct irradiance  $G_{\text{dir}}$ , the angle of solar incidence on the aligned surface  $\theta_{\text{sa}}$  and the solar elevation angle  $\gamma_{\text{s}}$  [5].

$$G_{\text{sa,dir}} = G_{\text{dir}} \cdot \frac{\cos(\theta_{\text{sa}})}{\sin(\gamma_{\text{s}})} \quad (2.17)$$

Due to a tilt of the considered surface, the direct irradiance  $G_{\text{sa,dir}}$  arriving at the aligned surface area can be larger than the horizontally incident direct irradiance  $G_{\text{dir}}$ . The calculation of the position of the Sun and the associated angles is described in Appendix B.

Since the density of the Sun's rays varies depending on the direction of incidence, an anisotropic approach is used to calculate the diffuse irradiance  $G_{\text{diff}}$ . The mathematical model of Klucher is used for the calculation of a diffuse irradiance  $G_{\text{sa,diff}}$  on an arbitrarily aligned surface area. A possible further model to calculate the diffuse irradiance on an aligned surface  $G_{\text{sa,diff}}$  is the model of Perez. This model provides more accurate results, but is also much more complex than the model of Klucher [5], [6].

Using the following Equation (2.18), the diffuse irradiance on a arbitrarily aligned surface  $G_{\text{sa,diff}}$  can be determined with the total horizontally incident solar irradiance  $G$  and diffuse irradiance  $G_{\text{diff}}$ , the angle of solar incidence  $\theta_{\text{sa}}$ , the solar elevation angle  $\gamma_{\text{s}}$  and the vertical tilt angle of the aligned surface  $\gamma_{\text{sa}}$  [5].

$$G_{\text{sa,diff}} = \frac{1}{2} \cdot G_{\text{diff}} [1 + \cos(\gamma_{\text{sa}})] \cdot \left[ 1 + \left( 1 - \left( \frac{G_{\text{diff}}}{G} \right)^2 \right) \cdot \sin^3 \left( \frac{\gamma_{\text{sa}}}{2} \right) \right] \cdot \left[ 1 + \left( 1 - \left( \frac{G_{\text{diff}}}{G} \right)^2 \right) \cdot \cos^2(\theta_{\text{sa}}) \cdot \cos^3(\gamma_{\text{s}}) \right] \quad (2.18)$$

In contrast to the calculation of the diffuse irradiance on an arbitrarily aligned surface  $G_{\text{sa,diff}}$ , an isotropic approach is sufficient for the calculation of the reflected irradiance  $G_{\text{refl}}$ . The albedo  $\alpha$  describes the reflectivity of the environment. The Albedo  $\alpha$  is standardised for specific objects according to the Table B.1. The reflected irradiance  $G_{\text{sa,refl}}$  can be calculated by using the horizontally incident solar irradiance

$G$ , the albedo  $\alpha$  of the environment immediately surrounding objects and the vertical tilt angle of the aligned surface  $\gamma_{sa}$  [5].

$$G_{sa,refl} = G \cdot \alpha \cdot \frac{1}{2} [1 - \cos(\gamma_{sa})] \quad (2.19)$$

Nowadays, solar systems are classically oriented towards the south. This orientation of solar systems has significant advantages concerning the maximum achievable output. However, if the peak loads of the demand are in the morning or afternoon hours, a demand-oriented positioning of the solar systems is recommended. The following Figure 2.7 explains the advantage of a demand-oriented positioning of solar systems [7].

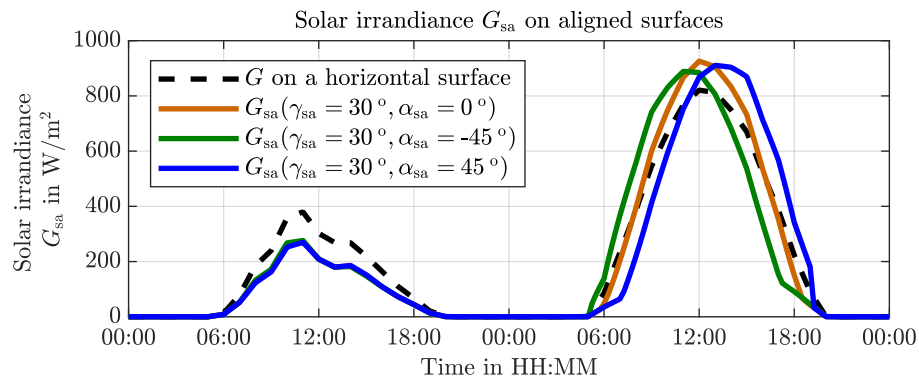


Figure 2.7: Comparison of solar irradiance at various alignments of surfaces

Figure 2.7 shows a comparison of the solar irradiance on various aligned surfaces for two days. On cloudy days, Figure 2.7 (first day), the diffuse part of the solar irradiance is present mostly, so no significant difference in irradiance on the different orientations of the surfaces occur. In contrast, on bright weather days such as Figure 2.7 (second day), the advantage of a demand-oriented positioning can be seen. An eastern alignment of the surface, Figure 2.7 (green line), shows an increased solar irradiance in the morning and a western alignment, Figure 2.7 (blue line), an increased solar irradiance in the afternoon in contrast to a south-oriented surface.

## 2.4 Energy Demand

With 23.9 % (AUT) and 25.7 % (EU-28) in 2017, the residential sector accounts for a significant share of total energy consumption in Austria and the EU-28 [8]. Although the energy efficiency of buildings and appliances improves, the energy demand of the residential sector has been increasing in recent years. This increase can be explained by a growing number of household equipment – entertainment, business devices and air conditioning systems – and a trend towards larger living spaces and single-person households. Refrigerators, freezers and washing machines are standard appliances in almost all households in Austria. These appliances are often reused as secondary devices even after replacement by a new device, e.g., a refrigerator [9]. The following Figure 2.8 shows the energy demand of the residential sector in Austria for the years 2017/18. According to Statistics Austria [10], the energy demand divides into the categories of space heating, domestic water heating, cooking, and domestic appliances and lighting.

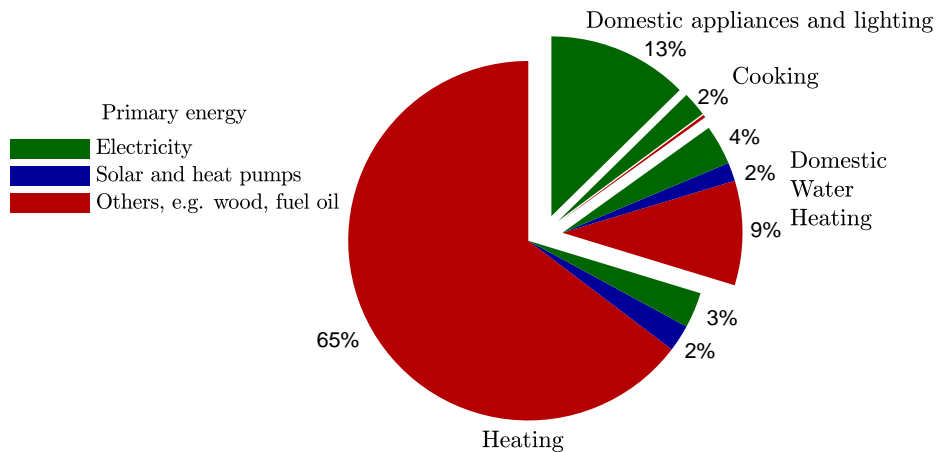


Figure 2.8: Energy demand of the residential sector in Austria, 2017/18 (custom representation,[10])

Mainly, the energy demand of residential households is used for space and domestic water heating. Together, these account for 85 % of the total energy demand of households. The energy sources used to cover this energy demand are mainly wood, fuel oil, natural gas and district heating. With a share of 22 % of the total energy demand of households, electricity covers mainly the energy demand for cooking, domestic appliances and lighting. The energy demand for charging electric vehicles, heat pumps, air conditioning and infrared heating is expected to increase sharply within the next years and will so increase both, the total electrical demand as well as its relative share within the residential sector.

The energy demand of a prosumer consists of the electrical demand, space heating and domestic hot water demand, cooling demand and the charging energy of the electric vehicle.

The electrical and hot water demand, as well as the presence of the electric vehicle at home, are generated by the LoadProfileGenerator (LPG) developed by Pflugradt [11]. The heating and cooling demand of a building are determined by applying the heating and cooling load calculations according to the standard ÖNORM B 8110-6 1:2019-01 [12] and Häupl et al. [13].

### LoadProfileGenerator by Pflugradt [11]:

The LoadProfileGenerator (LPG) is a simulation model for modelling the electrical and domestic hot water demand of households. Currently, simulations of business buildings and offices are not possible. The LPG simulates the psychological behaviour of persons living in households, and on this basis, the energy demand is determined. The psychological behaviour model prioritises specific activities, e.g., work is more important than watching television. Furthermore, the LPG takes availability times of the different activities into account. Compared to a probabilistic model, newly implemented activities will adapt automatically to the simulation. With a probabilistic model, however, new probability profiles must be generated when activities are added or removed [11].

The following Figure 2.9 shows the interaction of the person's needs, the activities and the necessary components.

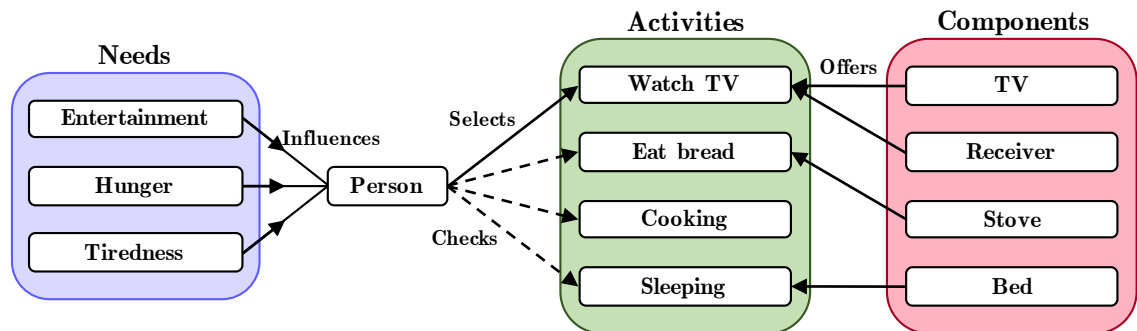


Figure 2.9: LPG - activity selection by a person (custom representation,[11])

A person checks which activity is necessary based on their needs. The various decision processes based on the needs result in device activation. If, for example, the activity „Watch TV“ is selected, the electrical demand of the television and the receiver occurs at a particular time. In order to represent the operation of a household more realistically, the LPG takes the following factors also into account [11].

- Locations, e.g., work and geographic location, e.g. Graz in Austria
- Holidays and vacations
- Temperature and date based profiles
- Autonomous devices

The LPG is validated by reviewing the simulation results concerning the plausibility criterion and comparing them with characteristic parameters from the literature. Furthermore, simulations of entire settlements, e.g., several hundred households,

are compared with the H0 standard load profile (SLP) for households [11]. The H0-SLP is an averaged and normalised measured load profile of a large number of households. When considering a total load of approximately 150 households, a symmetrical distribution around the mean value results and is therefore valid with restrictions [14].

### 2.4.1 Electrical Energy Demand – Domestic Appliances and Lighting

As described previously, the electrical energy demand of households is determined by domestic appliances, lighting and the electrical demand for cooking. Not considered are the technical systems such as heat pumps, gas boiler, circulation pumps and the electricity required for domestic hot water generation. The simulation model ProsOpt determines the electrical energy demand of the technical systems and the domestic hot water generation by optimising the operation of the investigated prosumers.

The following Figure 2.10 shows the electrical power of a selected household based on simulations of the LPG from Pflugradt [11]. The electrical power in Figure 2.10 is divided into the active (left) and reactive<sup>1</sup> (right) load.

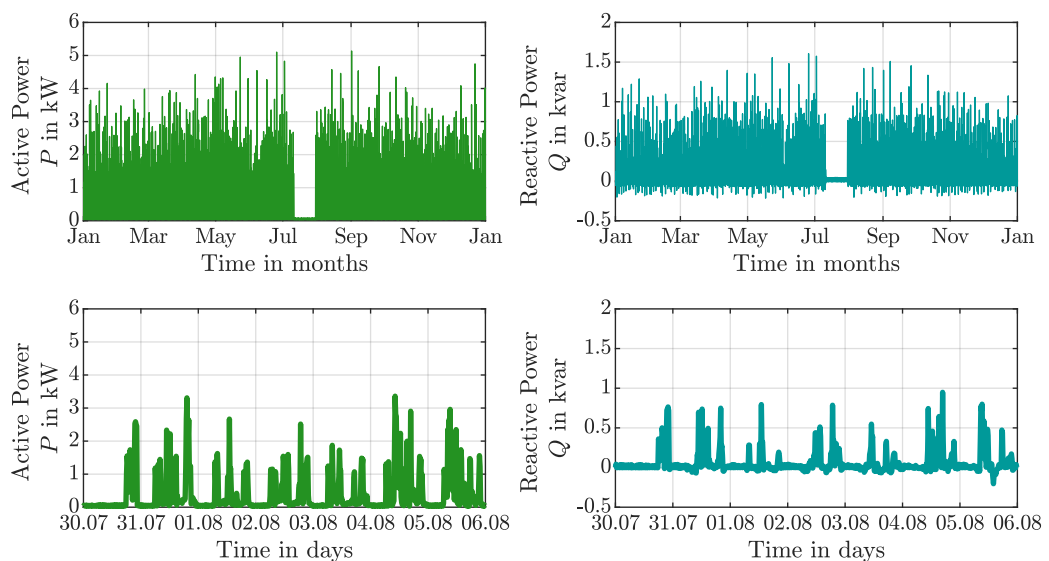


Figure 2.10: Electrical demand of a chosen household

The maximum transferred power at the Point of Common Coupling (PCC) of a household is limited physically by the house service connection and furthermore by a defined and contractually agreed power with the network operator. General the contractually agreed power with the network operator is between 3 and 5 kW according to the “Electricity System Charges Ordinance”. According to TAEV 2016 [15] and

<sup>1</sup> Reactive power  $Q > 0$ : inductive load (passive sign convention)  
Reactive power  $Q < 0$ : capacitive load (passive sign convention)

ÖVE/ÖNORM E 8016 [16] the maximum power of the house service connection of an Austrian household is 18 kW. Austrian households with an electric flow heater for domestic hot water generation must provide a maximum power of 24 kW. When using an electric heating system, e.g., infrared heating systems and an electric flow heater at the same time, a simultaneous operation must be prevented by using an interlock [14].

## 2.4.2 Heating and Cooling Demand

The thermal behaviour of buildings results from the interaction of internal and external factors with the building, the building construction itself, and the user behaviour. The balance of all influencing variables results in the heating demand in the cold season and the cooling demand in the summer. The heating and cooling demand are the amounts of energy required to maintain the room temperature of a room or building [13]. The following Figure 2.11 shows an overview of the internal and external factors influencing the thermal behaviour of a building. For reasons of clarity, the thermal energy flows are only shown for one zone, the ground floor, of the house.

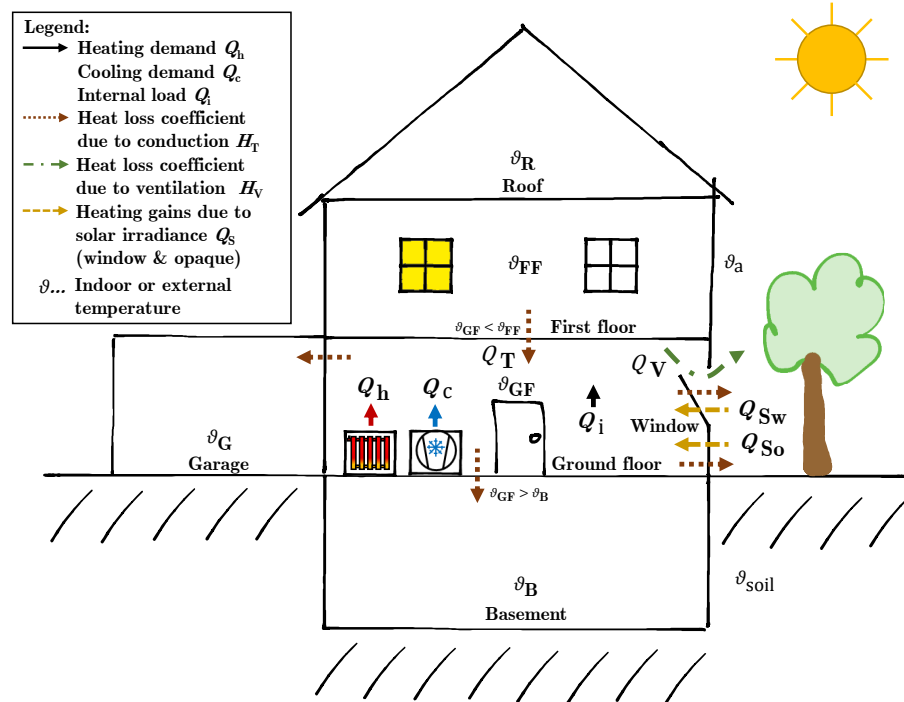


Figure 2.11: Overview of the internal and external factors influencing the thermal behaviour of a building.

The heating and cooling demand of a building can be determined using the following Equation (2.20) [13].

$$W_{h,c}(t) = (V_{\text{air}} c_{\text{air}} \rho_{\text{air}} + V_{\text{b}} c_{\text{b}} \rho_{\text{b}}) \frac{\Delta\vartheta_i(t)}{3600 \frac{\text{s}}{\text{h}}} + Q_i(t) - Q_T(t) - Q_V(t) + Q_S(t) \quad (2.20)$$

$\vartheta_i$	Indoor temperature in °C
$\rho$	Density in $\frac{\text{kg}}{\text{m}^3}$
air	Air volume
b	Building mass
c	Specific heat capacity in $\frac{\text{Wh}}{\text{kgK}}$
$Q_i$	Internal heat sources/sinks in Wh
$Q_S$	Heat gains due to solar irradiance in Wh
$Q_T$	Heat losses/gains due to conduction in Wh
$Q_V$	Heat losses/gains due to ventilation in Wh
V	Volume in $\text{m}^3$
$W_{h,c}$	Heating or cooling demand in Wh

As shown in Figure 2.11, the thermal behaviour of buildings is dependent on internal and external factors. Internal factors are internal heat sources such as lighting and the use of household appliances, as well as the attendance of persons. From the outside

- the induced heat due to solar irradiance through transparent components (windows),
- the absorbed solar irradiance of opaque building components (external walls, doors)
- heat conduction through windows and building components, and
- the exchange of air between the building and the environment

affects the thermal behaviour of buildings.

The calculation of all heat sources and sinks of the building shown in Figure 2.11 are explained in more detail below, using the following simplifications.

- The rooms on each floor are grouped into zones. A zone is characterised by the same usage, e.g., room temperature and air exchange, of the different rooms on each floor.
- The infiltration caused by leakages of the building are neglected.
- The building mass and the resulting effective heat storage capacity of the building  $C$  is calculated according to the simplified approach of the standard ÖNORM B 8110-6 1:2019-01 [17].

$$C = f_b \cdot V \quad (2.21)$$

$C$	Effective heat capacity in $\frac{\text{Wh}}{\text{K}}$
$f_b$	Specific heat capacity in $\frac{\text{Wh}}{\text{m}^3\text{K}}$
V	Gross volume in $\text{m}^3$

According to ÖNORM B 8110-6 1:2019-01 [17] the construction designs are divided as follows.

*Lightweight construction* ( $f_b = 10 \frac{\text{Wh}}{\text{K}}$ ):

Buildings in wooden construction without solid interior components

*Medium-heavy construction* ( $f_b = 20 \frac{\text{Wh}}{\text{K}}$ ):

Buildings in mixed construction, buildings in solid construction with suspended ceilings and predominantly light partition walls.

*Heavy construction* ( $f_b = 30$  to  $50 \frac{\text{Wh}}{\text{K}}$ ):

Buildings with a solid exterior and interior components, floating screeds and without suspended ceilings.

## Heat losses due to conduction

The heat losses due to conduction  $Q_T$  of a zone are calculated from the component surfaces with the respective overall heat transfer coefficient  $U$  and the temperature difference between inside and outside [13]. Furthermore, thermal bridges are taken into account with the thermal bridge correction factor  $\Delta U_{tb}$ . A common value for the thermal bridge correction factor is  $\Delta U_{tb} = 0.05 \frac{W}{m^2K}$ .

$$Q_{T,i}(t) = \sum_{j=1}^N (U_{eq\ i,j} \cdot A_{i,j} + \Delta U_{tb}) \cdot (\vartheta_{in,i}(t) - \vartheta_{out\ i,j}(t)) \quad (2.22)$$

$\Delta U_{tb}$	Thermal bridge correction factor in $\frac{W}{m^2K}$
$\vartheta_{in}$	Indoor temperature in $^{\circ}C$
$\vartheta_{out}$	Outside temperature in $^{\circ}C$ , e.g., air, soil or the temperature of other zones
$A$	Surface area of component in $m^2$
$i$	Zone of building
$j$	Component surface
$U_{eq}$	Equivalent overall heat transfer coefficient in $\frac{W}{m^2K}$

The equivalent overall heat transfer coefficient  $U_{eq} = U - g \cdot \frac{G}{\vartheta_{in} - \vartheta_{out}}$  considers in addition to the overall heat transfer coefficient  $U$  also the solar heat gains due to direct and diffuse solar irradiance  $G$ . The effective total energy transmittance  $g$  accounts a room's incoming solar energy, consisting of transmission  $\tau$  and absorption  $\alpha$  components. Typical values for the overall heat transfer coefficient  $U$  and effective total energy transmittance  $g$  can be found in Tables A.1 and A.2 in the Appendix.

## Heat losses due to ventilation

Heat losses  $Q_V$  caused by natural ventilation of the zones via doors, windows or by mechanical ventilation using fans has a significant impact on the thermal behaviour of buildings and their room air quality. The Equation (2.23) explains the calculation of heat losses from ventilation  $Q_V$ . According to ÖNORM B 8110-5 1:2019-01 [18], a ventilation rate of at least  $n = 0.28 h^{-1}$  must be selected for natural ventilation.

$$Q_{V,i}(t) = n_i \cdot V_i \cdot (\vartheta_{in,i} - \vartheta_a) \quad (2.23)$$

$\vartheta_a$	Ambient temperature in $^{\circ}C$
$\vartheta_{in}$	Indoor temperature in $^{\circ}C$
$i$	Zone of building
$n$	Ventilation rate in $h^{-1}$
$V$	Volume of zone in $m^3$

## Heat gains due to solar irradiance

Solar irradiance via opaque and transparent components can create additional heat sources and will reduce heat sinks. The influence of solar irradiance on a building for opaque components as external walls and roofs, and transparent building components is calculated according to the Equation (2.24) [13]. For opaque building components, the long-wave radiation is taken into account and, in contrast to transparent building components, the contribution of transmission is omitted.

$$\begin{aligned} \text{transparent: } Q_{\text{sw},i}(t) &= \sum_{j=1}^N G_{i,j}(t) \cdot F_{\text{F}} \cdot F_{\text{cs}}(t) \cdot g_{i,j} \cdot A_{i,j} \cdot \Delta t \\ \text{opaque: } Q_{\text{so},i}(t) &= \sum_{j=1}^N U_{i,j} \cdot A_{i,j} \cdot R_{\text{se}} \cdot (\alpha_{s,i,j} \cdot G_{i,j}(t) - F_{\text{f}} \cdot h_{\text{r}} \cdot \Delta\vartheta_{\text{er}}) \cdot \Delta t \end{aligned} \quad (2.24)$$

$\alpha_{\text{s}}$	Absorptivity of component
$\varepsilon$	Emissivity (external walls, roof, doors)
$\Delta\vartheta_{\text{er}}$	Temperature difference ambient air to sky in K; $\Delta\vartheta_{\text{er}} = 10 \text{ K}$
$\Delta t$	Timestep in h
$A$	Surface area of building component in $\text{m}^2$
$F_{\text{cs}}$	Reduction factor due to shading and sun protection; $F_{\text{cs}} = 0$ (no sun prot.), $F_{\text{cs}} = 0.25 - 0.5$ (manual sun prot.), $F_{\text{cs}} = 0.8$ (automatic sun prot.) [17]
$F_{\text{F}}$	Reduction factor due to frame share of windows; $F_{\text{F}} = 0.7$ [17]
$F_{\text{f}}$	Form factor (0.5 for vertical walls, otherwise 1)
$G$	Solar irradiance on building components $\frac{\text{W}}{\text{m}^2}$
$g$	Effective total energy transmittance, see [13], [17]
$h_{\text{r}}$	External radiation coefficient in $\frac{\text{W}}{\text{m}^2\text{K}}$ ; $h_{\text{r}} = 5 \cdot \varepsilon$
$i$	Zone of building
$j$	Component surface
$R_{\text{se}}$	External heat transfer resistance in $\frac{\text{m}^2\text{K}}{\text{W}}$ ; $R_{\text{se}} = 0.04 \frac{\text{m}^2\text{K}}{\text{W}}$ [17]
$U$	Overall heat transfer coefficient of a building component in $\frac{\text{W}}{\text{m}^2\text{K}}$ , see Table A.1

Essential for the calculation of the heat input by solar irradiance is the calculation of the irradiance on the arbitrary orientation of the component surfaces of the building, see Section 2.3. A north facade of a house, for example, has much less solar energy input than a south facade.

The developed simulation model ProsOpt calculates the heating and cooling demand of a house by using the building structure – size of the building,  $U$ -values and surface area proportions of respective components –, the geographical orientation of the building, weather data and the performance of the heating system. The following Figure 2.12 shows the calculated heating and cooling power of a single-family house. In this example, only the ground and first floor are conditioned.

The heating period starts on 1<sup>st</sup> October and ends on 30<sup>th</sup> April. During the summer months the building is cooled accordingly. To calculate the heating demand, a minimum setpoint indoor temperature of 22 °C and a maximum setpoint indoor temperature of 26 °C is selected for the cooling demand.

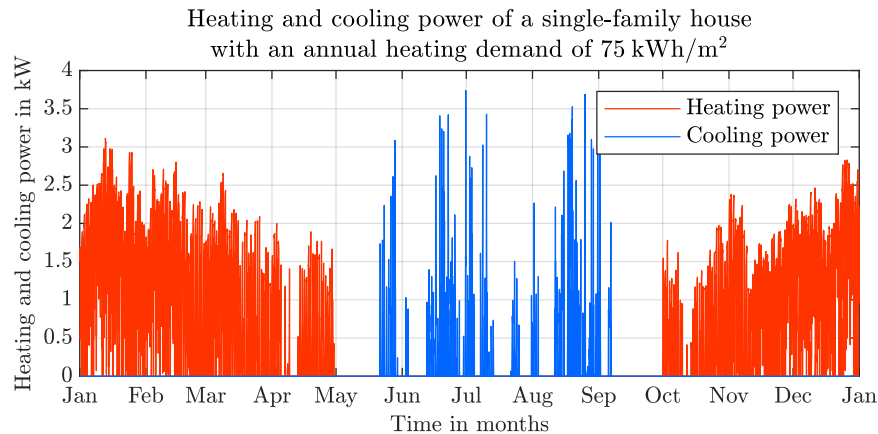


Figure 2.12: Heating and cooling power of the house with an annual heating demand of 75  $\frac{\text{kWh}}{\text{m}^2}$  and annual cooling demand of 6  $\frac{\text{kWh}}{\text{m}^2}$

## Validation

The developed model for calculating the heating and cooling demand was validated by the commercial software IDA ICE from the company EQUA Solutions AB [19]. The same parameters were chosen for both simulation models. The main parameters of these are,

- a minimum setpoint indoor temperature (heating season) of 22 °C,
- a maximum setpoint indoor temperature (cooling season) of 26 °C,
- an ventilation rate with natural ventilation of  $n = 0.5 \text{ h}^{-1}$  in the conditioned zones,
- an overall heat transfer coefficient  $U = 0.10 \frac{\text{W}}{\text{m}^2\text{K}}$  for external walls, ceilings and the roof, and  $U = 1.90 \frac{\text{W}}{\text{m}^2\text{K}}$  for windows,
- an effective total energy transmittance of the windows of  $g = 0.685$  in the heating period as well as a reduced total energy transmittance of  $g = 0.10$  in the summer months due to shading by, e.g., shutters.

The following Figure 2.13 shows a monthly comparison of the calculated heating and cooling demand from PosOpt and the IDA ICE simulation.

Figure 2.13 shows minimal deviations between the two simulations, which can be explained by the simplification of the calculation model of PosOpt mentioned above. The calculated annual heating demand deviates by 0.5 % and the annual cooling demand by 6.1 % from the results of the IDA ICE simulation. The developed calculation model is therefore adequately accurate for further applications.

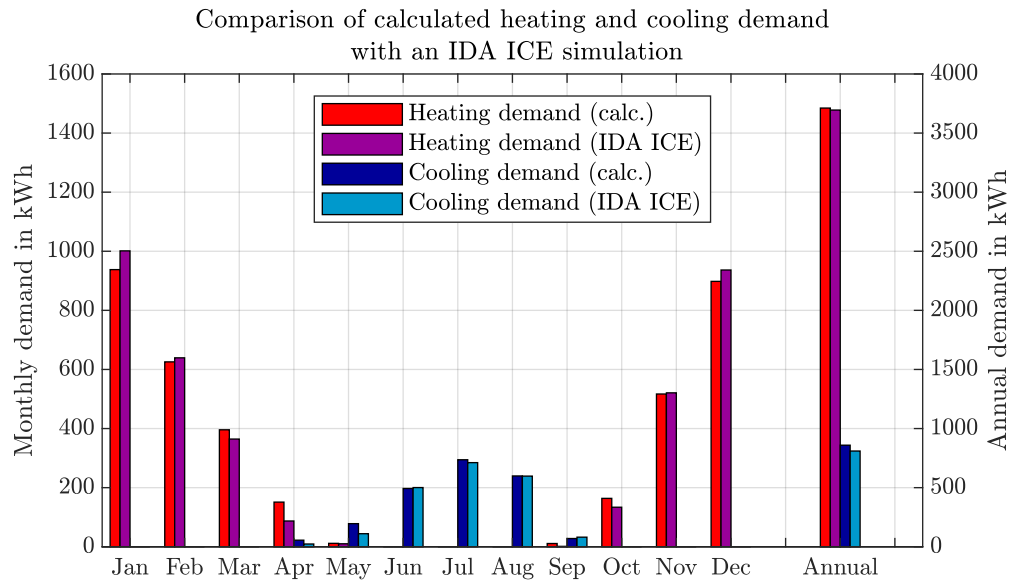


Figure 2.13: Comparison of the calculated heating and cooling demand with the results of the simulation software IDA ICE from EQUA Simulation AB [19]

### 2.4.3 Domestic Hot Water

The domestic hot water – at a temperature of 60 °C – in a household is primarily used in the kitchen and bathroom. The average domestic hot water demand of a household is 30 to 60 litres per person and day. There are different warm water temperatures required for each consumption point. For hygienic reasons, the domestic warm water is mixed from hot and cold water at the tap [20]. The cold water temperature is assumed to be 10 °C. According to Bohne [20], the following Table 2.1 lists average values for domestic warm water quantities and temperatures per use and different apartment sizes.

Table 2.1: Domestic warm water quantities and temperatures per use and different apartment sizes (own representation, [20], [21])

	Water demand per use or day	Water temperature
Tub bath	120 to 180l	40 °C
Shower	40 to 50l (5 minutes)	37 °C
Washing (washbasin)	5 to 20l	35 °C
Kitchen sink	10 to 40l	50 °C
1-room apartment or house (1 person)	50 to 95l/day	60 °C
2-room apartment or house (2-3 pers.)	70 to 200l/day	60 °C
3-room apartment or house (2-5 pers.)	95 to 250l/day	60 °C
4-room apartment or house (3-7 pers.)	120 to 500l/day	60 °C

The following Figure 2.14 shows the domestic hot water demand of a selected 2-person household based on the simulations of the LoadProfileGenerator (LPG).

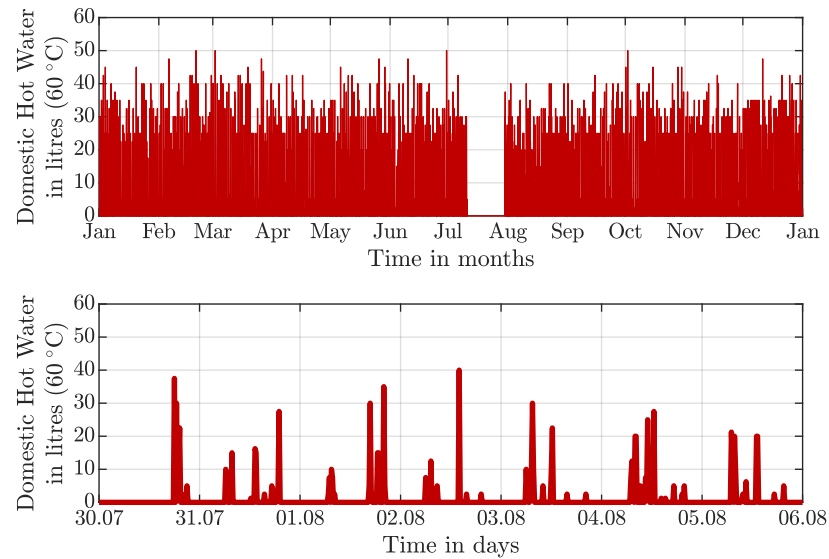


Figure 2.14: Domestic hot water demand of a chosen household

The average daily domestic hot water demand of the simulated 2-person household is 61 litres per person at a water temperature of 60 °C. Comparing the results of the selected household and other simulated households with the parameters according to the Table 2.1, plausible simulation results of the LoadProfileGenerator (LPG) by Pflugradt [11] are obtained.

## 2.4.4 Home Presence of Electric Vehicle

The used psychological behavioural model of the LPG by Pflugradt [11] simulates, additionally to the electrical and domestic hot water demand, the movements of the residents of a household. Different types of transportation devices, such as electric vehicles (EV's), buses as well as travel routes can be defined. The LPG limits the use of transportation devices for the residents. For example, if a person already uses the EV, another person must take the bus. Children cannot use the EV. The following Figure 2.15 shows the home presence of the EV over one year [22].

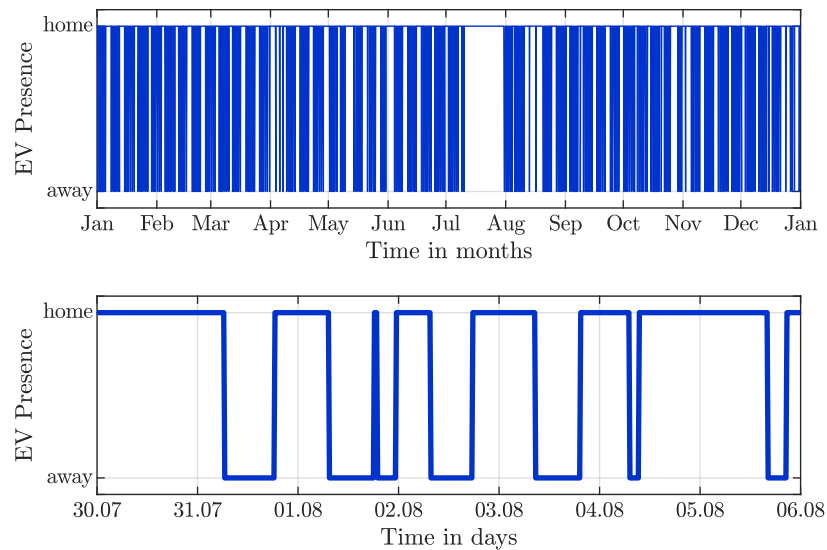


Figure 2.15: EV home presence of a chosen household

The developed simulation model ProsOpt uses the home presence of the EV for the optimised operation of the prosumer, intelligent charging and V2G/G2V. It is assumed that the EV is connected to the EVCS when at home.

## 2.5 Economic and Ecologic Assumptions

### Economic Assumptions

For the economic comparison of different technologies, the Levelised Cost of Energy (LCE or Levelized Cost of Electricity - LCOE) can be used. The LCE is calculated according to the net present value method including the capital and operating expenditures. The LCE is typically defined in Euros per kWh (€/kWh) [23].

$$\text{LCE} = \frac{I_0 + \sum_{j=1}^n \frac{A_j}{(1+i)^j}}{\sum_{j=1}^n \frac{W_j}{(1+i)^j}} \quad (2.25)$$

$A_j$	Operating expenditures for the year $j$ in $\frac{\text{€}}{\text{a}}$
$i$	Discount factor
$I_0$	capital expenditures in €
$n$	Expected service life in years
$W_j$	Amount of energy for the year $j$ in $\frac{\text{kWh}}{\text{a}}$

As shown in Figure 2.16, this thesis examines three different tariff models; the static and HT/NT tariffs commonly used in Austria and a newly offered dynamic tariff model.

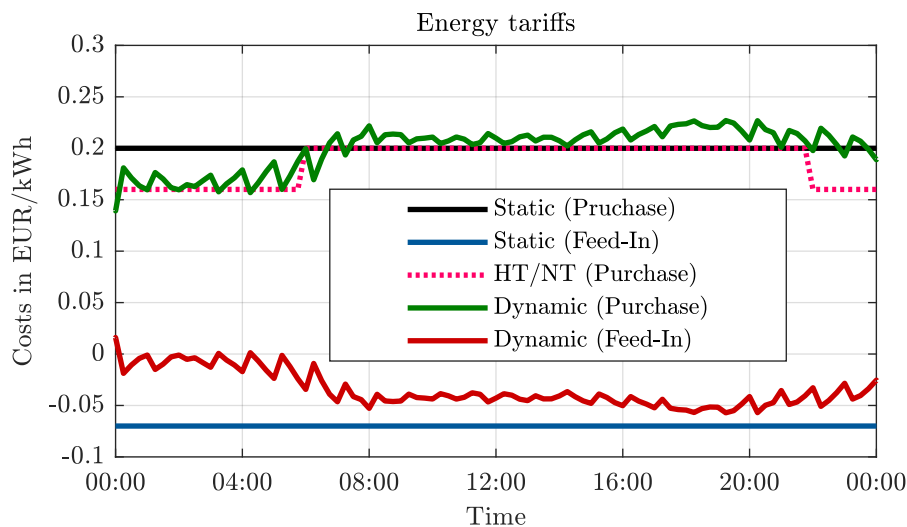


Figure 2.16: Static, HT/NT and dynamic tariff models

#### Static tariff:

The static tariff is a fixed rate agreed for a defined annual energy demand over a contractual period. The meter is read annually at the end of the contract period. If the agreed consumption is exceeded, the difference must be paid, otherwise, it will be credited. The electricity costs for consumers vary in Austria from 0.14 to 0.23 €/kWh (2018, [24]).

### HT/NT tariff:

The high (HT) and low tariff (NT) model is like the static tariff contractually agreed over a defined period. Other than the static tariff, a time range is defined for the low load (NT, 10 pm to 06 am) and high load times (HT, 06 am to 10 pm). This should provide incentives for power consumption in times of lower load. For this purpose, a second meter is installed. A centralized telecontrol signal usually selects the respective meter. The low tariff is approximately 70-80 % of the high tariff.

### Dynamic tariff:

Due to the planned installation of smart meters, the possibility of dynamic tariffs will be opened, such as tariffs of the Austrian company DAfi GmbH ([www.smartfox.at](http://www.smartfox.at)) [25]. A possible tariff model can be a tariff dependent on the electricity market (e.g., EPEX, Day-Ahead Auction). The dynamic tariff is calculated based on a monthly rate, taxes, network service charges and variable energy costs depending on the electricity market.

Since those costs vary in time depending on the operation and use of the technical components, additional sensitivity analyses must be performed at economic optimisations. Table 2.2 shows the assumed Levelised Cost of Energy and energy tariffs with typical prices in Austria (year 2018).

Table 2.2: Levelised Costs of Energy (LCE) for the used technologies and energy tariffs, typical prices in Austria, 2018

Purchase energy from the network (PCC)	Static tariff: 0.20 €/kWh
	HT/NT tariff: 0.2/0.16 €/kWh
	Dynamic tariff
Feed-in energy into the network (PCC)	Static tariff: 0.07 €/kWh
	Dynamic tariff
Photovoltaics (PV)	0.12 €/kWh
Electrical Energy Storage (EES)	$\geq 0.35$ €/kWh
Heat pump (HP)	0.15 €/kWh
Thermal energy storage (TES)	0.05 €/kWh
Air conditioner (AC)	0.20 €/kWh

Since consumption and production do not coincide in every time step, without the use of energy storage or demand-side management, it is necessary to purchase or feed-in energy at suboptimal tariffs or to adapt the load profile (i.e. consumer behaviour) according to the tariff situation. For example, at low feed-in tariffs, it is economical to use the surplus generation of the photovoltaic system locally using demand side management and thus to increase the self-consumption level or buffer it by using an electrical energy storage, or to cover/store the thermal demand.

## Ecologic Assumptions

For the ecological evaluation, the CO<sub>2</sub> balance of the technologies or system components is used. As listed in Table 2.3, CO<sub>2</sub> equivalents or the global warming potential (GWP), which are usually expressed in g<sub>CO<sub>2</sub></sub>/kWh, are used as an ecological objective for the linear optimisation algorithm.

Table 2.3: CO<sub>2</sub> equivalents or global warming potential (GWP) of the technologies used

Electricity mix (AUT)	250 g/kWh <sub>el</sub> [26]
Photovoltaics (PV)	60 g/kWh <sub>el</sub> [26], [27]
Electrical Energy Storage (EES)	100 g/kWh <sub>el</sub> [28]
Heat pump (HP)	140 g/kWh <sub>th</sub> [26], [29]
Air conditioner (AC)	140 g/kWh <sub>th</sub> (assumed as HP)
District heating (DH)	250 g/kWh <sub>th</sub> [26], [29], [30]

Since the numerical values of the CO<sub>2</sub> equivalents given in Table 2.3, as with the LCE, are based on a variation depending on use and system type, sensitivity analyses must be performed to evaluate the overall system. For example, the generation of electricity and heat (district heating) depends very strongly on the primary energy sources used.

## 2.6 Distributed Energy Generation and Storage Systems

### 2.6.1 Photovoltaic System

Photovoltaic systems convert solar energy into electrical energy. This conversion is possible through the photoelectric effect, which was discovered by the French physicist Alexandro Edmond Becquerel (1820-1891) and explained in detail by Albert Einstein. Albert Einstein was awarded the Nobel Prize in Physics for his explanation of the photoelectric effect in 1921. The first applied use of photovoltaic (PV) cells was presented in 1954 by Chapin, Fuller and Pearson at Bell Labs. Today's photovoltaic modules achieve efficiencies of 20 % to 25 % under laboratory conditions, depending on the cell technology under consideration [31]. In the following, the theoretical basics, such as the design and function of PV modules and inverters, are presumed and are not explained in detail.

The developed model to calculate a photovoltaic system uses weather data (solar irradiance, ambient temperature), technical characteristics of the PV modules and inverters (data sheets) as well as azimuthal orientations and inclinations of the PV modules to determine the expected energy output of the PV system. For reasons of transferability of the developed model, no shadowing analyses of surrounding objects, e.g., buildings are performed. The following Figure 2.17 shows the key parameters as well as the methodical approach for calculating the power output of a photovoltaic system. In the following section the parameters used in Figure 2.17 are explained in more detail.

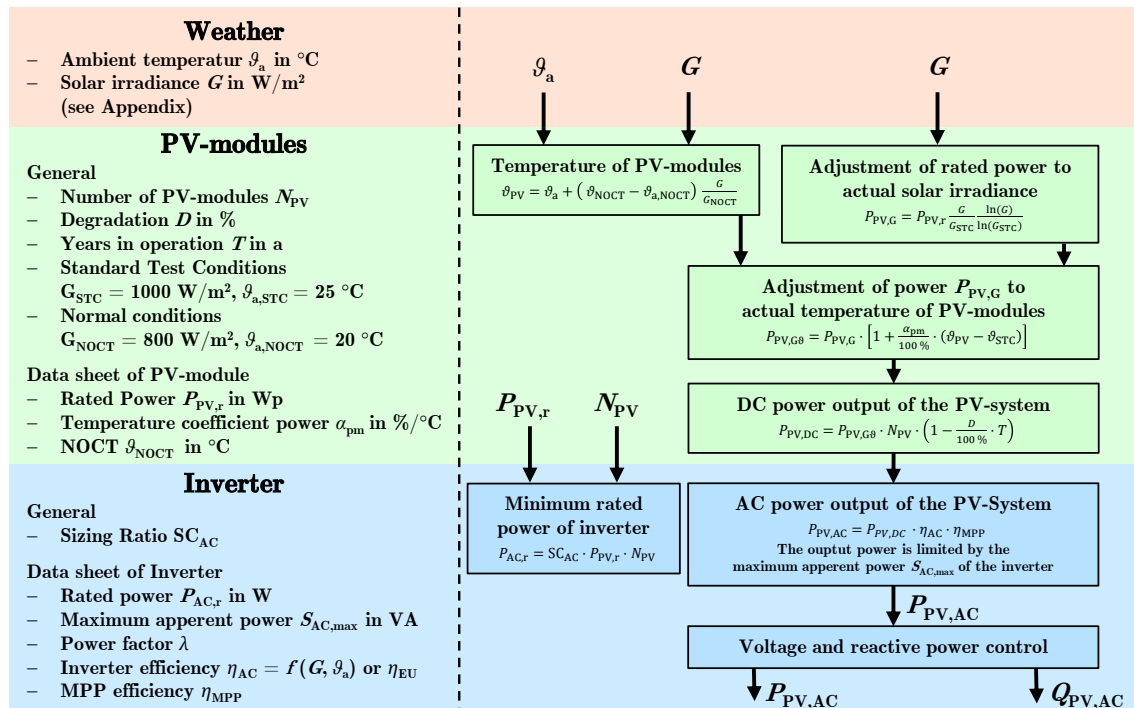


Figure 2.17: Methodical representation of the calculation process of the PV system

The efficiency of PV modules is determined according to the standard test conditions (STC), which are based on a solar irradiance  $G_{STC}$  of  $1000 \text{ W/m}^2$ , an ambient temperature  $\vartheta_{a,STC}$  of  $25^\circ\text{C}$  and an airmass of 1.5. The Airmass is the distance that sunlight travels through the earth's atmosphere to the Earth's ground. An airmass of 1.5 means an incidence angle of about  $48.2^\circ$ . As the STC rarely occur in reality, the nominal operating cell temperature (NOCT) is a further parameter of PV modules. The NOCT is determined under so-called normal conditions at a solar irradiance  $G_{NOCT}$  of  $800 \text{ W/m}^2$ , an ambient temperature  $\vartheta_{a,NOCT}$  of  $20^\circ\text{C}$ , a wind speed of  $1 \text{ m/s}$  and an Airmass of 1.5.

The efficiency of PV modules is highly dependent on external environmental influences. PV modules, such as monocrystalline PV modules, have a negative temperature coefficient  $\alpha_{pm}$ . Rising temperatures of PV modules lead to a decrease in efficiency. Both solar irradiance  $G$  and the ambient temperature  $\vartheta_a$  influence the PV module temperature  $\vartheta_{PV}$ . This influence on the efficiency  $\eta_{PV}$  of the PV modules is shown in Figure 2.18 below.

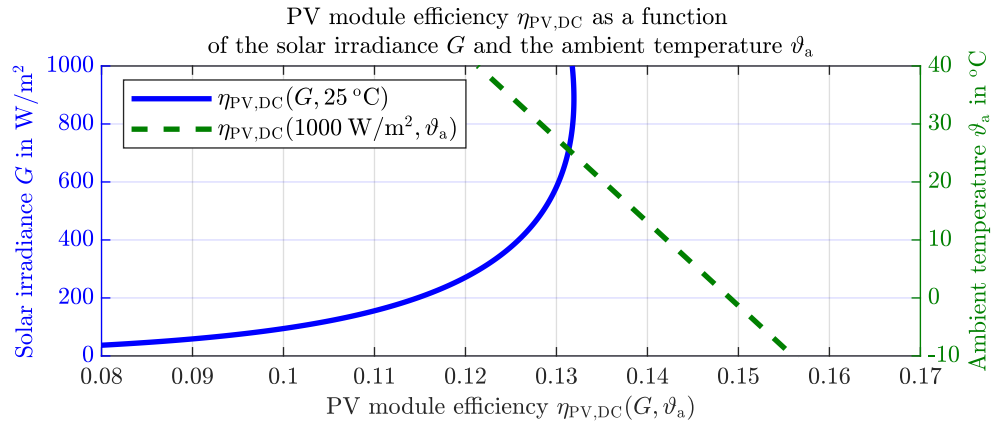


Figure 2.18: Efficiency of a PV module as a function of the ambient temperature  $\vartheta_a$  and the solar irradiance  $G$

Figure 2.18 shows the efficiency  $\eta_{PV}$  as a function of the solar irradiance  $G$  and the ambient temperature  $\vartheta_a$ . To show the influence of these two environmental dimensions separately, one dimension is considered constant in each case. Figure 2.18 shows a linear change of the efficiency  $\eta_{PV}$  at changing ambient temperatures  $\vartheta_a$ , as well as a non-linear relationship of the efficiency  $\eta_{PV}$  to the solar irradiance  $G$ . This relationship is considered in the following Equation (2.26).

The electrical energy output of a photovoltaic system is calculated as follows.

$$P_{PV,AC} = P_{PV,r} \frac{G}{G_{STC}} \frac{\ln(G)}{\ln(G_{STC})} \cdot \left[ 1 + \frac{\alpha_{pm}}{100\%} \left( \vartheta_a + \frac{\vartheta_{NOCT} - \vartheta_{a,NOCT}}{G_{NOCT}} G - \vartheta_{STC} \right) \right] \eta_{AC} \cdot \eta_{MPP} \left( 1 - \frac{D \cdot T}{100\%} \right) \quad (2.26)$$

PV modules work much better in cold seasons due to a negative temperature coefficient  $\alpha_{pm}$ . Nevertheless, in most cases, due to the significantly higher levels of solar irradiance  $G$  during the summer, the electrical output  $P_{PV}$  is higher at lower efficiency than in winter. PV modules lose their rated power  $P_{PV,r}$  over the years  $T$ . Many manufacturers of PV modules give a power guarantee of, e.g., 90% for the

first decade. In the model, therefore, an annual degradation  $D$  of the rated power of 1 %/a is expected [31].

## Inverter

The task of a grid-connected inverter is the efficient conversion of direct current into a sinusoidal alternating current, which is synchronous with the network frequency. Further tasks are the monitoring of the network (voltage, frequency, network impedance), personal safety and MPP tracking. In inverters, a so-called MPP tracker ensures that the solar modules are always operating at the point of maximum power (MPP) by adjusting the DC voltage appropriately [32]–[35].

The efficiency of inverters depends on their technical design, the MPP voltage, thus their operation point, and their actual load (partial versus maximum load). The following Figure 2.19 shows the efficiency curve  $\eta_{AC}(P/P_r)$  of a selected inverter. According to EN 50530 [36], the efficiency of the inverter  $\eta_{AC}$  is extended by the MPP efficiency  $\eta_{MPP}$  (inverter data sheet), as it is assumed that the MPP tracker does not always find the MPP. The total efficiency is the product of  $\eta_{AC}$  and  $\eta_{MPP}$  (data sheet of inverter;  $\eta_{MPP} > 0.99$  pu).

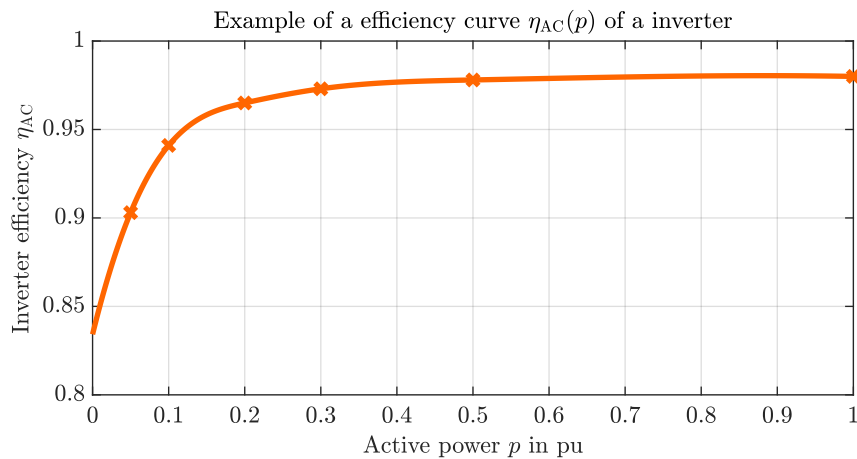


Figure 2.19: Efficiency of the inverter  $\eta_{AC}$  as a function of the active power output of the PV modules

In order to be able to compare different inverters, the efficiency  $\eta_{EU}$  has been defined in EN 50524 [37]. This efficiency weights the partial loads according to the relative incidence of the average irradiance conditions in Central Europe and is calculated for inverters as following in Equation (2.27).

$$\eta_{EU} = 0.03 \cdot \eta_{5\%} + 0.06 \cdot \eta_{10\%} + 0.13 \cdot \eta_{20\%} + 0.1 \cdot \eta_{30\%} + 0.48 \cdot \eta_{50\%} + 0.2 \cdot \eta_{100\%} \quad (2.27)$$

The compatibility of the inverter with the PV modules is essential for the maximum output that can be achieved. The sizing ratio  $SR_{AC}$  is defined as the quotient of the installed power of the PV system  $P_{PV,r}$  and the rated power of the inverter  $P_{AC,r}$ . To avoid losses at low loads, the inverter should not be oversized ( $SR_{AC} \approx 1$ ) [31].

## Requirements for network connection of generators

The standard EN 50160 [38] defines the voltage characteristics of electricity supplied by public electricity networks. This standard specifies that the supply voltage in low-voltage networks may change by a maximum of  $\pm 10\%$  to the nominal voltage  $V_N$ . In medium-voltage networks, the voltage change is related to an agreed supply voltage  $V_C$ .

In Austria, national rules – “TOR - Technische und organisatorische Regeln für Betreiber und Benutzer von Netzen [39]; [www.e-control.at/en/recht/marktregeln/tor](http://www.e-control.at/en/recht/marktregeln/tor)” – regulate the requirements for operators and users to connect with the public electricity network. These rules include the minimum requirements from national and European legal sources, such as the regulation (EU) 2016/631 [40]. According to these national rules, the reactive power capability for inverter-based generators with a maximum rated power  $S_r$  of less than 250 kW and a nominal voltage  $V_N$  less than 110 kV is defined as follows.

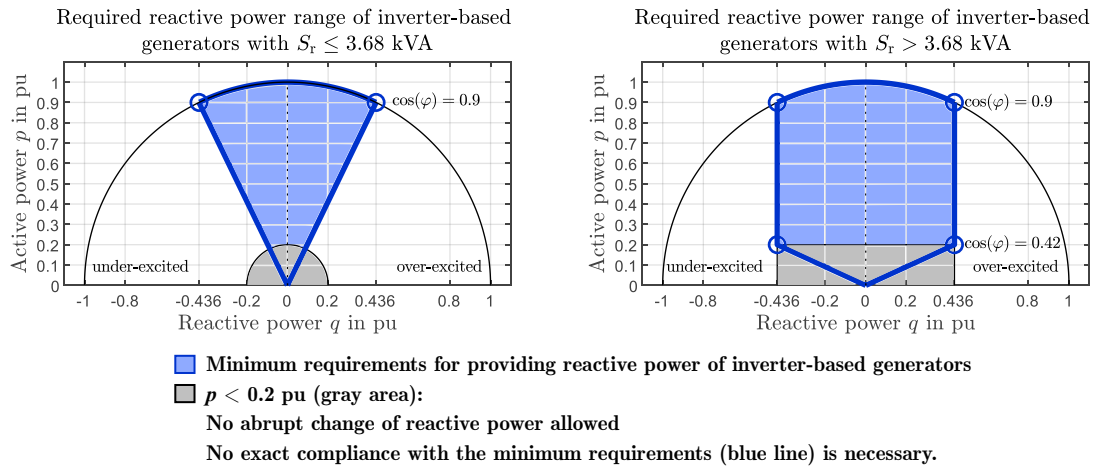


Figure 2.20: Reactive power capability for inverter-based generators (custom representation, [39])

Figure 2.20 shows the minimum requirements for providing reactive power to the network for inverter-based generators (blue area). The reactive power capability for inverter-based generators is divided into the two following types [39].

- Inverter-based generators  $S_r \leq 3.68$  kVA  
The required reactive power  $q$  increases linearly with increasing active power output  $p$ . The maximum required reactive power  $q_{\max}$  is set to 0.436 pu ( $\cos(\varphi) = 0.9$ ) at an active power  $p$  of 0.9 pu.
- Inverter-based generators  $S_r > 3.68$  kVA  
At an active power  $p$  between 0.2 pu and 0.9 pu, inverter-based generators greater 3.68 kVA must be able to provide at least a reactive power  $q$  of 0.436 pu.

At an active power  $p$  less than 0.2 pu (grey area), no abrupt changes of the reactive power  $q$  is allowed neither exact compliance with the minimum requirements (blue lines) is necessary. In order to comply with the voltage limits according to EN 50160, the following methods for voltage and reactive power control must be implemented [38].

*Constant power factor mode and constant reactive power mode:*

If there are no voltage and reactive power control specified by the network operator, the constant power factor mode is set to a unity power factor ( $\cos(\varphi) = 1$ ) as well as the reactive power mode is set to zero ( $Q = 0 \text{ var}$ ) [39], [41].

*Voltage-reactive power mode*

In the voltage-reactive power (volt-var) mode, the reactive power output  $q$  is actively controlled by the inverter as a function of the voltage  $v$ .

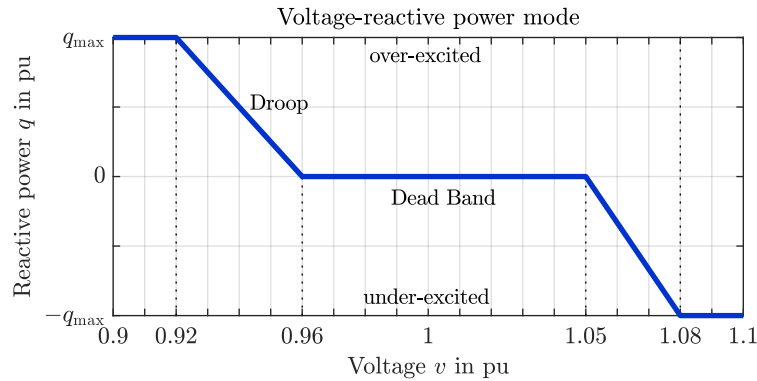


Figure 2.21: Voltage-reactive power mode for inverter-based generators

The piecewise linear characteristic of the (volt-var) mode, shown in Figure 2.21, is divided into the following areas [39].

- Over-excited operation of the inverter  
If the voltage level falls below  $0.96 V_N$ , the inverter will operate in an over-excited mode. The provided reactive power  $q$  as a function of the voltage  $v$  is linearly increased in the voltage range of  $0.96$  to  $0.92 V_N$  to the maximum reactive power  $q_{\max}$ .
- Dead Band  
In a voltage range from  $0.96$  to  $1.05 V_N$ , no reactive power ( $q = 0 \text{ pu}$ ) should be provided by the inverter. This is corresponding to the constant power factor mode with a unity power factor ( $\cos(\varphi) = 1$ ).
- Under-excited operation of the inverter  
At voltage levels above  $1.05 V_N$ , the inverter will operate in an under-excited mode. The provided reactive power  $q$  as a function of the voltage  $v$  is linearly decreased in the voltage range of  $1.05$  to  $1.08 V_N$  to the maximum reactive power  $-q_{\max}$ .

According to the Austrian national rules TOR, the required reactive power capability for inverter-based generators is set to  $0.436 \text{ pu}$ . Generators with rated apparent power  $S_r$  less or equal  $3.68 \text{ kVA}$  can set the required reactive power capability to  $0.312 \text{ pu}$  [39].

The volt-var mode offers more flexible control of the voltage, with a good compromise between voltage level and the provided reactive power, than the active power-power factor mode and the volt-watt mode. Further, the volt-var mode reduces network losses and offers savings in annual reactive energy. Otherwise, generators at the end

of the line, in particular, must participate very intensively in reactive power control [42].

*Active power-power factor mode*

The active power-power factor (watt-cos  $\varphi$ ) mode regulates the power factor  $\cos(\varphi)$  piecewise linearly as a function of the active power  $p$ . When reaching a setpoint of the active power  $p$ , e.g., 0.5 pu ( $1 \text{ pu} \hat{=} P_r$ ), the inverter operates in under-excited mode and reduces the power factor  $\cos(\varphi)$  linearly to a minimum of 0.9/0.95<sup>1</sup> [39].

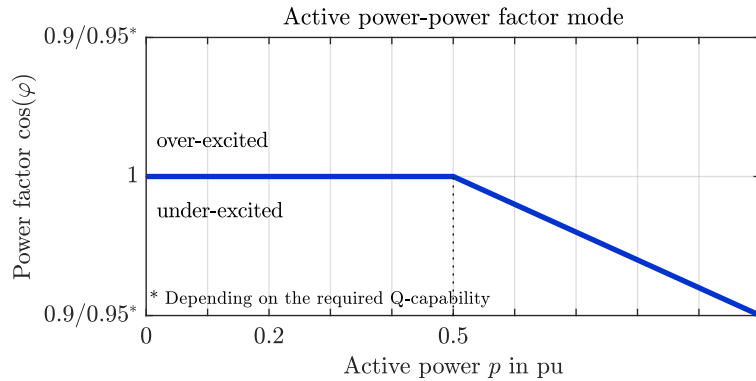


Figure 2.22: Active power-power factor mode for inverter-based generators

Compared to the volt-var mode, where individual generators must participate intensively in reactive power control, in the active power-power factor mode, all generators participate regardless of their position in the network in reactive power control [42].

*Voltage-active power mode*

Low voltage networks (LV-networks) are indicated by a high  $R/X$  ratio. Therefore the voltage  $v$  can be effectively influenced by controlling the active power output  $p$ .

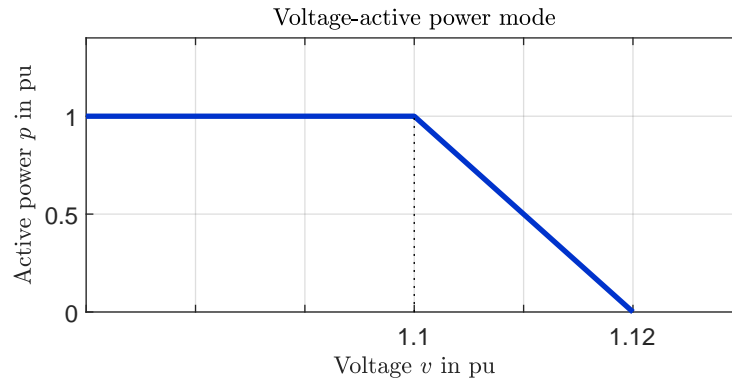


Figure 2.23: Voltage-active power mode for inverter-based generators

By exceeding a setpoint of the voltage level, e.g.,  $1.1 V_N$  ( $1 \text{ pu} \hat{=} V_n$ ), the voltage-active power (volt-watt) mode reduces the active power  $p$  of the generator linearly until the voltage  $v$  reaches a defined level, e.g.  $1.12 V_N$ . However, this will result in a loss of active power generation  $p$  [39].

<sup>1</sup> Depending on the required  $Q$ -capability

## 2.6.2 Electrical Energy Storage System

The purpose of an electrical energy storage (EES) system is to store energy in order to provide a demand-oriented supply [3]. As consumption and generation of consumers or prosumers do not correspond at all times, without the use of energy storage or demand-side management, it is either necessary to purchase or feed-in energy at sub-optimal tariffs or to adjust the load profile accordingly by adapting the customer behaviour. In the following, the storage of surplus generated electrical energy using electrochemical storage systems is investigated in more detail.

In their effect on the network, EES's are basically to be evaluated in the same way as electrical energy generation systems such as photovoltaic systems or consumer installations. Unless stated otherwise, the Austrian regulations apply equally to them [39]. For electrochemical storages in decentralised storage systems, Lithium-ion (Li-ion) batteries and Lead-acid (Pb-A) batteries are the dominant technologies in the building sector.

### *Lithium-ion (Li-ion) batteries:*

The expression Li-ion battery is an umbrella term for batteries which uses lithium compounds. By using different lithium compounds, it is possible to adapt the storage properties according to specific requirements [43]. Li-ion cells have an efficiency of up to 99 %. However, the entire EES system, including the inverter, achieves round-trip efficiencies of 83 to 86 % [44]. Li-ion batteries have low maintenance costs, can be operated within a wide temperature range and will allow fast charging. Most important, the energy density of Li-ion batteries is high. Many different fields, such as electronics and e-mobility, use Li-ion batteries [45].

The following Table 2.4 lists the essential specifications of Li-ion batteries. Li-ion batteries still have the potential for development. Table 2.4 also shows possible future improvement potential in addition to the actual status.

Table 2.4: Characteristics of Li-ion batteries (custom representation, [44])

Characteristics	Actual	Potential
<b>Cell efficiency</b>	95 - 99 %	95 - 99 %
<b>Round-trip efficiency</b>	80 - 85 %	85 - 90 %
<b>Energy density</b>	200 - 350 Wh/litre	250 - 550 Wh/litre
<b>Power density</b>	100 - 3500 W/litre	100 - 5.000 W/litre
<b>Cycle life</b>	1000 - 5000 cycles	3.000 - 10.000 cycles
<b>Calendar life</b>	5 - 20 a	10 - 30 a
<b>Depth of discharge</b>	up to 100 %	up to 100 %
<b>Self-discharge</b>	5 % monthly	1 % monthly

Barriers to the use of Li-ion batteries are the limited cycle life as well as the manufacturing costs. Nevertheless rapidly decreasing costs during the last years make Li-ion batteries attractive as a storage system in combination with photovoltaic systems. The requirements of Li-ion batteries as home storage systems differ significantly from mobile storage systems in design and dimensions. While

weight and volume play a major role in mobile applications, these factors are rather secondary in stationary applications. In stationary applications, calendar life and maintenance costs are more important [46].

*Lead-acid (Pb-A) batteries:*

Lead-acid (Pb-A) batteries have the largest market share for battery systems. The main application of Pb-A batteries is the automotive sector and emergency power supply in industry [45]. Pb-A batteries may produce hydrogen during load conditions. Therefore, the storage room of Pb-A batteries needs active ventilation due to the production of the hydrogen. Furthermore, Pb-A batteries require regular maintenance and refilling of the electrolyte. It is possible to bound the electrolyte as a gel form, to prevent the production of hydrogen. This prevention of gassing makes lead-gel batteries useful for domestic electrical energy storage systems [46].

The low cost and recyclability of Pb-A batteries, however, is contrasted by a low cycle life and energy density compared to Li-ion batteries. Besides, charging management prevents a deep discharge of the battery. The following Table 2.5 lists the essential characteristics of lead acid batteries and their future potential.

Table 2.5: Characteristics of Pb-A batteries (own representation, [44])

<b>Characteristics</b>	<b>Actual</b>	<b>Potential</b>
<b>Cell efficiency</b>	80 - 90 %	85 - 95 %
<b>Round-trip efficiency</b>	75 - 80 %	78 - 85 %
<b>Energy density</b>	50 - 100 Wh/litre	50 - 130 Wh/litre
<b>Power density</b>	10 - 500 W/litre	10 - 1.000 W/litre
<b>Cycle life</b>	500 - 2000 cycles	1.500 - 5.000 cycles
<b>Calendar life</b>	5 - 15 a	10 - 20 a
<b>Depth of discharge</b>	70 %	80 %
<b>Self-discharge</b>	0,1 - 0,4 % daily	0,05 - 0,2 % daily

The Pb-A batteries will also be used as a stationary storage battery soon, as it offers recyclability and is currently an alternative to the Li-ion batteries with low investment costs [44].

The inverter losses additionally influence the efficiency of an EES system. The inverter losses lead to a reduction of 10 to 15 % of the round-trip efficiency of the EES systems. The mode of operation, state of charge, depth of discharge and temperature have a strong influence on the calendar life. To spare possible lifetime of the battery, the depth of discharge is often only moderately and not fully utilised [44].

## Design and principle of operation of PV storage systems

Domestic EES systems using Li-ion and Lead-acid batteries dominate the market. There are various ways to integrate EES into PV systems. The coupling of the EES

to the PV system is possible on AC side as well as on DC side. An inverter converts the DC voltage generated by the PV modules to AC voltage. By extending a PV system with an EES, the use of either a separate inverter for both systems or a standard hybrid inverter is possible [47].

A charge controller controls the charging strategy and protects the EES from damage during the charging process. Especially For Pb-A batteries, it is necessary to disconnect the batteries from the PV system after complete charging, as otherwise overcharging would occur and result in so-called gassing in the battery. This gassing would cause long-term damage to the battery and significantly reduce its lifetime. A further task of the charge controller is to protect the storage from deep discharging. When the battery reaches a particular voltage level, the connection to the load is disconnected. This voltage is called the cut-off voltage and prevents the battery from being accidentally discharged. Furthermore, charge controllers have over-temperature protection which monitors and protects the cell temperature of the batteries. Besides, reverse polarity protection prevents damage to the battery by connecting the battery in reverse polarity [47].

In the following, different storage operation strategies of electrical energy storage systems are investigated. Constant efficiencies and a time-dependent self-discharge rate are assumed for the resulting charging and discharging processes. The charge controller is implemented optimally. This means that deep discharging or other critical operation modes do not occur in ProsOpt under any circumstances.

## Storage Operation Strategies

Grid-connected photovoltaic systems represent a relevant field of application for EES's. Especially in the future integrated smart grids and energy communities, decentralised and centralised electrical energy storage systems will be able to compensate the fluctuating generation from photovoltaic systems and the gap between generation and consumption in the short term. Suitable charging management can significantly improve the degree of autonomy as well as the degree of self-consumption. The EES stores the surplus generated energy so that it can be supplied according to demand and thus increase autonomy.

The operation strategies of PV-Storage systems allows to achieve specific targets. Often an increasing share of self-consumption or a limitation of the feed-in power (peak shaving) are preferred strategies. It is also possible to use a combination of operation strategies. In this way, it would be possible, for example, to ensure both operations optimised for self-consumption and peak-shaving.

## Degree of Autonomy and Self-Consumption

The degree of autonomy, as well as the degree of self-consumption, are essential indicators for the evaluation of the efficient use of the energy generated by renewable energy systems such as PV systems. The following Figure 2.24 shows a PV-Storage

system schematically with the connection to the power network. Further, Figure 2.24 exemplarily shows the PV generation (green line) and electrical demand of a household (black line) as well as the share of the generated power.

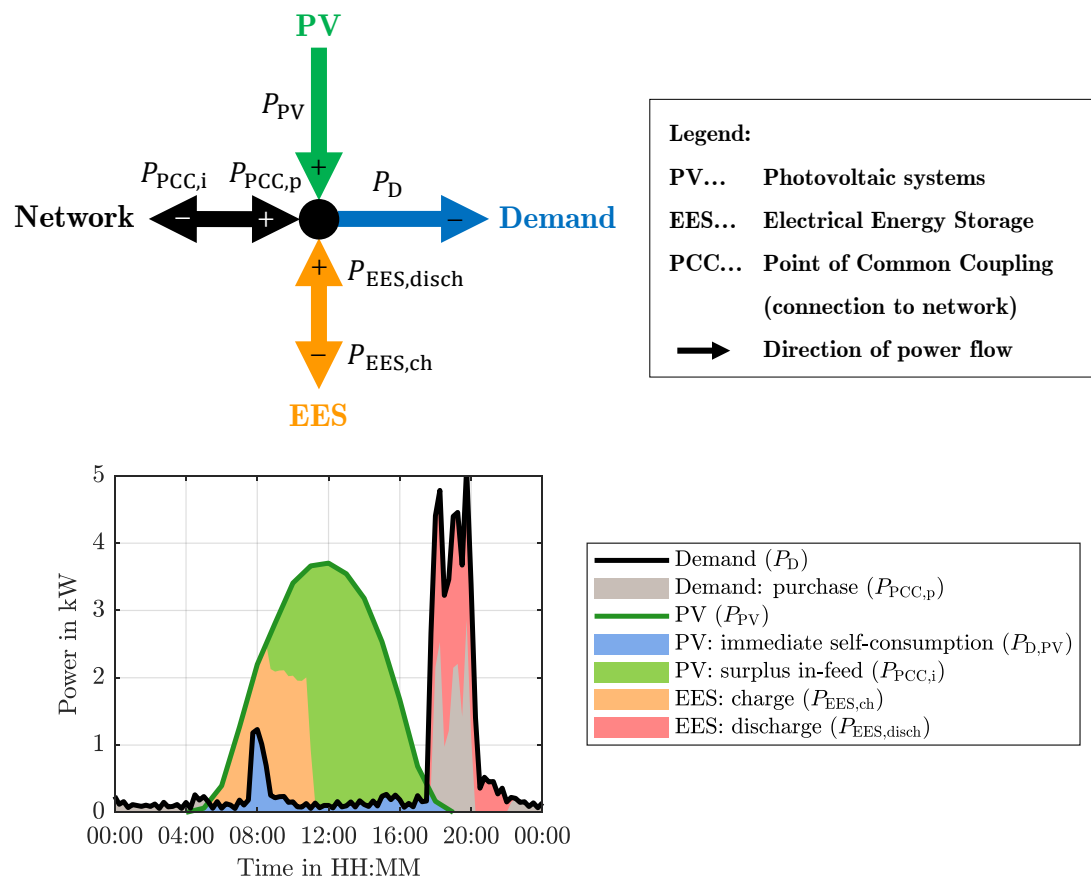


Figure 2.24: Schematic representation of a PV-Storage system and exemplary a comparison of the PV generation, the household's electrical demand, and the charging and discharging of an EES at limited charging/discharging power

The coloured areas in Figure 2.24 represent the proportional share of the PV generation to cover the electrical energy demand of a household. The areas in Figure 2.24 do not overlap. The generation is split into the energy used directly (blue area), the stored energy in the EES (orange area) and the surplus in-feed into the power network (green area). Furthermore, to cover the electrical demand, Figure 2.24 shows the energy purchased from the power network (grey area) as well as the energy discharged from the EES (red area).

*Degree of Self-Consumption (DSC):*

The degree of self-consumption indicates how much of the electrical energy generated by the PV system (Figure 2.24 - green line) is consumed without being fed into the power network (green area). In a PV-Storage system, the generated electrical energy is consumed either directly (blue area) or later through intermediate storing (orange area – charge EES, red area – discharge EES). The higher the degree of self-consumption, the less energy is fed into the power network by the PV system [46], [48], [49]. The degree of self-consumption

is calculated as follows and ranges between 0 and 1 pu (0 - 100 %).

$$\text{DSC} = \frac{\int_{t_1}^{t_2} P_{\text{PV}}(t) dt - \int_{t_1}^{t_2} P_{\text{PCC},i}(t) dt}{\int_{t_1}^{t_2} P_{\text{PV}}(t) dt} = \frac{\int_{t_1}^{t_2} P_{\text{D},\text{PV}}(t) dt + \int_{t_1}^{t_2} P_{\text{EES},\text{ch}}(t) dt}{\int_{t_1}^{t_2} P_{\text{PV}}(t) dt} \quad (2.28)$$

DSC	Degree of self-consumption
$P_{\text{D},\text{PV}}$	Demand directly covered by PV system in kW
$P_{\text{EES},\text{ch}}$	Charging power of electrical energy storage (EES) in kW
$P_{\text{PCC},i}$	Feed-in in the public electricity network in kW
$P_{\text{PV}}$	Generation of a photovoltaic system (PV) in kW
PCC	Point of Common Coupling

*Degree of autonomy (DA):*

The degree of autonomy indicates the share of demand covered by the PV directly (Figure 2.24 - blue area) and by intermediate storing with the EES (red area). The degree of autonomy thus indicates the independence from the power network and ranges between 0 and 1 pu (0 - 100 %). Increasing degree of autonomy results in more independence from the power network. The degree of autonomy is calculated as follows [46], [48].

$$\text{DA} = \frac{\int_{t_1}^{t_2} P_{\text{D}}(t) dt - \int_{t_1}^{t_2} P_{\text{PCC},p}(t) dt}{\int_{t_1}^{t_2} P_{\text{D}}(t) dt} = \frac{\int_{t_1}^{t_2} P_{\text{D},\text{PV}}(t) dt + \int_{t_1}^{t_2} P_{\text{EES},\text{disch}}(t) dt}{\int_{t_1}^{t_2} P_{\text{D}}(t) dt} \quad (2.29)$$

DA	Degree of autonomy
$P_{\text{D}}$	Demand in kW
$P_{\text{D},\text{PV}}$	Demand directly covered by PV system in kW
$P_{\text{EES},\text{disch}}$	Discharging power of electrical energy storage (EES) in kW
$P_{\text{PCC},p}$	Purchase of power from the public electricity network in kW
PCC	Point of common coupling

## Operation Strategy – Self-Consumption

The surplus generation of PV system charges the EES and thus increases the degree of self-consumption. This operation strategy reduces the amount of electrical energy purchased from the network and consequently increases the degree of autonomy. The EES stores the surplus generation of the PV system until the storage is fully charged. When fully charged, the surplus generation is usually fed-in into the network. The operation strategy “self-consumption” enables an increase in the degree of self-consumption, but the contribution to the reduction of the peak load to the network is limited [50]. Figure 2.25 shows the influence of an electrical energy storage system on the example of a single-family house with the operation strategy „self-consumption”. The dashed line represents the state of charge (SoC) of the storage system.

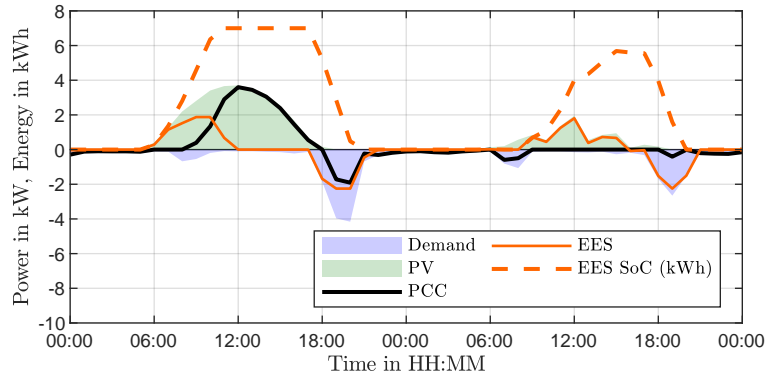


Figure 2.25: Operation strategy – self-consumption

### Operation Strategy – Peak-Shaving

A grid-optimised operation strategy takes a predefined limit of feed-in power of the PV-Storage system to the network into account. The EES stores the surplus generation of the PV system when exceeding the defined power limit. The EES gets charged with the power difference of the generation of the PV system and the peak power limit [50]. Figure 2.25 shows an example of a PV storage system with the operation strategy „peak-shaving”.

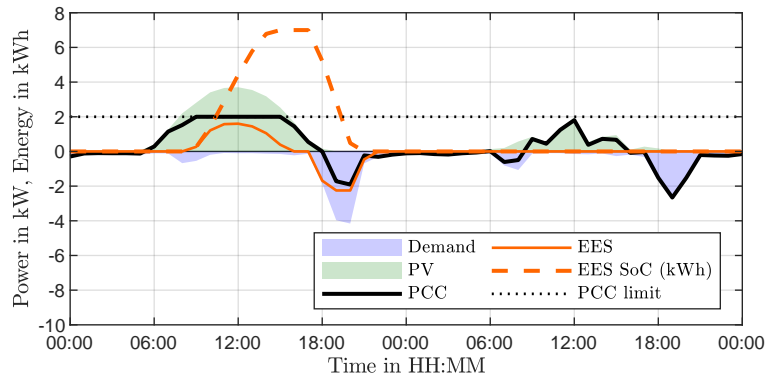


Figure 2.26: Operation strategy – peak-shaving

### Operation Strategy – Forecast

With a predictive operation strategy, it is possible to operate the EES optimally. Forecasts predict the future power generation of the PV system, the demand as well as possible changes in costs of energy tariffs. The EES system charges and discharges according to the weather forecasts and thus to the expected solar irradiance in order to ensure an optimal operation [46], [50]. The following Figure 2.27 shows the simulation results for a PV storage system with the operation strategy „forecast”.

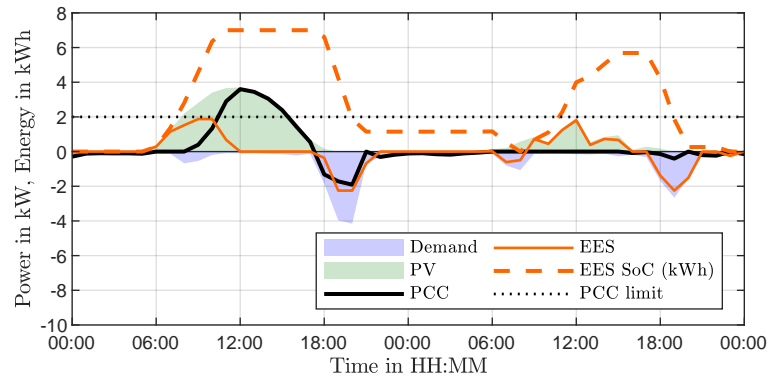


Figure 2.27: Operation strategy – forecast

By comparing Figures 2.25 and 2.27, a predictive operation strategy shows that due to the predicted reduced electricity generation on the next day, the electrical energy storage is not fully discharged. According to the predicted time range, the predictive operation strategy allows an efficient response to changes in generation, demand, and energy costs.

### 2.6.3 Electric Vehicles

Austria, like many other countries, has committed itself the goal of reducing CO<sub>2</sub> emissions. By the year 2050, Austria will achieve a mostly CO<sub>2</sub>-neutral transport sector. In addition to low-CO<sub>2</sub> fuels, electric mobility is a key technology for reaching energy and climate goals [51]. The introduction of electric vehicles (EV's) and the related installation of the required charging stations can significantly influence the planning and operation of electricity distribution networks, particularly in the LV and MV level (network level 5 to 7).

Due to the integration of EV's, LV distribution networks facing challenges such as

- high simultaneity of charging time<sup>1</sup>,
- high installed charging capacity of EV's,
- unknown behaviour in fault situations and
- unbalanced load in the network [53].

The integration of EV's will increase the electricity demand of households and the load on the network. According to the Austrian Energy Agency [54], Households in Austria currently have contractually the right to purchase between 3 and 5 kW over a specific time range. The charging capacity of EV's often reaches a multiple of the capacity of 3 to 5 kW. The maximum power supply for households in Austria usually is defined as 17.3 kW, limited by a 25 A fuse for each phase. Caused by the technical power limit of households, usually private charging stations with a charging capacity of 3.7 kW or 11 kW get installed [54]. A charging capacity greater than the commonly 11 kW respectively 22 kW is called fast charging. The supply of higher

<sup>1</sup> Charging events in the household sector may occur at the same time, e.g., in the evening [52].

charging capacities for households is technically difficult and cost-intensive to realise, e.g., installing of new cables and transformer.

The implementation of intelligent network-related solutions, such as demand-side management or tariff-based incentives, can limit the network load and thus reduce possible network expansions. Intelligent charging methods are based, for example, on the price of electricity, network capacity problems and local demand-side management [54], [55]. Since different measures can either increase the simultaneity of charging processes and thus limit the network or consumer load, an economically optimal compromise is necessary [56].

Losses occur when charging EV's. These charging losses are mainly composed of the converter losses and the thermal management of the battery [57]. The efficiency of charging an EV differs depending on the charging capacity. According to Sears et al. [58], Schäuble [57], Richardson et al. [59] and Garcia-Valle et al. [60] charging efficiencies between 85 % and 91 % can be achieved. The efficiency levels determined in the mentioned contributions are comparable with the efficiencies for Li-Ion batteries shown Table 2.4. The simulation model ProsOpt uses the round-trip efficiencies of EES listed in Table 2.4 for the EV calculation, see Section 2.2.1. Assuming identical losses during charging and discharging, for the charging/discharging process efficiencies between 89 % and 92 % are achieved, listed in Table 2.4.

### **Voltage and Reactive Power Control with EV's**

To comply the voltage limits according to national rules and standards [38], [39], inverter-based generators such as photovoltaic and electrical energy storage systems must implement voltage and reactive power control strategy's, see Section 2.6.1. In the field of EV's, the following restrictions influence the voltage and reactive power control in connection with EV charging processes. The EV is only available while the vehicle is connected to the electricity network. Further, the charging technology installed in the EV's itself hinders specific voltage and reactive power control strategies. However, measures such as voltage-active power mode, see Section 2.6.2, implemented in the charging station got already successfully tested in field tests [53], [55].

Wide network extensions and long radial feeders indicate rural low-voltage networks. This circumstance can lead to voltage problems at the connection point of the charging station under high load conditions due to high penetration of electric vehicles. To overcome this problem and comply with the standard EN 50160 [38], activation of the voltage-active power mode at the charging station can be chosen as measure.

Higher loads usually characterise urban low voltage networks with short cable lengths. Therefore, voltage problems like in the rural network are usually not a problem. In urban networks, overload problems can occur due to the higher number of network connection points [55].

## Range and Consumption of EV's

In 2012, 65 EV's available on the German market were evaluated by Probst [56] for their distribution and mean value of usable battery capacity, range and consumption. According to the results of this study, the battery capacities are multiplied by a factor of 0.8 and the ranges are divided by a factor of 1.625 in order to fit real-world conditions. The market study determined an average range of 100 km, with an average consumption of 20 kWh/100 km. The average usable battery capacity of EV was 20 kWh.

Since 2012, an improvement of the technology can be assumed. The ADAC Ecotest examined 19 EV's vehicles of different vehicle classes, in 2020 [61]. The evaluation of all vehicle classes showed an average range of 300 km, with an average energy consumption of 21 kWh/100 km. According to Statistics Austria [10] the average energy consumption of an EV in Austria is 15.7 kWh/100 km.

In mid-2018, the globally harmonized test procedure for passenger cars and light commercial vehicles WLTP<sup>1</sup> was introduced on a mandatory basis. This test procedure has replaced the European driving cycle NEDC<sup>2</sup>. Since this test procedure does not take into account power-consuming optional equipment such as air conditioning or seat heating. Therefore, a correction factor for consumption and range is calculated from the WLTP test conditions and the ADAC Ecotest, similar to Probst [56]. The evaluations have shown that the consumption is higher by approx. 1.16 to the consumption data of WLTP. The specified range of coverage for WLTP test conditions must be divided by the factor 1.20.

Using the LoadProfileGenerator LPG by Pflugradt [11], the information obtained on the consumption and range of electric vehicles is used to determine an electric vehicle's required electrical charging energy. For further information of the LoadProfileGenerator see sections 2.4 and 2.4.4.

## Electric Vehicle – V2G Model

Vehicle-to-Grid (V2G) describes the possible ability of an EV connected to the power network to act as an electrical energy storage (EES) system. Thus, an EV can compensate for the fluctuating generation of renewable energy sources or feed-back energy into the network [60]. The V2G function of an EV is implemented in the simulation model, as shown in Figure 2.28.

The storage capacity of the electric vehicle is separated into two parts. The yellow area shown in Figure 2.28 represents the capacity available for the V2G function. The blue area in Figure 2.28 is the capacity reserved for trips of the EV. This separation ensures that the V2G function does not use the full capacity of the EV to ensure

---

<sup>1</sup> Worldwide Harmonized Light Vehicles Test Procedure

<sup>2</sup> New European Driving Cycle

adequate capacity for trips. The storage capacities for V2G  $W_{V2G}$  and the trips  $W_D$  is calculated as follows.

$$\begin{aligned} W_{V2G} &= W_{EV} \cdot \text{DoD} \cdot k \\ W_D &= W_{EV} \cdot \text{DoD} \cdot (1 - k) \end{aligned} \quad (2.30)$$

DoD	Depth of Discharge in pu
$k$	Share of the storage capacity for V2G in pu
$W_D$	Storage capacity for trips in kWh
$W_{EV}$	Overall storage capacity of the Vehicle in kWh
$W_{V2G}$	Storage capacity for V2G in kWh

### Electric Vehicle – V2G Model

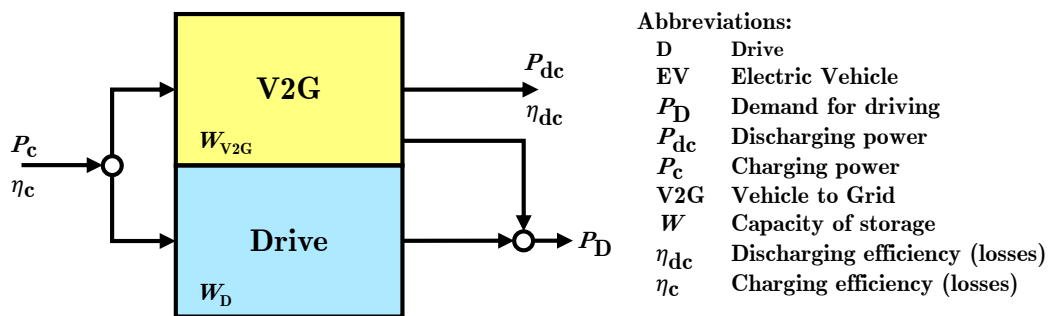


Figure 2.28: Electric Vehicle - V2G model

The EV is only available for the V2G function while the vehicle is connected to the power network. The LoadProfileGenerator (LPG) by Pflugradt [62] generates the arrival and departure times of the EV, see Section 2.4.4. The LPG simulates the behaviour of the occupants, e.g., driving to work. Thus arrival and departure times of the EV corresponds to the electrical demand of the household. The V2G function can easily deactivated by setting the factor  $k$  in Equation (2.30) to zero.

## 2.6.4 Solar Thermal System

In solar thermal systems, solar thermal collectors convert the solar irradiance into heat. This heat is used for, e.g., space heating and hot water needs, cooling as well as electrical power generation. The absorber of solar collectors is the essential component of a solar thermal system. The absorbed heat is then transferred to a heat transfer fluid, such as a water-glycol mixture [32]–[34]. The following three basic types of non-concentrated solar collectors are considered in detail.

### *Non-covered collector:*

These collectors are the technically simplest type available. Non-covered collectors consist of a solar absorber mat made of plastic with an integrated closely spaced piping system for the heat transfer fluid. These collectors are preferably used for heating open-air swimming pools. Since plastic is a poor heat conductor, the temperature of the heat transfer fluid is heated only slightly above or below the outside temperature. This small temperature difference to the environment leads to increased efficiency [32].

### *Flat plate collector:*

Flat plate collectors consist of an enclosure, a transparent cover such as glass, and an absorber. Compared to simple collectors, the enclosure of a flat plate collector alone reduces the heat losses to the environment. Furthermore, a selective coating of the absorber reduces heat radiation losses to the environment. Flat plate collectors thus achieve higher temperature levels and are used for producing hot water, district heating and process heat [32], [33].

A particular type is the combination of flat plate collectors with a heat storage tank as a single component. This collector is connected directly to the cold and warm water pipes, usually tap water. Thus, especially in Central and Eastern Europe, an additional electric heating cartridge is required to keep the system free of ice. For this reason, these collectors are mainly used in warmer regions. This design offers a compact construction but with the disadvantage of high heat losses at bad weather and at night [32].

### *Evacuated tube collectors:*

In evacuated tube collectors, glass tubes with a high vacuum significantly reduce heat losses through convection and thermal conduction, especially in the colder seasons. Evacuated tube collectors reach high operating temperatures above 100 °C. The absorber is located inside glass tubes so that the room behind the tubes is not fully used. Considering the total collector surface, the construction of evacuated tube collectors results in slightly lower efficiencies at low operating temperatures compared to flat plate collectors. A disadvantage of evacuated tube collectors is the significantly higher collector prices [32], [33].

Flat plate collectors have the largest market share in Europe. In China, on the other hand, evacuated tube collectors are used more frequently [32]. Next, the calculation

of collector efficiency for the collectors mentioned above, excluding the particular type of flat plate collectors, is explained in more detail.

The efficiency of a solar collector results from the absorbed solar irradiance reduced by thermal losses. The solar irradiance impinging on the collector is absorbed as heat by the absorber, taking into account a transmittance  $\tau$  of surrounding coverings. Neglecting losses, like reflection, convection and thermal radiation, results in maximum efficiency  $\eta_0$ . The following Equation (2.31) determines the collector efficiency  $\eta_c$  [33].

$$\eta_c = \eta_0 - \frac{a_1}{G_c} \cdot (\vartheta_c - \vartheta_a) - \frac{a_2}{G_c} \cdot (\vartheta_c - \vartheta_a)^2 \approx \eta_0 - \frac{a}{G_c} \cdot (\vartheta_c - \vartheta_a) \quad (2.31)$$

$\eta_0$	Maximum collector efficiency
$\eta_c$	Collector efficiency
$\vartheta_a$	Ambient temperature in °C
$\vartheta_c$	Collector temperature in °C
$a_{sol}$	Loss coefficient (linear fit) in $\frac{W}{m^2K}$
$a_1$	Linear loss coefficient in $\frac{W}{m^2K}$
$a_2$	Quadratic loss coefficient in $\frac{W}{m^2K^2}$
$G_c$	Irradiance on solar collector in $\frac{W}{m^2}$

This quadratic equation can be simplified as a linear function. To avoid too much inaccuracy by setting  $a_2$  to zero, the loss coefficient  $a$  must be determined as a fit from the linear function. Figure 2.29 shows the calculated collector efficiencies for different collector types.

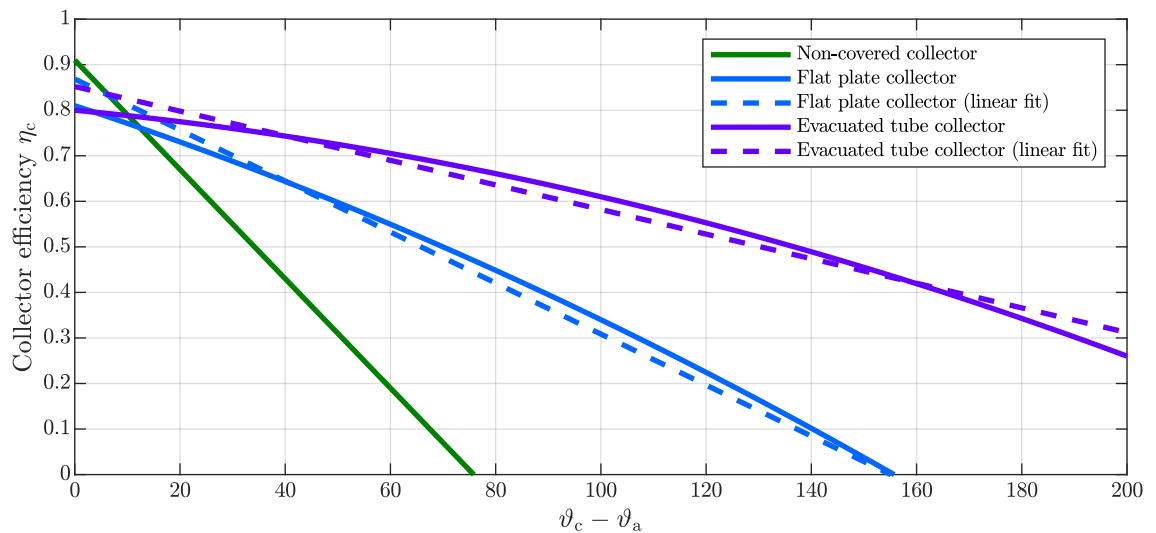


Figure 2.29: Collector efficiency for different temperature differences

Figure 2.29 shows the collector efficiency curve at different temperature differences. The collector efficiency increases with a raising irradiance  $G$ , which also leads to higher collector temperatures  $\vartheta_c$ . Further, the collector efficiency  $\eta_c$  decreases with lower ambient temperatures  $\vartheta_a$ . So the low collector efficiencies in winter times are caused by the low irradiance and the low ambient temperatures.

There is a small deviation due to the linear fit with a correlation coefficient of 99.28 % (R-square) for the flat plate collector and 97.69 % for the evacuated tube collector.

### Incidence angle modifier

A further influencing factor for the collector efficiency is the incidence angle  $\theta$  of the direct beam radiation  $G_{c,\text{dir}}$  on the collectors surface. As the incidence angle  $\theta$  increases, the reflections increase, which reduces the maximum efficiency  $\eta_0$  and must be corrected by the incidence angle modifier IAM. The incidence angle modifier IAM( $50^\circ$ ) at an incidence angle  $\theta$  of  $50^\circ$  as well as the absorption coefficient  $\alpha$  and the emissivity coefficient  $\tau$  can be found in data sheets of solar collectors. The maximum efficiency  $\eta_0$  depended on the incidence angle  $\theta$  can be described with the following Equation (2.32) [33], [63].

$$\eta_0(\theta) = \eta_{0i} \cdot \frac{F' \cdot \text{IAM}(\theta) \cdot G_{c,\text{dir}} + F' \cdot G_{c,\text{diff}}}{G_{c,\text{dir}} + G_{c,\text{diff}}} \quad (2.32)$$

with

$$\text{IAM}(\theta) = 1 - \left( \frac{1 - \text{IAM}(50^\circ)}{\arccos(50^\circ) - 1} \right) \cdot \left( \frac{1}{\cos(\gamma_s)} - 1 \right)$$

$\gamma_s$	Solar elevation angle (elevation) in $^\circ$
$\eta_{0i}$	Ideal collector efficiency
$\theta$	Incidence angle to the collector surface in $^\circ$
$F'$	Collector efficiency factor $\eta_0 = F' \cdot \alpha \cdot \tau = F' \cdot \eta_{0i}$
$G_{c,\text{diff}}$	Diffuse irradiance on the collector surface in $\text{W}/\text{m}^2$
$G_{c,\text{dir}}$	Direct beam irradiance on the collector surface in $\text{W}/\text{m}^2$
IAM	Incidence angle modifier

The incidence angle modifier IAM for the diffuse irradiance is neglected in Equation (2.32) and is assumed as unity. For evacuated tube collectors the incidence angle  $\theta$  is divided into a longitudinal  $\theta_l$  and a transversal  $\theta_T$  part.

$$\text{IAM}(\theta) = \text{IAM}_l(\theta_l) \cdot \text{IAM}_T(\theta_T)$$

with

$$\text{IAM}_l(\theta_l) = |\gamma_c + \arctan(\tan(90^\circ - \gamma_s) \cdot \cos(\alpha_s - \alpha_c))| \quad (2.33)$$

$$\text{IAM}_T(\theta_T) = \left| \frac{\arctan(\cos(\gamma_s) \cdot \sin(\alpha_s - \alpha_c))}{\cos(\theta)} \right|$$

$\alpha_c$	Geographical (azimuthal) orientation of the solar collector in $^\circ$
$\alpha_s$	Solar azimuth angle in $^\circ$
$\gamma_c$	Tilt angle of the solar collector in $^\circ$
$\gamma_s$	Solar elevation angle (elevation) in $^\circ$
$\theta_l$	Longitudinal incidence angle in $^\circ$
$\theta_T$	Transversal incidence angle in $^\circ$
$\text{IAM}_l$	Longitudinal incidence angle modifier
$\text{IAM}_T$	Transversal incidence angle modifier

## Mathematical Model of Solar Thermal System

Based on the Equations (2.31) and (2.32) the solar thermal system is implemented in ProsOpt similarly to an thermal energy storage. Which means, the gained energy from the environment – the solar irradiance  $G_c$  and the ambient temperature  $\vartheta_a$  – is stored in the fluid inside the collectors. Further, as shown in Figure 2.30, in addition to the environmental conditions, the inlet temperature  $\vartheta_{in}$ , the mass flow  $\dot{m}$  through the collector and the thermal capacity  $c$  of the heat transfer fluid influence the resulting collector temperature  $\vartheta_c$ . Thus the efficiency of the solar thermal system  $\eta_c$  is influenced by the environmental conditions, as well as the technical design of the thermal system [63].

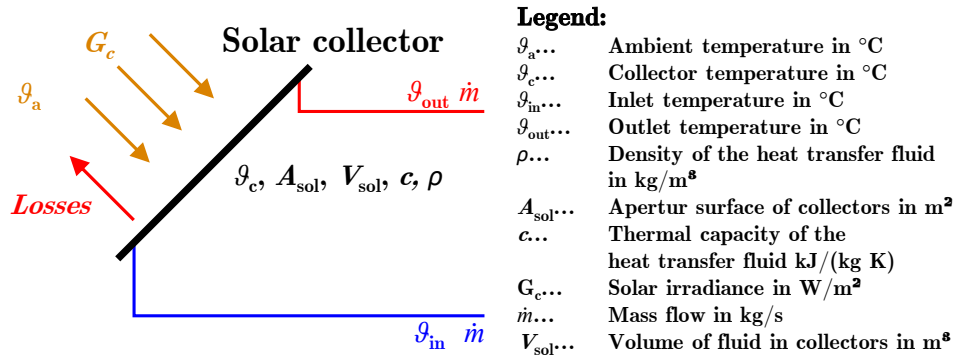


Figure 2.30: Schematic representation of a solar thermal system

The Equation (2.34) represents the mathematical description of the solar thermal system implemented in ProsOpt [63]. The solar thermal system's net thermal power  $\dot{Q}_{out}$  depends on the environmental energy input ( $G_c$ ,  $\vartheta_a$ ) and the actual mean collector temperature  $\vartheta_c$  (stored energy in the collector  $Q_{sol}$ ). The mean collector temperature  $\vartheta_c$  and thus, the stored energy  $Q_{sol}$  decrease as energy is extracted from the collector.

$$\dot{Q}_{out} = \dot{m} \cdot c \cdot (\vartheta_{out} - \vartheta_{in}) = G_c \cdot A_{sol} \left[ \eta_0(\theta) - \frac{a}{G_c} \cdot (\vartheta_c - \vartheta_a) \right] \quad (2.34)$$

The temperature of the solar heating system, shown in Figure 2.30 as the mean collector temperature  $\vartheta_c = \frac{\vartheta_{in} + \vartheta_{out}}{2}$ , also depends on the inlet temperature  $\vartheta_{in}$ . An increasing inlet temperature  $\vartheta_{in}$  will reduce the net thermal power  $\dot{Q}_{out}$  of the solar thermal system. Further, the actual mean collector temperature  $\vartheta_c$  of the solar thermals system can be calculated with the volume  $V_{sol}$  of the fluid inside the collectors and the actual energy level  $Q_{sol}$  in the collectors. The stored energy  $Q_{sol}$  results from the optimised operation of the hybrid energy system, see Section 2.2.1.

$$\vartheta_c = \frac{Q_{sol}}{V_{sol} \cdot \rho \cdot \frac{c}{3600 \frac{s}{h}}} + \vartheta_{ref} \quad (2.35)$$

$\vartheta_{ref}$   
 $Q_{sol}$

Reference temperature for energy calculations in °C  
Stored energy in the solar collector in kWh

## 2.6.5 Heat Pumps and Air Conditioners

Heat pumps and air conditioners are energy sources of heating systems which can regulate the room temperature of, e.g., a building. Both technologies are machines that raise heat from a lower to a higher level with the help of e.g. electric energy. Heat sources can be, e.g., ambient air, geothermal heat, groundwater and also waste heat from other processes. For thermodynamics, heat pumps and air conditioners do not differ from each other. Both the heat pump and air conditioner theoretically operate in a reversed Carnot cycle, which represents the maximum theoretical efficiency [5], [34], [64].

To simulate compression heat pumps and air conditioning machines, a catalogue data lookup approach is used. With this, the manufacturer's specifications of real-world machines are used to simulate the behaviour in different operating states via mathematical fit functions. These models are well suited to simulate machines already available on the market if they operate within the limits of the input variables [65].

The catalog data lookup approach is explained in more detail below. The following Figure 2.31 shows a surface plot of the manufacturer's specifications of the thermal power output  $\dot{Q}$  as a function of the flow  $\vartheta_{\text{flow}}$  and source inlet temperature  $\vartheta_{\text{source}}$  of a representative chosen air source heat pump.

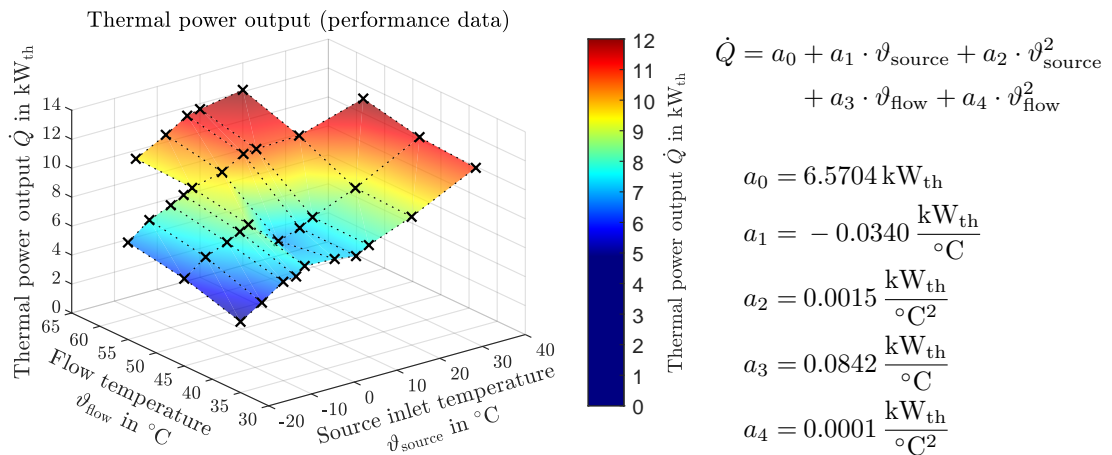


Figure 2.31: Thermal power output - performance data of a representative air source heat pump [66]

Using this catalogue data lookup approach, the mathematical fit functions determined for the electric power consumption  $P$  and the thermal power output  $\dot{Q}$  can be used to calculate the COP or, in the case of air conditioners, the EER (Energy Efficiency Ratio) according to the following equation.

$$\varepsilon_{\text{COP,EER}} = \frac{\dot{Q}}{P} \quad (2.36)$$

$\varepsilon_{\text{COP,EER}}$	Efficiency of heat pump (COP) or air conditioning system (EER)
$P$	Electric power consumption in kW
$\dot{Q}$	Thermal power output in kW <sub>th</sub>

This method can be used for air as well as ground source heat pumps. For the purpose of ground source heat pumps, the soil temperature  $\vartheta_{\text{soil}}$  can be determined from the ambient air temperature  $\vartheta_{\text{air}}$  using the following approach [67].

$$\vartheta_{\text{soil}}(t_i) = \vartheta_{\text{soil}}(t_{i-1}) + \frac{\Delta t \cdot k_{\text{soil}}}{c_{\text{soil}}(2 \cdot z_{\text{soil}})^2} \cdot (\vartheta_{\text{air}}(t_{i-1}) - \vartheta_{\text{soil}}(t_{i-1})) \quad (2.37)$$

$\Delta t$	Time step in s
$\vartheta_{\text{air}}$	Air temperature in °C
$\vartheta_{\text{soil}}$	Soil temperature in °C
$c_{\text{soil}}$	Volumetric heat capacity of the soil in J/m <sup>3</sup> K
$i$	Time index
$k_{\text{soil}}$	Thermal conductivity of the soil in W/mK
$t$	Time in s
$z_{\text{soil}}$	Depth in m

The following Figure 2.32 shows the calculated soil temperature  $\vartheta_{\text{soil}}$  as an annual curve (left) and at various depths (right). The optimum installation depth for horizontal earth collectors is below the frost line between 1.2 and 1.5 m [33]. For the simulations it is assumed that the soil temperature  $\vartheta_{\text{soil}}$  equals the source inlet temperature  $\vartheta_{\text{source}}$  for the heat pump. Typical values for the thermal conductivity  $k_{\text{soil}}$  and volumetric heat capacity  $c_{\text{soil}}$  for different kinds of soil are given in Table A.3 in the Appendix A.

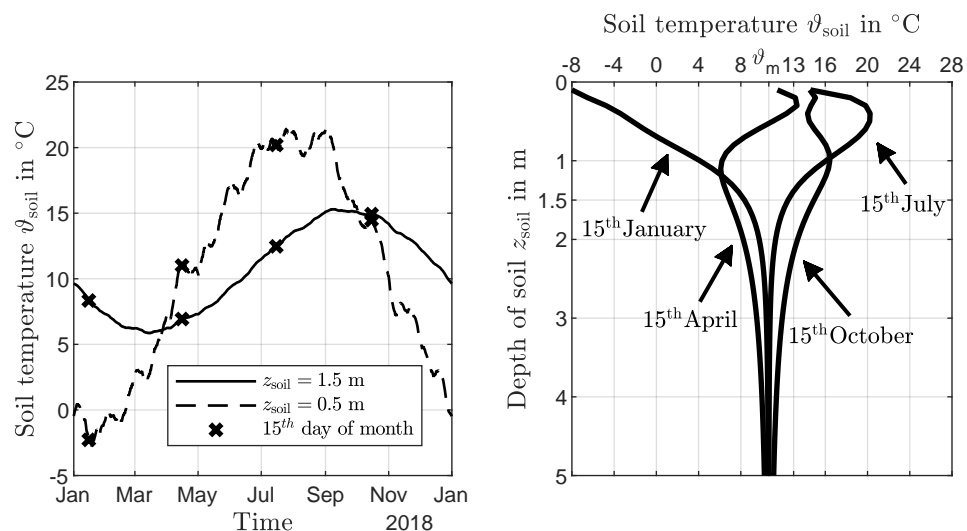


Figure 2.32: Soil temperature  $\vartheta_{\text{soil}}$  as an annual curve (left) and at various depths (right)

The Figure 2.32 (left) shows the soil temperature  $\vartheta_{\text{soil}}$  in a depth of 0.5 and 1.5 m. It can be seen that at a depth of 0.5 m the soil temperature  $\vartheta_{\text{soil}}$  gets within the frost line and the ground freezes in winter months. At a depth of 1.5 m the ground no longer freezes. Furthermore it can be seen that the soil temperature  $\vartheta_{\text{soil}}$  changes nearly sinusoidally within one year.

The Figure 2.32 (right) shows the soil temperature  $\vartheta_{\text{soil}}$  for four selected moments at different depths. The soil temperatures  $\vartheta_{\text{soil}}$  at shallow depths, e.g., 0.5 m are still strongly influenced by the air temperature  $\vartheta_{\text{air}}$ . At greater depths, e.g., 5 m, the soil temperature  $\vartheta_{\text{soil}}$  adapts to the mean air temperature  $\vartheta_{\text{m}}$ .

## 2.6.6 Domestic Gas Boiler

With a share of 23.5 % of primary heating systems (2017/2018), gas heating systems make a significant contribution to covering space heating and domestic hot water demand in Austria [68]. Conventional heating systems like domestic gas boilers are heating systems that use the chemically bound energy in fossil fuels to heat water. In a gas boiler, natural gas is burned in a combustion chamber and water is heated by means of a heat exchanger to cover the heat demand of a household.

It is not possible to use all the energy released during combustion. Small losses – usually about 1 % of the net heating value<sup>1</sup> (NHV) of natural gas – occur due to incomplete combustion (flue gas contains small amounts of unburned gases such as CO, H<sub>2</sub> and hydrocarbons), the energy content of the discharged ash and the heat transfer to the boiler installation room. The largest part of the losses are the flue gas losses, which are between 5 % and 15 % of the NHV, depending on the fuel of the boiler (natural gas, oil). In Austria, the NHV is often used as a reference value for calculating the boiler efficiency. If, however, partial condensation of the water contained in the flue gas occurs, it is recommended to use the gross heating value<sup>2</sup> (GHV) as a reference value for calculating the boiler efficiency, since using the NHV in this case results in a negative flue gas loss [70]. In a gas condensing boiler, the water vapour contained in the flue gas is condensed via heat exchangers and the condensation enthalpy is fed back to the heating system, improving boiler efficiency to around 93 % compared to the efficiency of standard gas boiler of about 85 % [71]–[73].

At a given reference temperature at standard conditions of 25 °C, the NHV and GHV links the enthalpies of the fuel and the minimum air volume with the enthalpy of the stoichiometric flue gas. The difference between NHV and GHV lies in the combustion products. At the NHV, the water contained in the stoichiometric flue gas is assumed to be gaseous. The GHV, on the other hand, refers to the dry stoichiometric flue gas and the completely condensed water [70].

The standard OENORM H 5056-1 [12] defines default values for calculating the efficiency of boilers with a nominal power  $P_N$  from 10 kW to 400 kW. The efficiency at full-load  $\eta_{\text{gas},100\%}$  and at part-load operation  $\eta_{\text{gas},30\%}$  of a gas boiler can be calculated according to OENORM H 5056-1 [12] with the help of Table 2.6 as follows.

$$\eta_{\text{gas},100\%} = (A + B \cdot \log(P_N)) \cdot \frac{1}{100\%} \quad (2.38)$$

$$\eta_{\text{gas},30\%} = (C + D \cdot \log(P_N)) \cdot \frac{1}{100\%} \quad (2.39)$$

<sup>1</sup> Net heating value (NHV) or lower heating value ( $H_i$ ): NHV = 10.22 kWh/Nm<sup>3</sup> in Styria, Austria [69]

<sup>2</sup> Gross heating value (GHV) or upper heating value ( $H_s$ ): GHV = 11.32 kWh/Nm<sup>3</sup> in Styria, Austria [69]

Table 2.6: Efficiencies of gas boiler according to [12]

Gas boiler type	Construction year	A	B	C	D
Gas boiler - Standard	from 1995	84 %	2 %	80 %	3 %
Condensing gas boiler	from 2015	95.9 %	1 %	106.7 %	1 %

### 2.6.7 District Heating

District heating (DH) is a type of heating system from which customers can obtain thermal energy via a heat distribution network. Various heat sources such as combined heat and power plants (CHP), waste heat from industry, heat pumps and solar thermal energy can be used to cover the thermal demand. The generation, as well as the distribution of heat in a DH-system, is not in the focus of this thesis. As a system boundary, the energy transfer station is used as an interface between the DH distribution system and the building heating system. The building heating system can be supplied via a direct or indirect connection to the DH distribution system. In the case of direct connection, the DH heating water flows through the building heating system to directly provide heat, e.g., to radiators. With an indirect connection, however, the DH heating water is separated hydraulically from the building heating system using a heat exchanger [74], [75].

The following two variants of heat supply have been implemented in ProsOpt within the scope of this thesis.

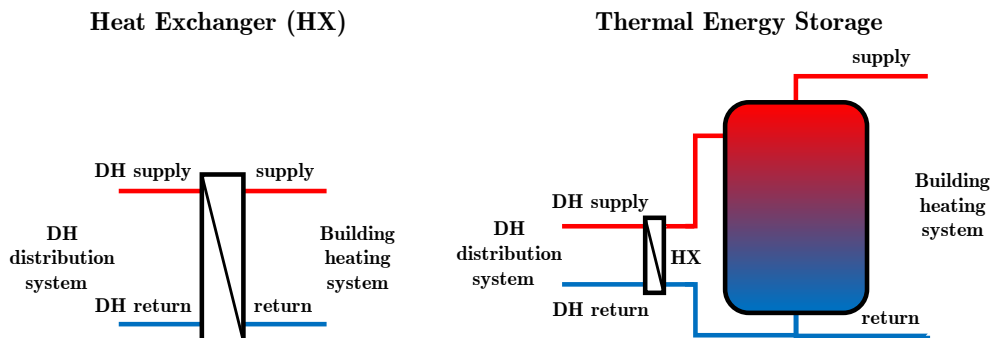


Figure 2.33: Implemented heat supply by district heating ([74], custom representation)

#### Heat Exchanger:

The supply water of the building heating system is heated by a heat exchanger only when needed. This means that the installed capacity of the HX to the DH distribution system must be sufficiently high to cover the heat demand at all times. The main advantages of this variant are the small space requirement combined with low costs and low heat losses in standby mode [74], [75].

#### Thermal Energy Storage:

The water in the thermal energy storage (TES) is heated by an external heat exchanger. Load peaks are covered by the TES, which means that the installed capacity of the HX can be reduced compared to the variant with a heat exchanger

without a thermal energy storage. However, this results in increased investment costs and additional heat losses caused by TES [74], [75].

The monthly losses of heat supply for space heating and hot water by district heating can be calculated according to the standard ÖNORM H 5056-1 [12] by Equation (2.40).

$$Q_{\text{DHlosses}} = 0.02 \cdot Q_{\text{load}} \quad (2.40)$$

$Q_{\text{DHlosses}}$	Monthly losses of heat supply for space heating and hot water in kWh
$Q_{\text{Load}}$	Monthly heating energy for space heating and hot water in kWh

Since district heating is used not only for heating but also for the domestic hot water supply of the household, supply temperatures higher than 60 °C are required at the customer's connection point to ensure safety against Legionella. The supply and return temperatures are different for each district heating network operator and season. This means that in the winter months supply temperatures between 95 °C and 155 °C and in the summer months supply temperatures between 70 °C and 85 °C are in use. The supply temperature in the summer months is lowered due to reduced consumption during this time of the year in order to reduce losses [76].

## 2.6.8 Thermal Energy Storage

Using thermal energy storage (TES), the use and expenditure of thermal energy can be temporally separated [77]. This means that the volatile generation of solar thermal systems can be temporarily stored or, in the case of a household sector, domestic heat water can be generated using electric cartridges depending on dynamic electricity tariffs. In this thesis, sensible thermal energy storage devices are considered for the short-term balance, several hours, between generation and demand for heating and cooling. Sensible heat is defined as a change in temperature during heat transport in a medium like water. The following Equation (2.41) gives the thermal energy as a function of temperature difference and heat capacity at constant pressure [78].

$$Q = m \cdot c_w \cdot \Delta\vartheta \quad (2.41)$$

$\Delta\vartheta$	Temperature difference in K
$c_w$	Specific heat capacity of water in J/kgK
$m$	Mass of water in kg
$Q$	Thermal energy in J

There are significant differences in the required temperature level of different heat sinks. Domestic hot water requires a temperature level of at least 60 °C to kill pathogens such as Legionella. Legionella proliferates mainly at temperatures between 25 °C and 45 °C and begins to die at 55 °C. To prevent legionella in drinking water, the stand-by volume of the thermal energy storage for reheating the drinking water should therefore never drop below 60 °C [74]. In contrast, heating water is operated with

significantly lower temperatures, such as flow temperatures of 35 °C for underfloor heating, in order to minimise heat losses.

Based on the approach of Steen et al. [4], a stratified thermal energy storage (TES) with three mixed zones (high (HT), low (LT) zones and the cold fresh water (CW) zones) is modelled as shown in the Figure 2.34.

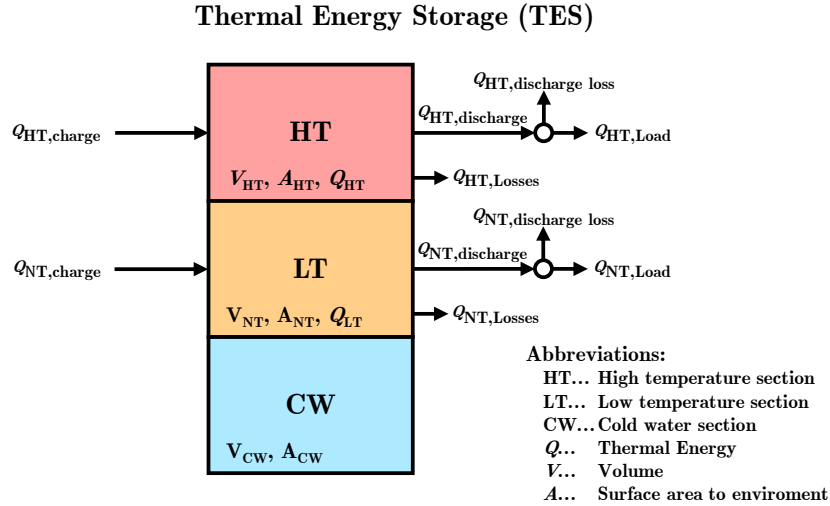


Figure 2.34: Schematic illustration of the used TES model

The approach of Steen et al.[4] do not consider the second law of thermodynamics, which accurately calculates the different temperature zones of the TES. This temperature calculations, however, cannot be used as a variable with the used optimisation algorithm and causes an endogenous optimisation problem that cannot be solved by the MILP solver (Mixed Integer Linear Programming).

For this reason, three temperature zones, each with a constant temperature level, are implemented, see Figure 2.34. This three temperature zones share the water volume of the TES. For example, discharging the HT zone results in a reduced volume of the HT zone and an increased volume of the CW zone. The storage capacity of each temperature zone, and the respective charging and discharging energy of the TES are variables of the MILP solver, see Section 2.2.1.

With the used approach of Steen et al. [4] to model a TES, heat sources with different temperatures, e.g., heat pumps and solar thermal systems, can be used together. The stored energy in each temperature zone in the TES and the storage losses to the ambient are calculated according to Equations (2.42) and (2.43).

$$Q_{\text{Storage}} = V \cdot \rho_w \cdot c_w \cdot (\vartheta - \vartheta_{\text{ref}}) \quad (2.42)$$

$$Q_{\text{Storage,Losses}} = U \cdot A \cdot (\vartheta - \vartheta_a) \quad (2.43)$$

$\vartheta$	Temperature of the medium in °C
$\vartheta_a$	Ambient temperature in °C
$\vartheta_{\text{ref}}$	Reference temperature in °C
$\rho_w$	Specific density of the medium kg/m <sup>3</sup>

$A$	Surface area of the TES to the environment in $\text{m}^2$
$c_w$	Specific heat capacity of the medium in $\text{J/kg K}$
$Q_{\text{Storage}}$	Stored thermal energy in TES in $\text{J}$
$Q_{\text{Storage, Losses}}$	Losses of the TES to the environment
$U$	Overall heat transfer coefficient of the TES in $\text{W/m}^2 \text{K}$
$V$	Volume of TES in $\text{m}^3$

## 2.7 Load Flow Calculations

In this thesis, time-series based load flow calculations are coupled with the developed simulation model ProOpt to investigate the influence of optimising prosumers on the low-voltage distribution network. The load flow calculations are performed with the software Matlab over one year and a temporal resolution of 15 minutes.

The load flow calculation is an analytical method to calculate electrical power networks and aims to calculate the voltages in the network nodes, the load flow in the elements as well as the active and reactive power losses, based on a particular load situation. A specific node type is assigned to each network node. According to the problem to be solved, there are different advantages and disadvantages in the simulation, depending on the node types. In the following Table 2.7 the different node types are listed [79], [80].

Table 2.7: Overview of the different node types - load flow calculation [79], [80]

Node type	Element	Given values	Calculated values	Annotation
Slack node	Power plant, Feed-in from the higher voltage level network	$\underline{V}$	$\underline{S}$	At least 1 slack node needed in network
		$V, \vartheta$	$P, Q$	$\vartheta = 0$
PQ	Load, power plant	$\underline{S}$ $P, Q$ $P, \cos(\varphi)$ $Q, \sin(\varphi)$	$\underline{V}$ $V, \vartheta$	Non-linear problem
PV	Power plant	$P, V$	$Q, \vartheta$	Non-linear problem Q limits must be monitored
I	Load	$I$ $I, \cos(\varphi)$	$\underline{V}$ $V, \vartheta$	Linear problem

The load flow calculation analytically determines the thermal limits of elements such as cables, overhead lines and transformers as well as the voltage limits [79], [80]. The standard EN 50160 [38] defines the voltage characteristics of electricity supplied by public electricity networks. This standard specifies that the supply voltage in low-voltage networks may change by a maximum of  $\pm 10\%$  of the nominal voltage  $V_N$ . In Austria, national rules – “TOR - Technische und organisatorische Regeln für Betreiber und Benutzer von Netzen [39]“ – regulate the requirements for operators and users to connect with the public electricity network. According to TOR, a maximum voltage increase in the low-voltage network, caused by power generation systems of  $\Delta v = 3\%$  at each node must be guaranteed.

In order to solve the non-linear problems, the Newton-Raphson method is used. The Newton-Raphson-method is an iterative method to solve non-linear problems and offers the advantage to converge fast to the end values. The power output of the prosumers at their respective PCC (Point of Common Coupling) – see Figure 2.2 – resulting from the optimised operation, are implemented in the load flow calculations as PQ-nodes. In Figure 2.35 the methodology of the Newton-Raphson method used for network calculations in combination with ProsOpt is explained in more detail using a flowchart.

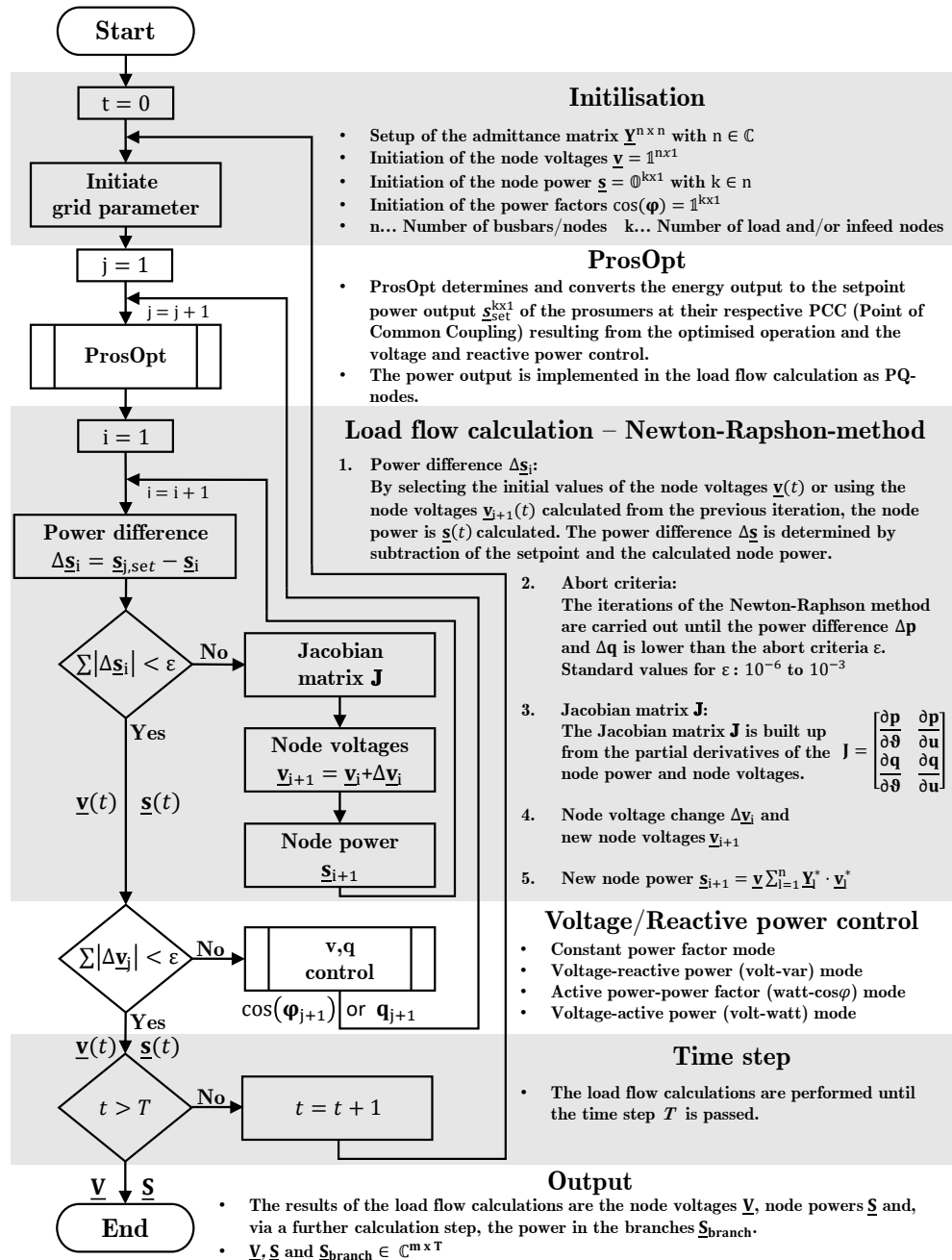


Figure 2.35: Methodology - load flow calculations

# 3 Optimisation of Hybrid Energy Systems

The developed simulation model ProOpt is used to analyse the operation of an optimising prosumer based on the example of a single-family house. With ProOpt, the optimal use of the energy generation and storage systems is determined using a linear optimisation algorithm (MILP – Mixed Integer Linear Programming), which taking the desired energy services, external boundary conditions, e.g., weather, and cost functions of the system components into account .

ProOpt can analyse a large number of scenarios, e.g., different types of technologies and optimisation objectives as well as varying consumers behaviour. Therefore, a corresponding prosumer set-up is defined in advance for subsequent investigations.

The energy demand of a single-family house is based on the electrical demand – domestic appliances and lighting – and the thermal demand, such as heating, cooling and domestic water heating. Furthermore, the construction of the building strongly influences the heating and cooling behaviour. With a share of 85 % of the total energy demand of households, space and domestic water heating have a significant impact on hybrid energy systems. Additionally, the charging of an electric vehicle is considered in the analyses.

Focus of the following analyses lies in the resulting electrical demand of prosumers, when the electrical and thermal systems are coupled together to a hybrid energy system. For this purpose, a heat pump is used to cover the heating demand and an air conditioning system to cover the cooling demand. In the following, a photovoltaic system in combination with electrical and thermal energy storages is used to cover a certain amount of the energy demand of a household.

In general, the following analyses are carried out to investigate an optimising prosumer:

1. *Degree of Autonomy and Self-Consumption of a Prosumer:*

The degree of autonomy, as well as the degree of self-consumption, are essential indicators to evaluate the efficient use of energy generated by renewable energy systems such as PV systems. A detailed analysis of the degrees of autonomy and self-consumption achievable by a prosumer, considering varying electrical generation and storage systems, is performed. Furthermore, the influence of different building structures and consumer behaviour is evaluated.

2. *Economic Optimum of a Prosumer:*

Both the capital and operating expenditures of photovoltaic (PV) and electrical energy storage (EES) systems significantly influence the profitability of a prosumer. The economic optimum of the examined prosumer is determined for different capital expenditures and system capacities (PV and EES), as well as for varying static electricity purchase tariffs and feed-in tariffs.

3. *Impact of Energy Tariffs on Prosumer Behaviour:*

Since consumption and generation do not coincide in every time step, without the use of energy storages or demand-side management, it is possibly necessary to purchase or feed-in energy at suboptimal tariffs or to adapt the load profile (i.e. consumer behaviour) according to the tariff situation. The impact of tariff regimes commonly used in Austria, the static, high and low tariffs (HT/NT) and a newly offered dynamic tariff are investigated.

4. *Storage Strategies: Forecast versus Self-Consumption:*

Grid-connected photovoltaic systems represent a relevant field of application for EES's, specifically to compensate the fluctuating generation from photovoltaic systems and the gap between generation and consumption in the short term. Suitable charging management can significantly improve the degree of autonomy as well as the degree of self-consumption. A commonly used storage strategy to maximise the degree self-consumption without any forecast methods getting compared with a forecast-based storage strategy.

5. *Economical and Ecological Optimisation of a Prosumer:*

For defined scenarios, the simulation model ProsOpt performs economical and ecological optimisations. For each defined scenario, a heat pump, thermal energy storage with a respective heating cartridge, and an air conditioning system couple the electrical and thermal systems and form a hybrid energy system. The analyses' main focus lies on the influence of the respective optimisation objectives – economic and ecological – on the annual energy costs and the annual CO<sub>2</sub> emissions of the prosumer.

In order to determine the significance of storage systems, the correlation between the demand and the generation of a PV system is formed. Times of demand, at which the PV system also generates energy, are identified. However, this does not imply that the PV system completely covers the electrical demand. Figure 3.1 graphically illustrates the correlation for each demand class, for every hour over one year and a power higher 100 W. Orange colour represents the PV system's generation. The blue areas illustrate the demand without correlation, and the green areas indicate the correlation between the demand and the generation of the photovoltaic system. Furthermore, as the the Pearson correlation coefficient  $\rho$  is calculated and displayed.

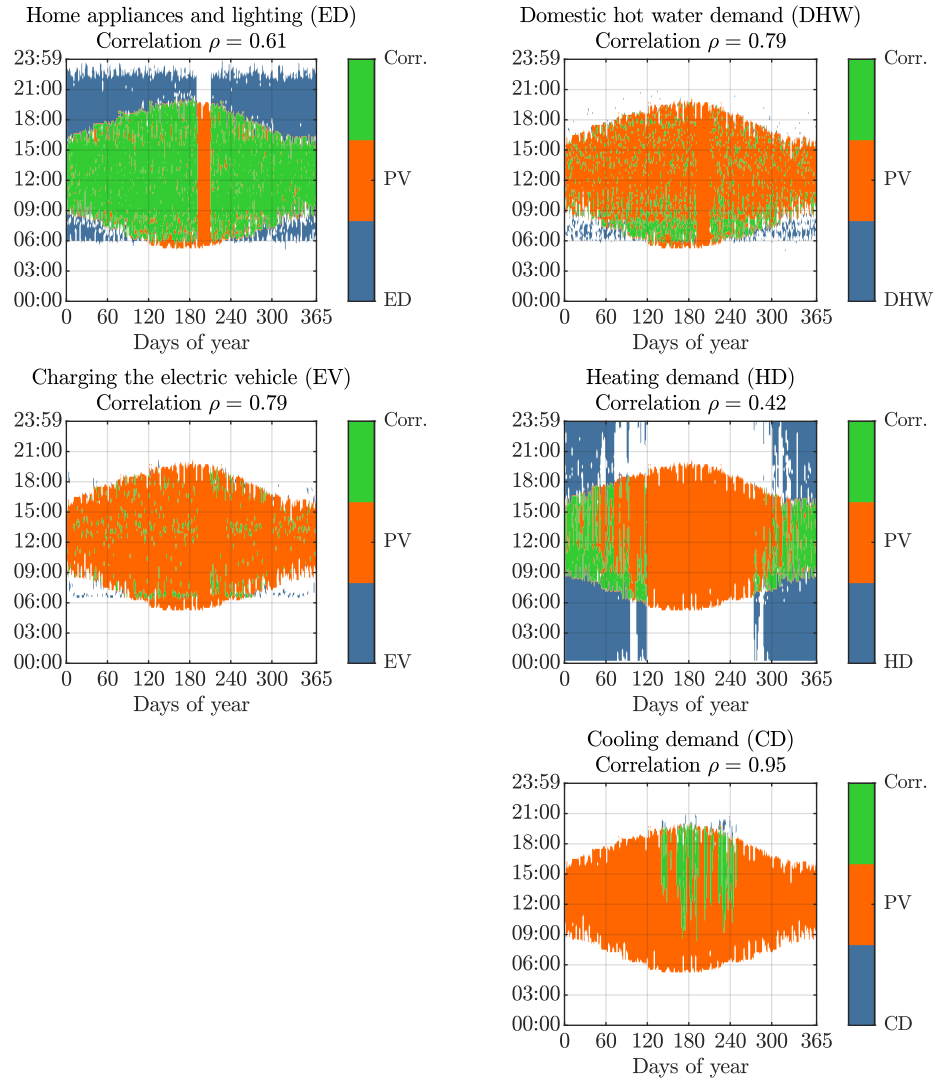


Figure 3.1: Correlation between demand and the generation of the PV system

Figure 3.1 shows the correlations between the electrical and thermal consumption and the PV generation of the respective prosumer. The correlation varies depending on consumer behaviour. In addition to the graphical illustration, the Pearson correlation coefficient is used to evaluate the correlation.

The Pearson correlation coefficient  $\rho$  measures the correlation between two continuous variables. The coefficient  $\rho$  is dimensionless and ranges between  $\pm 1$  (negative or positive linear correlation). At  $\rho = 0$ , there is no linear relationship between the two variables. The higher the Pearson correlation coefficient gets to  $\pm 1$ , the stronger the correlation. Compared to the According to Schober and Boer [81] the correlation coefficient can be interpreted as follows:

- Negligible correlation:  $\rho = 0.00 - 0.10$
- Weak correlation:  $\rho = 0.11 - 0.39$
- Moderate correlation:  $\rho = 0.40 - 0.69$
- Strong correlation:  $\rho = 0.70 - 0.89$
- Very strong correlation:  $\rho = 0.90 - 1.00$

*Domestic Appliances and Lighting (ED), and Charging of Electric Vehicle (EV):*

The electrical demand of the domestic appliances and lighting, and the charging demand of the electric vehicle, is highly dependent on consumer behaviour. General statements regarding the correlation between electrical demand and PV generation can not be concluded from Figure 3.1. An electrical energy storage (EES) system can be used to cover the demand of domestic appliances and lighting occurring at the evening and during night-time. In the case of the prosumer shown in Figure 3.1, the charging behaviour of the electric vehicle shows a strong correlation and thus corresponds well with the generation of the PV system.

*Domestic Hot Water Demand (DHW):*

The domestic hot water demand shows a strong correlation with the PV system. However, Figure 3.1 reveals that in winter in the morning hours, the domestic hot water demand and the PV generation no longer match. Therefore, in the simulations a thermal energy storage with heating cartridges is used to cover the domestic hot water demand.

*Heating (HD) and Cooling Demand (CD):*

Figure 3.1 shows a moderate correlation between heating demand and the generation of the PV system. As expected, the heating demand occurs in the cold season at low PV generation and especially during night time due to missing solar radiation. An energy storage system would improve the utilisation of the photovoltaic system to cover thermal demand.

In contrast to the heating demand, the cooling demand correlates perfectly with the generation of the photovoltaic system in summer. For this reason a cold storage is not taken into account in the simulations.

As the operation of the prosumer depends strongly on the demand and technology, the following initial parameter settings and loads are selected for simulations.

Table 3.1: Initial parameter settings - Prosumer (Scenario S1)

Photovoltaic system (PV):	Installed power $P = 6.1 \text{ kW}_p$
Electrical energy storage (EES):	Capacity $W = 7 \text{ kWh}$
Thermal energy storage (TES):	Volume $V = 300 \text{ litres}$
Heating cartridge - TES:	Power $P = 2 \text{ kW}$
Heat pump (HP):	Heating power $P = 7.63 \text{ kW}_{th}$ (A2/W35)
Air conditioner (AC):	Cooling power $P = 8.11 \text{ kW}_{th}$ (A35/W18)
Electrical demand (ED):	Annual demand $W = 4700 \text{ kWh/a}$
Electric vehicle (EV):	Annual charging demand $W = 1000 \text{ kWh/a}$
Heating demand (HD):	Annual demand $W = 75 \text{ kWh/m}^2\text{a}$ (min. indoor temperature $\vartheta = 22 \text{ }^\circ\text{C}$ )
Cooling demand (CD):	Annual demand $W = 6 \text{ kWh/m}^2\text{a}$ (max. indoor temperature $\vartheta = 26 \text{ }^\circ\text{C}$ )
Domestic hot water (DHW):	Annual demand $W = 2063 \text{ kWh/a}$ (max. water temperature $\vartheta = 60 \text{ }^\circ\text{C}$ )
Building	Conditioned floor area $A = 72 \text{ m}^2$

## 3.1 Degree of Autonomy and Self-Consumption of a Prosumer

In a PV-Storage system, the generated electrical energy is consumed either instantaneously or at a later time using storage systems. The degree of autonomy DA and the degree of self-consumption DSC are essential indicators in evaluating the efficient use of the energy generated by renewable generation systems such as PV systems. Both indicators can be expressed as follows. A more detailed explanation about DA and DSC can be found in Section 2.6.2.

The degree of autonomy DA indicates the share of demand covered by the PV combined with the EES. The degree of autonomy thus indicates the independence from the power network. [46], [48].

The degree of self-consumption DSC specifies how much of the PV's generated energy is consumed by the prosumer. The higher the degree of self-consumption, the less energy is fed into the power network by the PV system [46], [48], [49].

Based on the significance of these two indicators – DA and DSC – to evaluate the efficient use of the energy generated by the PV system, an optimising prosumer's operation, with the objective to maximise the DSC, is simulated with the simulation model ProsOpt. ProsOpt performs annual simulations with a time resolution of 15 minutes and an ideal forecast of 72 hours.

In the following and starting from the initial parameter settings stated in Table 3.1, the sensitivities of the DA and DSC according to varying PV and EES system sizes, changing consumer behaviour, and different building structures are evaluated. The following four main scenarios are analysed:

### *Scenario S1: Reference*

Reference scenario based on the chosen parameters in Table 3.1. The consumer behaviour for domestic appliances and lighting is characterised by loads peaks at the morning hours and mainly at midday. The annual heating demand of 75 kWh/m<sup>2</sup>a complies with a newly built standard house until the 2000s.

### *Scenario S2: Low-Energy House*

The house's thermal insulation is improved, resulting in an annual heating demand of 38 kWh/m<sup>2</sup>a. Compared to S1 (Reference), the annual heating demand is halved.

### *Scenario S3: Old Building*

The house corresponds, with an annual heating demand of 170 kWh/m<sup>2</sup>a, to an old house standard (1950s). Compared to S1 (Reference), the annual heating demand is more than twice as high.

### *Scenario S4: Morning Load Peaks*

The consumer behaviour for domestic appliances and lighting is characterised

by loads peaks mainly in the morning hours. Compared to S1, the annual electrical demand is reduced by 45 % to 2600 kWh/m<sup>2</sup>a. Furthermore, the electric vehicle is being charged more frequently at home, resulting in a more than doubled annual energy demand for charging of 2300 kWh/m<sup>2</sup>a compared to S1 (Reference).

The Table 3.2 below provides a summary overview of the annual energy demand according to the individual main scenarios.

Table 3.2: Scenarios – Annual energy demand according to the individual main scenarios

Demand	S1 Reference	S2 Low-Energy House	S3 Old Building	S4 Morning Load Peak
ED	4700 kWh/a	4700 kWh/a	4700 kWh/a	2600 kWh/a
EV	1000 kWh/a	1000 kWh/a	1000 kWh/a	2300 kWh/a
DHW	2063 kWh/a	2063 kWh/a	2063 kWh/a	1300 kWh/a
HD	75 kWh/m <sup>2</sup> a	38 kWh/m <sup>2</sup> a	170 kWh/m <sup>2</sup> a	75 kWh/m <sup>2</sup> a
CD	6 kWh/m <sup>2</sup> a	7 kWh/m <sup>2</sup> a	10 kWh/m <sup>2</sup> a	6 kWh/m <sup>2</sup> a

ED... Electrical demand      EV... Demand of electric vehicle  
 HD... Heating demand      DHW... Domestic hot water demand  
 CD... Cooling demand

For each of the four main scenarios, varying PV and EES system sizes are analysed:

- The installed power of the PV is varied from 0 kWp to 16 kWp.
- The storage capacity of the EES is varied from 0 kWh to 20 kWh.

In addition to these modifications, in the following analyses, the parameters chosen in Table 3.2 remain unchanged.

## Results

Figure 3.2 graphically represents the calculated degrees of autonomy and self-consumption as contour-plots for each scenario. In a contour plot, areas with the same colour and along the shown isolines correspond to the same degrees of autonomy DA and self-consumption DSC. There are two different ways to use the contour-plots shown in Figure 3.2.

- 1) The PV-Storage system is sized based upon the achievable DA and DSC using the isolines and coloured areas in Figure 3.2. For example, an exemplary sized PV-Storage system should achieve a DA of 50 % and the best possible DSC. As shown Figure 3.2 with black crosses (S1 Reference), a PV system's installed power of 6 kWp and an EES system's capacity of 7 kWh are sufficient to obtain this goal by reaching a DSC of 80 %. Selecting a larger EES, e.g., 20 kWh, would only result in a minor DSC improvement of 4 % to 84 %.

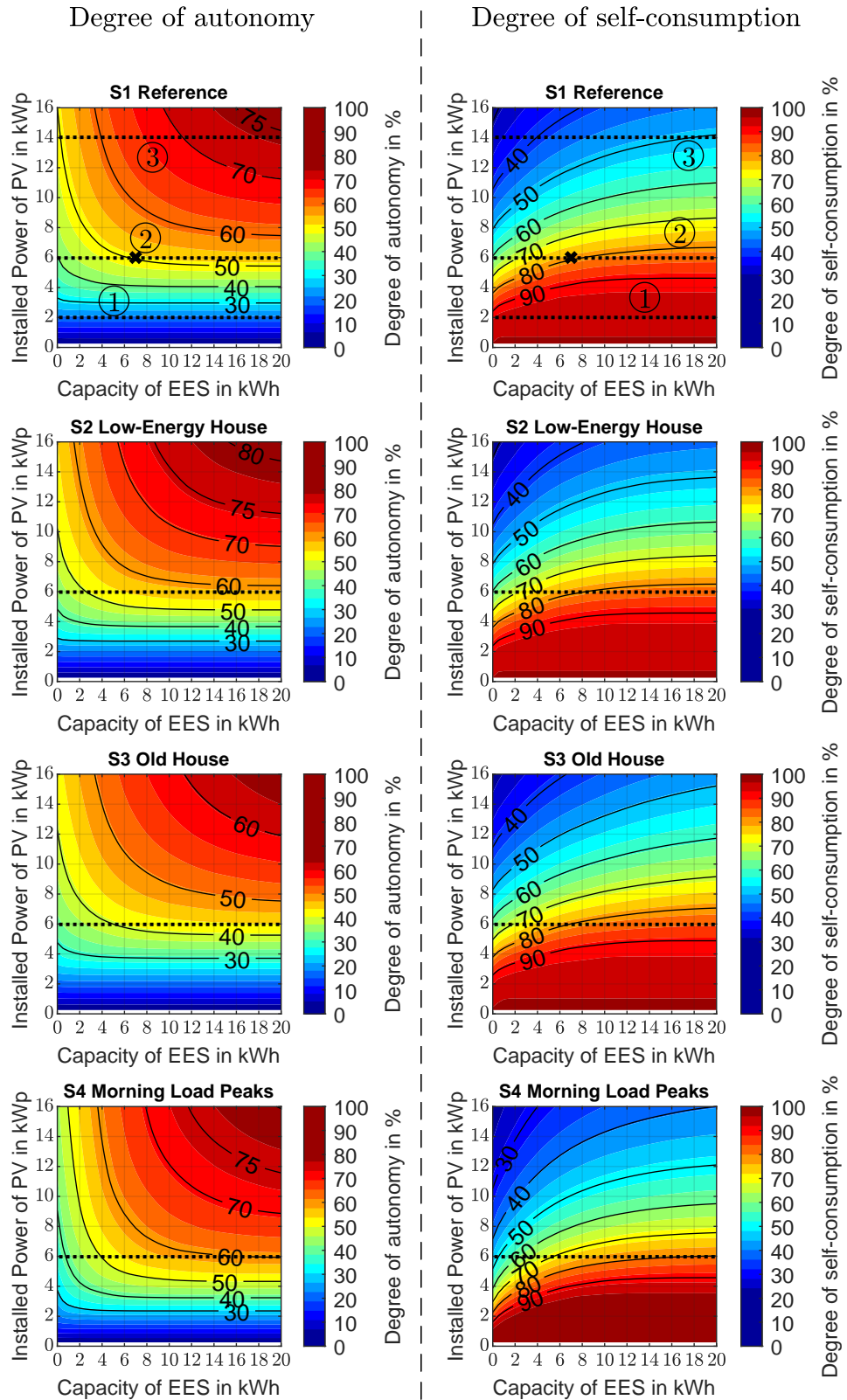


Figure 3.2: Degree of autonomy and self-consumption of prosumers – Scenarios S1 to S4

- 2) Based on a given PV system, the DA and DSC improvements by using an EES system can be determined. In the following, the influence of different EES system capacities on the DA and DSC for Scenario S1 (Reference) and three selected PV systems (①: 2 kWp, ②: 6 kWp, ③: 14 kWp) is examined in detail.
- ① The installation of a 2 kWp PV system without using an EES leads to a DA of 18.1 %. Due to the high DSC of 94 % achieved by the PV system alone, the EES usage results only in a marginal increase of the DA of 0.2 % to 18.3 %. Nearly the entire PV generation is consumed instantaneously by the prosumer.
  - ② The installation of a 6 kWp PV system, commonly installed in Austrian household sector, leads to a degree of autonomy of 40 %. The DA can be increased by using an EES system. With an EES capacity of 20 kWh, the DA is raised to 53 %. However, there is no significant increase in the DA above a storage capacity of approximately 7 kWh. An increase of the EES capacity from 7 kWh to 20 kWh, thus a tripling of capacity, increases the DA just by 3 % from 50 % to 53 %. This means that the EES with a storage capacity of 7 kWh already uses most of the available surplus generation of the PV system. Larger EESs are not entirely utilised and increase the DA and DSC only in a few moments of the year where the 7 kWh EES would be already fully charged.
  - ③ The 14 kWp PV system without using an EES system leads to a DA of 49 %. Since most of the demand coinciding with the PV generation is already covered by the 6 kWp system, the DA of the 14 kWp system increases by only 9 %, even though the PV system is more than doubled. Compared to ②, the DA can be significantly increased by using an EES system. With an EES capacity of 20 kWh, the DA is raised to 75 %.

The degree of autonomy and self-consumption depends, in addition to the size of the PV and EES system, mainly on the prosumer's demand and consumer behaviour. In order to show the sensitivity of the DA and DSC, the simulation results (S2 to S4) with changed thermal and electrical demand compared to S1 (Reference) are analysed.

*Scenario S2 & S3 - House with Changed Heating and Cooling Demand:*

- In scenario S2 (Low-Energy House), the heating demand of the investigated building is halved from 75 kWh/m<sup>2</sup>a (S1 Reference) to 38 kWh/m<sup>2</sup>a. This reduction of the thermal demand, supplied by a heat pump, affects the DA, which is increased. However, the DSC remains almost the same in comparison to scenario S1 (Reference).

This small impact of the thermal demand on the DSC can be explained by the fact, that the heating demand occurs during the cold season mainly at night and at times of low or no PV generation. The generated energy of the PV system gets mainly consumed by the domestic appliances and lighting, the

domestic water heating as well as the charging of the electric vehicle.

- In scenario S3 (Old House), the building's heating demand is more than doubled from 75 kWh/m<sup>2</sup>a (S1 Reference) to 170 kWh/m<sup>2</sup>a. Similar to scenario S2 (Low-Energy House), the change of the heat pump supplied thermal demand mainly influences the DA, which is reduced due to the significantly increased energy demand. Due to the same reasons as in scenario S2, the DSC is only slightly affected by the increased thermal demand.

*Scenario S4 - Morning Load Peaks:*

In Scenario S4, the consumer behaviour is changed compared to Scenario S1 (Reference), while the heating and cooling demand remains the same. The change in consumer behaviour affects the use of domestic appliances and lighting, reduced by 45 % to 2600 kWh/a, the domestic hot water demand, reduced by 37 % to 1300 kWh/a, as well as the charging behaviour of the electric vehicle, increased by 130 % to 2300 kWh/a.

Due to the changed consumer behaviour in scenario S4 with load peaks occurring most frequently during the morning hours, there exists only a small correlation between PV generation and demand, since in the morning hours the PV can not cover the increased demand. Therefore, the DA is reduced compared to scenario S1 (Reference), although the annual energy demand of S4 is about 1000 kWh lower than S1. The installation of 6 kWp PV system without using an EES leads to a degree of autonomy of 35 %.

Because of the small correlation between PV generation and demand, and the reduced energy demand, an EES system installation results in a higher impact on the DA than scenarios S1 to S3. With an EES capacity of 20 kWh the DA is raised from 35 % to 60 %.

*General Statements:*

In general, Figure 3.2 shows that the combination of PV and EES can significantly increase the DA as well as the DSC. However, even with a PV system with a installed power of 16 kWp (17.2 MWh/a) and a EES system with a capacity of 20 kWh, the maximum achievable DA is between 77 % (S1 Reference) and 81 % (S3 Old House). Although, with a DSC between 40 % (S4 Morning Load Peaks) and 48 % (S3 Old House), less than the half of the generated energy is consumed by the prosumer itself. This discrepancy results from the seasonal difference between generation, highest yield during summer, and demand, highest demand in the winter, of the prosumer.

Photovoltaic and electrical energy storage systems require an optimal dimensioning of their system capacities. To achieve autarky (DA = 100 %), PV-Storage systems need to be dimensioned in a disproportionate size so as to cover the high energy demand in winter and during long periods of reduced energy generation.

A further possibility to efficiently use the generated energy and therefore to increase the DA and the DSC, is the adaption of the energy demand to the generation of the PV system. This adaptation process is often difficult to achieve due to the consumers' lack of flexibility. Such flexibilities in the household sector could be

the domestic appliances' coordinated operation or a changed heating behaviour by increasing the room temperature during day time. Further, with market-dependent or special prosumer tariffs, the prosumer can be motivated to use the generated energy efficiently.

## 3.2 Economic Optimum of a Prosumer

Both the capital (CAPEX) and operating (OPEX) expenditures of photovoltaic (PV) and electrical energy storage (EES) systems significantly influence the profitability of a prosumer. Therefore, the investigated prosumer's economic optimum of the annual energy costs is determined at varying capital expenditures and system capacities for the PV and the EES system, as well as varying electrical energy purchase and feed-in tariffs.

In the following, the annual energy costs of an optimising prosumer, with the objective to maximise the degree of self-consumption, are calculated for different chosen scenarios using ProsOpt. The simulation model ProsOpt performs annual simulations with a time resolution of 15 minutes and an ideal forecast of 72 hours.

As shown in Table 3.3, eight main scenarios are defined to analyse the sensitivities of the annual energy costs for the investigated optimising prosumer with the initial parameter settings stated in Table 3.1 to varying capital expenditures and energy tariffs. Further, for each of the eight main scenarios, the following varying PV and EES system sizes are analysed:

- The installed power of the PV is varied from 0 kWp to 16 kWp.
- The storage capacity of the EES is varied from 0 kWh to 20 kWh.

For each analysed scenario, the Levelized Costs of Electricity (LCOE) of the PV and the EES systems are calculated. The LCOE is calculated according to the net present value method, including the CAPEX and OPEX and the PV or EES's annual generated/stored energy. A detailed explanation about the LCOE can be found in Section 2.5.

Using the technologies' levelised costs of electricity (LCOE) and at the given energy tariffs, the total annual energy costs for the prosumer's optimising operation are subsequently calculated. For an easier comparison of the results, each scenario's calculated total annual energy costs at varying PV and EES system sizes are normalised to the corresponding economic minimum.

The CAPEX of PV and EES systems and the electrical energy tariffs significantly affect the annual energy costs of a prosumer. Typical CAPEX for PV and EES systems and electrical energy tariff costs for Austria and Germany are given below.

### *CAPEX of PV Systems:*

According to Biermayer et al. [82], the average CAPEX in Austria for a grid-connected PV system is 1569 €/kWp in 2019. Based on analyses of Figgener et al. [83], the mean CAPEX of a PV system in Germany ranged from

1000 €/kW<sub>p</sub> to 1800 €/kW<sub>p</sub> in 2018, with an average CAPEX of 1400 €/kW<sub>p</sub>.

*CAPEX of EES Systems:*

The CAPEX of an EES system, depending on the usable storage capacity, range in Germany between 1000 €/kWh and 2250 €/kWh, at average CAPEX of 1400 €/kWh in 2018 [83].

*Electrical Energy Tariffs:*

The electricity costs for consumers vary in Austria according to e-control [24] from 0.14 to 0.23 €/kWh, whereas the electricity costs in Germany are considerably higher, averagely 0.3 €/kWh [84]. The energy tariffs for feed-in the energy generated by a PV system vary in Austria, according to e-control (TARIFkalkulator) [85], from 0.03 to 0.08 €/kWh.

Since the CAPEX for PV and EES systems vary depending on the system size and possible funding, the following CAPEX, as shown in Table 3.3, are assumed for subsequent analysis. Further, two different energy tariffs are analysed for purchase as well as feed-in energy. Scenarios C1 to C4 investigate current and scenarios C5 to C8 possible future CAPEX of PV and EES.

Table 3.3: Considered CAPEX and energy tariffs

Scenario	CAPEX - PV	CAPEX - EES	Energy tariff (purchase)	Energy tariff (feed-in)
C1			0.2 €/kWh	0.07 €/kWh
C2	1500 €/kW <sub>p</sub>	1500 €/kWh	0.3 €/kWh	0.03 €/kWh
C3			0.3 €/kWh	0.07 €/kWh
C4			0.3 €/kWh	0.03 €/kWh
C5		800 €/kWh	0.2 €/kWh	
C6	800 €/kW <sub>p</sub>		0.3 €/kWh	0.03 €/kWh
C7		400 €/kWh	0.2 €/kWh	
C8			0.3 €/kWh	

In addition to the CAPEX and in order to calculate the LCOE, the following parameters are assumed:

- A service life of the PV system of 25 years [86], [87].
- A service life of the EES system of 15 years [3].
- A discount rate of 2.8 %/a [87].
- The OPEX of the PV and the EES are 2 %/a of the respective CAPEX [23].
- An annual degradation of 1 %/a of the PV system's installed power and the EES system's storage capacity.

## Results

Figure 3.3 graphically represents the calculated prosumers annual energy costs for the chosen scenarios and at different PV and EES system sizes as contour-plots. In the

shown contour plots, areas with the same colour and the shown isolines correspond to the same costs. Each scenario's annual energy costs are normalised to their respective economic optimum. This economic optimum is marked in Figure 3.3 with green crosses.

#### *Current Capital Expenditures - Scenarios C1 to C4*

Scenarios C1 to C4, left row of plots in Figure 3.3, are dealing with current capital expenditures of PV and EES systems – PV: 1500 €/kWp, EES: 1500 €/kWh – at different energy tariff situations.

- Scenarios C1 and C2:  
Scenario C1 (purchase: 0.2 €/kWh, feed-in: 0.07 €/kWh) and C2 (purchase: 0.2 €/kWh, feed-in: 0.03 €/kWh) representing the current Austrian energy tariff situation. A PV systems installed power of 3.8 kWp results in the economic optimum for scenario C1. In scenario C2, the PV systems installed power decreases due to the lower feed-in tariff gains to 3.3 kWp. In both scenarios, the implementation of an EES system results in significantly increasing annual energy costs. By installing the determined PV systems (C1 and C2; green crosses), the annual energy costs can be reduced by 6 % to 8 % compared to a system without PV generation (PV: 0 kWp, EES: 0 kWh).
- Scenarios C3 and C4:  
With the increase of the energy tariff (purchase) from 0.2 €/kWh to 0.3 €/kWh, the minimum of the annual energy costs is reached with an PV system's installed power of 5.9 kWp in C3 and 4.3 kWp in C4. The same as in C1 and C2, the reduction of the feed-in tariff from 0.07 €/kWh to 0.03 €/kWh leads to smaller PV system sizes. Due to the higher energy costs of 0.3 €/kWh, a PV system installation (C3 and C4; green crosses) can reduce the annual energy costs by 13 % to 16 % compared to a system without PV generation (PV: 0 kWp, EES: 0 kWh). Still, the implementation of an EES system results in significantly increasing annual energy costs.

#### *Possible Future Capital Expenditures - Scenarios C5 to C8*

Scenarios C5 to C8, right row of plots in Figure 3.3, are dealing with possible future capital expenditures of PV and EES systems – PV: 800 €/kWp, EES: 400 €/kWh (C7 and C8) to 800 €/kWh (C5 and C6) – at different energy tariff situations.

- Scenarios C5 and C6:  
Compared to the current situation analysed in the previous scenarios C1 to C4, the CAPEX in scenarios C5 and C6 is reduced to 800 €/kWp for the PV system and 800 €/kWh for the EES system. Scenario C5 (purchase: 0.2 €/kWh, feed-in: 0.03 €/kWh) representing the current Austrian energy tariff situation. In scenario C6, the energy tariff is increased from 0.2 €/kWh to 0.3 €/kWh.  
  
A PV system's installed power of 5.9 kWp results at the economic optimum for scenario C5. In scenario C6 and at the economic optimum, the PV systems installed power increases due to the higher energy tariff of 0.3 €/kWh to 8.4 kWp. Further, an EES system's capacity of 0.5 kWh is preferable in C6. By

installing the determined PV systems, the annual energy costs can be reduced by 17 % (C5; green cross) and 24 % (C6; green cross) compared to a system without PV generation (PV: 0 kWp, EES: 0 kWh).

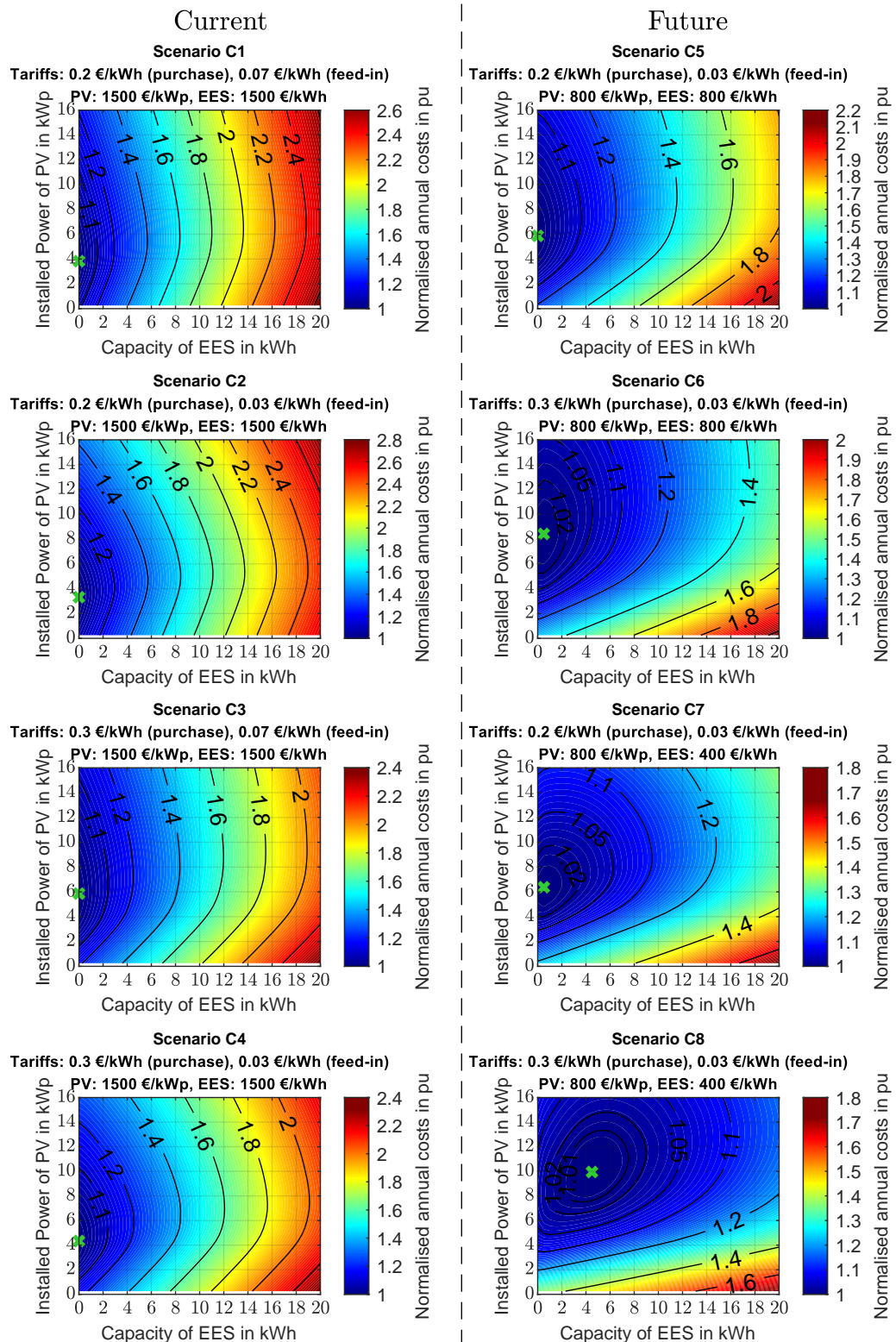


Figure 3.3: Economic optimum of a prosumer

Although the CAPEX for PV and EES in scenarios C5 and C6 is almost halved compared to scenarios C1 to C4, an EES system's implementation still results in C5 and C6 in increasing annual energy costs even though the relative increase of costs is smaller in relation to C1 to C4.

- Scenarios C7 and C8:

In Scenario C7 and C8, the EES system's CAPEX is further reduced to a very optimistic 400 €/kWh. The CAPEX of the PV system stays with 800 €/kWp the same compared to scenarios C5 and C6. Again, scenario C7 (purchase: 0.2 €/kWh, feed-in: 0.03 €/kWh) representing the current Austrian energy tariff situation and in scenario C8, the energy tariff is increased from 0.2 €/kWh to 0.3 €/kWh.

A PV system's installed power of 6.4 kWp and an EES system's capacity of 0.5 kWh results in the economic optimum for scenario C7, marked with a green cross. Although the EES systems CAPEX is halved again compared to C5, the use of an EES is still not profitable at the current Austrian energy tariff situation. By installing the determined PV-Storage system (C7, green cross), the annual energy costs can be reduced by 17 % compared to a system without PV generation and EES.

In scenario C8, the energy tariff increases from 0.2 €/kWh to 0.3 €/kWh. Due to these increased energy costs, the use of an EES becomes profitable. Now, a PV system's installed power of 10 kWp and an EES system's capacity of 5 kWh results in the economic optimum for scenario C8. The annual energy costs can be reduced by 4 % compared to a system with a 10 kWp PV system and without an EES. Further, with the determined PV-Storage system (PV: 10 kWp, EES: 5 kWh), the annual energy costs can be reduced by 26 % compared to a system without PV generation.

*General Statements:*

Installing a PV system at typical Austrian CAPEX and energy tariffs will reduce the annual energy costs of a prosumer compared to installing a system without PV generation. Hence, the annual energy costs of the investigated prosumer (Table 3.3) could be reduced by 6 % to 8 %. Most important, the analyses clearly showed that installing an EES system is unprofitable at current Austrian EES' CAPEX and energy tariffs.

Reducing the CAPEX, e.g., to a highly optimistic 400 €/kWh, combined with an increased energy tariff to 0.3 €/kWh, will significantly influence an EES system's profitability. A PV-Storage system becomes now profitable. As shown in Figure 3.3, installing a PV-Storage system (PV: 10 kWp, EES: 5 kWh) reduces the prosumer's annual energy costs by 26 % compared to installing a system without PV generation.

Even with EES systems' falling prices in Austria, the low electricity prices (0.2 €/kWh) represent a significant barrier to investing in an EES system. Nevertheless, installing a PV system alone – without using an EES system – will reduce the annual energy

costs, even at current Austrian CAPEX. For example, a 6 kWp PV system, commonly installed within the Austrian household sector, can reduce the investigated prosumer's annual energy costs by about 2 % to 6 %.

### 3.3 Impact of Energy Tariffs on Prosumer Behaviour

The integration of new meter functions and services (smart metering) in hybrid energy systems such as prosumers will enable market-dependent dynamic or special consumer and prosumer tariffs. Since demand and generation do not correlate within every time step, it is usually essential, without using energy storages or demand-side management, to purchase or feed-in energy at sub-optimal tariffs or to adjust demand accordingly. In the case of unprofitable feed-in tariffs, it can be economical to use the photovoltaic system's surplus generation on-site through demand-side management and thus increase the degree of self-consumption, to buffer it in energy storages, or to cover the thermal demand (e.g., domestic hot water demand).

Therefore, the impact of tariff regimes commonly used in Austria on optimising prosumers, the static, high and low tariff (HT/NT) and a newly offered dynamic tariff are examined using the simulation model ProsOpt. Both the static and the HT/NT tariff are tariff models with fixed agreed costs for a defined annual energy demand over a contractual period. By using smart meters, a dynamic tariff model dependent on the electricity market is possible. A detailed explanation about the energy tariffs can be found in Section 2.5.

The simulation model ProsOpt performs annual simulations

- with a time resolution of 15 minutes,
- an ideal forecast of 72 hours,
- and the objective to minimise the investigated prosumer's energy costs.

An optimising prosumer's response to the different energy tariffs is analysed based on the thermal (TES) and electrical (EES) energy storage system's operation. The used thermal energy storage covers the domestic hot water demand by using heating cartridges. The parameter settings of the investigated prosumer can be found in Table 3.1.

#### Results

Figure 3.4 shows the state of charge (SoC) of the electrical (EES) and thermal (TES) energy storage system at the three chosen energy tariffs (static, HT/NT and dynamic tariff) during four exemplary selected days. Furthermore, the PV system's generation (green area), the electrical energy demand (grey area) and the thermal demand (red area) are shown. The electrical demand is composed of the lighting, the household appliances, and the electric vehicle's charging power, and the thermal demand is

composed of the heating and the domestic hot water – load peaks in the red area – demand. Due to poor weather conditions, the PV systems’ generation is reduced on day three and four. The demand stays similar for the investigated days.

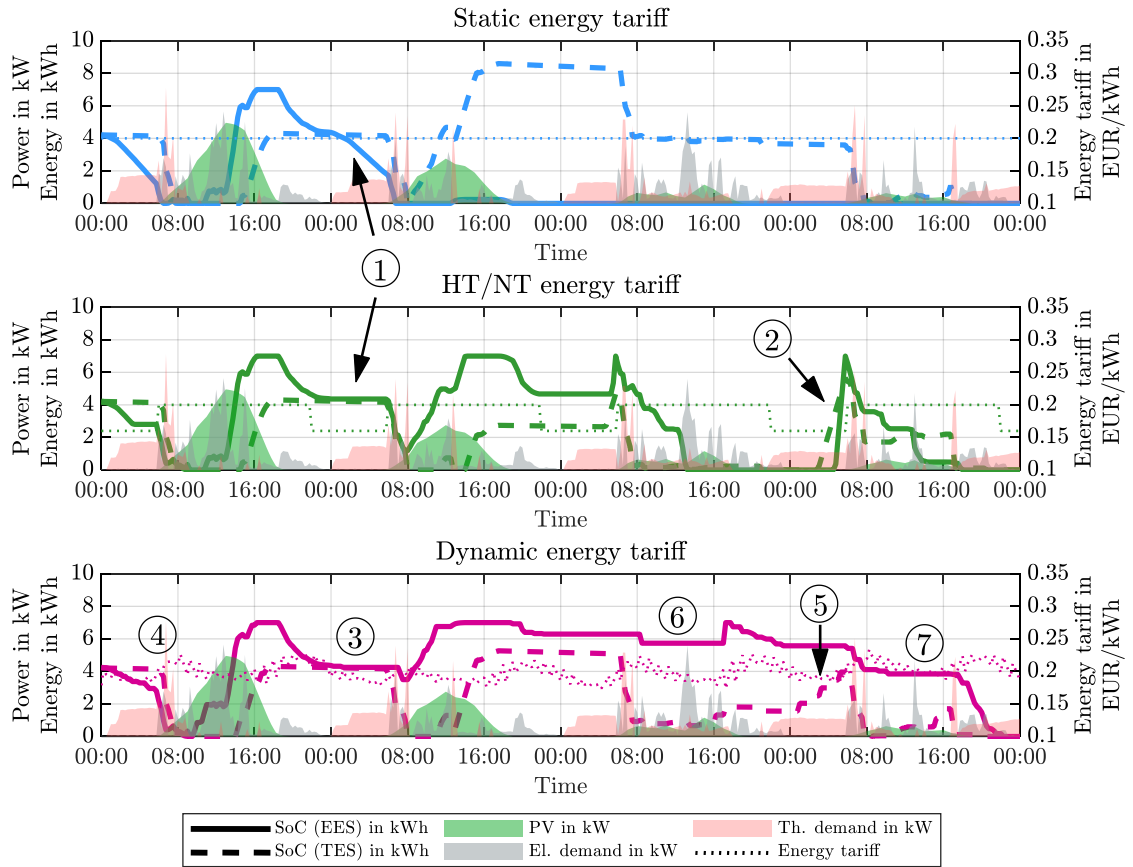


Figure 3.4: Impact of energy tariffs on optimising prosumer storage charging behaviour

*Static Energy Tariff:*

At a static energy tariff, both storage systems – EES and TES – are operating independently from the energy tariff. The prosumer’s forecast-based storage management mainly depends on the energy generation of the PV system, the energy demand and the assumed investment and operating expenditures of the technologies. Mainly based on the assumed costs of the technologies, it is economically preferable to fully charge the TES system with the PV generation in the case of the upcoming poor weather conditions - decrease in PV generation – during the last two days (Figure 3.4) instead of using the EES system. The stored energy in the TES is then used to cover the domestic hot water demand on the following poor weather days. Further shown in Figure 3.4 ① (static energy tariff), the EES system is used to cover the heat pump supplied heating demand at night, until the EES system completely discharged on the morning of day two.

*HT/NT Energy Tariff:*

The storage management of the optimising prosumer is now reacting to differing electrical energy costs. The costs of the HT/NT tariff changes according to a given time range for the

- low load NT from 10 pm to 6 am (night-time) and
- high load HT from 6 am to 10 pm (day-time).

Comparing the HT/NT- with the static energy tariff in Figure 3.4, marked with ①, it can be observed that at low tariff times (NT, 10 pm to 06 am) and due to the prosumer's forecast-based operation, with an ideal weather, demand and tariff forecast of 72 hours, the EES system holds the state of charge and will not cover the heating demand. Later, at high tariff times (NT, 06 am to 10 pm), the prosumer's energy demand gets covered by the storages (EES and TES).

Further, as shown in Figure 3.4 ②, at times of low or no PV generation and low tariff times, it can be observed that caused by the forecast-based operation of the prosumer the storage systems – EES and TES – are charged from the power network briefly before switching from NT to HT times. After switching from NT to HT, the charged energy is used to cover the prosumer's energy demand.

#### *Dynamic Energy Tariff:*

The prosumer's optimised storage management at a dynamic tariff behaves similar but smoother than the HT/NT tariff. The energy costs at dynamic tariff show a market-dependent periodically behaviour, as shown in Figure 3.4. The energy costs decrease at times of high generation of the PV system and low load (night) and increase again at times of high loads, such as in the morning and evening.

Compared to the HT/NT tariff, a similar behaviour is observed for the dynamic tariff. At low tariff times ③, ⑥ and ⑦, mainly on midday and night, the storage systems holds their state of charge and will not cover the energy demand. At increasing energy costs ④, the storages – EES and TES – are then used to cover the energy demand. Similar to the HT/NT tariff ②, at times of low or no PV generation and low costs, caused by the forecast-based operation of the prosumer, the storage systems is charged, see ⑤, via the power network.

Since the low and high tariff times change more frequently in the dynamic energy tariff than the HT/NT energy tariff, the EES is barely used during the two bad weather days as almost no electrical energy is consumed at high tariff times and at low tariff times the demand gets preferably covered with power network. Only on the last day – shown in Figure 3.4 ⑦ – the EES is discharged early in the morning because the ideal 72 hours forecast predicts a high PV generation for the upcoming days (not shown in Figure 3.4) and the possibility to charge the storages again.

#### *General Statements:*

The use of time-varying energy tariffs, such as a dynamic market-dependent energy tariff, also leads to changes in the prosumers' hybrid energy system's operation. An optimising prosumer considering weather, demand and tariff forecasts of, e.g., the next 72 hours, will react to changing energy tariffs to achieve an economic optimum as well as change the storage system's charging and discharging behaviour.

The analyses reveals that with time-varying energy tariffs, the optimising prosumer's energy storages would possibly get charged at times of low or no PV generation and low costs, resulting in increased demand at unusual times. Therefore, the impact of

optimising prosumers at such dynamic energy tariffs on the low-voltage network are analysed in Section 4.2.

### 3.4 Storage Strategies: Forecast versus Self-Consumption

By combining PV- and EES systems, the fluctuating PV generation and the gap between generation and demand in the short term can be compensated. A suitable charging management of the EES system can significantly improve the degree of autonomy DA as well as the degree of self-consumption DSC.

With the operating strategies of PV-Storage systems, specific objectives can be achieved. Often, increasing the degree of self-consumption or a limitation of the feed-in power (peak shaving) are preferred strategies. Further, with the simulation model ProsOpt, it is also possible to simulate optimising prosumers with a forecast-based – weather, demand and tariffs – storage strategy. A more detailed explanation of storage operation strategies can be found in Section 2.6.2.

In the following, a forecast-based storage strategy is compared with the commonly used traditional storage strategy, with the objective to maximise the degree of self-consumption without using forecasts. The forecast-based storage strategy uses the simulation model ProsOpt, which performs annual simulations with a time resolution of 15 minutes, an ideal forecast of 72 hours and the objective to increase the degree of self-consumption.

#### Results

Figure 3.5 illustrates the absolute deviation of the DA and DSC between the forecast-based storage strategy and the traditional strategy to maximise the DSC without any forecast methods. A positive difference in Figure 3.5 indicates an xx % higher DA or DSC of the forecast-based storage strategy compared to the traditional storage strategy.

As shown in Figure 3.5, the forecast-based storage strategy reaches only minimal higher values for the DA and the DSC than the analysed traditional storage strategy. Depending on the system size, the forecast-based storage strategy achieves up to 0.6 % higher degrees of autonomy and up to 0.8 % higher degrees of self-consumption. However, Figure 3.5 shows areas – ② and ③ – where the forecast-based storage strategy achieves better DA and DSC than the traditional storage strategy.

#### *Small PV- or EES-System Sizes ①:*

Figure 3.5 (blue area, marked ①) shows that for small PV system sizes between 2 to 5 kW<sub>p</sub> and depending on the capacity EES, the forecast-based storage strategy achieves similar DA and DSC compared to the traditional storage strategy.

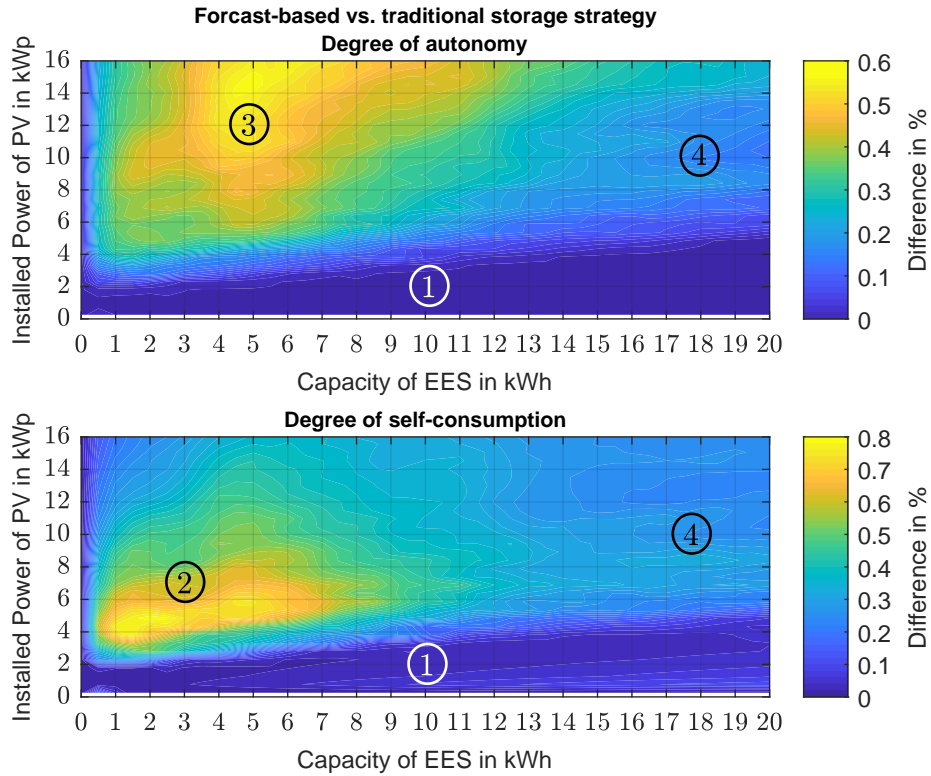


Figure 3.5: Forecast-based versus traditional storage strategy - difference in degree of autonomy and degree of self-consumption

For small PV system sizes, the generated energy is either consumed instantly, or only a low surplus generation is available for the EES system. Due to this low surplus generation, considering forecasts within the storage strategy of several days becomes obsolete, as the stored energy is already consumed on the same day.

*Degree of Self-Consumption DSC ② and Degree of Autonomy DA ③:*

With PV system sizes larger than 4 kWp and using an EES system larger than 2 kWh, the PV systems' generated energy is more efficiently used when using a forecast-based storage strategy compared to the traditional storage strategy.

As shown in Figure 3.5 ②, an increase in EES capacity in the forecast-based storage strategy results in higher efficient use of the generated electrical energy of up to 0.8 % (PV: 5 kWp, EES: 2 kWh). The forecast-based storage strategy uses the limited generation and storage capacity between 3 and 8 kWp (PV) and 1 and 7 kWh (EES) due to the forecast over several days better and thus achieve a slight improvement in the DSC compared to the traditional storage strategy. This slightly more efficient use of the generated energy also results, in the range between 6 and 16 kWp (PV) and 1 and 9 kWh (EES), in minimal higher degrees of autonomy, with a maximum difference of the DA ④ of up to 0.6 % (PV: 14.5 kWp, EES: 5 kWh).

Further, a forecast-based storage strategy can result in a minimal higher degree of autonomy DA of up to 0.6 % (PV: 14.5 kWp, EES: 5 kWh). Dependent on the PV system size, the DA's increase is limited by the storage capacity ③. In the range

between 6 and 16 kWp (PV) and 1 and 9 kWh (EES), the forecast-based storage strategy can use the surplus generation efficiently at limited storage capacity where the surplus generation is already optimally used, and an increase of the storage capacity no longer has a significant influence.

*General Statements:*

As shown in Figure 3.5, the forecast-based storage strategy reaches only minimally higher values for the DA and the DSC than the analysed traditional storage strategy. Using a forecast-based storage strategy, with the objective of increasing the degree of self-consumption, results in no significant efficient use of the PV system's generated energy compared to the traditional storage strategy without any forecasts methods.

However, ProsOpt's simulations are performed at an ideal forecast of 72 hours. Thus, forecast uncertainties have not been considered, indicating the absolute difference between the forecast-based storage strategy and the traditional storage strategy may indeed be smaller. It can be assumed that due to the forecast uncertainties, the effectiveness of the forecast-based storage strategy will decrease.

### 3.5 Economical and Ecological Optimisation of a Prosumer

In following the simulation model ProsOpt optimises a prosumer's – single-family house – operation with a coupled thermal and electrical energy system. Depending on the respective analysed scenario, ProsOpt performs annual simulations with a time resolution of 15 minutes, an ideal forecast of 72 hours, and with the objective to minimise the investigated prosumer's

- annual energy costs (€/a) or
- annual CO<sub>2</sub> emissions (kgCO<sub>2</sub>/a).

The analyses' main focus encompasses the influence of the respective optimisation objectives – economic and ecological – have on prosumer's annual energy costs and the annual CO<sub>2</sub> emissions. Therefore, the sensitivity analyses of the technologies Levelized Cost of Energy LCE (Levelized Cost of Electricity - LCOE) and the CO<sub>2</sub> equivalents are performed. A more detailed explanation of LCE/LCOE and CO<sub>2</sub> equivalents can be found in Section 2.5.

- The Levelized Cost of Energy LCE (Levelized Cost of Electricity - LCOE) allows an economic comparison of different technologies. These are calculated, as shown in Equation (2.25), taking into account the energy demand using the net present value, including capital (CAPEX) and operating (OPEX) expenditures. The LCE is usually expressed in Euro per kWh (€/kWh).

As the LCEs differ depending on the technical components' operation and use, additional sensitivity analyses must be carried out. The used basic assumptions of the LCE, shown in Table 3.5, are determined through market studies and

own calculations, whereby these correspond to typical prices in Austria for 2018.

- The ecological evaluation of the system components can be performed by using the CO<sub>2</sub> equivalents or global warming potentials (GWP) listed in Table 3.5, which are usually expressed in g<sub>CO<sub>2</sub></sub>/kWh. Since the CO<sub>2</sub> equivalent values stated in Table 3.5, like the LCEs, depending on the usage and type of the system, sensitivity analyses must be performed to evaluate the entire system.

Traditional heating systems such as gas and oil boilers get increasingly replaced by alternatives such as heat pumps. The thermal supply of the optimising prosumer is investigated in detail by using a heat pump as the primary heating system. Therefore, a heat pump (HP), thermal energy storage (TES, with heating cartridges), and an air conditioning system (AC) couple the electrical and thermal systems to form a hybrid energy system. Table 3.4 lists the selected parameter settings and demand for the subsequent analyses.

Table 3.4: Parameter settings - economical and ecological optimisation of a prosumer

Photovoltaic system (PV):	Installed power $P = 5 \text{ kWp}$
Electrical energy storage (EES):	Capacity $W = 10 \text{ kWh}$
Thermal energy storage (TES):	Volume $V = 300 \text{ litres}$
Heating cartridge of the TES:	Power $P = 2 \text{ kW}$
Heat pump (HP):	Heating power $P = 5.2 \text{ kW}_{\text{th}}$
Air conditioner (AC):	Cooling power $P = 2.4 \text{ kW}_{\text{th}}$
Electrical demand (ED):	Annual demand $W = 4970 \text{ kWh/a}$
Heating demand (HD):	Annual demand $W = 45 \text{ kWh/m}^2\text{a}$
Cooling demand (CD):	Annual demand $W = 3.4 \text{ kWh/m}^2\text{a}$
Domestic hot water (DHW):	Annual demand $W = 2100 \text{ kWh/a}$
Building	Conditioned floor area $A = 150 \text{ m}^2$

### Heat Pump as the Primary Heating System - Results

A heat pump is used as the primary heating system and covers the investigated prosumer's heating demand. Sensitivity analyses of the system components starting from the initial state, stated in the following Table 3.5, are carried out, and the resulting annual energy costs and CO<sub>2</sub> emissions are presented graphically in Figures 3.6 and 3.7. For easier readability,

- economically optimised simulation results are drawn as solid lines and
- ecological optimised simulation results are drawn as dashed lines.

In both cases, black circles represent the initial state values of the sensitivity analyses. Note, that in the following Figures 3.6 and 3.7, a sensitivity from the initial state of exemplary -30 % means on the example of

Table 3.5: Assumed initial values of levelised costs of energy (LCE) and CO<sub>2</sub> equivalents

Electricity costs (purchase)	0.20 €/kWh	
Electricity costs (feed-in)	-0.07 €/kWh	
Electricity mix (AUT)		250 g/kWh <sub>el</sub>
Photovoltaics (PV)	0.12 €/kWh	90 g/kWh <sub>el</sub>
Electrical energy storage (EES)	0.35 €/kWh	100 g/kWh <sub>el</sub>
Heat pump (HP)	0.15 €/kWh	140 g/kWh <sub>th</sub>
Air conditioner (AC)	0.20 €/kWh	140 g/kWh <sub>th</sub>

- electricity costs – solid black line – a reduction from 0.20 €/kWh (0 %) to 0.14 €/kWh (-30 %), or in the case of the
- electricity mix – dashed black line – a reduction from 250 g/kWh (0 %) to 175 g/kWh (-30 %).

The LCE are based on presumed

- capital and operating expenditures and
- the annual amount of energy generated or stored by the system components.

For each changed sensitivity in the LCE or CO<sub>2</sub> equivalent (GWP) of the respective technology, annual simulations are performed to determine the resulting annual energy costs and CO<sub>2</sub> emissions.

Based on these selected parameters, the optimal operation of the prosumer's technologies to minimise the energy costs or CO<sub>2</sub> emissions is determined.

- Thus, the used optimisation algorithm selects only the technologies/systems contributing to an energy cost or CO<sub>2</sub> reduction.
- Since due to the optimal operation of the technologies/systems the initially selected generated or stored annual energy amounts changes, the LCE or the CO<sub>2</sub> equivalents (GWP) also change respectively.

Therefore, the following analyses perform sensitivity analyses based on the initial LCE or CO<sub>2</sub> equivalents (GWP) to consider these changes and determine when a technology/system will reduce energy costs or CO<sub>2</sub> emissions.

#### Annual Energy Costs:

The following Figure 3.6 shows the economically (solid lines) and ecologically (dashed lines) optimising prosumer's resulting annual energy costs at different sensitivities of the LCE (€/kWh) or GWP (g/kWh).

The determined annual energy costs at the initial values of the LCE (black circle at solid lines) for the economically optimising prosumer is 2294 €/a. In the case of ecological optimisation (black circle at dashed lines), the resulting annual energy costs of 2770 €/a are 476 € higher than the economically optimising prosumer.

As shown in Figure 3.6, changing values of LCE or GWP of the following system components show a high gradient which results in high sensitivity and, therefore, a high impact on the annual energy costs of the investigated prosumer.

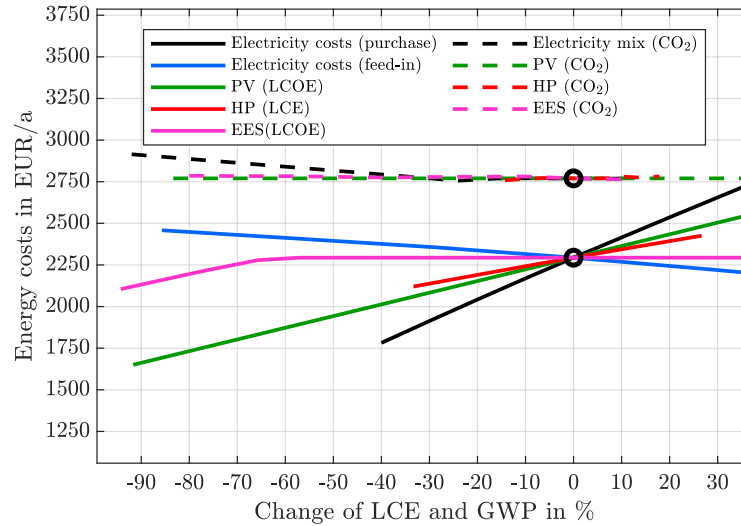


Figure 3.6: Sensitivity analyses of annual energy costs - heat pump as the primary heating system PV... photovoltaic system, HP... heat pump, EES... electrical energy storage system LCE and GWP values are normalised to the initial values stated in Table 3.5, e.g., electricity costs of 0.2 €/kWh or the electricity mix of 250 g/kWh equals 0 %

*Optimising Prosumer with an Economic Objective:*

Since a heat pump covers the prosumer’s thermal energy demand, the prosumer’s total annual energy demand is covered via the electrical system. This, in turn, leads to the highest sensitivity in the electricity costs (purchase, solid black line), followed by the LCOE of the PV system (solid green line) and the HP (solid red line).

The EES system cannot significantly reduce annual energy costs until the LCOE of EES (pink solid line) reaches approximately 0.12 €/kWh, respectively -65 %. Above this LCOE of 0.12 €/kWh, the EES system remains too expensive and is not considered by the prosumer’s used optimisation algorithm.

*Optimising Prosumer with an Ecologic Objective:*

In an ecologically optimised system, only the electricity mix (dashed black line) shows a slight influence on the annual energy cost when reducing the CO<sub>2</sub> equivalents of the electricity mix from 250 g/kWh (0 %) significantly to approximately less than 125 g/kWh (-50 %).

When reducing the electricity mix by less than half of the initial value, an increasing amount of electricity is purchased from the power network at electricity costs of 0.20 €/kWh and will also be stored in the EES system, with an CO<sub>2</sub> equivalent of 100 g/kWh and an LCOE of 0.35 €/kWh, resulting in higher annual energy costs.

### Annual CO<sub>2</sub> Emissions:

Further analysis focuses on the annual CO<sub>2</sub> emissions of the investigated optimising prosumer. The following Figure 3.7 shows the economically (solid lines) and ecologically (dashed lines) optimising prosumer's resulting annual CO<sub>2</sub> emissions at sensitivities of the LCE (€/kWh) or GWP (g/kWh).

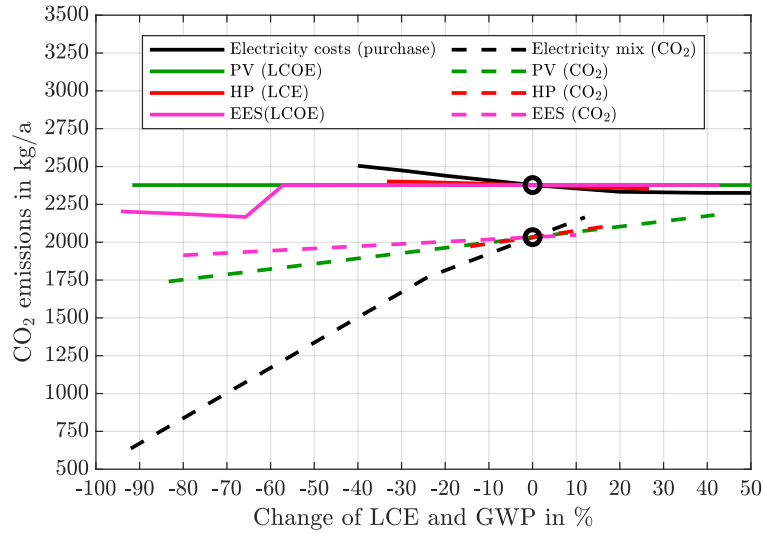


Figure 3.7: Sensitivity analyses of annual CO<sub>2</sub> emissions - heat pump as the primary heating system PV... photovoltaic system, HP... heat pump, EES... electrical energy storage system LCE and GWP values are normalised to the initial values stated in Table 3.5, e.g., electricity costs of 0.2 €/kWh or the electricity mix of 250 g/kWh equals 0 %

The determined annual CO<sub>2</sub> emissions at the initial values of the LCE (black circle at solid lines) for the economically optimising prosumer is 2377 kg/a. In the case of ecological optimisation (black circle at dashed lines), the resulting annual CO<sub>2</sub> emissions of 2033 kg/a are 344 kg less compared to the economically optimising prosumer.

As shown in Figure 3.7, changing values of LCE or GWP of the following system components show a high gradient, resulting in high sensitivity and, therefore, in a high impact on the investigated prosumer's annual CO<sub>2</sub> emissions.

#### *Optimising Prosumer with an Economic Objective:*

The EES system (solid pink line) shows, together with the electricity costs (solid black line), the highest sensitivity of the annual CO<sub>2</sub> emissions.

By reducing the electrical energy storage system's LCOE to approximately 0.12 €/kWh (- 65 %, significant jump in the pink solid line), the EES is cheap enough and is considered by the prosumer's used optimisation algorithm used. Caused by the assumed GWP of the EES system of 100 g/kWh<sub>el</sub>, this leads to reduced annual CO<sub>2</sub> emissions.

*Optimisation with an Ecologic Objective:*

The electricity mix (dashed black line) shows the most significant sensitivity in an ecologically optimised system followed by the PV system. This high sensitivity in the electricity mix can be explained by the fact that a prosumer remains nonetheless highly dependent on the power network as presented in Section 3.1.

**General Statements:**

The economic and ecological sensitivity analyses show that even when decentralised generation and storage systems are used, the economic and ecological dependence on primary energy sources from the electricity network remains very high. In the case of a prosumer with a heat pump as the primary heating system, the most efficient way to reduce the CO<sub>2</sub> emissions is choosing an electricity provider who is offering 100 % renewable energy.

# 4 Influence of Prosumers on Distribution Networks

The increasing share of decentralised energy generation and storage systems in distribution networks, the integration of electric vehicles, the coupling of electrical and thermal systems, as well as the increasing implementation of Information and Communication Technologies (ICT) are leading to significant changes in planning and operation of distribution networks. Formerly systems such as single-family houses, commercial and industrial buildings, now become so-called prosumers (producers and consumers) who feed back energy into the network at certain times.

Subsequent, the developed simulation model ProsOpt – see Section 2.2 – is used to analyse the influence of self-optimising prosumers on a rural distribution network. Therefore the energy management model of ProsOpt is linked with load flow calculations of the power network. For the network analyses, the benchmark network “1-LV-rural1-0-sw” from the German project “SimBench” [88] is used. The “Simbench” project aims to create several chosen benchmark networks for the development of new methods and solutions in the field of network analysis, network planning and network operation management. By using benchmark networks in a variety of studies, the results are reproducible, comparable and transparent. The SimBench datasets are completely and publicly available on the project homepage “simbench.de” [88].

The rural low-voltage distribution network of the benchmark network “1-LV-rural1-0-sw” shown in Figure 4.1 consists of four feeders and a total of 13 households. The household loads and the decentralised generation systems from SimBench dataset are replaced by the simulation model ProsOpt. Low-voltage cables of the type NAYY 4x150SE 0.6/1kV with a thermal rating of 270 A are used [88]. The low voltage network is fed by a 160 kVA transformer from a 20 kV medium-voltage network. In order to analyse the influence of prosumers on different feeder lengths and assuming the voltage level on the high-voltage side of the transformer is not constant, the following changes are made in contrast to the SimBench data sets:

- Additionally, a 10 km long medium-voltage cable is connected between the 20 kV medium-voltage network and the transformer. The medium-voltage cable type A2XHCJ2YV 150 has a thermal rating of 319 A [89].
- The length of cable C5 extends from 50 m to 500 m.
- The length of cable C13 extends from 133 m to 1000 m.

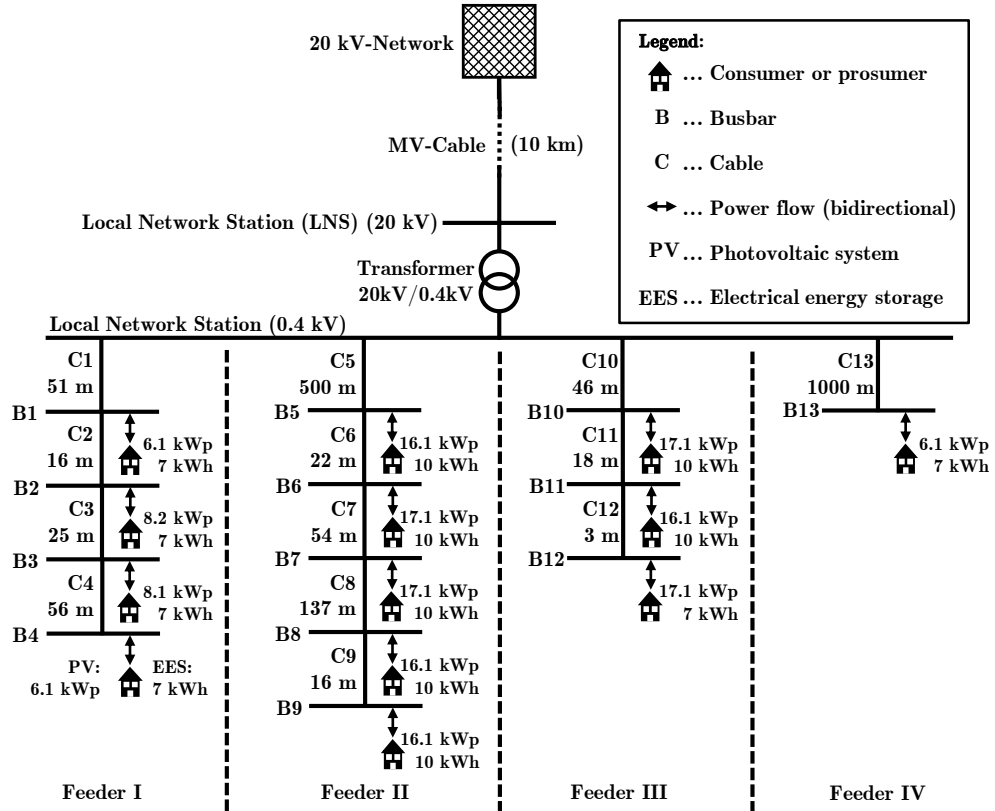


Figure 4.1: Low-voltage network, consisting of four feeders and the considered thirteen prosumers

The electrical parameters of the network components are listed in the following Table 4.1.

Table 4.1: Electrical parameters of the network components [88]–[90]

Component	Nominal voltage $V_n$ in kV	Rated power $S_r$ in kVA	Impedance $\underline{Z}'$ in $\Omega/\text{km}$	Capacity $C'$ in nF/km	Thermal rating $I_{th}$ in A
NAYY 4x150SE	0.4	-	$0.2067 + 0.080i$	500	270
A2XHCJ2YV 150	20	-	$0.2060 + 0.121i$	254	319
Transformer	20/0.4	160	$0.025i$	-	231

The thirteen prosumers are connected to the busbars B1 – B13 of the low-voltage network in Figure 4.1. The energy demand of each prosumer consists of the electrical demand, space heating, domestic hot water demand, cooling demand and the charging energy of the electric vehicle. The electrical and hot water demand, as well as the presence of the electric vehicle at home, are generated by the LoadProfileGenerator (LPG) developed by Pflugradt [11], see Section 2.4. The heating and cooling demand of each building are determined by applying the heating and cooling load calculations according to the standard ÖNORM B 8110-6 1:2019-01 [12] and Häupl et al. [13], see Section 2.4.2. The annual energy demand of the thirteen prosumers is listed in Table C.1 in the appendix.

The thirteen prosumers connected to the low-voltage network use linear optimisation algorithms to optimise the operation of the hybrid energy systems (single-family houses). Therefore, the optimal use of the energy generation and storage systems is determined using linear optimisation (MILP – Mixed Integer Linear Programming) taking into account the desired energy services, external boundary conditions (e.g., weather) and cost functions of the system components. There is no exchange of information between the prosumers nor is an so-called energy community formed. The optimisation objectives of the prosumers aims to individually maximise the degree of autonomy as well as minimising the annual energy costs. A detailed explanation about the optimisation of prosumers (hybrid energy systems) can be found in Section 2.2.1.

The following time-series based load flow calculations are performed for one year and a time resolution of 15 minutes for the low voltage distribution network shown in Figure 4.1. Using the methodology described in Section 2.7, the load flow calculations are executed with Matlab by using the Newton-Raphson method.

The feeding 20 kV medium-voltage network, see Figure 4.1, is implemented as a slack node with a voltage level of  $v = 1$  pu. The power output of the prosumers at their respective PCC (Point of Common Coupling) – see Figure 2.2 – resulting from the optimised operation, are implemented in the load flow calculations as PQ-nodes (see Table 2.7). The house service lines from the households to the busbars of the distribution network are neglected in the analyses.

In the following analyses, the influence of optimising prosumers on the power network is investigated under consideration of different scenarios. Generally, the following analyses are carried out to investigate the influence of optimising prosumer:

1. *Increasing Hybridisation Levels of Households:*

Due to the coupling of the thermal and electrical systems using heat pumps, air conditioners and heating cartridges, and charging the electric vehicle increases the household's electrical demand accordingly. This increased electrical demand will also affect distribution networks. The influence of the households changed electrical demand combined with renewable generation and energy storages on a low-voltage network is investigated.

2. *Dynamic Energy Tariffs and Peak-Shaving:*

The introduction of dynamic energy tariffs has a significant impact on prosumers' optimised operation when using energy storage systems, see Section 3.3. An optimising prosumer considering weather, demand, and tariff forecasts will react to changing energy tariffs and adapt the storage systems' charging and discharging behaviour accordingly, resulting possibly in increased electrical demand at unusual times. Therefore, the impact of optimising prosumers at such dynamic energy tariffs on the low-voltage network is analysed. Further, measures to limit the households peak power, such as peak-shaving, are being investigated.

3. *Impact of Voltage and Reactive Power Control on the Distribution Network:*  
In order to comply with the voltage limits according to EN 50160 [38] and the Austrian national rules TOR [39], the effectiveness of different methods for voltage and reactive power control are determined.

Table 4.2 lists the analysed scenarios. Changes in technologies and energy demand per scenario affect all thirteen investigated prosumers equally. An “x” or the technologies’ abbreviation indicates that the technology or demand is considered in the examined scenario. Each prosumer’s electrical and thermal demand is listed in Table C.1 in the appendix.

Table 4.2: Defined scenarios - network analysis

Section	Scenario	ED	EV	DHW	HD	CD	PV	EES	PCC Limit	Voltage/Reactive power control	Energy tariff
4.1	N1			DH	DH					not applicable	
	N2	x							17.3 kVA		static
	N3		x	TES-HC	HP						
	N4						x	x		$\cos(\varphi) = 1$	
4.2	N5								17.3 kVA		dynamic
	N6	x	x	TES-HC	HP	x	x	x	8 kVA	$\cos(\varphi) = 1$	static
	N7										dynamic
4.3	N8									$\cos(\varphi) = 0.95$	
	N9	x	x	TES-HC	HP	x	x	x	17.3 kVA	volt-var mode	static
	N10									watt-cos $\varphi$ mode	
CD...	Cooling demand				DH...	District heating					
DHW...	Domestic hot water demand				EES...	Electrical energy storage					
ED...	Electrical demand				EV...	Demand of electric vehicle					
HC...	Heating cartridge				HP...	Heat pump					
PCC...	Point of common coupling				TES...	Thermal energy storage					

#### Scenario N1:

In Scenario N1, the households’ electrical demand (ED), consisting of the lighting and household appliances, and the air-conditioning system covering the cooling demand (CD), is supplied by the power network. The heating demand (HD) and domestic hot water demand (DHW) are covered by district heating. The households in N1 neither have electric vehicles (EV), photovoltaic systems (PV), nor energy storage systems. At the PCC, the technical power limit is set to a typical value for Austrian households to 17.3 kVA (25 A fuse for each phase).

#### Scenarios N2 to N10:

Heat pumps are used to cover the heating demand (HD) of the households. The domestic hot water demand are covered by a thermal energy storages (TES) using electric cartridges (HC). The investigated households own an electric vehicle (EV), which can be charged at home with a typical single-phase charging power of 3.7 kVA (16 A fuse) [54].

- In the scenarios N4 to N10, a photovoltaic system and an electrical energy storage system, as shown in Figure 4.1, are considered at each household. Except for N8 to N10, all inverter of the prosumers work in a constant power factor mode set to a unity power factor ( $\cos(\varphi) = 1$ ). The installed power of the PV systems of 167 kWp in the entire network is chosen to study extreme

PV situations in rural networks.

Formerly, inverters are set to a constant power factor not equal unity to comply with the voltage limits according to the standard EN 50160 [38] and the Austrian national rules TOR [39]. Therefore, the inverters in N8 are specified to work in under-excited (voltage-reducing) mode with a constant  $\cos(\varphi)$  of 0.95.

- Scenarios N4 and N6 analyse the impact of dynamic energy tariffs on the prosumers' optimised operation when using energy storage systems.
- To investigate the effectiveness of the measure "peak-shaving", the peak power of the households is more than halved from 17.3 kVA to 8 kVA in N5 and N6.

### Box plots

In the following analyses, box plots are used to visualise the results of the performed load flow calculations, such as the transformer loading and the LV-network losses. A box plot provides a graphical representation of the statistical evaluation of a data series. This contains within the box (blue boxes)

- the median value (horizontal red line),
- upper (75 %-) and lower (25 %-) quantile,

and outside the box,

- the upper and lower antennas or whiskers, calculated using the upper and lower quantiles multiplied with a constant factor of 1.5, and
- and the outliers (red dots), which represent in the following analyses the peak loads in the network [14].

## 4.1 Increasing Hybridisation Levels of Households

Due to the coupling of the thermal and electrical systems using heat pumps, air conditioners and heating cartridges and the charging of electric vehicle increases the household's electrical demand accordingly. This increased electrical demand will also affect distribution networks. In this section, the influence of the households' changed electrical demand combined with renewable generation and energy storages on a low-voltage network is investigated. Using the developed simulation model ProOpt, the optimal use of the PV generation and storage systems is simulated for different prosumers. It is assumed that all prosumers use the same optimisation algorithm with the same objective, a combination of increasing the degree of self-consumption and reducing energy costs, as in the previous Sections 3.1 to 3.4. The simulations are performed for one year with a time resolution of 15 minutes.

## Transformer Loading and LV-Network Losses

Figure 4.2 shows for the analysed scenarios N1 to N4, the active power flow across the transformer  $p_T$ , the transformer loading  $i_T$  and the network losses  $s_{\text{loss}}$ . The rated power of the transformer  $S_T$  and the respective voltage level  $V_n$  are selected as the base values (pu-system).

The following assumptions apply to the sign of the electrical power at the transformer:

- Power  $p_T > 0$ : load flow from the medium-voltage network to the low-voltage network (top-down)
- Power  $p_T < 0$ : load flow from the low-voltage network to the medium-voltage network (bottom-up)

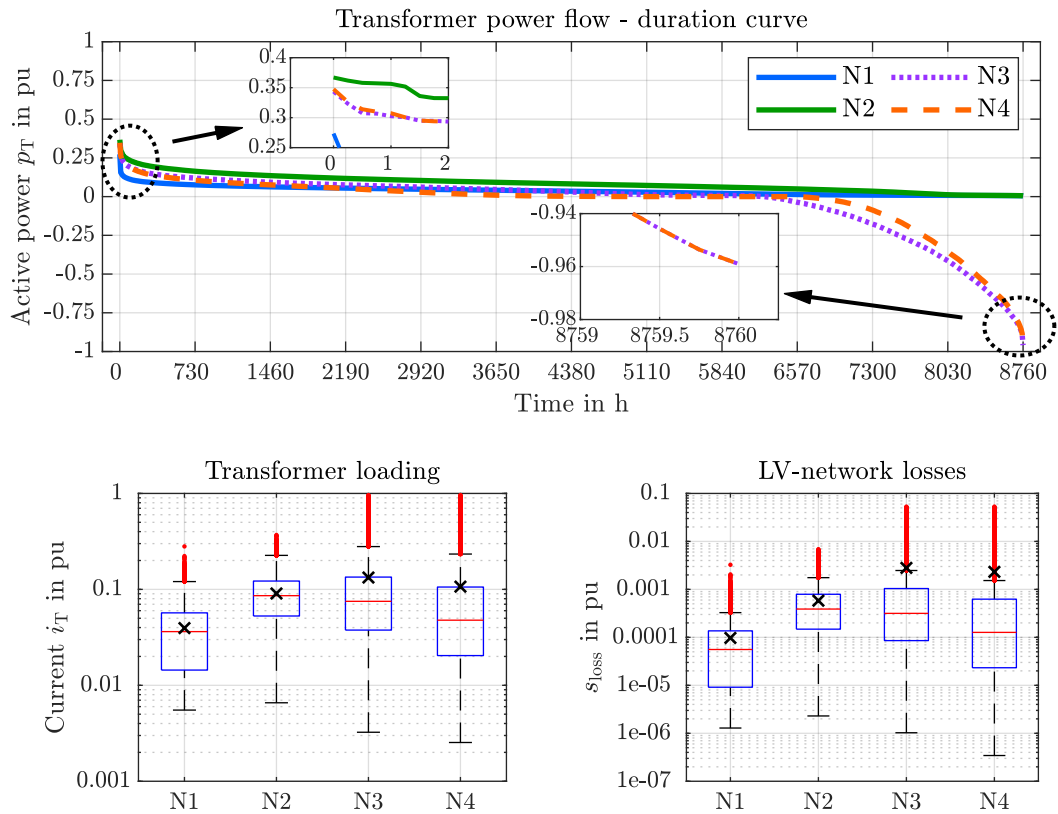


Figure 4.2: Active power flow  $p_T$  across the transformer, transformer loading  $i_T$  and LV-network losses  $s_{\text{loss}}$ — Scenario N1-N4:

N1: District heating, w/o photovoltaic's and electrical energy storages

N2: Heat pumps (heating demand), thermal energy storages with heating cartridges (domestic hot water demand), home charging of the electric vehicles, w/o photovoltaic's and electrical energy storages

N3: N2 with photovoltaic's added

N4: N2 with photovoltaic's and electrical energy storages added

Box plots: Black crosses represent the average values

*Scenario N1 - District Heating as Primary Heating System of Households:*

The electrical demand of the households is composed of domestic appliances, lighting and air conditioning. The households in N1 neither have electric vehicles (EV), photovoltaic systems (PV), nor energy storage systems. This leads, as shown in Figure 4.2 (solid green line), to a uni-directional load flow from the medium-voltage network to the low-voltage network (top-down).

On average, the transformer is loaded by 0.04 pu. At peak load times, a maximum transformer loading of 0.280 pu occurs. The network losses  $s_{\text{loss}}$  in the LV-network amount on average 0.0001 pu and a maximum of 0.003 pu.

*Scenario N2 - Heat Pumps as Primary Heating System of Households:*

In scenario N2, the households use heat pumps and thermal energy storages with heating cartridges to cover the thermal demand. Further, home charging of electric vehicles is considered. No PV systems are considered, leading to a uni-directional load flow (solid blue line) from the medium-voltage network to the low-voltage network (top-down).

Due to the increased annual electrical energy demand caused by thermal and electrical systems' coupling in scenario N2, the maximum transformer loading increases compared to N1 by 32 % to 0.369 pu.

The increased electrical energy demand also results in an increase of the average annual transformer loading  $i_T$  from 0.040 pu (N1) to 0.091 pu (N2). Similarly, the average annual network losses in the LV-network increase from 0.0001 pu (N1) to 0.0006 pu (N2).

*Scenario N3 - Heat Pump as Primary Heating System of Households and Installed Photovoltaic Systems:*

In Scenario N3, the generation of photovoltaic systems is additionally considered with a total installed power of 167 kWp, see Figure 4.1. Compared to Scenario N2, the generation of PV systems reduces the load flow  $p_T$  from the medium-voltage (MV) network (top-down) by 7 % to 0.344 pu. However, in Scenario N3, a reverse load flow from the LV network to the MV network occurs due to the photovoltaic systems' in-feed. In the worst case, a maximum load flow  $p_T$  to the MV network of 0.959 pu is reached. The integration of PV systems in scenario N3 increases the average transformer loading from 0.091 pu (N2) to 0.133 pu (N3).

The analysed average (black crosses) and median values (red line in boxplot) in scenarios N1 and N2 barely deviate, as seen in Figure 4.2. For scenario N3, the average value of 0.133 pu and the median value of 0.075 pu of the transformer loading differs significantly. This difference of the average and median values is referred to a non-symmetrical distribution of the load flow across the transformer caused by integrating the photovoltaic systems. Since the non-symmetrical distribution affects the median value less than the mean value, in the further analyses of scenarios N3 to N10, which consider PV generation, the average and maximum values are used to evaluate the simulation results instead of the median values.

### Scenario N<sub>4</sub> - Heat Pump as Primary Heating System of Households and Installed Photovoltaic- and Electrical Energy Storage Systems:

In Scenario N<sub>4</sub>, electrical energy storage (EES) systems are installed at the households. The use of EES systems increases the peak power  $p_T$  purchased from the MV network slightly from 0.344 pu (N<sub>3</sub>) to 0.348 pu (N<sub>4</sub>), which equals an increase of 1.2 %. However, the maximum power in-feed from the LV network to the MV network by the PV systems remains the same in both scenarios. Using EES systems, the annual average transformer loading is, compared to N<sub>3</sub>, reduced by 19.6 % to 0.107 pu and the network losses by 18 % to 0.0023 pu.

#### Note:

- The implementation of EES systems in households can achieve a significant reduction in the average transformer loading and LV-network losses.
- However, the EES system cannot contribute to reducing the power peaks caused by the PV feed-in.

## Line Loading

Figure 4.3 shows the results of the load flow calculations regarding the line loading of the scenarios N<sub>1</sub> to N<sub>4</sub>. The average and maximum line loadings are presented. The line loadings are normalised to the low-voltage cables' thermal rating (NAYY 4×150SE) of 270 A.

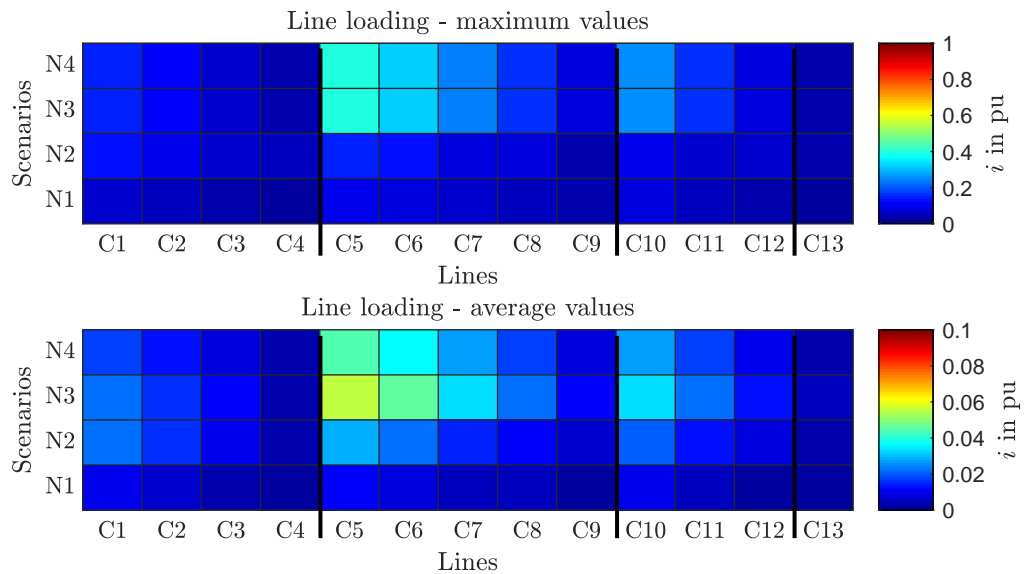


Figure 4.3: Line loading - scenarios N<sub>1</sub> to N<sub>4</sub>, cables C<sub>1</sub>... C<sub>13</sub>: 1 pu =  $I_{th} = 270$  A (see Figure 4.1)  
N<sub>1</sub>: District heating, w/o photovoltaic's and electrical energy storages  
N<sub>2</sub>: Heat pumps (heating demand), thermal energy storages with heating cartridges (domestic hot water demand), home charging of the electric vehicles, w/o photovoltaic's and electrical energy storages  
N<sub>3</sub>: N<sub>2</sub> with photovoltaic's added  
N<sub>4</sub>: N<sub>2</sub> with photovoltaic's and electrical energy storages added

The highest loadings for each feeder occur in the cables C1, C5 and C10 located at the respective feeders' beginning. Due to the high installed PV power in feeder II of 82.5 kW<sub>p</sub>, the cable C5 shows the maximum line loading of 0.4 pu at times of high power feed of the PV systems. The line loadings in the LV-network are well below the thermal rating of the respective cables.

Even with the increased demand due to the coupling of the thermal and electrical systems, the charging demand of the EVs and the high feed-in of the PV systems leads to no significant increase in the line loading in rural networks.

## Node Voltages

The results of the load flow calculations regarding the node voltages of the busbars of the analysed LV-network for scenarios N1 to N4 are shown in Figure 4.4. The limits of the node voltages are defined by the standard EN 50160 [38]. This standard specifies that the supply voltage in low-voltage networks may change by a maximum of  $\pm 10\%$  to the nominal voltage  $V_N$ . According to the Austrian national rules TOR [39], a maximum voltage rise in the low-voltage network, caused by power generation plants of  $\Delta v = 3\%$  at each node (house service connection) must be guaranteed.

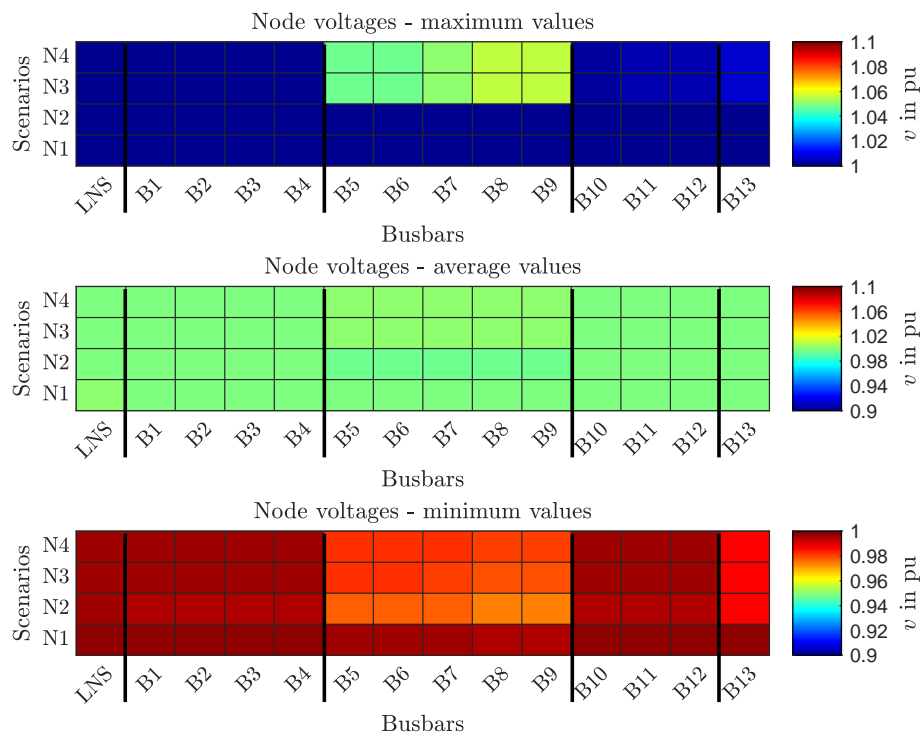


Figure 4.4: Node voltages – scenario N1 to N4, busbars LNS and B1... B13 (see Figure 4.1)

N1: District heating, w/o photovoltaic's and electrical energy storages

N2: Heat pumps (heating demand), thermal energy storages with heating cartridges (domestic hot water demand), home charging of the electric vehicles, w/o photovoltaic's and electrical energy storages

N3: N2 with photovoltaic's added

N4: N2 with photovoltaic's and electrical energy storages added

Figure 4.4 shows that due to the short cable lengths of the feeders I and III between 16 m and 56 m, no significant changes in the node voltages occur. However, the longer cable lengths of up to 500 m in feeder II lead to significant voltage changes at the busbars B5 to B9. The most affected household is connected at the end of feeder II at busbar B9. A maximum voltage rise to 1.056 pu (N3 and N4) and a maximum voltage decrease to 0.974 pu (N2) appears. As the peak loads only occur in a few hours per year, the busbars' average voltage level is still around 1 pu (N1 to N4).

## Summary

The coupling of the thermal and electrical systems using heat pumps, air conditioners, heating cartridges and the charging of electric vehicle increases the household's electrical demand accordingly. The investigated households' electrical demand has more than doubled, with an average increase of 124 %. This increased electrical demand will also affect distribution networks.

- Even when a household's demand for electrical energy is more than doubled, the transformer's maximum loading only increases by 32 %.

Although the implementation of PV systems reduces the load flow from the MV-network (top-down), the generation plant's surplus leads to a reversal of the load flow into the MV-network (bottom-up). Depending on the installed PV power in the LV-network, this surplus power in-feed can increase by multiple of the initial loading.

- The investigated rural network with an installed photovoltaic capacity of 167 kWp reached, in the worst case, a maximum load flow to the MV network (bottom-up) of 0.959 pu at a rated power of the transformer of 160 kVA. This is an increase of 178 % compared to the transformer's former maximum loading (top-down) without PV in-feed. It must be noted that the total installed photovoltaic capacity of 167 kWp in the network represents an extreme photovoltaic scenario, resulting in this heavy loading of the transformer. Nevertheless, the installed photovoltaic capacity per household falls within realistic limits.
- Furthermore, the increased demand or PV systems' high feed-in leads to no significant increase in the line loading in rural networks with a maximum loading of 0.4 pu ( $1 \text{ pu} = I_{\text{th}} = 270 \text{ A}$ ).

The implementation of electrical energy storage systems in households reduces average transformer loading and network losses. Here, the average transformer loading is reduced by 19.6 % and the network losses by 18 %.

- However, most interesting is that the implementation of electrical energy storage systems in households will not reduce the peak power in the rural network.

Due to the PV systems' power in-feed, the voltage increases in the worst case to 1.056 pu at busbar B9, located at the end of feeder II with relatively long cable lengths. To guarantee a maximum voltage rise of  $\Delta v = 3 \%$  at each busbar, see

Section 2.7, further measures are necessary. Possible measures are explained in the following Sections 4.2 and 4.3.

## 4.2 Dynamic Energy Tariffs and Peak-Shaving

New metering functions and services (smart metering) allow market-dependent dynamic or special consumer and prosumer-oriented tariffs. In the simplest case, the consumer can be motivated to increase the energy efficiency or change the behaviour by the increased information gain, e.g., by presenting the current tariff situations, the self-consumption or associated costs.

Since consumption and generation do not coincide in every time step, without energy storage or demand-side management, it is possibly necessary to purchase or feed-in energy at suboptimal tariffs or adapt the load profile (i.e. consumer behaviour) according to the tariff situation. For example, at low feed-in tariffs, it is economical to use the surplus generation of the photovoltaic system locally using load management and thus to increase the degree of self-consumption level or buffer it by using energy storages.

Subsequently, the effects of economically optimising prosumers on the LV network are examined for different tariff situations and at a given power limitation at the PCC's. The scenarios N4 to N7 get investigated in detail. Further, see Table C in the appendix and Table 4.2 for a specific scenario overview.

Figure 4.5 shows for the analysed scenarios N4 to N7 the active power flow across the transformer  $p_T$ , the transformer loading  $i_T$  and the network losses  $s_{\text{loss}}$ . The rated power of the transformer  $S_T$  and the respective voltage level  $V_n$  are selected as the base values (pu-system).

The introduction of dynamic energy tariffs (N5 and N7) has a significant impact on the optimised operation of prosumers. Figure 4.5 shows that at dynamic energy tariffs, the peak power of prosumers increases both in terms of power demand and surplus feed-in.

### *Scenario N5 - Dynamic Energy Tariff:*

Scenario N5 achieves the peak load in winter at times of no PV generation, a high heating and domestic hot water demand and at times of low energy costs. As a result of the low energy costs, almost all prosumers simultaneously charge their thermal energy storages via the power network. The electrical energy storages are not discharged at those times. Compared to scenario N4, in scenario N5, the load flow  $p_T$  from the MV network increases from 0.348 pu to 1.040 pu. A detailed explanation about the response of optimising prosumers on dynamic energy tariffs can be found in Section 3.3.

In addition to peak load, the surplus feed-in to the LV network increases at times of high PV generation combined with high energy costs (purchase) and high feed-in tariffs in scenario N5. Nearly the entire PV generation of the prosumers is fed into the LV network. The energy storages will not be charged at those times. Compared

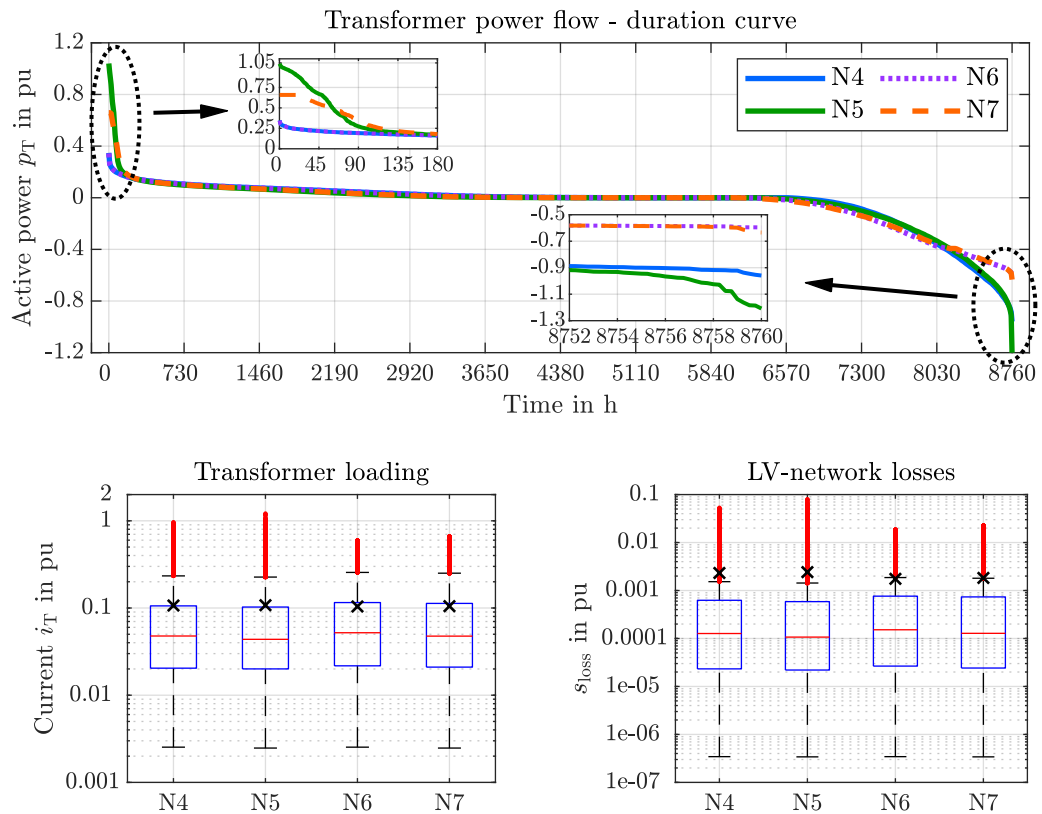


Figure 4.5: Active power flow  $p_T$  across the transformer, transformer loading  $i_T$  and LV-network losses  $s_{loss}$  – Scenario N4-N7

**N4:** Heat pumps (heating demand), thermal energy storages with heating cartridges (domestic hot water demand), home charging of the electric vehicles, photovoltaic's, electrical energy storages, static energy tariffs and PCC limits set to 17.3 kVA

**N5:** N4 with dynamic energy tariffs

**N6:** N4 performing peak-shaving with PCC limits set to 8 kVA

**N7:** N4 with dynamic energy tariffs and performing peak-shaving with PCC limits set to 8 kVA

Box plots: Black crosses represent the average values

to scenario N4, in scenario N5, the power in-feed into the MV network increases from 0.959 pu to 1.208 pu.

The introduction of dynamic tariffs combined with optimising prosumers increases the purchasing power and feed-in power. In both cases – purchase and in-feed – the transformer gets overloaded at peak times, about five hours a year. However, in contrast, the average transformer loading  $i_T$  and network losses  $s_{loss}$  in scenarios N4 and N5 remains almost the same.

#### *Scenario N6 and N7 - Peak-Shaving:*

By limiting the maximum power per household, the maximum transformer loading can be significantly reduced. This limitation of the power can be achieved by smart metering and, for example, by introducing power-based tariffs, at which exceeding a

defined power limit for a specific time result in increased electricity costs.

A power limit of exemplary 8 kVA at the PCC of the households is set in scenarios N6 and N7. The maximum power flow  $p_T$  from the MV-Network to the LV-network in N5 is reduced by using peak-shaving in N7 by 37 % from 1.04 pu to 0.659 pu (N7). Similarly, the maximum power at surplus feed-in decreases by 51 % from 1.208 pu (N5) to 0.634 pu (N7).

Performing peak-shaving, both the purchased peak power from the MV-network and the feed-in peak power to the MV-network can be significantly reduced.

## Line Loading

Figure 4.6 shows the results of the load flow simulations regarding the line loading of the scenarios N4 to N7. The average and maximum line loadings are presented. These cable loadings are normalised to the low-voltage cables' thermal rating (NAYY  $4 \times 150SE$ ) of 270 A.

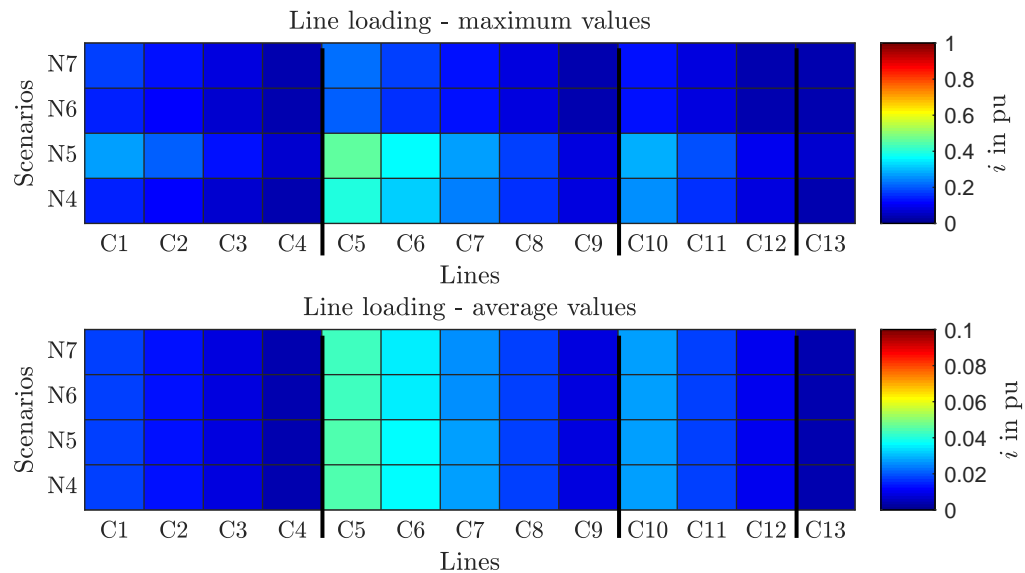


Figure 4.6: Line loading – scenarios N4 to N7, cables C1... C13:  $1 \text{ pu} = I_{th} = 270 \text{ A}$  (see Figure 4.1)  
**N4:** Heat pumps (heating demand), thermal energy storages with heating cartridges (domestic hot water demand), home charging of the electric vehicles, photovoltaic's, electrical energy storages, static energy tariffs and PCC limits set to 17.3 kVA  
**N5:** N4 with dynamic energy tariffs  
**N6:** N4 performing peak-shaving with PCC limits set to 8 kVA  
**N7:** N4 with dynamic energy tariffs and performing peak-shaving with PCC limits set to 8 kVA

The highest line loadings occur in the cables C1, C5 and C10 located at the beginning of the respective feeder. The maximum line loading with 0.46 pu (N5) at cable C5 appears at the maximum power in-feed of the feeders II PV systems. The introduction of a power limit at the PCC of the households in N6 and N7 leads to a significant

reduction in line loading. Thus, the cable C5 with the previously highest loading reduces from 0.46 pu (N5) to 0.22 pu (N7). Even with the increased power due to the implementation of dynamic energy tariffs, no significant line loadings occur in rural networks at peak times.

## Node Voltages

The results of the load flow calculations regarding the node voltages of the busbars of the analysed LV-network for scenarios N4 to N7 are shown in Figure 4.7. The limits of the node voltages are defined by the standard EN 50160 [38]. This standard specifies that the supply voltage in low-voltage networks may change by a maximum of  $\pm 10\%$  to the nominal voltage  $V_N$ . According to the Austrian national rules TOR [39], a maximum voltage rise in the low-voltage network, caused by power generation plants of  $\Delta v = 3\%$  at each node (house service connection) must be guaranteed.

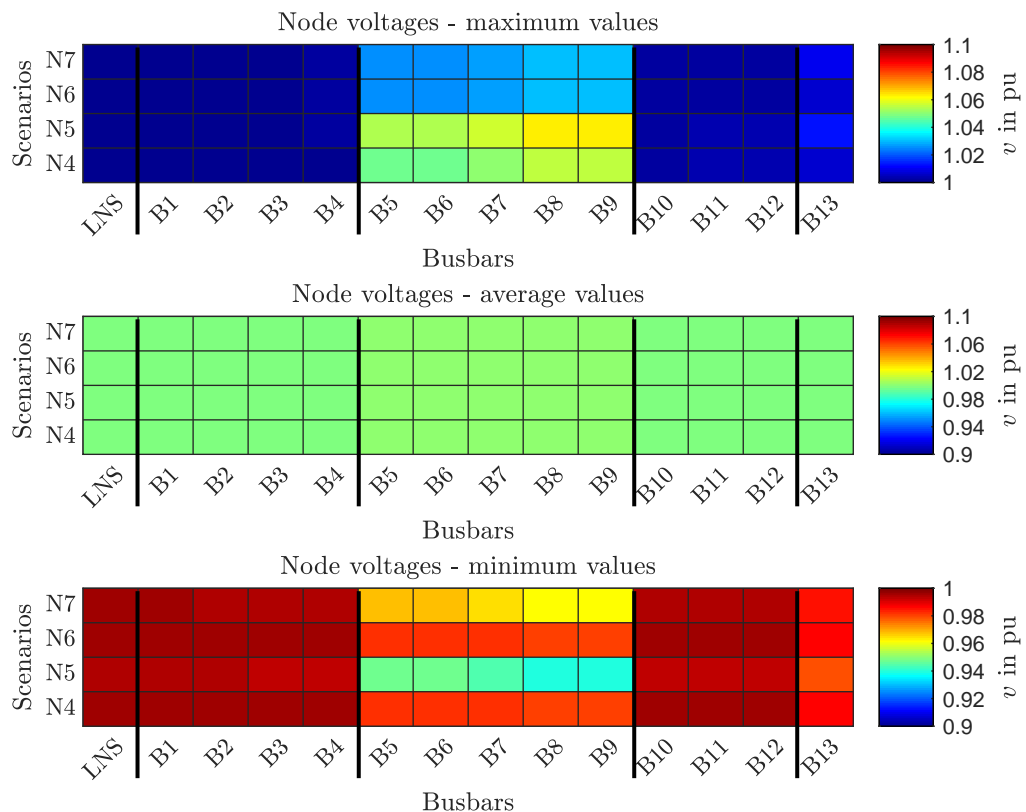


Figure 4.7: Node voltages – scenarios N4 to N7, busbars LNS and B1... B13 (see Figure 4.1)

N4: Heat pumps (heating demand), thermal energy storages with heating cartridges (domestic hot water demand), home charging of the electric vehicles, photovoltaic's, electrical energy storages, static energy tariffs and PCC limits set to 17.3 kVA

N5: N4 with dynamic energy tariffs

N6: N4 performing peak-shaving with PCC limits set to 8 kVA

N7: N4 with dynamic energy tariffs and performing peak-shaving with PCC limits set to 8 kVA

The introduction of dynamic tariffs in N5 and N7 results in increased peak power

at the cables, causing the highest voltage changes in scenario N5 (dynamic energy tariff, w/o power limits). Due to the long cable length of 500 m of cable C6, the most affected household is connected at the end of feeder II at busbar B9. A maximum voltage of 1.064 pu (N5) and a minimum voltage of 0.94 pu (N5) appears. As the peak loads only occur in a few hours per year, the busbars' average voltage level is still around 1 pu (N4 to N7).

Introducing a power limit at the households' PCC's reduces the occurring maximum node voltage rise or decrease. Compared to scenario N5, the maximum voltage rise in scenario N7 is reduced from 1.064 pu to 1.03 pu. Furthermore, the voltage decrease is reduced from 0.94 pu to 0.962 pu.

## Summary

The analyses of the investigated rural network show that the introduction of dynamic tariffs combined with prosumers' optimising operation increases both

- the purchasing power from 0.348 pu to 1.040 pu and
- feed-in power from 0.959 pu to 1.208 pu,

which leads in both cases to an overloading of the transformer at peak times, about five hours a annually.

The increased power caused by using dynamic tariffs combined with prosumers' optimising operation leads to no significant increase in the line loading in rural networks with a maximum line loading of 0.46 pu ( $1 \text{ pu} = I_{\text{th}} = 270 \text{ A}$ ).

However, the increased power results in a minimum voltage of 0.94 pu (purchased power) and a maximum voltage of 1.064 pu (power in-feed) appears. As the peak loads only occur in a few hours per year, the busbars' average voltage level is still around 1 pu.

Performing peak-shaving by setting a power limit of exemplary 8 kVA at the households' PCC, both

- the purchased peak power from the MV-network (reduced by 37 % from 1.04 pu to 0.659 pu) and the
- feed-in peak power to the MV-network (reduced by 51 % from 1.208 pu to 0.634 pu)

can be significantly reduced.

The introduction of dynamic energy tariffs has a significant impact on the optimised operation of prosumers. The power exchange between the prosumer and electrical distribution network also changes due to the altered charging behaviour of electrical and thermal energy storage systems. Measures to limit the power exchange, such as peak-shaving, can significantly reduce the peak power.

The performed simulations reveal that the introduction of dynamic energy tariffs will fundamentally change prosumers' operation, directly influencing the load flow in

distribution networks. The power increases significantly at the same energy demand, considering that households pay for the purchased or fed-in amount of energy (energy-based tariffs). Performing peak-shaving by setting power limits at the households' PCC the optimising prosumers' respective peak power to be reduced.

### 4.3 Impact of Voltage and Reactive Power Control on the Distribution Network

Due to the optimising prosumers' operation and the in-feed of the surplus generation of the PV systems into the LV-network, the node voltages are influenced. As shown in Section 4.1 and 4.2, a high in-feed into the LV-network (scenario N4) leads to a node voltage rise to 1.06 pu. Section 4.1 shows that voltage changes mainly occur in networks with long cable lengths. To comply with the voltage limits according to EN 50160 [38] and the Austrian national rules TOR [39], the effectiveness of the following methods for voltage and reactive power control are determined.

- *Scenario N4 – Constant Power Factor Mode:*

The generation plants of the prosumers operate at a constant power factor mode with a unity power factor ( $\cos(\varphi) = 1$ ).

- *Scenario N8 – Constant Power Factor Mode:*

To reduce the voltage rise in the rural network caused by the generation plants of the prosumers, a constant power factor  $\cos(\varphi) = 0.95$  (under-excited) is set.

- *Scenario N9 – Voltage-Reactive Power Mode:*

To limit the voltage rise and voltage decrease, the voltage-reactive power (volt-var) mode is used to actively control the reactive power output of the inverter as a function of the voltage  $v$ . A detailed explanation about the volt-var mode can be found in Section 2.6.1.

A dead band of  $\pm 2\% v_n$  ( $1 \text{ pu} = v_n = 0.4 \text{ kV}$ ) as well as a droop of  $2\% v_n$  is set. According to the Austrian national rules TOR, the required reactive power capability for inverter-based generators  $q_{\max}$  is set to 0.436 pu, corresponding to a power factor  $\cos(\varphi)$  of 0.9.

- *Scenario N10 – Active Power-Power Factor Mode:*

In Scenario 10, the active power-power factor (watt-cos  $\varphi$ ) mode is used. The active power-power factor (watt-cos  $\varphi$ ) mode regulates the power factor  $\cos(\varphi)$  piecewise linearly as a function of the active power  $p$ .

When reaching an active power of  $p = 0.5$  ( $1 \text{ pu} \hat{=} P_r$ ), the inverter operates in under-excited mode and reduces the power factor  $\cos(\varphi)$  linearly to a minimum of 0.9 pu. Further informations of the watt-cos  $\varphi$  mode can be found in Section 2.6.1.

To ensure the set power factors or the reactive power in scenarios N8 to N10, the inverter's active power might be curtailed at times of high generation of the PV systems. To minimise the curtailment of the active power, the selected inverters have a Sizing Ratio of  $SR = 1.1$ . A detailed explanation of PV modelling and the voltage and reactive power control can be found in Section 2.6.1.

## Transformer Loading and LV-Network Losses

Figure 4.8 shows the active power flow for the analysed scenarios N4 and N8 to N10 over the transformer  $p_T$ , the transformer loading  $i_T$  and the network losses  $s_{\text{loss}}$  of the low-voltage (LV) network. The rated transformer power  $S_T$  and the respective voltage level  $V_n$  are selected as the base values (pu-system).

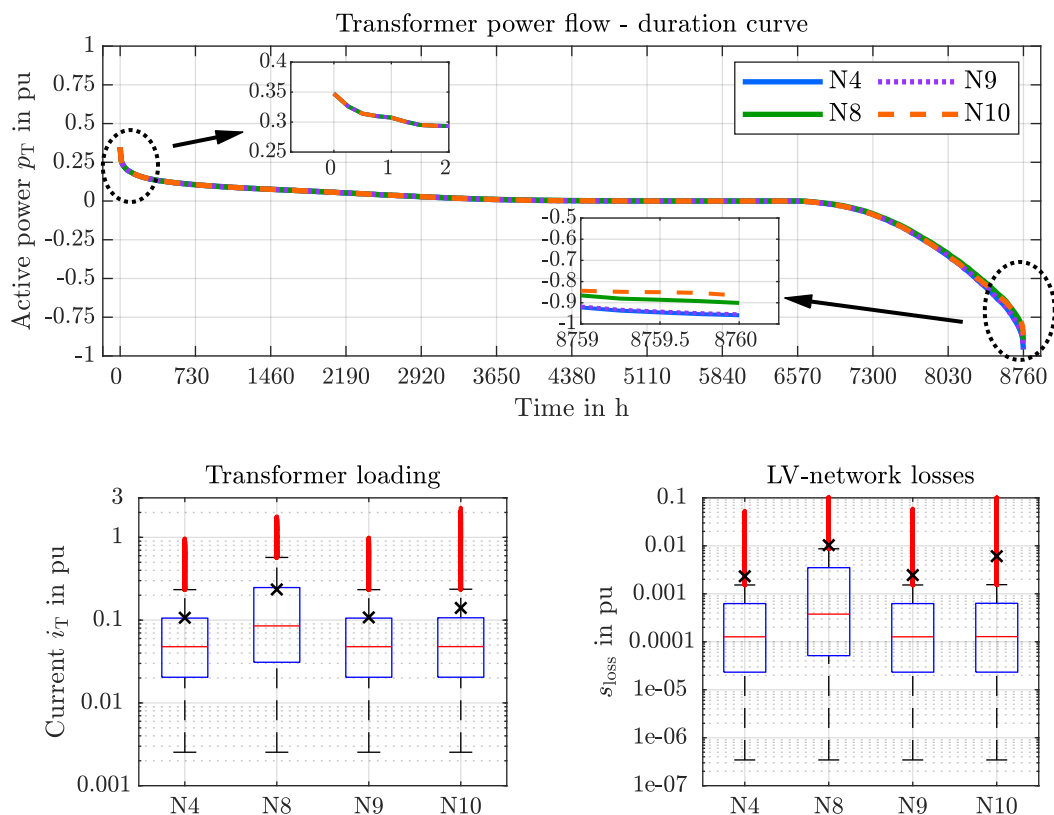


Figure 4.8: Active power flow  $p_T$  across the transformer, transformer loading  $i_T$  and LV-network losses – Scenarios N4 and N8 to N10

N4: Heat pumps (heating demand), thermal energy storages with heating cartridges (domestic hot water demand), home charging of the electric vehicles, photovoltaic's, electrical energy storages, static energy tariffs, PCC limits set to 17.3 kVA and the inverters are operating in a constant power factor mode  $\cos(\varphi) = 1$

N8: N4 and the inverters are operating in a constant power factor mode  $\cos(\varphi) = 0.95$  (under-excited)

N9: N4 and the inverters are operating in volt-var mode

N10: N4 and the inverters are operating in watt-cos  $\varphi$  mode

Box plots: Black crosses represent the average values

The following assumptions apply to the sign of the electrical power at the transformer:

- Power  $p_T > 0$ : load flow from the medium-voltage network to the low-voltage network (top-down)
- Power  $p_T < 0$ : load flow from the low-voltage network into the medium-voltage network (bottom-up)

Compared to the scenarios N4 and N9, a reduced active power in-feed of the prosumers in the scenarios N8 (constant power factor mode,  $\cos(\varphi) = 0.95$ ) and N10 (watt- $\cos \varphi$  mode) occur. The active power in-feed of the prosumers in scenarios N8 and N10 is curtailed at times of high generation of the PV systems to guarantee the respective set power factors  $\cos(\varphi)$ . This high active power in-feed of the prosumers to the LV network leads to a reverse load flow from the LV network to the MV network.

Compared to N4 and N9, the PV in-feed is curtailed at peak times (between 540 h/a (N8) and 314 h/a (N10)). This leads to a reduced power in-feed to the MV network from 0.959 pu (N4) to 0.901 pu in N8 and 0.867 pu in N10, as shown in Figure 4.8 (transformer power flow - duration curve).

Due to the provided reactive power by the inverters of the prosumers, the transformer loading as well as the LV-network losses are influenced significantly and increased especially in the scenarios N8 (constant power factor mode:  $\cos(\varphi) = 0.95$ ) and N10 (watt- $\cos \varphi$  mode), as the provided reactive power is mainly depended on the active power in-feed of the PV systems.

#### *Scenario N8 - Constant Power Factor Mode*

By choosing a constant power factor  $\cos(\varphi)$  of 0.95 (under-excited), the prosumers' inverters provide reactive power at any time. This provided reactive power leads in total to an increasing transformer loading and higher LV-network losses compared to scenario N4 ( $\cos(\varphi) = 1$ ), both in average and for maximum values. The maximum transformer loading increases from 0.96 pu (N4) to 1.78 pu, which heavily overloads the transformer.

#### *Scenario N10 - Active Power-Power Factor Mode*

In Scenario N10, the power factor  $\cos(\varphi)$  is, after reaching the setpoint of  $p = 0.5$  pu ( $1 \text{ pu} \hat{=} P_r$ ), linearly reduced to a minimum of 0.9 pu at  $p = 1$  pu. With the chosen settings of the watt- $\cos \varphi$  mode, the average transformer loading is slightly increased from 0.107 pu (N4) to 0.140 pu (N10).

According to the chosen settings with a power factor of  $\cos(\varphi) = 0.9$  at a active power of the inverter of  $p = 1$  pu, a maximum transformer loading of 2.26 pu occurs.

Note, in scenarios N8 and N10, the transformer is heavily overloaded at feed-in peak times.

- Therefore, both chosen methods – constant power factor with  $\cos \varphi = 0.95$  and watt- $\cos \varphi$  mode – for reactive power control are not recommended for the investigated network at the chosen extreme PV scenario.

- A limitation of the feed-in power (peak-shaving), reduction of the installed PV power in the network or selecting other setpoints of the power factors  $\cos(\varphi)$  are recommended to reduce the transformer loading significantly.

#### Scenario N9 – Voltage-Reactive Power Mode:

Differently to the watt- $\cos\varphi$  mode, in scenario N10, the volt-var mode actively controls the inverter's reactive power output as a function of the voltage  $v$ . The volt-var mode barely affects the average transformer loading and the LV-network losses. The average transformer loading is increased from 0.107 pu (N4) to 0.108 pu. With the volt-var mode's chosen settings, a maximum transformer loading of 0.99 pu occurs.

## Line Loading

Figure 4.9 shows the results of the load flow simulations regarding the line loading of the scenarios N4, N8 to N10. The average and maximum line loadings are presented. The line loadings are normalised to the thermal rating of the low voltage cables (NAYY 4×150SE) of 270 A.

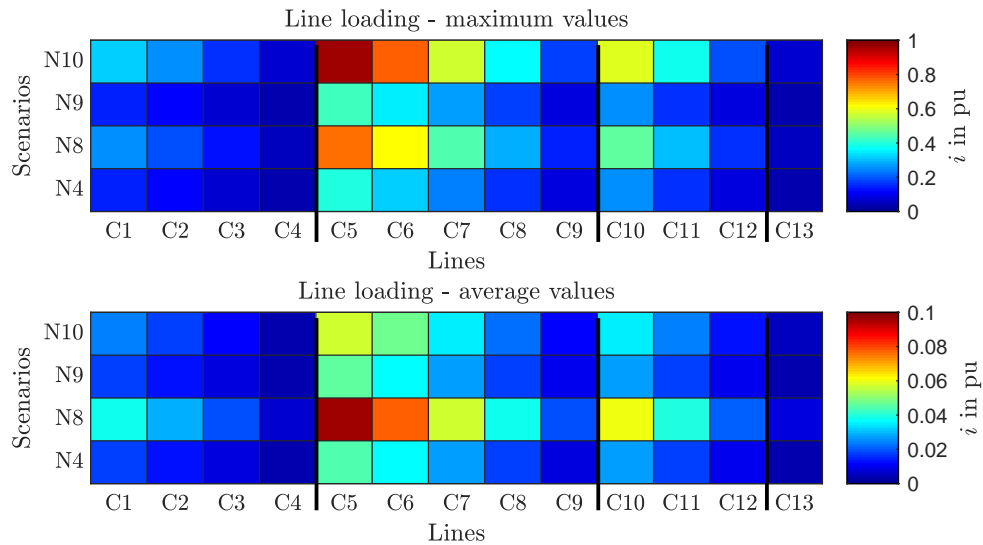


Figure 4.9: Line loading – scenario N4 and N8 to N10, cables C1... C13: 1 pu =  $I_{th} = 270$  A (see Figure 4.1)

N4: Heat pumps (heating demand), thermal energy storages with heating cartridges (domestic hot water demand), home charging of the electric vehicles, photovoltaic's, electrical energy storages, static energy tariffs, PCC limits set to 17.3 kVA and the inverters are operating in a constant power factor mode  $\cos(\varphi) = 1$

N8: N4, inverters are operating with a constant power factor of 0.95 (under-excited)

N9: N4 and the inverters are operating in volt-var mode

N10: N4 and the inverters are operating in watt- $\cos\varphi$  mode

The high amount of provided reactive power in scenario N8, constant power factor mode ( $\cos(\varphi) = 0.95$ ), and in scenario N10, watt- $\cos\varphi$  mode, to the LV network

shows the highest degree of line loading in the analysed scenarios. The maximum line loading of 0.97 pu occurs in scenario N10 at the cable C5. As the constant power factor mode (N8) with a  $\cos(\varphi) = 0.95$  (under excited) provide at any time reactive power of power in-feed, results in general to higher loading of the lines, compared to any scenario with applied reactive power management.

The volt-var mode is characterised by flexible, reactive power control as a function of the node voltages  $v$  and shows no significant increase in cable loading in combination with effective voltage control.

## Node Voltages

Based on the performed load flow calculations for the scenarios N4 and N8 to N10, the effectiveness of the investigated methods for voltage and reactive power control are investigated in detail by analysing the node voltages. Figure 4.10 shows the node voltages of the busbars of the analysed LV-network. The limits of the node voltages are defined by the standard EN 50160 [38]. This standard specifies that the supply voltage in low-voltage networks may change by a maximum of  $\pm 10\%$  to the nominal voltage  $V_N$ . According to the Austrian national rules, TOR [39], a maximum voltage rise in the low-voltage network, caused by power generation plants of  $\Delta v = 3\%$  at each node (house service connection) must be guaranteed.

Figure 4.10 shows that in feeder II, due to the long cable C5 (500 m) at the beginning of the feeder and the high installed power of the PV systems of the prosumers, significant changes in the node voltages of the busbars B5 to B9 occur. However, a shorter length of the cables, about 50 metres, in the feeder I and III lead to no significant voltage changes.

### *Scenario N8 - Constant Power Factor Mode:*

At a unity power factor  $\cos(\varphi)$  in scenario N4, a maximum voltage rise to 1.056 pu and voltage decrease to 0.98 pu occurs at the busbar B9. Setting a constant power factor  $\cos(\varphi)$  of 0.95, in scenario N8, the maximum voltage rise caused by power in-feed of the generation plants is compared to scenario N4 significantly reduced to a maximum node voltage of 1 pu for the entire network area.

The circumstance that at a constant power factor  $\cos(\varphi)$  of 0.95 (under-excited) all inverters of the prosumers in the LV-network provide at any times of power in-feed, reactive power to the LV-network, leads to a significant voltage decrease in the entire network, reaching a minimum node voltage of 0.921 pu at busbar B9. The node voltage at the LNS (0.4 kV) is now also affected significantly and is reduced to 0.937 pu.

### *Scenario N10 - Voltage-Reactive Power Mode:*

Similar to a constant power factor  $\cos(\varphi)$  in scenario N8, the watt- $\cos\varphi$  mode in scenario N10 also affects the node voltages in the entire network area equally.

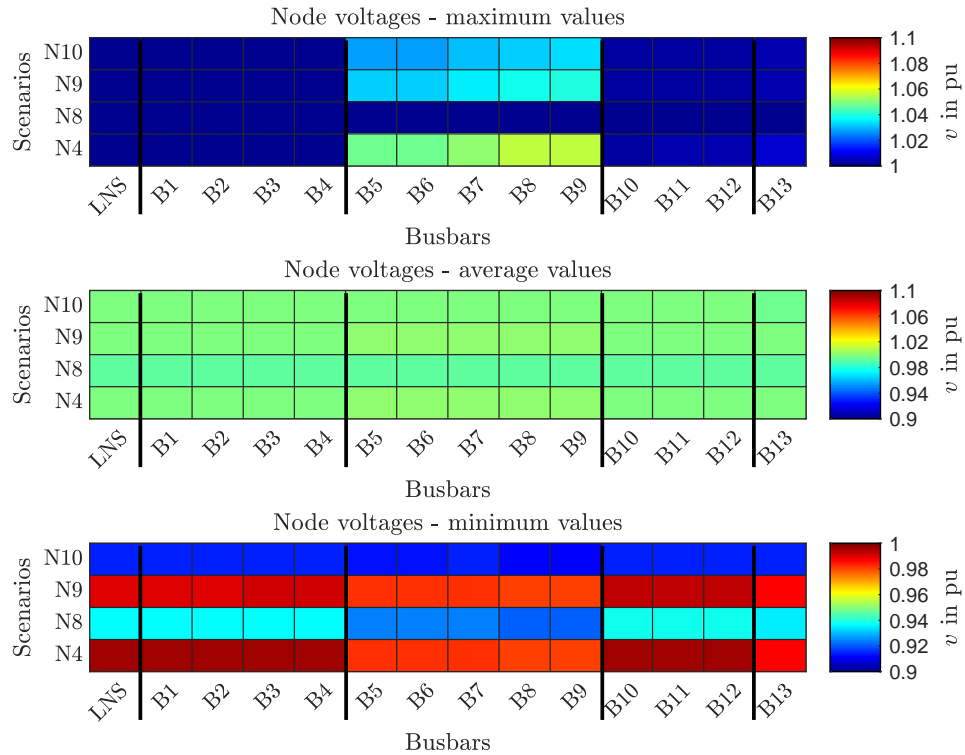


Figure 4.10: Node voltages - scenarios N4,N8 - N10, busbars LNS and B1-B13 (see Figure 4.1)

N4: Heat pumps (heating demand), thermal energy storages with heating cartridges (domestic hot water demand), home charging of the electric vehicles, photovoltaic's, electrical energy storages, static energy tariffs, PCC limits set to 17.3 kVA and the inverters are operating in a constant power factor mode  $\cos(\varphi) = 1$

N8: N4, inverters are operating with a constant power factor of 0.95 (under-excited)

N9: N4 and the inverters are operating in volt-var mode

N10: N4 and the inverters are operating in watt-cos  $\varphi$  mode

In Scenario N10, the power factor  $\cos(\varphi)$  is, after a power level of  $p = 0.5$  pu, linearly reduced up to a minimum of 0.9 at  $p = 1$  pu. The chosen power factor  $\cos(\varphi)$  of 0.9 at  $p = 1$  pu results in high voltage decrease in the entire network and to a minimum node voltage at busbar B9 of 0.911 pu.

In comparison to scenario N4, the voltage rise caused by the prosumers' generation plants reduces significantly, with a maximum reduction of the node voltage at busbar B9 from 1.056 pu (N4) to 1.033 pu.

#### *Scenario N9 – Active Power-Power Factor Mode:*

In scenario N9, the voltage-reactive power (volt-var) mode actively controls the inverter's reactive power output as a function of the node voltage  $v$  (B1... B13), which leads to the lowest transformer loading as well as an effective voltage control. The volt-var mode offers more flexible control of the voltage, than the watt-cos  $\varphi$  mode. So it offers a good compromise between voltage level and the provided reactive power, than the watt-cos  $\varphi$  mode.

The generation plants connected to the feeders I, III and IV rarely provide reactive

power, as the voltage level is mostly between 0.98 pu and 1.02 pu (dead band). However, only the generation plants at feeder II must actively provide reactive power to minimise the voltage rise. The maximum voltage rise at busbar B9 is decreased from 1.056 pu (N4) to 1.039 pu (N9).

*Characteristic Curves and Operating Range of Voltage-Reactive Power Mode and Active Power-Power Factor Mode:*

Caused by the high cable lengths and the power in-feed of the generation plants in feeder II, the greatest need for reactive and voltage power control occurs here. Figure 4.11 shows the general characteristic curves and the operating range, based on the performed load flow calculations, for the volt-var mode, Scenarios N9, and the watt-cos  $\varphi$  mode, Scenario N10, for the generation plants of feeder II in detail.

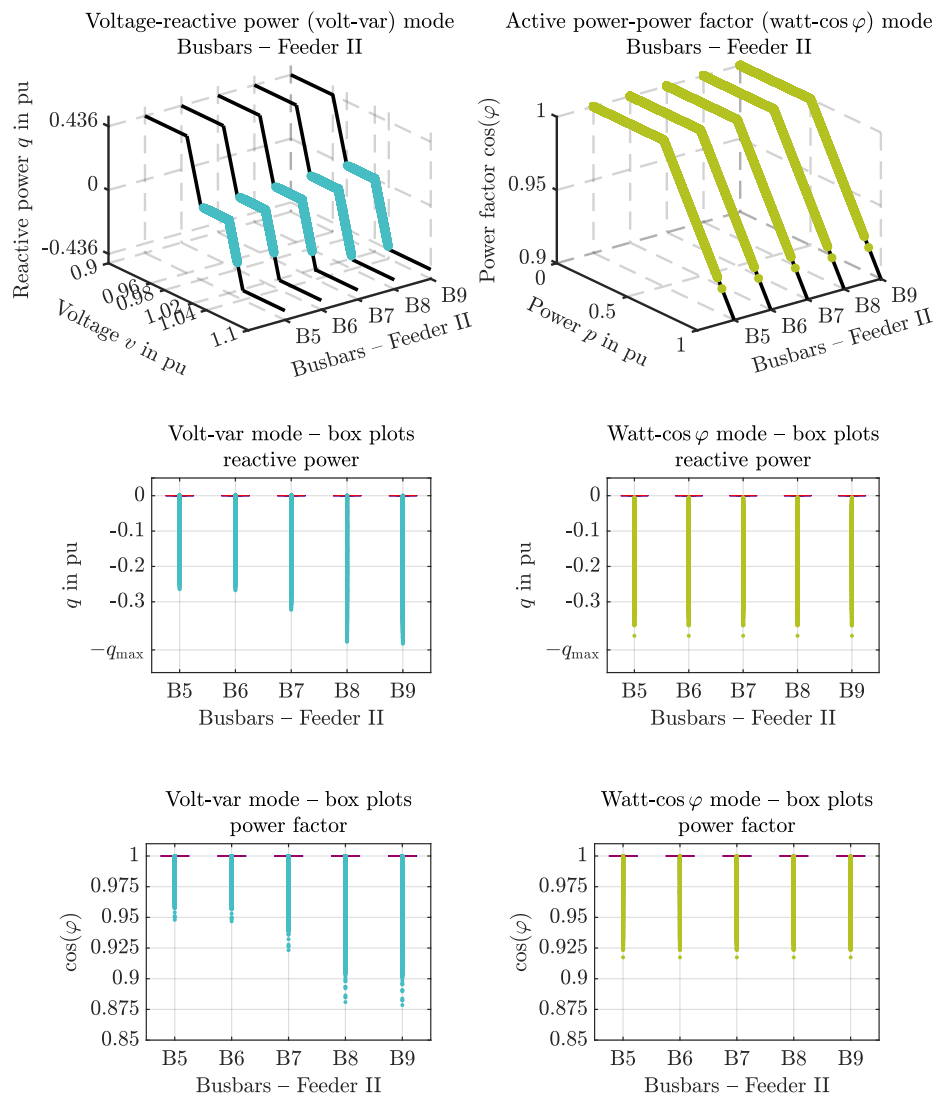


Figure 4.11: Characteristic curves of the volt-var mode (left) and the watt-cos  $\varphi$  mode (right) for feeder II

Figure 4.11 (left) shows the characteristic curve (black line) of the voltage-reactive

power (volt-var) mode of the prosumers of the feeder II for the busbars B5 to B9. The cyan dots show every moment the volt-var mode is actively providing reactive power to the network. The volt-var mode actively controls the inverter's reactive power output as a function of the node voltage  $v$ .

Generally, generation plants operating in volt-var mode at the beginning of the feeder do only slightly participate in reactive power control. The further away the generation plants are located at the feeder from the feeding network (local network station), the higher the participation in reactive power control.

Figure 4.11 (right) shows the characteristic curve (black line) of the watt- $\cos\varphi$  mode of the prosumers at the respective busbar. The yellow dots show every moment the watt- $\cos\varphi$  mode is actively providing reactive power to the network. In contrast to the volt-var mode, at the watt- $\cos\varphi$  mode the power factor  $\cos(\varphi)$  is, after reaching the setpoint of  $p = 0.5$  pu, linearly reduced to a minimum of 0.9 pu (under-excited).

Compared to the volt-var mode, where generation plants at the end of the feeder must participate more in reactive power control, in the watt- $\cos\varphi$  mode each generation plant participates equally in the voltage control.

## Summary

Due to the optimising prosumers' operation and the in-feed of the surplus generation of the PV systems into the LV-network, the busbars' voltage levels are influenced accordingly. In scenario N4 – constant power factor mode with a unity power factor – the voltage increases in the worst case to 1.06 pu at busbar B9, located at the end of feeder II with relatively long cable lengths. To guarantee a maximum voltage rise of  $\Delta v = 3\%$  at each busbar, the following three measures are analysed in detail:

- Constant Power Factor Mode  $\cos(\varphi) = 0.95$  (under-excited)
- Active Power-Power Factor (watt- $\cos\varphi$ ) Mode
- Voltage-Reactive Power (volt-var) Mode

To ensure the set power factors or the reactive power, the inverter's active power might be curtailed at times of high generation of the PV systems. To minimise the active power's curtailment, the selected inverters have a Sizing Ratio of  $SR = 1.1$ .

*Constant Power Factor Mode  $\cos(\varphi) = 0.95$  (under-excited):*

By choosing a constant power factor  $\cos(\varphi)$  of 0.95 (under-excited), the prosumers' inverters provide reactive power at any time. This provided reactive power leads to an increasing transformer loading, higher LV-network losses, and a higher loading of the lines compared to any scenario with applied reactive power management, both in average and for maximum values, reaching a maximum transformer loading of 1.78 pu and therefore a heavily overloading of the transformer.

The PV in-feed is curtailed at peak times (around 540 h/a), which leads to a reduced active power in-feed to the MV network from 0.959 pu (constant power factor mode with a unity power factor) to 0.901 pu.

Setting a constant power factor  $\cos(\varphi)$  of 0.95, the maximum voltage rise caused by power in-feed of the generation plants is significantly reduced in the entire network to a maximum node voltage of 1 pu and a minimum node voltage of 0.921 pu at busbar B9. The node voltage at the local network station (LNS - 0.4 kV) is now also affected significantly and is reduced to 0.937 pu.

*Active Power-Power Factor (watt-cos  $\varphi$ ) Mode:*

The active power-power factor (watt-cos  $\varphi$ ) mode regulates the power factor  $\cos(\varphi)$  piecewise linearly as a function of the active power  $p$ . When reaching an active power of  $p = 0.5 p_r$ , the inverter operates in under-excited mode and reduces the power factor  $\cos(\varphi)$  linearly to a minimum of 0.9 pu. Whereas, at the watt-cos  $\varphi$  mode, each generation plant participates equally in the voltage control.

With the chosen settings of the watt-cos  $\varphi$  mode, the transformer loading is slightly increased to an average value of 0.140 pu and a maximum of up to 2.26 pu. Furthermore, the line loading is also increased on average, reaching a maximum line loading of 0.97 pu at cable C5.

The PV in-feed is curtailed at peak times (around 314 h/a), which leads to a reduced maximum power in-feed to the MV network from 0.959 pu (constant power factor mode with a unity power factor) to 0.867 pu. Nevertheless, the transformer is heavily overloaded at those feed-in peak times.

- Therefore, both chosen methods – constant power factor with  $\cos \varphi = 0.95$  and watt-cos  $\varphi$  mode – for reactive power control are not recommended for the investigated network at the chosen extreme PV scenario.
- Recommendations for reducing the transformer loading significantly include limiting the feed-in power (peak-shaving), reducing the installed PV power in the network or selecting other setpoints of the power factors  $\cos(\varphi)$ .

Similar to a constant power factor  $\cos(\varphi)$  mode, the watt-cos  $\varphi$  mode also affects the node voltages in the entire network area equally, resulting in a voltage decrease in the entire network leading at the busbar B9 to a minimum node voltage of 0.911 pu and a maximum voltage of 1.033 pu.

*Voltage-Reactive Power (volt-var) Mode:*

The volt-var mode can be used to limit both the voltage rise and voltage decrease and actively control the inverter's reactive power output as a function of the voltage  $v$ . A dead band of  $\pm 2 \% v_n$  ( $1 \text{ pu} = v_n = 0.4 \text{ kV}$ ) as well as a droop of 2 % is set.

The volt-var mode only barely affects the average transformer loading, the LV-network losses and the line loading. The average transformer loading is increased minimal 0.107 pu to 0.108 pu and leading to an increase of maximum transformer loading from 0.96 pu (N4) of 0.99 pu. The volt-var mode with a flexible, reactive power control as a function of the node voltages  $v$  shows no significant increase in cable loading.

The volt-var mode actively controls the inverter's reactive power output as a function of the node voltage  $v$  (B1... B13), which leads to the lowest transformer loading as well as an effective voltage control.

The generation plants connected to the feeders I, III and IV rarely provide reactive power, as the voltage level is mostly between 0.98 pu and 1.02 pu (dead band). However, caused by long line lengths and high PV in-feed, the generation plants at feeder II must actively provide reactive power to minimise the voltage rise. The maximum voltage rise at busbar B9 is decreased from 1.056 pu to 1.039 pu.

The volt-var mode offers more flexible control of the node voltage, with a good compromise between voltage level and the provided reactive power, than the watt-cos  $\varphi$  mode. Otherwise, generators at the end of the feeder, in particular, must participate very intensively in reactive power control. Compared to the volt-var mode, in the watt-cos  $\varphi$  mode all generators participate regardless of their position in the network in reactive power control.

# 5 Summary and Outlook

## Simulation Model – ProsOpt

(Sections 2.2 to 2.6.8)

Within ProsOpt, a powerful simulation model was developed in the software Matlab to model, simulate and analyse the behaviour and steady-state energy flows of hybrid energy systems such as single-family houses. Using linear optimisation algorithms, ProsOpt determines in a forecast-based manner the optimal use of decentralised energy generation and storage systems. It does so by considering different optimisation objectives, desired energy services (heating, cooling, electrical energy services), external boundary conditions (e.g., building structure, weather), individual technical components, as well as selected energy tariffs.

The following list outlines possible applications for the developed simulation model ProsOpt according to the energy-based analysis of prosumers.

- Optimisation of the prosumers operation considering various objectives, such as increasing the degree of self-consumption or achieving an economically or ecologically optimal advantage.
- Dimensioning and optimal operation of generation and storage systems.
- Coupling a prosumer's thermal and electrical energy system.
- Optimal operation management of thermal and electrical energy storage systems.
- Analysis of various energy tariffs' influence on prosumers' operation.
- Integration of electric vehicles including Vehicle2Grid / Grid2Vehicle.
- Determination of optimising prosumers' behaviour in low-voltage distribution networks taking into account voltage and reactive power control strategies.
- Investigation of specific building construction designs on the energy demand of prosumers.

ProsOpt is designed to perform as a standalone application for the detailed analysis of prosumers' optimised operation and as a sub-function in load-flow calculations. ProsOpt also considers different voltage and reactive power control methods.

The design of ProsOpt's methodology is transferable to other hybrid energy systems, e.g., industrial companies. ProsOpt's methodology was also implemented in the project "REsys - Regelungsstrategien zur Effizienzsteigerung komplexer hybrider Energiesysteme" funded by the Austrian "Klima- und Energiefonds" as a part of the "Energieforschungsprogramm 2015".

*Future Work:*

- Plug-in in commercial power system analysis software:  
In this thesis, ProsOpt is linked with the load flow calculations of power networks. As ProsOpt is implemented in Matlab, the load flow calculations are also performed in this software. Therefore, future projects plan to implement the simulation model ProsOpt as a plug-in for commercial power system analysis software.
  
- Web-based simulation model:  
The Matlab-based simulation model ProsOpt should be implemented as a web-based simulation model, in which everyone can optimise their specific household with consideration of the coupling of thermal and electrical systems, integration of electric vehicle charging stations as well as desired energy services (heating, cooling, electrical energy services), external boundary conditions, e.g., building structure and weather, individual technical components, and selected energy tariffs.
  
- Forecast considering uncertainties:  
Additionally, in this thesis, an ideal forecasts for demand, weather and energy tariffs is used to perform optimisations. Uncertainties due to forecast models for weather as well as electrical and thermal demand will be addressed in future work.

## Optimisation of Hybrid Energy Systems

### (Section 3)

The developed simulation model ProOpt is used to analyse the operation of an optimising prosumer based on the example of a single-family house, taking the following points into consideration:

- the electrical demand (domestic appliances and lighting),
- the heating and cooling demand at specific building constructions,
- the domestic hot water demand
- and the charging of an electric vehicle.

With ProsOpt, the optimal use of the energy generation and storage systems is determined using a linear optimisation algorithm (MILP – Mixed Integer Linear Programming), which take the desired energy services, external boundary conditions, e.g., weather and cost functions of the system components into account .

The analyses' focus lies in the resulting electrical demand of prosumers when the electrical and thermal systems are coupled together to a hybrid energy system. For this purpose, a heat pump is used to cover the heating demand and an air conditioning system to cover the cooling demand. Furthermore, a photovoltaic system combined

with electrical and thermal energy storages is used to cover a certain amount of the household's energy demand.

## Degree of Autonomy and Self-Consumption of a Prosumer (Section 3.1)

The degree of autonomy (DA) and the degree of self-consumption (DSC) are essential indicators in evaluating the efficient use of energy generated by renewable energy systems such as photovoltaic (PV) systems. A detailed analysis of the degrees of autonomy and self-consumption achievable by a prosumer, which takes the varying electrical generation and storage systems into consideration, is performed. Furthermore, the influence of different building structures and consumer behaviour are evaluated. The main results can be summarised as follows:

- Predominantly, the combination of the photovoltaic system with an electrical energy storage system significantly increases the degree of autonomy as well as the degree of self-consumption.
- However, even with a large installed photovoltaic capacity of 16 kWp (17.2 MWh/a) and a large electrical energy storage capacity of 20 kWh, a maximum value of the degree of autonomy, which primarily depends on consumer behaviour and the building structure, of about 79 % is achieved.
- In the same scenario, a degree of self-consumption of around 44 % is achieved, i.e., approximately half of the generated energy is consumed by the prosumer him/herself. This discrepancy results from the seasonal difference between the generation and demand, with the highest generation during summer and the highest demand in winter.

Photovoltaic (PV) and electrical energy storage (EES) systems require an optimal dimensioning of their system capacities. To achieve autarky (DA = 100 %), PV-Storage systems need to be dimensioned in a disproportionate size so as to cover the high energy demand in the winter season and during long periods of reduced energy generation caused by bad weather.

A further possibility to efficiently use the generated energy and, thereby, increase the degree of autonomy and self-consumption is to adapt the energy demand to the photovoltaic system generation. This adaptation process is often difficult to achieve due to the consumers' lack of flexibility. With market-dependent or special prosumer tariffs, the prosumer can be motivated to use the generated energy efficiently.

## Economic Optimum of a Prosumer

### (Section 3.2)

Both the capital and operating expenditures of photovoltaic (PV) and electrical energy storage systems significantly influence a prosumer's profitability. Therefore, the investigated prosumer's economic optimum of the annual energy costs is determined at varying capital expenditures and system capacities for the photovoltaic and electrical energy storage systems, as well as at varying electrical energy purchase and feed-in tariffs.

Installing a photovoltaic system at typical Austrian capital expenditures and energy tariffs reduces the annual energy costs compared to installing a system without photovoltaic generation.

- Hence, the annual energy costs of the investigated prosumer are reduced by about 7 %.
- Most importantly, the analyses clearly showed that installing electrical energy storage systems is unprofitable at current Austrian capital expenditures for electrical energy storage systems and energy tariffs (2019, capital expenditures and tariffs are provided in Section 3.2).

Reducing the electrical energy storage system's capital expenditures to a highly optimistic 400 €/kWh (-73 % compared to the current costs), combined with an increased energy tariff to 0.3 €/kWh (+50 % compared to the current tariffs), will significantly influence an EES system's profitability. The PV-Storage system becomes now profitable, e.g., by installing a PV-Storage system with a capacity of 10 kWp (PV) and 5 kWh (Storage) reduces the prosumer's annual energy costs by about 26 % compared to installing a system without photovoltaic generation.

Even with electrical energy storage systems' falling prices in Austria,

- the current Austrian low electricity prices (about 0.2 €/kWh) represent a significant barrier to investing in an electrical energy storage system.

Nevertheless, installing a photovoltaic system alone – without using an electrical energy storage system – will reduce the annual energy costs, even at current Austrian photovoltaic systems capital expenditures. A 6 kWp photovoltaic system, commonly installed within the Austrian household sector, can reduce the investigated prosumer's annual energy costs by about 4 %.

## Impact of Energy Tariffs on Prosumer Behaviour

### (Section 3.3)

Since consumption and generation do not coincide within every time step, without energy storages or demand-side management it is necessary to purchase or feed-in energy at suboptimal tariffs or adapt the load profile i.e., consumer behaviour, according to the tariff situation. The impact of tariff regimes commonly used in

Austria, the static, high and low tariffs (HT/NT) and a proposed dynamic tariff are examined herein.

The use of time-varying energy tariffs, such as a dynamic market-dependent energy tariff, also leads to changes in the prosumers' hybrid energy system's operation. An optimising prosumer considering weather, demand and tariff forecasts of, e.g., the next 72 hours, will react to changing energy tariffs to achieve an economic optimum as well as change the storage system's charging and discharging behaviour.

The analyses reveals that with time-varying energy tariffs, the optimising prosumer's energy storages would possibly get charged at times of low or no PV generation and low costs, resulting in increased demand at unusual times.

## Storage Strategies: Forecast versus Self-Consumption

### (Section 3.4)

A suitable charging management of electrical energy storage systems can compensate for the gap between the fluctuating photovoltaic generation and demand in the short-term. This will significantly improve the degree of autonomy and self-consumption. Traditionally preferred storage operation strategies are

- to maximise the degree of self-consumption (commonly used)
- and/or to limit the feed-in power (peak shaving).

The simulation model ProsOpt, uses another possible storage operation strategy along with the forecast-based storage strategy which encompasses weather, demand and tariffs. By considering forecasts of, e.g., 72 hours, the prosumer reacts to changing weather, demand or energy tariffs to achieve an optimal operation, e.g., economically, and respectively adapts the charging and discharging behaviour of the storage systems. A more detailed explanation of storage operation strategies can be found in Section 2.6.2.

The simulation model ProsOpt performed annual simulations with a time resolution of 15 minutes, an ideal forecast of 72 hours, a static energy tariff (purchase and in-feed) and with the objective of increasing the degree of self-consumption. The forecast-based storage strategy of ProsOpt is compared with the commonly used traditional storage strategy of maximising the degree of self-consumption without using forecasts.

The forecast-based storage strategy reaches only minimally higher values for the degree of autonomy (+0.6 %) and the degree of self-consumptions (+0.8 %) than the analysed traditional storage strategy. Using a forecast-based storage strategy, with the objective of increasing the degree of self-consumption, results in no significant efficient use of the PV system's generated energy compared to the traditional storage strategy without any forecasts methods.

However, ProsOpt's simulations are performed at an ideal forecast of 72 hours. Thus, forecast uncertainties have not been considered, indicating the absolute difference between the forecast-based storage strategy and the traditional storage strategy may

indeed be smaller. It can be assumed that due to the forecast uncertainties, the effectiveness of the forecast-based storage strategy decreases.

## Economical and Ecological Optimisation of a Prosumer

### (Section 3.5)

The simulation model ProsOpt optimises a prosumer's operation in a single-family house environment with a coupled thermal and electrical energy system. Depending on the scenario, ProsOpt performs annual simulations with a time resolution of 15 minutes, an ideal forecast of 72 hours, and the objective of minimising the investigated prosumer's

- annual energy costs (€/a) or
- annual CO<sub>2</sub> emissions (kgCO<sub>2</sub>/a).

The analyses' main focus encompasses the influence of the respective optimisation objectives – economic and ecological – have on the prosumer's annual energy costs and the annual CO<sub>2</sub> emissions. Therefore, the sensitivity analyses of the technologies Levelized Cost of Energy LCE (Levelized Cost of Electricity - LCOE) and the CO<sub>2</sub> equivalents are performed.

The used optimisation algorithm used (Mixed-Integer Linear Programming – MILP) determines the minimum annual energy costs or CO<sub>2</sub> emissions of the prosumer based on the LCE or CO<sub>2</sub> equivalents of the system components. At a too high of an LCE or CO<sub>2</sub> equivalent of a system component, the system component will not contribute to minimising the costs or CO<sub>2</sub> emissions, and therefore, the optimisation algorithm will not consider the certain system component.

#### **Annual Energy Costs:**

The following system components shows the highest gradient in the sensitivity analyses which results in high sensitivity and, therefore, a high impact on the annual energy costs of the investigated prosumer.

#### *Optimising Prosumer with an Economic Objective:*

Since a heat pump covers the prosumer's thermal energy demand, the prosumer's total annual energy demand is covered via the electrical system. This, in turn, leads to the highest sensitivity in the electricity costs (tariff) followed by the LCOE of the photovoltaic system system and the heat pump.

The electrical energy storage system cannot significantly reduce annual energy costs until the LCOE of electrical energy storage system reaches an LCOE of approximately 0.12 €/kWh (-66 % compared to the initial value of 0.35 €/kWh). Above this LCOE of 0.12 €/kWh, the EES system remains too expensive and is not considered by the prosumer's used optimisation algorithm.

**Annual CO<sub>2</sub> Emissions:**

The following system components shows the highest gradient in the sensitivity analyses which results in high sensitivity and, therefore, a high impact on the investigated prosumer's CO<sub>2</sub> emissions.

*Optimising Prosumer with an Economic Objective:*

The electrical energy storage system shows, together with the electricity costs, the highest sensitivity of the annual CO<sub>2</sub> emissions.

By reducing the electrical energy storage system's LCOE to approximately 0.12 €/kWh (-66 % compared to the initial value of 0.35 €/kWh), the electrical energy storage is cheap enough and is considered by the prosumer's used optimisation algorithm used. Caused by the assumed GWP of the electrical energy storage system of 100 g/kWh<sub>el</sub>, this leads to reduced annual CO<sub>2</sub> emissions.

*Optimisation with an Ecologic Objective:*

The electricity mix exhibited the most significant sensitivity in an ecologically optimised system followed by the photovoltaic system. This high sensitivity in the electricity mix can be explained by the fact that a prosumer remains nonetheless highly dependent on the power network (Section 5).

**General Statement:**

The economic and ecological sensitivity analyses show that even when decentralised generation and storage systems are used, the economic and ecological dependence on primary energy sources from the electricity network remains very high. In the case of a prosumer with a heat pump as the primary heating system, the most efficient way to reduce the CO<sub>2</sub> emissions is choosing an electricity provider offering mostly 100 % renewable energy.

## Influence of Prosumers on Distribution Networks

**(Section 4)**

The developed simulation model ProsOpt is used to analyse the influence of self-optimising prosumers on a rural distribution network in different scenarios. Therefore, the energy management model of ProsOpt is linked with load-flow calculations of a selected low-voltage network. For the network analyses, the benchmark network "1-LV-rural1-0-sw" from the German project "SimBench" [88] is used.

### Increasing Hybridisation Levels of Households

**(Section 4.1)**

The coupling of the thermal and electrical systems using heat pumps, air conditioners, heating cartridges and the charging of electric vehicles increases the household's

electrical demand. The influence of the households' changed electrical demand combined with renewable generation and energy storages on a low-voltage network is investigated.

Due to the aforementioned hybridisation, the households' electrical demand more than doubles (+124 %) compared to a system with no heat pumps or charging of electric vehicles at home. This increased electrical demand affects the transformer loading and the network losses in distribution networks.

- Even when a household's demand for electrical energy is more than doubled, the transformer's maximum loading only increases by 32 %.

Although the implementation of photovoltaic systems reduces the load flow from the MV-network (top-down), the plant's generation surplus leads to a reversal of the load flow into the MV-network (bottom-up). Depending on the installed PV power in the LV-network, this surplus power in-feed can increase the network loading significantly.

- The investigated rural network with an installed photovoltaic capacity of 167 kWp reaches, in the worst case, a maximum load flow to the MV network (bottom-up) of 96 % at a rated power of the 160 kVA transformer. This is an increase of 178 % compared to the transformer's former maximum loading (top-down) without photovoltaic in-feed.

It must be noted that the total installed photovoltaic capacity of 167 kWp in the network represents an extreme photovoltaic scenario, resulting in this heavy loading of the transformer. Nevertheless, the installed photovoltaic capacity per household falls within realistic limits.

- Furthermore, neither the increased demand nor the photovoltaic systems' high feed-in leads to a significant increase in the line loading in rural networks.

The implementation of electrical energy storage systems in households reduces average transformer loading and network losses. Here, the average transformer loading is reduced by 20 % and the network losses by 18 %.

- However, perhaps most notable is the fact that the implementation of electrical energy storage systems in households will not reduce the peak power in the rural network.

Due to the photovoltaic systems' power in-feed, the voltage increases in the worst case to 106 % at the most affected busbar. To guarantee a maximum voltage rise of  $\Delta v = 3$  % at each busbar (Section 2.7) further measures are necessary. Possible measures are explained in detail in Sections 4.2 and 4.3.

## Dynamic Energy Tariffs and Peak-Shaving

### (Section 4.2)

The introduction of dynamic energy tariffs has a significant impact on the optimised operation of prosumers. The power exchange between the prosumer and electrical distribution network also changes due to the altered charging behaviour of electrical

and thermal energy storage systems. Measures to limit the power exchange, such as peak-shaving, can significantly reduce the peak power.

The analyses of the investigated rural network show that the introduction of dynamic tariffs combined with prosumers' optimising operation increases both

- the purchasing power by 200 % and
- feed-in power by 26 %,

which leads to an overloading of the transformer at peak times for about five hours annually.

The increased power caused by using dynamic tariffs combined with prosumers' optimising operation leads to no significant increase in the line loading in rural networks.

However, the increased power results in a minimum voltage of 94 % (purchased power) and a maximum voltage of 106 % (power in-feed) results.

Performing peak-shaving by setting a power limit of exemplary 8 kVA at the households' Point of Common Coupling (PCC), the purchased peak power from the MV-network decreases by 37 % and the feed-in peak power to the MV-network decreases by 51 %.

The introduction of dynamic energy tariffs has a significant impact on the optimised operation of prosumers. The power exchange between the prosumer and electrical distribution network also changes due to the altered charging behaviour of electrical and thermal energy storage systems. Measures to limit the power exchange, such as peak-shaving, can significantly reduce the peak power.

The performed simulations reveal that the introduction of dynamic energy tariffs will fundamentally change prosumers' operation, directly influencing the load flow in distribution networks. The power increases significantly at the same energy demand, considering that households pay for the purchased or fed-in amount of energy (energy-based tariffs). Performing peak-shaving by setting power limits at the households' PCC allows the optimising prosumers' respective peak power to be reduced.

## **Impact of Voltage and Reactive Power Control on the Distribution Network**

### **(Section 4.3)**

To comply with the voltage limits according to EN 50160 [38] and the Austrian national rules TOR [39], the effectiveness of various methods for voltage and reactive power control are determined.

Due to the optimising prosumers' operation and the in-feed of the photovoltaics systems' surplus generation into the LV-network, the busbars' voltage levels are influenced. When photovoltaic converters operate at unity power factor, the voltage increases up to 106 % for the busbar most distant from the feeder connection. To

guarantee a maximum voltage rise of  $\Delta v = 3 \%$  at each busbar, the following three measures are analysed in detail:

- Constant Power Factor Mode  $\cos(\varphi) = 0.95$  (under-excited<sup>1</sup>)
- Active Power-Power Factor (watt-cos  $\varphi$ ) Mode
- Voltage-Reactive Power (volt-var) Mode

In case the operating strategy leads to an exceedance of the inverter's apparent power capability, the active power is reduced. This guarantees operation within the required reactive power levels. To minimise active power curtailment, the selected inverters have a Sizing Ratio of  $SR = 1.1$ .

*Constant Power Factor Mode  $\cos(\varphi) = 0.95$  (under-excited):*

By choosing a constant power factor  $\cos(\varphi)$  of 0.95 (under-excited), the prosumers' inverters provide reactive power at any time. This provided reactive power leads to an increased transformer loading, higher LV-network losses, and a higher loading of the lines compared to any scenario with applied reactive power management. With a maximum transformer loading up to 178 %, the transformer is significantly overloaded.

The photovoltaic in-feed is curtailed for 6 % annually at peak feed-in, which leads to a reduced active power in-feed to the MV network from 96 % (constant power factor mode with a unity power factor) to 90 %.

Setting a constant power factor  $\cos(\varphi)$  of 0.95, the maximum voltage rise caused by power in-feed of the generation plants is significantly reduced in the entire network to a maximum node voltage of 1 pu and a minimum node voltage of 92 % at the most affected busbar. The node voltage at the local network station (LNS - 0.4 kV) is now also affected significantly and is reduced to 94 %.

*Active Power-Power Factor (watt-cos  $\varphi$ ) Mode:*

The active power-power factor (watt-cos  $\varphi$ ) mode regulates the power factor  $\cos(\varphi)$  as a function of the active power  $p$ . When reaching an active power level of 0.5, the inverter operates in under-excited mode and reduces the power factor  $\cos(\varphi)$  to a minimum of 0.9 pu. Whereas, at the watt-cos  $\varphi$  mode, each generation plant participates equally in the voltage control.

The watt-cos  $\varphi$  mode's application yields increased transformer loading up to a maximum loading level of 226 %, whereby the transformer is heavily overloaded. Furthermore, the line loading is also increased on average, reaching a maximum line loading of 97 % at the most affected cable.

The photovoltaic in-feed is curtailed for 4 % annually at peak feed-in, which leads to a reduced maximum active power in-feed to the MV network from 96 % (constant power factor mode with a unity power factor) to 87 %. Nevertheless, the transformer is heavily overloaded at those feed-in peak times.

---

<sup>1</sup> Voltage reducing

- Therefore, both chosen methods – constant power factor with  $\cos \varphi = 0.95$  and watt- $\cos \varphi$  mode – for reactive power control are not recommended for the investigated network in the case of strong photovoltaic expansion.
- Recommendations for reducing the transformer loading significantly include limiting the feed-in power (peak-shaving), reducing the installed PV power in the network or selecting other setpoints of the power factors  $\cos(\varphi)$ .

Similar to a constant power factor  $\cos(\varphi)$  mode, the watt- $\cos \varphi$  mode also affects the node voltages in the entire network area equally, resulting in a voltage decrease in the entire network leading to a minimum node voltage at the most affected busbar of 91 % and a maximum voltage of 103 %.

#### *Voltage-Reactive Power (volt-var) Mode:*

The volt-var mode is used to limit both the voltage rise and voltage decrease as well as actively control the inverter's reactive power output as a function of the voltage  $v$ . A dead band of  $\pm 2 \% v_n$  ( $1 \text{ pu} = v_n = 0.4 \text{ kV}$ ) as well as a droop of 2 % is set.

The volt-var mode only barely affects the average transformer loading, the LV-network losses and the line loading. A maximum transformer loading of 99 % is reached. The volt-var mode with a flexible, reactive power control as a function of the node voltages  $v$  shows no significant increase in cable loading.

The volt-var mode actively controls the inverter's reactive power output as a function of the node voltage  $v$ , which leads to the lowest transformer loading as well as an effective voltage control.

The generation plants connected to feeders with relatively short line lengths rarely provide reactive power, as the voltage level mostly lies within the volt-var curve's dead band. However, caused by long line lengths and high photovoltaic in-feed, the generation plants at feeder II must actively provide reactive power to minimise the voltage increase. The maximum voltage increase at the most affected busbar decreased from 106 % to 104 %.

The volt-var mode offers more flexible control of the node voltage, providing a good compromise between voltage level and the provided reactive power. Otherwise, generators at the end of the feeder, in particular, must participate very intensively in reactive power control. As opposed to the volt-var mode, in the watt- $\cos \varphi$  mode all generators participate regardless of their position in the network in reactive power control.

# References

- [1] J. Kallrath, *Gemischt-ganzzahlige Optimierung: Modellierung in der Praxis*, 2nd ed. Wiesbaden, Germany: Springer, 2013.
- [2] A. Koop and H. Mooock, *Lineare Optimierung - eine anwendungsorientierte Einführung in Operations Research*, 2nd ed. Berlin, Heidelberg, Germany: Springer Spektrum, 2018.
- [3] M. Sterner and I. Stadler, *Energiespeicher - Bedarf, Technologien, Integration*, 2nd ed. Berlin, Germany: Springer Vieweg, 2017.
- [4] D. Steen, M. Stadler, G. Cardoso, M. Groissböck, N. DeForest, and C. Marnay, “Modeling of thermal storage systems in MILP distributed energy resource models,” *Applied Energy*, vol. 137, pp. 782–792, 2015.
- [5] V. Quaschnig, *Regenerative Energiesysteme: Technologie - Berechnung - Klimaschutz*, 8th ed. Munich, Germany: Carl Hanser Verlag, 2013.
- [6] M. Fürnschuß, “Prognose des elektrischen Energieertrags von Photovoltaikanlagen sowie dessen Integration in Stromversorgungsnetze,” M.S. thesis, IEAN, TU Graz, Graz, Austria, 2018.
- [7] M. Fürnschuß, M. A. Lagler, and E. Schmautzer, “Bedarfsorientierte Konzeptionierung von Photovoltaikanlagen,” in *15th EnInnov*, Graz, Austria, 2018.
- [8] “Energie in Österreich 2018 - Zahlen, Daten, Fakten,” Bundesministerium für Nachhaltigkeit und Tourismus, Vienna, Austria, 2018.
- [9] *Thema Energieverbrauch*, E-control, May 15, 2020. Accessed on: May 15, 2020. [Online]. Available: <https://www.e-control.at/konsumenten/energiesparen/thema-energieverbrauch>.
- [10] *Energiestatistik: Mikrozensus Energieeinsatz der Haushalte 2017/2018*, Statistik Austria, September 15, 2019. Accessed on: December 07, 2020. [Online]. Available: [http://www.statistik.at/wcm/idc/idcplg?IdcService=GET\\_PDF\\_FILE&RevisionSelectionMethod=LatestReleased&dDocName=034835](http://www.statistik.at/wcm/idc/idcplg?IdcService=GET_PDF_FILE&RevisionSelectionMethod=LatestReleased&dDocName=034835).
- [11] N. D. Pflugradt, “Modellierung von Wasser- und Modellierung von Wasser- und Energieverbräuchen in Haushalten,” Ph.D dissertation, Technische Universität Chemnitz, Chemnitz, Germany, 2016.
- [12] *Energy performance of buildings – Part 1: Energy use for heating systems*, ÖNORM H 5056-1:2019. 2019.
- [13] P. Häupl, G. Höfker, M. Homann, C. Kölzow, A. Maas, C. Nocke, and O. Riese, *Lehrbuch der Bauphysik: Schall - Wärme - Feuchte - Licht - Brand - Klima*, 8th ed. Wiesbaden, Germany: Springer Vieweg, 2017.

- [14] T. Wieland, “Eine neuartige probabilistische Methode zur Betriebsmitteldimensionierung in aktiven urbanen Niederspannungsnetzen,” Ph.D dissertation, IEAN, TU Graz, Graz, Austria, 2016.
- [15] *Bundeseinheitliche Fassung: Technische Anschlussbedingungen für den Anschluss an öffentliche Versorgungsnetze mit Betriebsspannungen bis 1000 Volt, mit Erläuterungen der einschlägigen Vorschriften*, TAEV. 2016.
- [16] *Elektroinstallationen - Hausanschlüsse, Hauptleitungen, Messeinrichtung*, ÖVE/ÖNORM E 8016:2012-01-01. 2012.
- [17] *Thermal insulation in building construction: Principles and verification methods — Heating demand and cooling demand*, ÖNORM B 8110-6-1:2019-01-15. 2019.
- [18] *Thermal insulation in building construction: Part 5: Model of climate and user profiles*, ÖNORM B 8110-5:2019-03-15. 2019.
- [19] *IDA Indoor Climate and Energy (IDA ICE)*, EQUA - Simulation Software, October 10, 2020. Accessed on: October 10, 2020. [Online]. Available: <https://www.equa.se/en/about-us/about-equa>.
- [20] D. Bohne, *Technischer Ausbau von Gebäuden: Und nachhaltige Gebäudetechnik*, 10th ed. Wiesbaden, Germany: Springer Vieweg, 2014.
- [21] H. Brünner, *Der Gas- und Wasserleitungsinstallateur: Fachkunde für Schule und Praxis, mit Berechnungsbeispielen*, 3rd ed. Vienna, Austria: Bohmann, 1977.
- [22] N. Pflugradt and U. Muntwyler, “Synthesizing Electromobility Charging Profiles,” in *25th International Conference on Electricity Distribution*, Madrid, Spain, 2019.
- [23] T. Weiglhofer, M. Aigner, and E. Schmautzer, “Ermittlung unterschiedlicher Einflüsse auf Stromgestehungskosten fossiler und erneuerbarer Erzeugungstechnologien,” in *14th EnInnov*, Graz, Austria, 2016.
- [24] E-control, Accessed on: February 02, 2018. [Online]. Available: [www.e-control.at](http://www.e-control.at).
- [25] SMARTFOX, DAfi GmbH, 2021. Accessed on: May 14, 2021. [Online]. Available: <http://www.smartfox.at>.
- [26] *GEMIS 4.95*, IINAS - Internationales Institut für Nachhaltigkeitsanalysen und strategien GmbH, January 23, 2019. Accessed on: January 23, 2019. [Online]. Available: [www.iinas.org](http://www.iinas.org).
- [27] L. Rausch and U. R. Fritsche, “Aktualisierung von Ökobilanzdaten für Erneuerbare Energien im Bereich Treibhausgase und Luftschadstoffe,” Öko-Institut e.V., Germany, 2012.
- [28] S. Schidler, “Stromspeicher: ökologischer Hintergrund, graue Energie, Lebenszyklus, Recycling,” FH-Technikum Wien, Vienna, Austria, 2018.
- [29] *Heizkostenvergleich - CO<sub>2</sub>-Emissionen*, Austrian Energy Agency, Accessed on: January 23, 2019. [Online]. Available: <https://www.energyagency.at/fakten-service/heizkosten/co2-emissionen.html>.

- [30] *OIB-Richtlinien (OIB-RL 6)*, Österreichisches Institut für Bautechnik. 2015.
- [31] K. Mertens, *Photovoltaik: Lehrbuch zu Grundlagen, Technologie und Praxis*, 4th ed. Munich, Germany: Springer Spektrum, 2018.
- [32] M. Kaltschmitt, W. Streicher, and A. Wiese, *Erneuerbare Energien: Systemtechnik, Wirtschaftlichkeit, Umweltaspekte*, 5th ed. Berlin, Germany: Springer Vieweg, 2014.
- [33] V. Quaschnig, *Regenerative Energiesysteme: Technologie - Berechnung - Klimaschutz*, 10th ed. Munich, Germany: Carl Hanser Verlag, 2015.
- [34] H. Watter, *Regenerative Energiesysteme*, 5th ed. Wiesbaden, Germany: Springer Vieweg, 2019.
- [35] H.-G. Wagemann, H. Eschrich, and P. N. Khoi, *Photovoltaik*, 2th ed. Wiesbaden, Germany: Vieweg + Teubner, 2013.
- [36] *Overall efficiency of grid connected photovoltaic inverters*, ÖVE/ÖNORM EN 50530:2010 + A1:2013. 2014.
- [37] *Data sheet and name plate for photovoltaic inverters*, ÖVE/ÖNORM EN 50524:2009. 2010.
- [38] *Voltage characteristics of electricity supplied by public electricity networks*, ÖVE/ÖNORM EN 50160:2010. 2010.
- [39] *Technische und organisatorische Regeln für Betreiber und Benutzer von Netzen: TOR Erzeuger: Anschluss und Parallelbetrieb von Stromerzeugungsanlagen des Typs A und von Kleinsterzeugungsanlagen*, E-control, 2019. Accessed on: March 03, 2020. [Online]. Available: <https://www.e-control.at/recht/marktregeln/tor>.
- [40] *Commission Regulation (EU) 2016/631 - Establishing a network code on requirements for grid connection of generators*, The European Commission. 2016.
- [41] *IEEE Standard for Interconnection and Interoperability of Distributed Energy Resources with Associated Electric Power Systems Interfaces*, IEEE 1547-2018. 2018.
- [42] “U-Control: Technische Wirksamkeit, Robustheit und Wirtschaftlichkeit neuer Verfahren zur Sicherung der statischen Spannungshaltung in Verteilnetzen mit starker dezentraler Einspeisung,” TU Braunschweig, TU München, RWTH Aachen, FGH e.V., Germany, 2018.
- [43] “Vor- und Nachteile verschiedener Energiespeichersysteme,” Deutscher Bundestag, 2014.
- [44] G. Fuchs, B. Lunz, M. Leuthold, and D. U. Sauer, “Technology Overview on Electricity Storage: Overview on the potential and on the deployment perspectives of electricity storage technologies,” Smart Energy for Europe Platform GmbH, iSEA RWTH Aachen, Aachen, Germany, 2012.
- [45] A. R. Dehghani-Sani, E. Tharumalingam, M. B. Dusseault, and R. Fraser, “Study of energy storage systems and environmental challenges of batteries,” *Renewable and Sustainable Energy Reviews*, vol. 104, pp. 192–208, 2019.

- [46] J. Weniger, J. Bergner, T. Tjaden, and V. Quaschnig, *Dezentrale Solarstromspeicher für die Energiewende*, 1st ed. Berlin, Germany: Berliner Wissenschafts-Verlag, 2015.
- [47] S. Höger, M. Greif, and S. Schramm, “Modularer Inselwechselrichter mit integriertem Energiespeicher für den afrikanischen Markt,” Project, Hochschule München, Munich, Germany, 2015.
- [48] S. H. Ibrahim, “Erstellung eines Berechnungstools zur Dimensionierung von Akkuspeichersystemen für netzgekoppelte Photovoltaikanlagen,” M.S. thesis, Hochschule für Angewandte Wissenschaften Hamburg, Hamburg, Germany, 2013.
- [49] W. Hennings, P. Stenzel, and N. Pflugradt, “Performance of a photovoltaic plus battery home system with load profile scenarios changing over the system life,” *Energy Procedia*, vol. 142, pp. 3252–3257, 2017.
- [50] J. Figgner, D. Haberschusz, K.-P. Kairies, O. Wessels, B. Tepe, M. Ebbert, R. Herzog, and D. U. Sauer, “Wissenschaftliches Mess- und Evaluierungsprogramm Solarstromspeicher 2.0: Jahresbericht 2017,” iSEA RWTH Aachen, 2017. [Online]. Available: <http://www.speichermonitoring.de>.
- [51] “Nationaler Strategierahmen Saubere Energie im Verkehr,” bmvit - Bundesministerium für Verkehr, Innovation und Technologie, 2016.
- [52] J. Liebl, *Netzintegration der Elektromobilität 2018*. Wiesbaden, Germany: Springer Fachmedien Wiesbaden, 2018.
- [53] A. Kampker, D. Vallée, and A. Schnettler, *Elektromobilität: Grundlagen einer Zukunftstechnologie*, 2nd ed. Berlin, Germany: Springer Vieweg, 2018.
- [54] *EP Elektromobilität braucht starke und intelligente Netze - Fact Sheet*, Österreichs Energie, 2017. Accessed on: December 7, 2020. [Online]. Available: <http://oesterreichsenergie.at>.
- [55] “Abschlussbericht des EP Elektromobilität,” EP Elektromobilität des AK Verteilernetze, Österreichs Energie, 2018.
- [56] A. Probst, “Auswirkungen von Elektromobilität auf Energieversorgungsnetze analysiert auf Basis probabilistischer Netzplanung,” Ph.D dissertation, Universität Stuttgart, Stuttgart, Germany, 2014.
- [57] J. Schauble, “Generating electric vehicle load profiles from empirical data of three EV fleets in Southwest Germany,” *Journal of cleaner production*, 2017.
- [58] J. Sears, D. Roberts, and K. Glitman, “A comparison of electric vehicle Level 1 and Level 2 charging efficiency,” *2014 IEEE Conference on Technologies for Sustainability (SusTech)*, pp. 255–258, 2014.
- [59] P. Richardson, D. Flynn, and A. Keane, “Local Versus Centralized Charging Strategies for Electric Vehicles in Low Voltage Distribution Systems,” *IEEE Transactions on Smart Grid*, vol. 3, pp. 1020–1028, 2012.
- [60] R. Garcia-Valle and J. A. Peças Lopes, *Electric Vehicle Integration into Modern Power Networks*. New York, NY: Springer New York, 2013.

- [61] Jochen Wieler, *Elektroauto Reichweiten & Stromverbrauch im Vergleich — ADAC*, ADAC, April 14, 2020. Accessed on: April 16, 2020. [Online]. Available: <https://www.adac.de/rund-ums-fahrzeug/tests/elektromobilitaet/stromverbrauch-elektroautos-adac-test/>.
- [62] N. Pflugradt, *LoadProfileGenerator*, April 6, 2020. Accessed on: April 16, 2020. [Online]. Available: <https://www.loadprofilegenerator.de/>.
- [63] C. Richter, D. Lincot, and C. A. Gueymard, *Solar Energy*. New York, NY: Springer New York, 2013.
- [64] J. Unger and A. Hurtado, *Alternative Energietechnik*, 5th ed. Wiesbaden, Germany: Springer Fachmedien Wiesbaden GmbH, 2015.
- [65] C. Glück, “Generische Simulationsmodelle für Sorptionswärmepumpen zum Heizen und Kühlen,” Ph.D dissertation, Karlsruher Institut für Technologie, Karlsruhe, Germany, 2015.
- [66] “Planungsanleitung: VITOCAL 300-A / Typ AWO-AC 301.B,” Viessmann, 2017.
- [67] T. K. K. Rankinen and D. Butterfield, “A simple model for predicting soil temperature in snow-covered and seasonally frozen soil: model description and testing,” *Hydrology and Earth System Sciences*, vol. 8, pp. 706–716, 2004.
- [68] *Primäres Heizsystem nach überwiegend eingesetztem Energieträger und Art der Heizung*, Statistik Austria, July 10, 2019. Accessed on: January 11, 2020. [Online]. Available: [https://www.statistik.at/wcm/idc/idcplg?IdcService=GET\\_PDF\\_FILE&RevisionSelectionMethod=LatestReleased&dDocName=022721](https://www.statistik.at/wcm/idc/idcplg?IdcService=GET_PDF_FILE&RevisionSelectionMethod=LatestReleased&dDocName=022721).
- [69] *Erdgasparameter 2019*, Energienetze Steiermark GmbH, 2019. Accessed on: January 13, 2020. [Online]. Available: <https://www.e-netze.at/downloads-data/Gas/4.%20Erdgasparameter/Erdgasparameter%202019.pdf>.
- [70] H. Baehr and S. Kabelac, *Thermodynamik - Grundlagen und technische Anwendungen*, 16th ed. Berlin, Germany: Springer Vieweg, 2016.
- [71] J. Schweitzer, “Facts and figures about domestic gas boilers,” Danish Gas Technology Centre, Hørsholm, Denmark, February 15, 2016. [Online]. Available: [http://www.dgc.eu/sites/default/files/filarkiv/documents/R1603\\_facts\\_gas\\_boilers.pdf](http://www.dgc.eu/sites/default/files/filarkiv/documents/R1603_facts_gas_boilers.pdf).
- [72] A. Müller, P. Biermayr, L. Kranzl, R. Haas, F. Altenburger, I. Bergmann, G. Friedl, W. Haslinger, R. Heimrath, R. Ohnmacht, and W. Weiss, “Heizen 2050: Systeme zur Wärmebereitstellung und Raumklimatisierung im österreichischen Gebäudebestand: Technologische Anforderungen bis zum Jahr 2050,” Research project, Austria, 2010.
- [73] S. Ernst, “Modellierung der Entwicklung von Treibhausgasemissionen und Energieverbrauch für Raumwärme und Warmwasser im österreichischen Wohngebäudebestand unter der Annahme verschiedener Optimierungsziele,” Ph.D dissertation, TU Wien, Vienna, Austria, 2007.

- [74] J. Andres, T. Nussbaumer, S. Thalmann, and J. Ködel, “Planungshandbuch Fernwärme: Schlussbericht,” EnergieSchweiz, Bundesamt für Energie BFE, Bern, Switzerland, April 6, 2017. [Online]. Available: [www.qmfernwaerme.ch](http://www.qmfernwaerme.ch).
- [75] B. Skagestad and P. Mildenstein, “District Heating and Cooling Connection Handbook,” International Energy Agency, 2002.
- [76] S. Böhmer and M. Gössl, “Optimierung und Ausbaumöglichkeiten von Fernwärmesystemen,” Umweltbundesamt, Vienna, Austria, 2009.
- [77] J. Dohmann, *Thermodynamik der Kälteanlagen und Wärmepumpen*, 1st ed. Berlin, Germany: Springer Vieweg, 2016.
- [78] O. S. Burheim, “Engineering energy storage,” *Academic Press, London and San Diego, California*, 2017.
- [79] D. Oeding and B. R. Oswald, *Elektrische Kraftwerke und Netze*, 8th ed. Berlin, Germany: Springer Vieweg, 2016.
- [80] M. A. Lagler, “Rechnergestützte Analyse eines urbanen 20-kV-Mittelspannungsnetzes,” M.S. thesis, IEAN, TU Graz, Graz, Austria, 2015.
- [81] P. Schober and C. Boer, “Correlation Coefficients: Appropriate Use and Interpretation,” in *Anesthesia and Analgesia*, Department of Anesthesiology, VU University Medical Center, Amsterdam, the Netherlands, 2018.
- [82] P. Biermayr, C. Dißauer, M. Eberl, and M. Enigl, “Innovative Energietechnologien in Österreich Marktentwicklung 2019: Biomasse, Photovoltaik, Solarthermie, Wärmepumpen und Windkraft,” Bundesministerium für Klimaschutz, Umwelt, Energie, Mobilität, Innovation und Technologie, 2020.
- [83] J. Figgenger, D. Haberschusz, Kai-Philipp Kairies, O. Wessels, S. Zurmühlen, and D. U. Sauer, “Speichermonitoring BW - Jahresbericht 2019,” iSEA RWTH Aachen, Aachen, Germany, 2019.
- [84] Bundesnetzagentur, 2018. [Online]. Available: [www.bundesnetzagentur.de](http://www.bundesnetzagentur.de).
- [85] E-control, Accessed on: February 12, 2021. [Online]. Available: [www.e-control.at/konsumenten/service-und-beratung/toolbox/tarifkalkulator#/](http://www.e-control.at/konsumenten/service-und-beratung/toolbox/tarifkalkulator#/).
- [86] C. Kost, J. Mayer, J. Thomsen, and N. Hartmann, “Studie: Stromgestehungskosten erneuerbare Energien,” Fraunhofer-Institut für Solare Energiesysteme ISE, Germany, 2013.
- [87] P. Biermayr, C. Dißauer, M. Eberl, M. Enigl, H. Fechner, K. Leonhartsberger, F. Maringer, S. Moidl, C. Schmidl, C. Strasser, W. Weiss, P. Wonisch, and E. Wopienka, “Innovative Energietechnologien in Österreich - Marktentwicklung 2016: Biomasse, Photovoltaik, Solarthermie, Wärmepumpen und Windkraft,” Bundesministerium für Verkehr, Innovation und Technologie, 2017.
- [88] “SimBench - Elektrische Benchmarknetzmodelle,” Universität Kassel, Fraunhofer IEE, RWTH Aachen University, Technische Universität Dortmund, Germany, 2020. [Online]. Available: [simbench.de](http://simbench.de).
- [89] G. Wurzer, “Verkabelung von Verteilernetzen kleiner 20kV,” M.S. thesis, IEAN, TU Graz, Graz, Austria, 2013.

- [90] H. Gremmel, *ABB Schaltanlagen Handbuch*, 9th ed. Berlin, Germany: Cornelsen, 1998.
- [91] “Ratgeber G1 – U-Wert,” Ich tu’s, Energie Agentur Steiermark, 2020.
- [92] J. M. Andújar Márquez, M. Á. Martínez Bohórquez, and S. Gómez Melgar, “Ground Thermal Diffusivity Calculation by Direct Soil Temperature Measurement. Application to very Low Enthalpy Geothermal Energy Systems,” *Sensors*, vol. 16, p. 306, 2016.
- [93] H. Watter, *Regenerative Energiesysteme*, 4th ed. Wiesbaden, Germany: Springer Vieweg, 2015.
- [94] “PVGIS,” European Commission, Joint Research Centre Energy Efficiency and Renewables Unit, 2018.
- [95] V. Quaschnig, *Simulation der Abschattungsverluste bei solarelektrischen Systemen*, 1st ed. Berlin, Germany: Köster, 1996.
- [96] I. Bostan, A. Gheorghe, V. Dulgheru, I. Sobor, V. Bostan, and A. Sochirean, *Resilient Energy Systems: Renewables: Wind, Solar, Hydro*. Dordrecht, Netherlands: Springer Netherlands, 2013.

# Appendices

# Appendix A

## Methodology, Modelling, Calculations

Table A.1: Comparison of typical overall heat transfer coefficients  $U$  ( $[U] = 1 \frac{\text{W}}{\text{m}^2\text{K}}$ ) for different building types [91]

Building components	Passive house	Low-energy house	House (poor insulation)
Basement ceilings	0.10	0.20	0.50 - 1.70
External walls	0.10	0.20	0.60 - 2.40
Floors with soil contact	0.10	0.20	1.50 - 2.60
Roofs	0.10	0.15	0.70 - 1.80
Walls with soil contact	0.10	0.20	1.10 - 4.00
Windows and doors	0.80	1.20	2.50 - 4.60

Table A.2: Typical values for the total energy transmittance  $g$  of transparent components [17]

Window type	Window structure	
	in mm	$g$
Single glas	4	0.85
Double insulated glass	4/Air/4	0.76
Double thermal insulated glass	4/Argon/4	0.47 - 0.65
Triple thermal insulated glass	4/Argon/4/Argon/4	0.50 - 0.54
Double insulated vacuum glass	4/0.6/4	0.54
Double insulated sun protection glass	6/Argon/4	0.32 - 0.42
Triple insulated sun protection glass	6/Argon/4/Argon/6	0.23 - 0.35

Table A.3: Thermal conductivity  $k_{\text{soil}}$ , volumetric heat capacity  $C_{\text{soil}}$  for different kinds of soil [92]

Rock Type	Thermal Conductivity $k_{\text{soil}}$ in W/mK *	Volumetric Heat Capacity $C_{\text{soil}}$ in MJ/m <sup>3</sup> K
Basalt	1,3 - (1,7) - 2,3	2,6
Greenstone	2,0 - (2,6) - 2,9	2,9
Gabbro	1,7 - (1,9) - 2,5	2,6
Granite	2,1 - (3,4) - 4,1	3,0
Peridotite	3,8 - (4,0) - 5,3	2,7
Gneiss	1,9 - (2,9) - 4,0	2,4
Marble	1,3 - (2,1) - 3,1	2,0
Mica schist	1,5 - (2,0) - 3,1	2,2
Shale sedimentary	1,5 - (2,1) - 2,1	2,5
Limestone	2,5 - (2,8) - 4,0	2,4
Loam	1,5 - (2,1) - 3,5	2,3
Quartzite	3,6 - (6,0) - 6,6	2,2
Salt	5,3 - (5,4) - 6,4	1,2
Sandstone	1,3 - (2,3) - 5,1	2,8
Siltstones and argillites	1,1 - (2,2) - 3,5	2,4
Dry gravel	0,4 - (0,4) - 0,5	1,6
Water saturated gravel	1,8 - (1,8) - 1,8	2,4
Dry sand	0,3 - (0,4) - 0,6	1,6
Water saturated sand	1,7 - (2,4) - 5,0	2,9
Dry clay/silt	0,4 - (0,5) - 1,0	1,6
Water saturated clay/silt	0,9 - (1,7) - 2,3	3,4
Peat	0,2 - (0,4) - 0,7	3,8

\* Min - (Typ) - Max

# Appendix B

## Solar Irradiance

In a so-called sidereal year, the Earth travels 365.26 times around its geographic north-south axis, whereby a sidereal year is a time that the Earth needs to orbit the Sun to a certain reference point compared to an infinitely distant fixed star. The Earth's orbit is an ellipse, with a low numerical eccentricity of  $\varepsilon = 0.017$  [6].

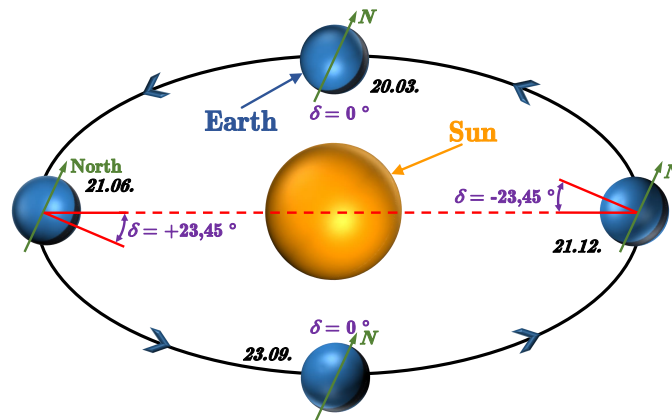


Figure B.1: Illustration of Sun's declination  $\delta$  (not to scale, year: 2018, time zone: UTC+1) [6]

Further, the Earth tilts around its equatorial plane, described by the declination  $\delta$ . The absolute maximum value of the declination is about  $23.45^\circ$  in the Winter and  $-23.45^\circ$  in the summer (Northern hemisphere). At a declination of  $0^\circ$  the astronomical spring or fall begins [6].

Thus, the Sun is not a fixed point and continuously changes its position on the sky, leads

- to a day and night rhythm caused by the rotation of the Earth around its geographic north-south axis and
- to different densities of the solar irradiance due to Earth's rotation around the sun and the declination [93].

The following Figure B.2 illustrates the yearly sum of solar irradiation on optimally-inclined south-orientated photovoltaic modules.

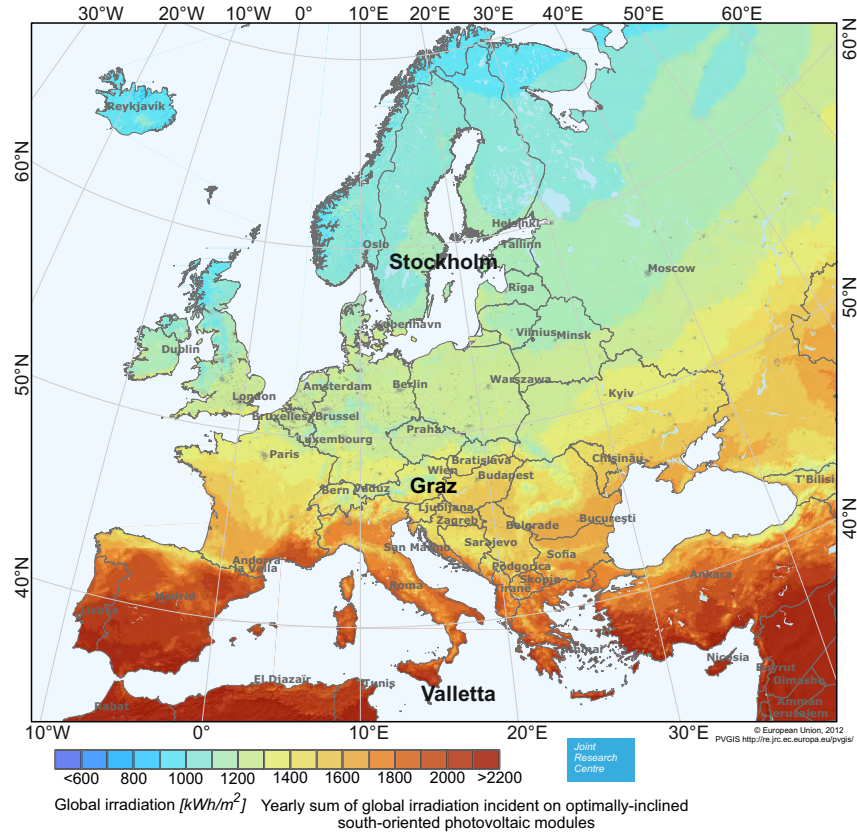


Figure B.2: Yearly sum of solar irradiation incident on optimally-inclined south-orientated photovoltaic modules – Europe [94]

As seen in Figure B.2, the solar irradiation — solar irradiance integrated over time — descent towards the north pole and reverse it decreases towards the equator. Due to the declination, the maximum annual solar irradiation on Earth do not occur at the equator but somewhat north or south of it [6].

This circumstance is explained in more detail using the following three exemplary selected European cities.

**Stockholm, Sweden:**

- Latitude  $\varphi = 59.334591$  ( $59^\circ 20' 4.5276''$  N)
- Longitude  $\lambda = 18.063240$  ( $18^\circ 3' 47.6640''$  E)

**Graz, Austria:**

- Latitude  $\varphi = 47.076668$  ( $47^\circ 4' 36.0048''$  N)
- Longitude  $\lambda = 15.421371$  ( $15^\circ 25' 16.9356''$  E)

**Valletta, Malta:**

- Latitude  $\varphi = 35.896343$  ( $35^\circ 53' 46.8348''$  N)
- Longitude  $\lambda = 14.512982$  ( $14^\circ 30' 46.7352''$  E)

The following Figure B.3 shows for the three exemplary cities the monthly and yearly solar irradiation on optimal inclined south orientated photovoltaic modules for the year 2016 by using the solar radiation database "PVGIS-SARAH" from the

Photovoltaic Geographical Information System (PVGIS). PVGIS is provided by the Joint Research Center of the European Commission. It is a database containing annual averaged solar radiation data from Europe, Africa and Western Asia. With this data, the average expected irradiation in a certain area and period can be determined. The

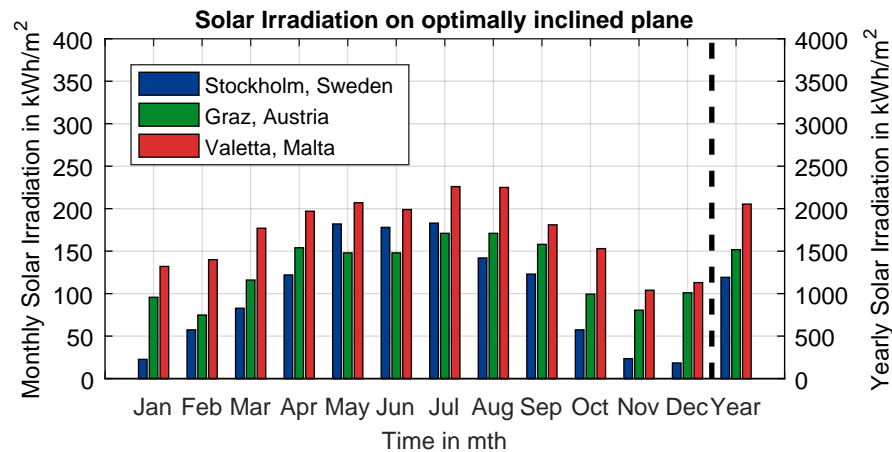


Figure B.3: Monthly and yearly solar irradiation of three different cities

decrease in solar irradiation along the longitudes shows the Figure B.3 by comparing the yearly solar irradiation of the chosen cities. Besides, it can be seen that in the summer months, due to the Sun declination caused longer light days in Stockholm, the possible monthly energy yield in comparison to Graz can be higher.

## Position of the Sun in the Sky

The position of the sun in the sky can be calculated quite generally, e.g., “DIN algorithm for determining the position of the sun (DIN 5034-2)” [95]. From this, statements can be made about the solar radiation incident on the earth’s surface.

Subsequent simplifications for the calculation [6]:

- Neglecting the difference between solar and apparent solar altitude
- Determination of the summer solstice on the 21.06.
- Determination of the winter solstice on the 21.12.
- Zero crossings of the declination angle on 21.03. and 21.09.

Two angles can clearly describe the position of the Sun in the sky, the solar azimuth angle  $\alpha_s$  and the solar elevation angle  $\gamma_s$  from an observer point.

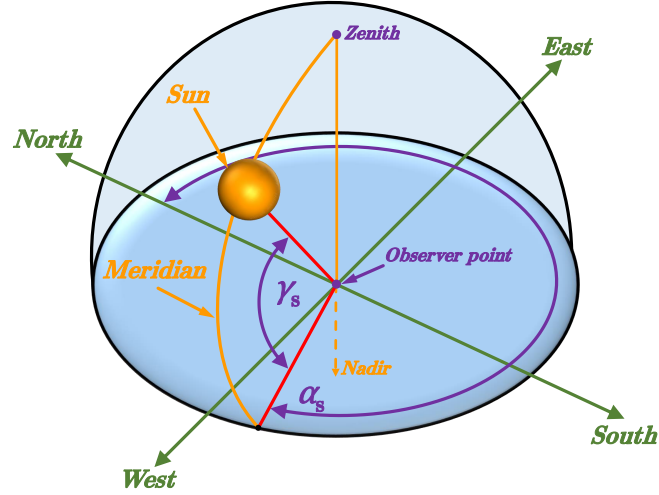


Figure B.4: Position of the sun in the sky [6]

The position of the sun depends mainly on geographical coordinates, defined by the longitude  $\lambda$  and latitude  $\varphi$ , and the time.

The declination angle  $\delta$  can be calculated as follows, taking into account a day depending angle  $J'$  (current day of the year):

$$\delta(J') = 0.3948 - 23.2559 \cdot \cos(J' + 9.1^\circ) - 0.3915 \cdot \cos(2 \cdot J' + 5.4^\circ) - 0.1764 \cdot \cos(3 \cdot J' + 26^\circ) \quad (\text{B.1})$$

$\delta$	Declination in $^\circ$
$J'$	Day depending angle $J' = 360^\circ \cdot \frac{n}{N}$
$N$	Total number of days in one year
$n$	Day of the year

The equation of time  $x$  caused by the declination  $\delta$  results as follows:

$$x(J') = 0.0066 + 7.3525 \cdot \cos(J' + 85.9^\circ) + 9.9359 \cdot \cos(2 \cdot J' + 108.9^\circ) + 0.3387 \cdot \cos(3 \cdot J' + 105.2^\circ) \quad (\text{B.2})$$

$J'$	Day depending angle $J' = 360^\circ \cdot \frac{n}{N}$
$N$	Total number of days in a year
$n$	Day of the year
$x$	Equation of time in minutes

With the result of the equation of time  $x$  and due to the declination  $\delta$ , the correct local solar time LST is given by applying the following equation.

$$\text{LST} = \text{LT} - \text{TZ} + 4 \cdot \lambda \cdot 1 \text{ min}/^\circ + x \quad (\text{B.3})$$

$\lambda$	Longitude
LST	Local solar time in minutes
LT	Local time in minutes
TZ	Time zone deviation to UTC (coordinated universal time)
$x$	Equation of time in in minutes

The hour angle  $\omega$  is a time depending coordinate (equatorial coordinate system), next to the declination  $\delta$ , to determine the sun's position in the sky [96].

$$\omega = (12 \text{ pm} - \text{LST}) \cdot 15^\circ/\text{h} \quad (\text{B.4})$$

$\omega$	Hour angle in minutes
LST	Local solar time in minutes

By using the hour angle  $\omega$ , the latitude  $\varphi$  and declination angle  $\delta$  the solar elevation angle  $\gamma_s$  can be calculated:

$$\gamma_s = \sin^{-1}(\cos(\omega) \cdot \cos(\delta) + \sin(\varphi) \cdot \sin(\delta)) \quad (\text{B.5})$$

$\gamma_s$	Solar elevation angle in $^\circ$
$\delta$	Declination
$\varphi$	Latitude

The solar azimuthal angle  $\alpha_s$  depends on the declination  $\delta$ , solar elevation angle  $\gamma_s$  and the latitude  $\varphi$ , and gets calculated with the equation.

$$\alpha_s = \begin{cases} 180^\circ - \cos^{-1} \frac{\sin(\gamma_s) \cdot \sin(\varphi) - \sin(\delta)}{\cos(\gamma_s) \cdot \cos(\varphi)} & \text{for LST} \leq 12 \text{ pm} \\ 180^\circ + \cos^{-1} \frac{\sin(\gamma_s) \cdot \sin(\varphi) - \sin(\delta)}{\cos(\gamma_s) \cdot \cos(\varphi)} & \text{for LST} > 12 \text{ pm} \end{cases} \quad (\text{B.6})$$

The following Figure B.5 shows a sun path chart for the three selected cities – Stockholm, Graz and Valetta.

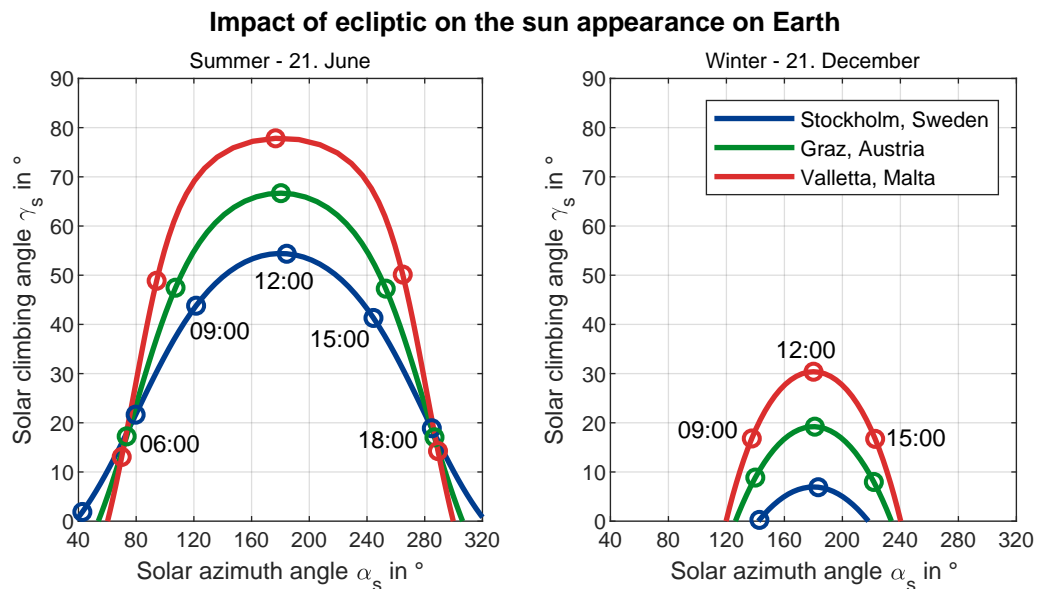


Figure B.5: Solar path

## Orientation and Tilt of Aligned Surfaces

The geographical orientation  $\alpha_{sa}$  and tilt  $\gamma_{sa}$  of aligned surfaces, e.g., roofs and photovoltaic modules, are essential parameters for the calculation of the solar irradiance falling on certain surfaces. The vertical tilt  $\gamma_{sa}$  of surfaces is measured from the horizontal. Parallel to the horizontal, the vertical tilt is  $0^\circ$ , and orthogonal to the horizontal it is  $+90^\circ$ . The azimuthal alignment of the surface is related to the geographical direction south. An azimuthal orientation of the surface to the south corresponds to a  $\alpha_{sa}$  of  $0^\circ$  or to the west of  $+90^\circ$ .

## Solar Incidence on Aligned Surfaces

The sun's angle on an arbitrary aligned surface can be calculated using the angles previously determined to describe the position of the sun and the orientation and vertical tilt of the surface. The determination of the sun's angle of incidence is essential for the calculation of the solar irradiance on arbitrarily aligned surfaces, as explained in the chapter. The following Figure B.6 shows the essential angular relationships.

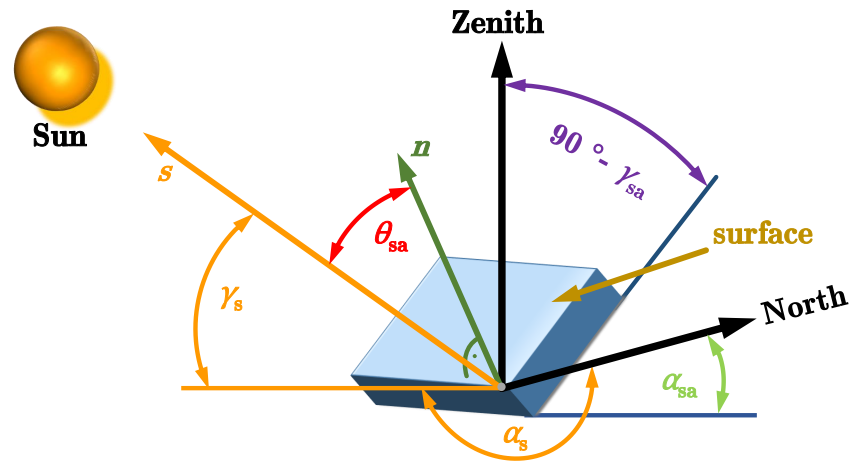


Figure B.6: Overview of the different angles [6]

The normal vector  $\mathbf{n}$  is orthogonal to the surface under consideration. The Sun vector  $\mathbf{s}$  points from the considered surface to the centre of the sun. The angle of incidence can be calculated from the Arcuscosine of the scalar product of the two vectors. Here, the sun's position, which is given in spherical coordinates, must be converted into the Cartesian coordinate system. The Sun's angle of incidence can be calculated without conversion of the Sun's position [95].

$$\theta_{sa} = \cos^{-1} [-\cos(\gamma_s) \cdot \sin(\gamma_{sa}) \cdot \cos(\alpha_s - \alpha_{sa}) + \sin(\gamma_s) \cos(\gamma_{sa})] \quad (\text{B.7})$$

## Albedo

The following Table B.1 lists the different albedo values  $\alpha$  according to Quaschnig [95]. If the environment is unknown, the albedo must be defined as  $\alpha = 0.2$ .

Table B.1: Albedo values  $\alpha$  for different surfaces according to Quaschnig [95]

Surface	Albedo $\alpha$	Surface	Albedo $\alpha$
Grass	0.25	Asphalt	0.15
Turf	0.18 ... 0.23	Forests	0.05 ... 0.18
Dry grass	0.28 ... 0.32	Heathland and sandy areas	0.10 ... 0.25
Uncultivated fields	0.26	Water area ( $\gamma_s > 45^\circ$ )	0.05
Plain floor	0.17	Water area ( $\gamma_s > 30^\circ$ )	0.08
Gravel	0.18	Water area ( $\gamma_s > 45^\circ$ )	0.12
Concrete, weathered	0.2	Water area ( $\gamma_s > 10^\circ$ )	0.22
Concrete, clean	0.3	Fresh snow cover	0.80 ... 0.90
Cement, clean	0.55	Snow cover	0.45 ... 0.70

# Appendix C

## Influence on Distribution Networks

Table C.1: Energy demand of households connected to B1 to B13

Branch	Bubsar	ED in kWh/a	EV in kWh/a	HD in kWh/m <sup>2</sup> a	DHW in kWh/a	CD in kWh/m <sup>2</sup> a
Branch I	B1	4743	932	74	2063	6
	B2	4753	985	38	2071	7
	B3	3561	730	168	2068	10
	B4	2765	696	74	1449	6
Branch II	B5	4889	1335	38	2269	7
	B6	4384	1260	168	1979	10
	B7	1551	1603	74	1029	6
	B8	3371	1663	38	1068	7
	B9	3901	687	168	2053	10
Branch III	B10	7004	1213	74	3456	6
	B11	3518	664	38	2041	7
	B12	4625	1356	168	1992	10
Branch IV	B13	2683	1307	74	894	6

ED... Electrical demand

EV... Demand of electric vehicle

HD... Heating demand

DHW... Domestic hot water demand

CD... Cooling demand